University of Nevada, Reno

Spatial and Temporal Relationships between Carlin-style Gold and Polymetallic Mineralization at the Deep Cove Gold-Silver Deposit, Lander County, Nevada

A thesis submitted in partial fulfillment of the requirements for the degree of Master of Science in Geology

by
Wilson M. Bonner

Dr. John L. Muntean/Thesis Advisor

December, 2019

THE GRADUATE SCHOOL

We recommend that the thesis
prepared under our supervision by

Wilson M. Bonner

Entitled

Spatial and Temporal Relationships Between Carlin-style Gold and Polymetallic Mineralization at the Deep Cove Gold-Silver Deposit, Lander County, NV

be accepted in partial fulfillment of the
requirements for the degree of

Master of Science

Dr. John L. Muntean , Advisor

Dr. Michael W. Ressel , Committee Member

Dr. Adam Kirn , Graduate School Representative

David W. Zeh, Ph.D., Dean, Graduate School

December, 2019

ABSTRACT

Cove is a late Eocene previously mined Au-Ag deposit in the Battle Mountain district of Lander County, Nevada that contains both Carlin-style and polymetallic mineralization. It has been interpreted as a distal disseminated deposit approximately 1.6 km northeast of the Eocene McCoy Au skarn deposit and adjacent late Eocene quartz monzonite Brown stock. Previous geologic mapping, stable isotope data, and geochronology have suggested the mineralization at Cove is genetically associated with an Eocene magmatic-hydrothermal system also responsible for the skarn mineralization at McCoy (Johnston et al., 2008). Exploration drilling by Premier Gold Mines, Ltd since 2012 at Cove has further defined the Carlin-style Helen and CSD deposits and discovered the Carlin-style Gap zones and the 2201 polymetallic zone.

The mineralization at the Helen and Gap zones is hosted in Middle Triassic silty limestones overlying dolostones. All three deposits occur along the axis of the northwest trending Cove anticline at depths of 350 – 550 m below surface. Carlin-style mineralization in the CSD, Gap, and Helen zones is controlled by intersections of NE- (and NS-) striking faults and dikes and the NW trending Cove anticline. The ore fluids propagated out from these faults and dike contacts along the axis of the anticline by taking advantage of stratigraphic contacts and pre-mineral mafic sills. The polymetallic mineralization at the 2201 zone, occurs beneath the CSD zone, approximately 600 - 900 m below surface. It is characterized by mostly pyrite-sphalerite-galena carbonate veins and disseminations with lesser but higher-grade precious and base metals in pyrite-sphalerite-galena-quartz-siderite-(chalcopyrite-arsenopyrite-pyrrhotite-electrum) veins hosted in Early to Middle Triassic conglomerates and carbonate sandstones. At the contact of the siliciclastics overlying limestone, there manto-style replacement sulfides bodies locally formed as a result of a strong pH gradient.

Although all Carlin-style ore zones display similar associated decarbonatization and silicification alteration, the pyrite textures and geochemistry varies among zones based on distance from the polymetallic minerals.

Arsenian pyrite in the Helen zone is more commonly very fine-grained, anhedral (“fuzzy”), and lacks well-defined rims whereas the arsenian pyrites in the CSD zone are fine-grained, often euhedral to subhedral, and display well defined As- (Ag-)bearing rims. Ag was first detected in Carlin-style pyrite rims at the CSD zone using energy dispersive spectroscopy (EDS) on a scanning electron microscope (SEM) and later confirmed with an electron microprobe. The results of the microprobe work show Ag can exist in Carlin-style rims up to 1.5 wt %. The Carlin-style mineralization at Cove has variable Ag/Au ratios that average ~1.5 across the deposit and generally decrease along the Cove anticline to the northwest from the CSD zone averaging ~12 to the Helen zone averaging ~0.5. Beneath the CSD zone, we observe Carlin-style mineralization overprinting preexisting manto-style polymetallic mineralization in the basal Favret limestone.

This study describes the mineralization at Cove including pyrite geochemistry and district-scale geochemical trends, reports new geochronology for the district, and places Cove along a continuum between Carlin-type gold deposits and distal disseminated sedimentary rock-hosted deposits.

ACKNOWLEDGEMENTS

Many thanks to Premier Gold Mines who supported this thesis and provided much of the data presented in this study. Barrick Gold Corporation also contributed data and ideas presented here. I benefited from conversations with and work done on the Cove project by Mike Ressel, Marcus Johnston, Chris Henry, Brian Cousens, Ken Coleman, Chad Peters, Mia O'Neal, Warren Thompson, Page Anderson, Vladimir Ispolatov, Liz Stock, Nick Williams, Paul Dobak, and Meghan Jackson. I appreciate the professional support from Ewan Downie and Steve McGibbon at Premier Gold Mines and from Glenn Asch and Kevin Creel at Barrick given to me in order to complete this work. Thanks to Dave Browning and others at TerraCore for acquiring and interpreting hyperspectral data reported in Appendix B and to Andrew Zehr for his help compiling Appendix A. I also appreciated advice from Moira Smith, Joe Laravie, Stephen Shaver, Maeve Boland, Murray Hitzman, Jon Price, Nancy Richter, Chris Clinkscales, and my family throughout my master's studies. I received a grant in 2016 from the Society of Economic Geologists Foundation for which I am very grateful. Thanks to all the sponsors of the Center for Research in Economic Geology at the University of Nevada, Reno. Special and distinct thanks to Tyler Hill and John Muntean. Guess I'll keep on RAMBLIN ON!

TABLE OF CONTENTS

LIST OF TABLES

LIST OF FIGURES

INTRODUCTION

Carlin-type gold deposits in north-central Nevada constitute one of the world's largest gold districts (Muntean, 2018) and have been the focus of many research projects since their economic importance began to be recognized in the 1990's (Cline, 2018). Research in the last 10-15 years has mostly centered on deposits within the four major gold-producing districts – the Carlin Trend , the Jerritt Canyon district, the Getchell district, and the Cortez district (Cline, 2018). Controversy still remains, however, whether Carlin-type gold deposits are the distal products of magmatic-hydrothermal systems (Muntean et al. 2011; Johnston and Ressel, 2004; Sillitoe and Bonham, 1990) or whether they form solely from meteoric and/or metamorphic fluids (Seedorff, 1991; Ilchik and Barton, 1997; Large et al., 2011). Much of this controversy is driven by the fact that Carlin-type deposits formed from relatively low-temperature fluids (<250˚C), and show no evidence for higher temperature alteration and mineralization (e.g, skarn), resulting in a lack of elemental or mineralogical zoning, that would be expected if there was a temporal and spatial relationship with an underlying pluton. Further controversy exists whether Carlin-type gold deposits form from different processes than distal disseminated deposits – Carlin-style gold deposits with a spatial and temporal relationship to plutons (Sillitoe and Bonham, Jr., 1990). Hofstra and Cline (2000) distinguished distal disseminated deposits from Carlin-type deposits by their strong zoning (alteration, mineralogy, geochemistry), temporal and spatial relationships to calc-alkaline granitoid intrusions, common early polymetallic skarn and/or veins and carbonate replacement bodies, along with much higher Ag/Au ratios than Carlin-type deposits.

The Cove-McCoy district contains many styles of mineralization, including skarn at McCoy, adjacent to the Eocene Brown stock, and polymetallic veins, manto-style carbonate replacement bodies, and Carlin-style disseminated gold mineralization at Cove, located 1.6 km northeast of McCoy. The Carlin-style mineralization at Cove was interpreted by Sillitoe and Bonham (1990) as a distal product of magmatic-hydrothermal mineralization associated with the Brown stock and was classified as a distal disseminated deposit as defined by the U.S. Geological Survey (Cox and Singer 1990) . Johnston et al. (2008) presented

geologic mapping, petrographic studies, geochronology, stable isotope, fluid inclusion, and other geologic evidence at Cove to better understand the zonation and genetic relationship between the McCoy skarn and the polymetallic and disseminated Carlin-style mineralization at Cove. Although Johnston's studies were inconclusive in establishing a precise temporal relationship between the spatially separate gold-bearing polymetallic mineralization and Carlin-style mineralization at Cove, the work did establish based on sulfur isotopes that the hydrothermal fluids responsible for the Carlin-style mineralization and alteration had a magmatic component and could have been an evolved expression of the same magmatic-hydrothermal system responsible for the higher temperature mineralization at both Cove and McCoy. Based in part on this work, Johnston and Ressel (2004) suggested that Cove could be placed along a continuum of distal disseminated deposits and Carlin-type gold deposits.

Since Johnston's work in the mid 2000's, exploration at the Cove property has further defined and discovered deeper zones of both Carlin-style mineralization (Helen, Gap, CSD zones) and polymetallic mineralization (2201 zone). These deeper discoveries have permitted a reevaluation of the timing relationship between the two styles of gold mineralization, along with testing of the hypothesis that Carlin-style distal disseminated mineralization forms a continuum with Carlin-type mineralization, as defined by the large deposits on the Carlin trend, and the Cortez, Getchell, and Jerritt Canyon camps.

Through petrography, trace element geochemistry, geochronology, and detailed core logging and documentation of cross-cutting relationships, this study presents results from deeper mineralization at Cove unavailable to previous researchers that supports a continuum between distal disseminated deposits and Carlin-type deposits and contributes to the debate at large on the origin of Carlin-type gold deposits in Nevada.

MCCOY MINING DISTRICT AND PREVIOUS RESEARCH

The Cove gold-silver deposit is located within the Fish Creek Mountains about 22 km south of the Battle Mountain district and 48 km southwest of the town of Battle Mountain, Lander County, Nevada (Figure 1).

It exists within the McCoy mining district, which contains numerous historic producing mines and prospects. Joseph H. McCoy first discovered placer gold deposits in the district in 1914, and the Gold Dome Mine produced ~1000 ounces of gold from 1930 to 1931 in the vicinity of the current McCoy open pit (Emmons and Eng, 1995). The district has seen production and been extensively explored since then by several companies including Echo Bay Minerals. Echo Bay discovered Cove in 1987 through a soil sampling survey and began open pit mining in 1988. The grade of ore produced from Cove from 1987 to 2001 averaged 1.29 g/t Au and 4.41 g/t grams Ag per tonne. Total production at McCoy and Cove from 1986 through 2006 totaled 3,409,451 ounces of gold and 110,207,329 ounces of silver (Practical Mining, LLC, 2013). Current exploration efforts by Premier Gold Mines and Nevada Gold Mines are focused on Carlin-style mineralization in deeper host rocks than what was previously mined from the Cove resource.

Figure 1. Location of the Cove-McCoy Mining District in northern Nevada.

The geology of the McCoy mining district was mapped and described by Emmons and Eng (1995), who also reported K-Ar geochronology on sericite, biotite, and hornblende from the Brown stock and proximal dikes (Table 2). Brooks (1994) completed a dissertation on the petrology, geochronology, and geochemistry of the Brown stock and McCoy skarn wherein he proposed two pulses of mineralization: an early, sub-economic skarn deposit associated with an oxidized, magnetite-bearing intrusion and a late, higher-grade skarn deposit associated with an ilmenite-bearing, reduced intrusion. He dated the first phase of magmatism and mineralization, based on K-Ar ages of hydrothermally altered sericite and magmatic hornblende and biotite from the Brown stock, at ~40.1 Ma and the second phase, dated by a K-Ar adularia age on mineralization, was determined to be ~39 Ma. The economic gold and silver mineralization was associated with the second phase that is characterized by quartz-pyrite ± adularia and retrograde alteration assemblages and had a correlation with As, Bi, Te, and Zn. Based on fluid inclusion microthermometry, Brooks (1994) reported the homogenization temperatures of the fluid responsible for the early prograde skarn event at McCoy as 330° - 590°C and salinities up to 39.8 eq. wt % NaCl based on analyses of fluid inclusions in pyroxene and garnet. Fluid inclusions in retrograde epidote homogenized at lower temperatures, 200 - 350°C, and contained salinities of ~11 eq. wt. % NaCl eq.

After Kuyper et al. (1991), Johnston (2003) was the first comprehensive study of the geology and geochemistry of the Cove deposit. This work and the publications that emanated from it (Johnston et al., 2008; Johnston and Ressel, 2004) reported updated geologic mapping of the open pit, petrographic observations, and fluid inclusion, stable isotope, and geochronology results. Johnston (2003) analyzed quartz fluid inclusions from seven different polymetallic vein samples collected in the Cove pit. These produced homogenization temperatures ranging from 207° to 370° C with a mean of 304° C. Stable isotope results on sulfides from both McCoy and Cove suggested a common source of sulfur in the ore fluids. Stable isotopes of oxygen and hydrogen analyzed from hydrothermal illite and hydrothermal quartz suggested the fluids were partly of magmatic origin.

METHODS

For this research, a select subset of 15 core holes from Premier Gold Mines drilling were selected across a series of northwest and northeast cross sections. The northeast section was constructed to intersect the 2201 zone, the CSD zone, and the Helen zone. These holes were re-logged in detail with a focus on mineralogy, alteration, igneous rocks, and lithologies within defined formations. During this work, over 600 individual samples were selected from these holes to support further petrographic and geochronologic work (Table 2Table 2. Collected samples from Cove deposit by formation and mineralization type.
). Preference for additional analytical work was made for samples that were located along a transect from unmineralized to weakly mineralized to ore-grade mineralization in each deposit. No samples from the Gap deposit were initially collected as the deposit had not been discovered at the time.

Collected samples by formation		Collected samples by mineralization type	
Panther Canyon Formation	44	**Carlin-style**	214
Home Station Member	82	*Helen Zone*	*68*
Favret Formation	194	*CSD Zone*	*146*
Dixie Valley Formation	162	**Polymetallic mineralization**	137
Havallah Formation	24	**manto**	57
Undifferentiated igneous rocks	105		
other	26		
Total	**637**		

Table 2. Collected samples from Cove deposit by formation and mineralization type.

Premier Gold Mines made available their complete geochemical dataset, which consisted of ICP-MS analyses of 48 elements using a four acid digestion on one gram pulps that were conducted on the same intervals as 10 gram fire assay gold samples. Premier drill core and rotary samples were assayed by Inspectorate/Bureau Veritas (2013 – 2015) and ALS Labs (2015 – 2016) and check samples were assayed by American Assay. Differences in the digestion method between labs led us to re-assay the volatile elements (As, Sb, and Hg) using the incipient dryness method (heating sample to its original dryness before hydrochloric acid digestion) prior to ICP-MS to establish more consistent comparisons.

Element ratios and trends were explored using Reflex's ioGAS software and both GEMS and Leapfrog Geo three-dimensional modeling software. Further lithogeochemical plotting and analysis were constructed with R software using the classification and geotectonic diagrams found within the GCDKit package for R (Janousek et al., 2006). Skeletonized drill samples were scanned with TerraCore's hyperspectral imaging spectrometers in Reno in 2015. Data were analyzed and interpreted by TerraCore staff.

Drill core samples were first described using a binocular scope and scanned to high resolution images before selecting a subset to be cut for thin section petrography and microscopy. Type samples of igneous rocks were prepared for both thin section preparation and whole rock geochemistry (ALS Labs). After detailed observations were recorded using transmitted light and reflected light petrography of the unmineralized and mineralized samples, a subset was chosen for further analysis with the University of Nevada, Reno (UNR) JEOL JSM-6010LA tungsten-filament scanning electron microscope (SEM). This instrument was used to acquire high-resolution back scatter electron images of pyrite textures and energy dispersive spectroscopy (EDS) spot analyses of certain mineral phases. The UNR JEOL JSM-7100 FT field emission SEM was used to complete element maps of unique grains first recognized on the tungsten-filament SEM. The same samples were then taken to the University of Nevada, Las Vegas Electron Microanalysis and Imaging Laboratory (EMiL) to use the JEOL JXA-8900 electron microprobe microanalyzer (EPMA).

Samples for geochronology were chosen based on their observed cross-cutting relationships to Carlin-style mineralization, polymetallic, and skarn mineralization. Mineral separates were completed by GeoSep Services in Moscow, ID. Six samples were analyzed at the United States Geological Survey (USGS)-Stanford University Sensitive High-Resolution Ion Microprobe (SHRIMP) – Reverse Geometry lab in 2016. Individual zircons were selected for each sample with a bias towards the most euhedral, inclusion-free grains. These were mounted to epoxy grain mounts and imaged with cathodoluminescence (CL) using a CL detector mounted to a scanning electron microscope (SEM) at Stanford University. U-Pb and trace element analysis were completed following guidelines of Barth and Wooden (2006). Concentrations were calibrated against reference standards MADDER (Barth and Wooden, 2010; Coble et al., 2018) and TEMORA 1 (Black et al., 2003).

Thermodynamic modeling and metal solubilities were calculated using CHNOSZ, a package for R (Dick, 2019), using the most recent recommended thermodynamic properties for Au and Ag complexes (Pokrovski et al., 2014).

REGIONAL GEOLOGY

The Fish Creek Mountains and Cove-McCoy district are located on the western edge of the rifted North American craton near a lithospheric terrane boundary with accreted oceanic terranes to the west delineated by several isotopic systems including Sr and Pb. While many notable Carlin-type deposits are hosted within Paleozoic miogeoclinal rocks, the Cove orebody is hosted within Triassic sedimentary rocks of the Star Peak Group (Nichols and Silberling, 1977), which were deposited unconformably over the Havallah sequence in a back-arc setting. The Havallah sequence was emplaced eastward along the east-verging Golconda thrust during the Late Permian-Early Triassic Sonoma orogeny (Silberling and Roberts, 1962; Dickinson, 2006). In the Early to Middle Triassic, differential uplift and subsidence produced repeating sequences of carbonate and coarse-grained clastic rocks, the Star Peak Group, until the late Middle to Late Triassic when thick accumulations of marine rocks, locally present at Cove-McCoy, as the Auld Lang Syne Group, occurred across the western Basin and Range Province (Wyld, 2000). This back-arc basin was subsequently closed off tectonically by collisional tectonism and arc accretion forming the Luning-Fencemaker fold-and-thrust belt in the Late Triassic-Early Jurassic. Intrusion of back-arc plutons, including the ~157 Ma McCoy pluton within the McCoy district (Emmons and Eng, 1995), was common in the Late Jurassic (Oldow, 1983; Wyld, 2000). Continued magmatism in the Mesozoic was responsible for the Late Cretaceous (~89 Ma) Fish Creek granitic porphyry at the north end of the Fish Creek Mountains (Miller and Silberman, 1977) and several Cretaceous intrusions in the nearby Battle Mountain district (Theodore, 2000; King, 2017). By 45 Ma, rollback of the shallowly subducting Farallon plate initiated a magmatic flare up (Humphreys, 1995) that swept across the Great Basin progressively from north to south. This episode was responsible for many of the plutonic rocks at Cove-McCoy including the ~38 Ma Brown stock, many granodiorite dikes and sills, and the Davenport granodiorite stock east of the Cove deposit under pediment alluvial cover. Volcanism in the late Eocene resulted in the formation of calderas and various other volcanic centers in the Fish Creeks and adjacent mountain ranges, including the emplacement of the 34.45 ± 0.06 Ma Tuff of Cove Mine (John, et al., 2008), and the 34.24 ± 0.07 Ma Pinnacle Mountain rhyolite dome (Cousens et al., 2019) south of the McCoy deposit. Beginning at ~17 Ma, northern Nevada experienced the main phase of Basin and Range

extension (Colgan et al., 2006a; Colgan et al., 2006b), though the Cove-McCoy district displays only minimal post-mineral movement along faults (Johnston et al., 2008).

DISTRICT GEOLOGY

The stratigraphy and structural geology of Cove-McCoy (Figure 2**Error! Reference source not found.**) and the north Fish Creek Mountains has been mapped and described by Stewart et al. (1977), Emmons and Eng (1995), Johnston (2001; 2003), and Thompson et al (2015).

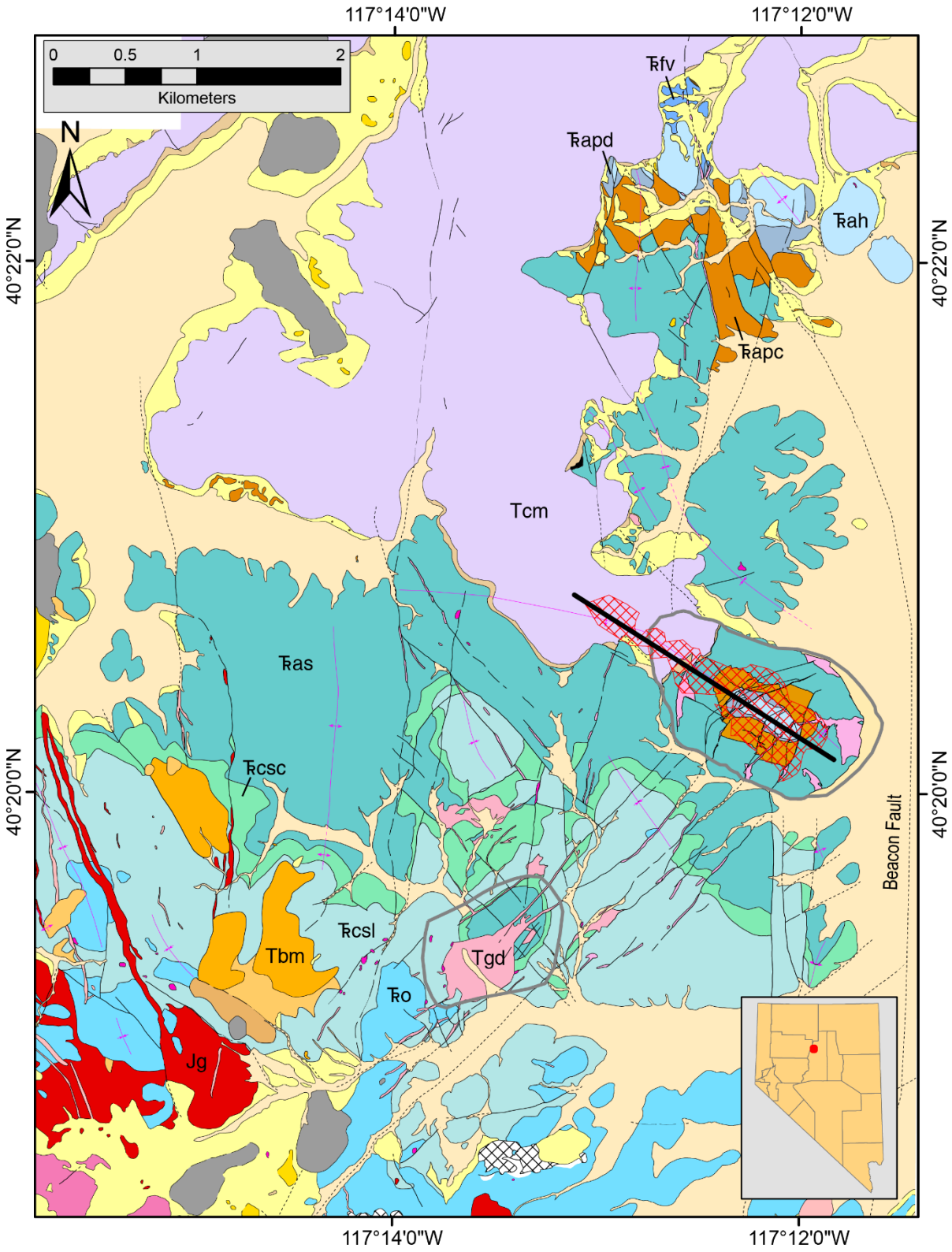
117°14'0"W
117°12'0"W
40°22'0"N
40°20'0"N
0
0.5
1
2
Kilometers
N
Tfv
Tapd
Tah
Tapc
Tcm
Tas
Tcsc
Tcsl
Tbm
Tgd
To
Jg
Beacon Fault

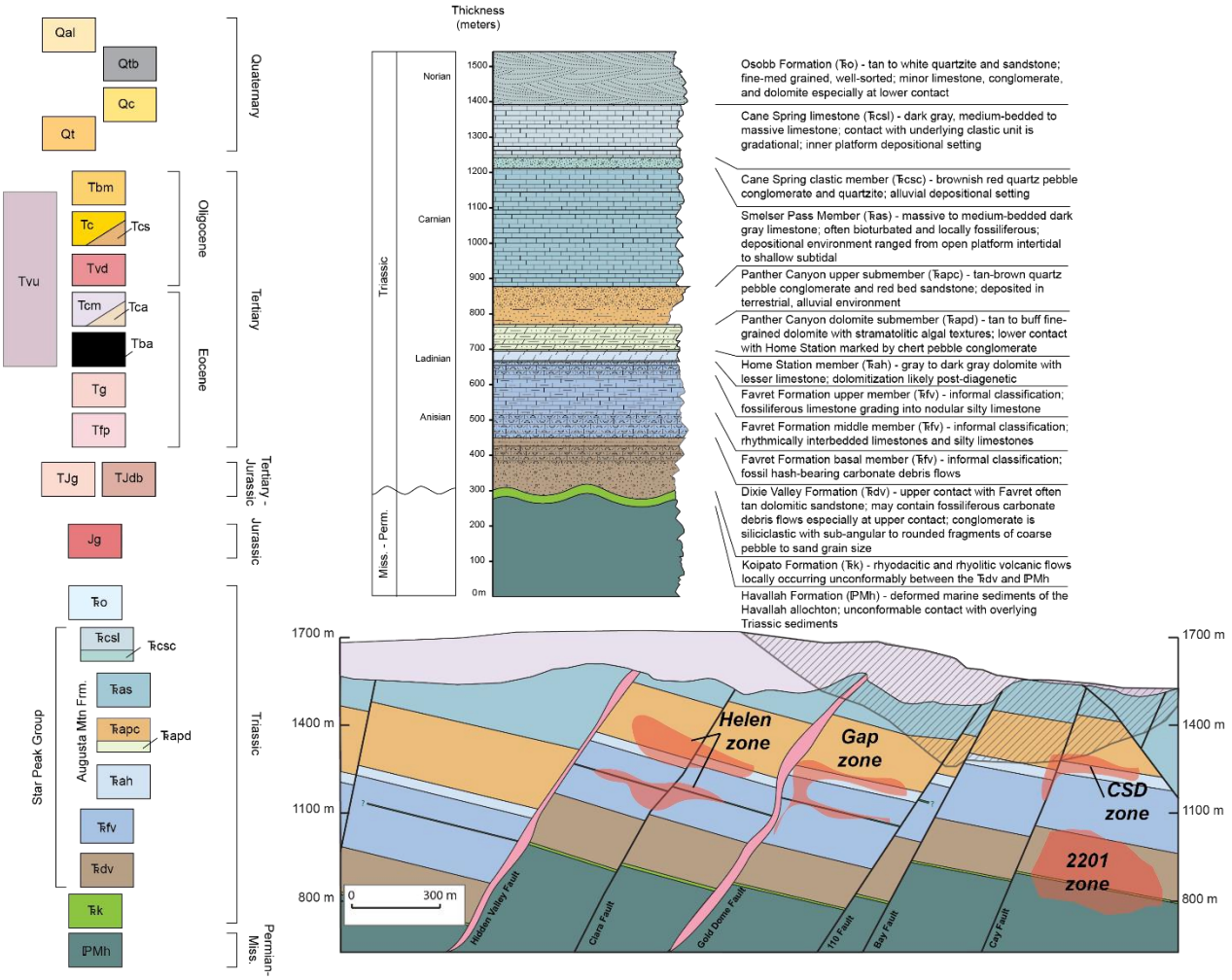

Figure 2. Geologic map of the Cove-McCoy Mining District adapted from Emmons and Eng (1995) and a description of map units. Cross section line is drawn on geologic map and is looking northeast along hinge of Cove anticline. Grid is in WGS84.

Stratigraphy

The oldest exposed unit is the allochthonous Mississippian-Permian Havallah sequence consisting of allochthonous, metamorphosed marine sediments (Silberling and Roberts, 1962). It crops out on the northern and northwestern flanks of the range at Buffalo Valley and is encountered in the deepest exploration drill holes at the 2201 zone. The Havallah is unconformably overlain regionally by either Early Triassic Koipato volcanic rocks or Early to Middle Triassic Star Peak Group (Nichols and Silberling, 1977). This contact is not exposed in surface geology, but when encountered in drilling is defined by a thin rhyodacite tuff that may

be part of the early Triassic Koipato group. The oldest unit in the Star Peak Group is the late Spathian to middle Anisian Dixie Valley Formation (TRdv). It is the main host of the polymetallic 2201 zone and contains dolomitic sandstones, conglomerates, and minor beds of fossiliferous carbonate debris flows at its upper conformable contact with the Favret Formation.

The Favret Formation (TRfv) is the main host of Carlin-style mineralization at the Helen and Gap deposits and is consistently 200 - 215 m thick. The Favret consists of three previously undifferentiated informal units defined as an upper fossiliferous unit, a middle unit containing alternating thin beds of silty limestone and limestone, and a basal fossiliferous debris flow unit. The middle unit is the best host rock for Carlin-style mineralization on the property due to its permeability and concentrations of reactive iron. Its < 10 cm thick limestone and silty limestone interbeds are interpreted to have been deposited in a slope setting within a bac arc basin further offshore than the shelfal facies of the upper and basal fossiliferous units. The silty limestone interbeds of the middle unit contain calcite, quartz, apatite, dolomite, and minor monazite ((Ce, La)PO_4) allowing it to be easily distinguished from the upper and basal members with downhole multielement geochemistry. The Favret crops out approximately four kilometers north of the Cove deposit.

The Augusta Mountain Formation conformably overlies the Favret Formation and comprises four members in the Cove-McCoy district. The Home Station member has a gradational contact with the underlying Favret Formation. The Home Station is a massive, gray to dark gray dolostone that contains local recrystallized ammonites and bivalve fossils. The dolomite is only locally ferroan based on potassium ferricyanide staining. The Home Station is consistently altered and mineralized in the Helen, Gap, and CSD deposits though it rarely contains concentrations > 5 g/t Au. Its upper contact with the Panther Canyon dolomite submember is defined by a chert pebble conglomerate marker bed and change in bedding thickness. The thickness of the Home Station member ranges between 15 and 45 m.

The Panther Canyon member, which is 180 m thick, is divided into two members – an older dolomite member (TRapd) and a younger upper member (TRapc) containing a coarsening upward sequence of carbonate

cemented silt- and sandstone to pebble conglomerate. The dolomite submember is differentiated from the Home State member dolostone by its thin bedding, tan to buff color, and lack of fossils. The Panther Canyon dolostone submember is the main host of the CSD deposit and upper Helen zone. It contains more ferroan dolomite and lower concentrations of phosphorous allowing it to be distinguished by geochemistry from the lower Home Station member. The upper submember was the main host rock for the mined Cove open pit deposit. Its carbonate sandstone beds were a strong control on disseminated mineralization; however, they are rarely altered or mineralized in the Helen and Gap areas.

The youngest member of the Augusta Mountain Formation is the Smelser Pass Member consisting of massive to medium-bedded gray limestone and minor fossiliferous limestone. It hosted oxidized, supergene mineralization in the Cove pit but was otherwise unmineralized. It crops out extensively across the property; however, its homogeneity and 300 – 340 m thickness complicate estimations of offset along mapped faults.

The Cane Spring Formation is the youngest unit in the Star Peak Group at Cove-McCoy and is divided into a basal clastic member and an upper limestone member. The basal unit is a coarse-grained, quartz pebble conglomerate that ranges in thickness from 45 to 60 m. The upper limestone member is a massive poorly bedded gray limestone that is difficult to distinguish from the Smelser Pass when the basal clastic member is present. Both informal members of the Cane Spring Formation hosted oxide and sulfide skarn mineralization at McCoy.

Conformably overlying the Augusta Mountain Formation is the Osobb Formation of the Auld Lang Syne Group (Emmons and Eng, 1995). It displays extensive contact metamorphism in the Cove-McCoy district based on its proximity to the Jurassic McCoy Pluton in outcrop. It consists of white to tan sandstone (now quartzite) and is at least 150 m thick, though true thickness is unknown due to erosion. It hosts Jurassic magnetite-hematite deposits along its southern contact with the McCoy pluton (Stewart et al., 1977).

Structure

The Triassic sedimentary rocks consistently dip 10 – 20 degrees to the south across the property exposing the oldest units at the northern end of the range. Late Triassic or Jurassic compression resulted in low amplitude, broad anticlines and synclines trending north-south and northwest (Cove anticline) across the property. These folds were offset by later extensional events, forming steeply dipping (~70 degrees) northwest-striking faults, northeast-striking faults, and late north south-striking faults (Johnston 2001). Offsets along the northwest- and northeast-striking sets are 40 – 75 m whereas the north south-striking faults can display offsets of greater than 200 m. All faults mapped and logged in detail on the property display complex cross-cutting relationships and evidence for multiple generations of reactivation. Most, however, are pre- or syn-mineral with only minimal post-mineral movement.

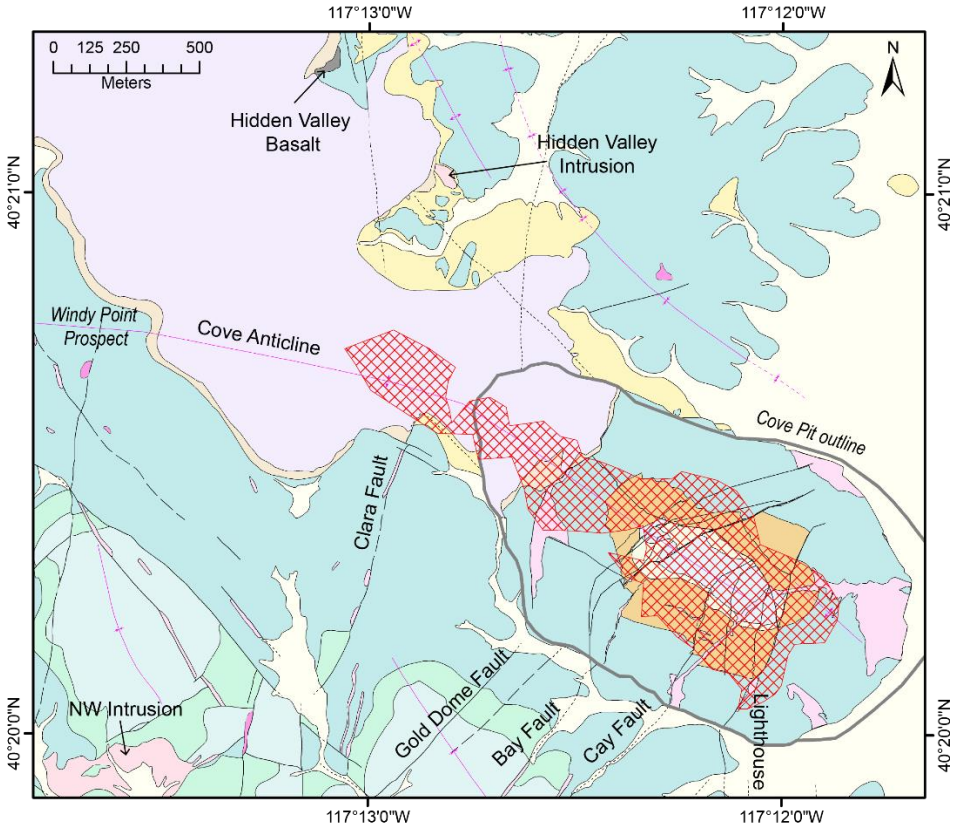

Figure 3. Cove pit map and labeled structures and features referenced in text. From Emmons and Eng (1995) and Johnston et al. (2008)

IGNEOUS GEOLOGY OF COVE-MCCOY

Granitic Intrusions

The Cove-McCoy district contains several intrusions of different ages ranging from Jurassic to Eocene. The oldest intrusive body is the Jurassic (157 Ma K-Ar date; Silberman and McKee 1971) McCoy pluton at the southern edge of the property (Figure 2). It is a polyphase, porphyritic to equigranular intrusion containing phases of granite, granodiorite, quartz monzonite, and minor diorite composition (Emmons and Eng, 1995). The Eocene Brown stock occurs at the McCoy mine and is quartz monzonite to granodiorite in composition (Emmons and Eng, 1995; Johnston et al., 2008). Brooks (1994) identified five sequential intrusive phases based on cross-cutting relationships and compositional variations.

Airborne geophysics by Echo Bay identified a magnetic anomaly under alluvial cover to the east of the Cove pit, which was drilled in the 1990's. Several drill holes intersected an Eocene (Emmons and Eng, 1995) granitic to granodioritic intrusion with a sill-like geometry, which was later named the Davenport intrusion. Importantly, the sill-like geometry of the intrusion based on historic drill logs does not match the location or depth of the magnetic anomaly and there may be an undrilled larger deeper intrusion under the sill. Other granitic to granodioritic intrusions on the property include the Hidden Valley intrusion and the Northwest intrusion, which are undistinguishable from the Brown stock in hand sample and geochemistry, although they are spatially discrete bodies (Figure 3).

The Cove-McCoy property contains abundant dikes and sills evident both in surface mapping and drilling (Figure 2). Emmons and Eng (1995) divided them into Eocene feldspar porphyry granodiorite dikes, Jurassic granodiorite dikes, and Tertiary-Jurassic dikes of unknown age. Many of the northeast- and north-south-striking faults on the property are occupied by granodiorite feldspar porphyry dikes that can extend for > 1 km strike lengths. These dikes are light gray to white in color due to sericitic or argillic alteration. The Gold Dome dike, the most commonly drilled granodioritic dike, is ~35 m thick. Less altered samples collected from the Cove open pit retain evidence for secondary biotite replacing hornblende suggesting a weak potassic alteration event that was overprinted by lower temperature alteration events at depth. The Gold Dome is the most prominent granodiorite dike at Cove and is cross-cut by both polymetallic veins and id pervasively affected by weak Carlin-style mineralization and illite alteration attributed to it.

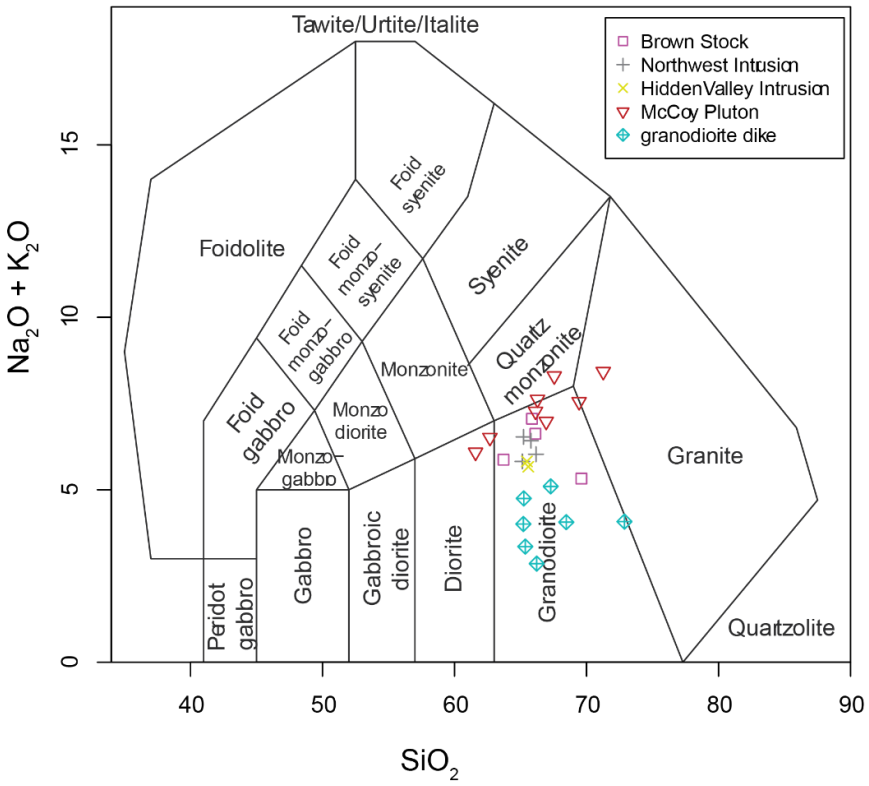

Figure 4. Middlemost (1994) geochemical discrimination plot showing the compositions of the granitic rocks of the Cove-McCoy district. The McCoy pluton is Jurassic while other samples are dated or presumed to be Eocene. The granodiorite samples have some degree of alteration, which has removed most of the sodium.

Mafic Intrusions

Though not as abundant as feldspar porphyry granodiorite dikes, mafic dikes and sills are commonly encountered in surface mapping and drilling at Cove. However, due to extensive alteration, many mafic rocks have been unidentified or incorrectly grouped with the granodiorite dikes in historic logs. Detailed logging of a transect across the Helen zone in 2015 observed a close spatial association of mafic sills with disseminated gold mineralization which led to an effort to better understand their features and age. Whole rock geochemistry has identified at least three pre-mineral mafic intrusive phases in the Cove deposit: calc-

alkaline basalt sills, calc-alkaline to shoshonitic basaltic andesite dikes and sills, and shoshonitic basaltic andesite dikes.

The basalt sills can easily be distinguished from the other mafic phases due to their high V/Ni ratio (Figure 5a). They are almost always observed in drilling across the Cove deposit in the middle unit of the Favret formation, where they cut bedding at a low angle. They are typically less than three meters thick, are dark green, contain abundant calcite, and are locally magnetic. Though they have a strong spatial association with Carlin-style gold mineralization and alteration, they are unmineralized even in direct contact with mineralized limestone.

The basaltic andesite dikes are more difficult to identify in hand sample due to intensive illite/illite-kaolinite alteration. They are generally light green to white in color and can be magnetic where they are less clay-altered. They can also share a spatial association to Carlin-style mineralization though not as strong as the basalt sills. Unlike the basalt sills, however, the basaltic andesites can be mineralized (up to 20 ppm Au and 20 ppm Ag). During a whole rock geochemistry study of the mafic rocks, a subset of basaltic andesites were identified by their high LREE concentrations typical of shoshonitic volcanism (Figure 5d, Figure 5e). Though alteration has had some affect on the concentrations of LREE (note wide range of La values in Figure 5b), we are confident there is a lithologic difference since they are both altered, and once classified and put into spatial context, the shoshonitic basaltic andesite appears as a clear northwest-striking, near vertical, <5 meter wide dike. This also appears to represent a heretofore unrecognized southwestern margin to Carlin-style mineralization in the Cove deposit. The Fire Dike is cut by northeast-striking Eocene faults implying that it is pre- or syn-Eocene, though geochronology is difficult to attain given the basaltic andesite composition (lack of dateable zircons) and strong degree of alteration.

Hidden Valley Basalt

A small outcrop of weakly altered Eocene basalt occurs on the eastern margin of the Cove mesa at Hidden

Valley (Figure 3) and extends under the younger Eocene Tuff of Cove Mine volcanic cover to at least the northeast edge of the Helen zone based on drilling.

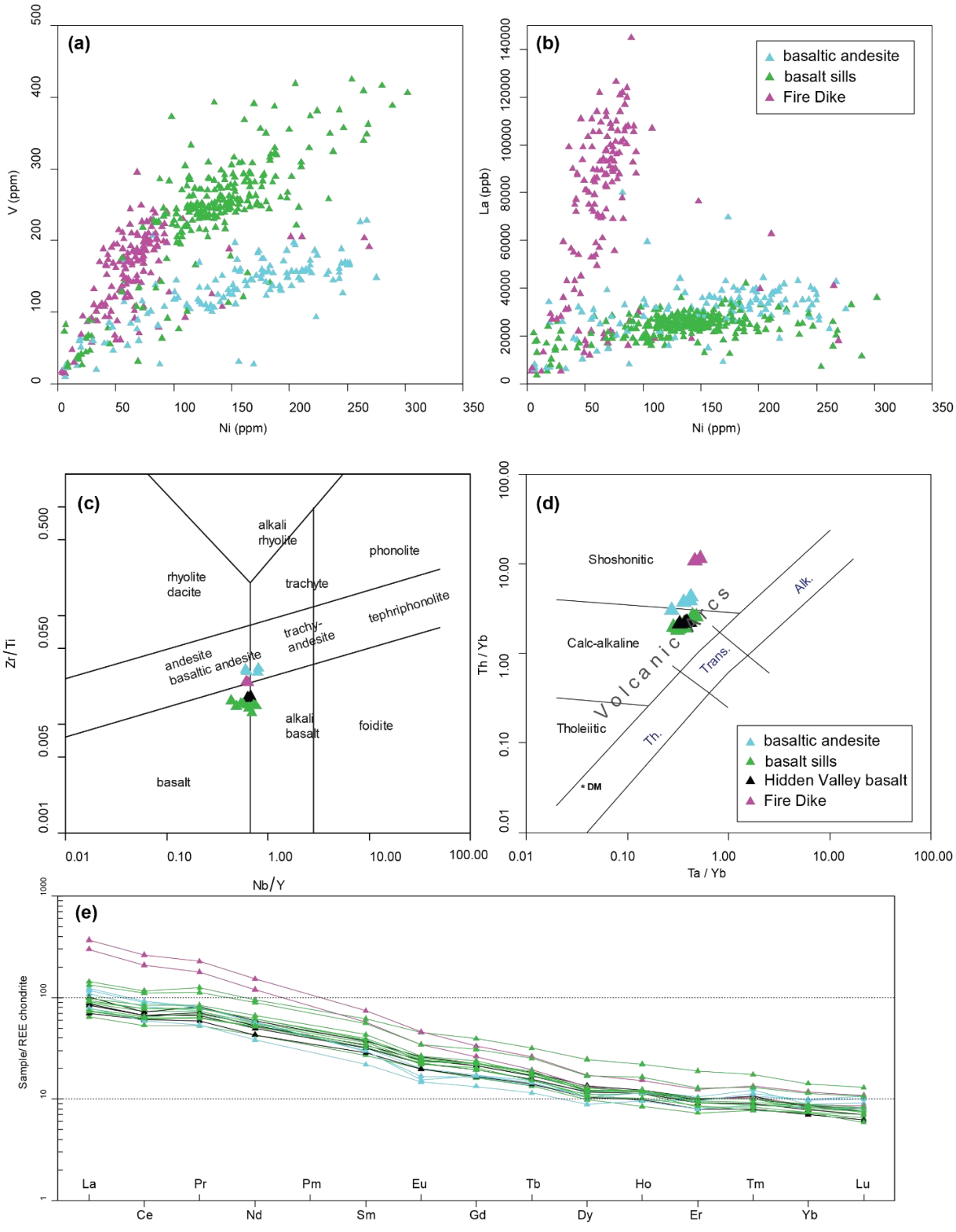

Figure 5. Various plots of the Cretaceous sill, basaltic andesite, Fire dike, and Hidden Valley basalt flow (Nakamura, 1974; Pearce, 1982; Pearce, 1996). Figures 4a and 4b are results of four acid digestion multi-element

analysis while Figures 4c, 4d, and 4e are the results of whole rock fusion. See Appendix A for complete whole rock analyses.

GEOCHRONOLOGY

The feldspar porphyry dikes and related intrusions had previously been dated with K-Ar at 38.8 to 40.3 Ma (biotite; Emmons and Eng 1995) and $^{40}Ar/^{39}Ar$ at 39.01 ± 0.22 Ma (biotite; Johnston et al., 2008). Brooks (1994) reported K-Ar previously acquired K-Ar age dates suggesting the age of the Brown stock to be between ~38 and 42 Ma. For mineralization, Groff et al. (1997) reported an $^{40}Ar/^{39}Ar$ adularia age for the skarn mineralization at McCoy at 38.26 ± 0.24 Ma and Johnston et al. (2008) presented an $^{40}Ar/^{39}Ar$ plateau age 39.37 ± 0.23 Ma for hypogene illite in the altered Bay dike and interpreted the date to represent the timing of polymetallic mineralization at Cove.

This U/Pb zircon study aimed to better asses the age of the Brown stock at McCoy and granodiorite feldspar porphyry dikes from Cove. We report new U-Pb zircon dates for five pit wall samples from the Brown stock (BS-1, BS-2, BS-3, BS-4bt, BS-5) and one drill core sample from the Gold Dome dike (Figure 6). Samples were analyzed at USGS-Stanford SHRIMP (Sensitive High Resolution Ion Microprobe) laboratory in 2016 (see Appendix C). One spot was analyzed per zircon chosen after grains were imaged with cathodoluminescence microscopy. Four to ten zircon spots, with a preference on zircon growth rims rather than cores, were used to calculate a date per sample. The SHRIMP beam spot size was approximately 22 µm. The Brown stock samples all yielded ^{204}Pb corrected $^{206}Pb/^{238}U$ weighted mean dates between 38.60 ± 0.22 Ma and 37.42 ± 0.17 Ma, which are interpreted as crystallization ages. The Gold Dome dike yielded a ^{204}Pb corrected $^{206}Pb/^{238}U$ weighted mean date of 37.60 ± 0.37 Ma suggesting the Gold Dome and other granodiorite feldspar porphyry dikes were emplaced during intrusion of the Brown stock, which is consistent with the dikes emanating from the Brown stock based on field mapping (Emmons and Eng, 1995). The Gold Dome dike is crosscut locally by polymetallic veins (Figure 7Figure 7) and is pervasively altered and enriched in elements associated with Carlin mineralization (Au, As, Sb, Tl, Ag).

However, previously reported overlapping $^{40}Ar/^{39}Ar$ isochron ages for Cove mineralization and the Bay dike (~39.1 – 39.2 Ma) are older than the U/Pb zircon mean ages. Given the high mean square weighted deviation (all > 1) of all reported samples, there is likely analytical variation not considered in the uncertainties. In either case, the relative timing of events remains the same.

Previously Published Geochronology of the McCoy-Cove Mining District							
Sample name	**Location**	**Rock Type**	**Mineral**	**Method**	**Age plus uncertainty (Ma)**	**Comments**	**Reference**
USGS(M)-M273	McCoy Pluton	granodiorite	biotite	K-Ar	157 ± 3	corrected age from originally published 151 ± 3 Ma	Silberman and McKee (1971)
M151A	North Fish Creek Porphyry	Quartz monzonite	sericite	K-Ar	89.5 ± 2.7	hydrothermally altered (sericitic) iron-stained quartz monzonite porphyry	Miller and Silberman (1977)
McCoy-1	McCoy Deposit	Quartz monzonite	biotite	K-Ar	38.0 ± 1.2	"fresh" intrusive phase 5	Brooks (1994)
Ad-5080	McCoy Deposit	vein adularia	Adularia	K-Ar	39.1 ± 1.5	McCoy gold deposit	Brooks (1994); Emmons and Eng (1995)
McCoy 4840-III	McCoy Deposit	vein adularia	Adularia	K-Ar	38.7 ± 1.1	McCoy gold deposit	Emmons and Eng (1995)
CV-1 4925B	Cove	Bio-fsp porphyry	Biotite	K-Ar	40.3 ± 1.2	Bay dike; hydrothermally altered displaying biotite replacement by calcite+illite	Brooks (1994); Emmons and Eng (1995)
CV-5 4895B	Cove	Felsic porphyry	Biotite	K-Ar	39.4 ± 1.2	Cay dike; displays weak alteration, biotite fresh	Brooks (1994); Emmons and Eng (1995)
CV-3 4865A	Cove	Biotite granodiorite	Biotite	K-Ar	40.0 ± 1.2	Weak alteration, biotite rimmed by calcite	Brooks (1994); Emmons and Eng (1995)
GMC-1 460-462'	McCoy Deposit	Biotite qtz-monzonite	Sericite	K-Ar	40.0 ± 1.5	Brown stock	Brooks (1994); Emmons and Eng (1995)
GMC-3 257 - 263'	McCoy Deposit	Quartz monzonite	Sericite	K-Ar	40.9 ± 1.6	Brown stock	Brooks (1994); Emmons and Eng (1995)
GMC-1 729.5 - 731'	McCoy Deposit	Biotite qtz-monzonite	Biotite	K-Ar	41.6 ± 1.6	Brown stock	Brooks (1994); Emmons and Eng (1995)
GMC-4 507 - 514'	McCoy Deposit	Altered quartz-monzonite	Sericite	K-Ar	42.9 ± 1.9	Brown stock	Brooks (1994); Emmons and Eng (1995)
MCW-3	McCoy Deposit	"mafic dike"	Biotite	K-Ar	48.6 ± 2.0	Collected north of McCoy deposit	Brooks (1994); Emmons and Eng (1995)
Td-W1	McCoy Deposit	"dike"	Hornblende	K-Ar	64.5 ± 3.1	Dike near NW Brown zone	Brooks (1994); Emmons and Eng (1995)
143581	McCoy Deposit	Feldspar porphyry	Hornblende	K-Ar	37.0 ± 2.2	McCoy decline	Emmons and Eng (1995)
PP-3-89	Davenport	Feldspar porphyry	Biotite	K-Ar	39.9 ± 1.6	sill within Smelser Pass limestone under pediment cover at Davenport	Emmons and Eng (1995)
CVC-1-158-159	Cove	granodiorite	Biotite	K-Ar	39.5 ± 1.5	Bay dike	Brooks (1994); Emmons and Eng (1995)
CV-4865B	Cove	granodiorite	biotite	K-Ar	38.8 ± 1.1	Southeast intrusion at Cove	Emmons and Eng (1995)
WAF-16	Pinnacle Mountain	rhyolite	biotite	K-Ar	34.1 ± 0.9		Emmons and Eng (1995)
WAF-18	Pinnacle Mountain	rhyolite	biotite	K-Ar	32.9 ± 0.9		Emmons and Eng (1995)
WMC-2-88-530-535	McCoy Pluton	granodiorite	Whole rock	K-Ar	140 ± 6	Drill cuttings; McCoy pluton	Emmons and Eng (1995)
WMC-7-55-235-240	McCoy Pluton	granodiorite	Whole rock	K-Ar	139 ± 7	Drill cuttings; McCoy pluton	Emmons and Eng (1995)
L#2100	McCoy Deposit	vein adularia	adularia	^{40}Ar-^{39}Ar	38.26 ± 0.24	vein adularia associated with quartz-pyrite-gold mineralization	Groff et al. (1997)
4145E -19	Cove	granodiorite	illite	^{40}Ar-^{39}Ar	39.37 ± 0.23	altered Bay dike; age interpreted to represent timing of replacement of biotite by hypogene sericite/illite	Johnston et al. (2008)
AR44955E-2	Cove	granodiorite	biotite	^{40}Ar-^{39}Ar	39.01 ± 0.22	Fresh exposure of the West intrusion slightly propylitized though biotite contains no secondary sericite/illite, quartz, or calcite; interpreted to represent timing of deposition of igneous biotite	Johnston et al. (2008)
05-DJ-8	Cove	tuff	sanidine	^{40}Ar-^{39}Ar	34.45 ± 0.06	Tuff of Cove Mine	John et al. (2008)
H10-53	Pinnacle Mountain	rhyolite	sanidine	^{40}Ar-^{39}Ar	34.24 ± 0.07		Cousens et al. (2019)

Table 3. Previously published geochronology of the Cove-McCoy Mining District. Ages from Brooks (1994) include ages originally acquired or published by Gold Fields Mining Co., Echo Bay Minerals, and from Kuyper et al., 1991.

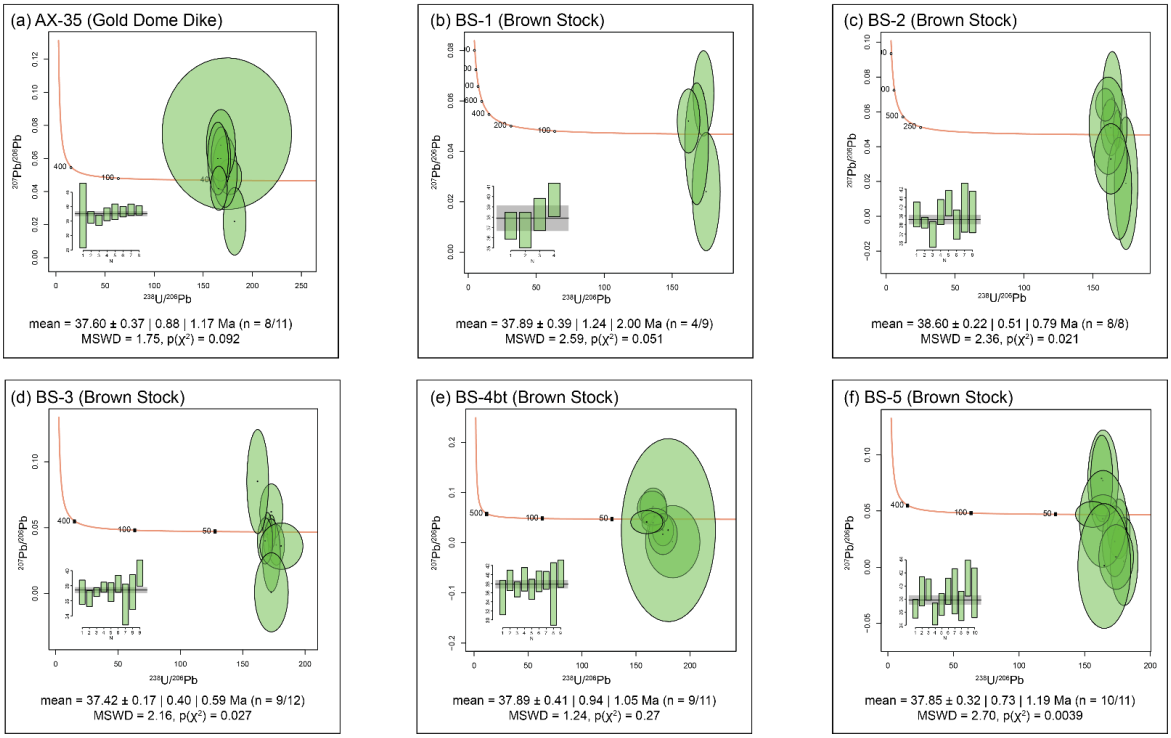

Figure 6. Tera-Wasserburg diagrams for the Gold Dome dike and Brown stock samples analyzed at the USGS-Stanford SHRIMP. Ages are weighted mean ^{204}Pb-corrected ^{206}Pb/^{238}U ages. Only showing concordant results. Values are the weighted mean age with standard error, confidence interval for the weighted mean, lower and upper half-widths of the confidence interval, number of grains used per sample, mean square of the weighted deviates, and the p-value of a Chi-square test using n as degrees of freedom. Calculated with R package IsoplotR (Vermeesch, 2018). See Appendix C1 for complete data.

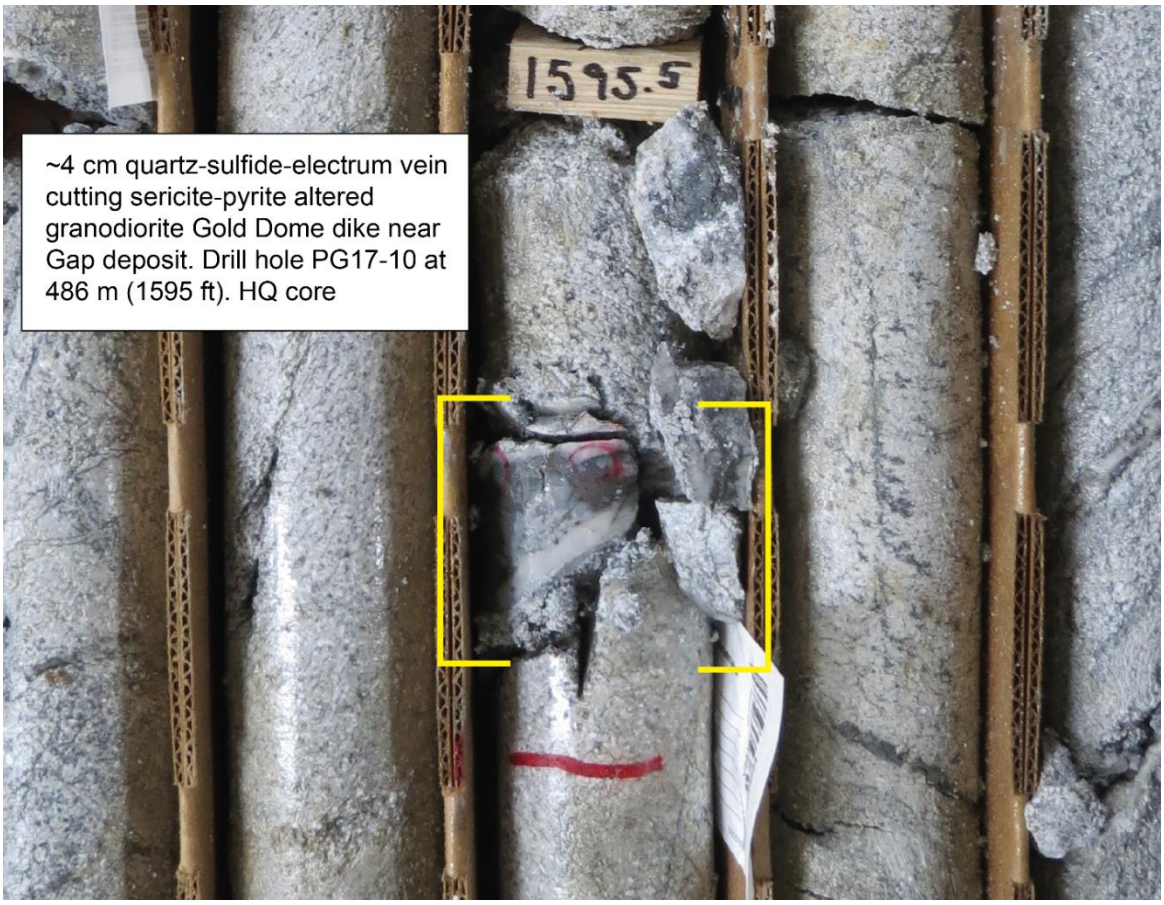

Figure 7. Polymetallic vein cutting the Gold Dome dike in Premier Gold Mines exploration drill hole PG17-10 near the Gap deposit.

HYDROTHERMAL MINERALIZATION AND ALTERATION

McCoy Skarn

Mineralization at McCoy is hosted within the Cane Spring Formation and Smelser Pass and Panther Canyon members of the Augusta Mountain Formation. It is divided into two stages roughly coeval with phases of skarn metasomatism associated with the progressive emplacement of the Brown stock (Brooks et al., 1991). Stage 1 mineralization occurs with early garnet-pyroxene skarn as disseminated pyrite and chalcopyrite (py:cpy ~15:1). Accessory sulfides include sphalerite, pyrrhotite, and galena. Stage 2 mineralization is associated with retrograde skarn alteration and later quartz-pyrite ± adularia. Stage 2 mineralization is best developed where these later alteration assemblages have partially or completely replaced prograde skarn. Stage 2 mineralization is spatially associated with dikes and sills and occurs as both veins and disseminated

pyrite and chalcopyrite (py:cpy ~20:1). Bornite is also commonly observed with chalcopyrite when stage 2 mineralization is hosted in the Panther Canyon Member of the Augusta Mountain Formation. Stage 2 accessory sulfides include pyrrhotite, sphalerite, galena, arsenopyrite, hedleyite (Bi_7Te_3), native Bi, and hessite (Ag_2Te). Total sulfide content during stage 2 is lower than in stage 1. The late quartz-pyrite±adularia mineralization associated with stage 2 is fracture-controlled and commonly occurs as veins in the clastic rocks of the Panther Canyon Member and more pervasive replacement bodies in limestone in the Smelser Pass Member. Quartz-pyrite ± adularia mineralization cross cuts both prograde and retrograde skarn alteration. It is the latest phase of hypogene mineralization in the deposit and constituted most of the ore that was mined at McCoy. Geochemically, the stage 2 mineralization has significantly higher concentrations of Pb, Zn, and higher Au/Cu ratios than stage 1 mineralization. Supergene processes replaced chalcopyrite with copper oxides including covellite, digenite, chalcocite, and cuprite.

Mineralization and Alteration

2201 Zone

The 2201 Zone below the Cove pit is hosted within conglomerates and dolomitic sandstones of the Dixie Valley Formation, the Koipato Formation, and the Havallah Sequence. The mineralization occurs as veins and disseminated sulfides characterized by predominantly pyrite-sphalerite-galena assemblages with minor chalcopyrite, arsenopyrite, pyrrhotite, and electrum (Figure 8). The polymetallic mineralization in the 2201 zone is enveloped by a broad zone of illite/sericite alteration and distal chlorite alteration of the conglomerate matrix and talc alteration of the dolomitic sandstones. Zones of (NH_4-)illite are confined to local occurrences of electrum-bearing quartz veins within the broader non-ammonium illite-sericite and illite-chlorite alteration zones (Figure 10b). The extent of illite-sericite alteration surrounding mineralization is unknown. Minor silicification is common, especially in the conglomerate.

The most common gangue phases in veins are carbonates including calcite, dolomite, and siderite. Quartz and quartz-carbonate veins are less common but have higher gold concentrations. Carbonate veins are generally 0.1 – 2 cm thick, discontinuous, and predominate at elevations depths less than 945 meters. Quartz and quartz-carbonate veins are generally 2 – 7 cm wide, have straight vein edges, and predominate at depths

greater than 945 meters. A paragenesis of the 2201 zone based on cross-cutting relationships observed in 12 drill holes is early quartz and quartz-calcite-sulfide veins cut by later quartz-siderite-sulfide veins and latest calcite-pyrite-sphalerite-galena veins and veinlets. Late barren carbonate veins cut all other phase where observed together (Figure 8a).

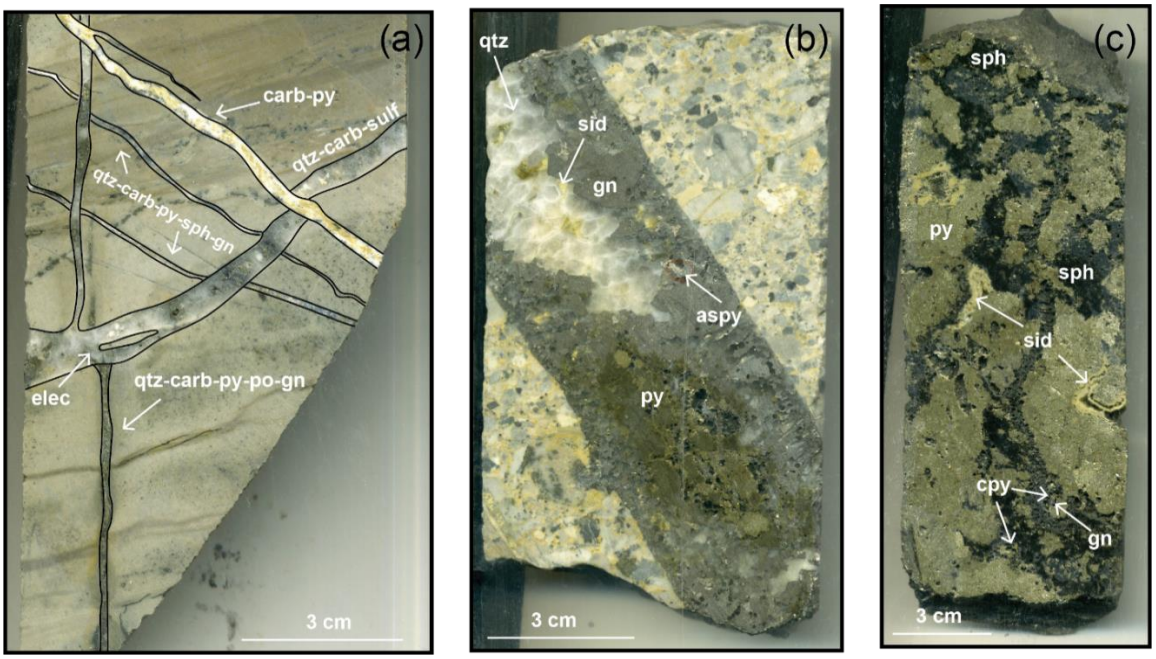

Figure 8 (a) Cross-cutting relationship of polymetallic veins from sample PG1415-2486.5 ft (11.796 g/t Au, 25.1 g/t Ag) displaying early qtz-carb-py-sph-gn veins cut by qtz-carb-py-po-gn veins which are then cut by electrum-bearing qtz-carb-sulf veins hosted by dolomitic sandstone of Dixie Valley Formation. Late carbonate-pyrite veins cut all other assemblages. (b) Sample PG1410-2654.5 in Dixie Valley Formation conglomerate displaying a polymetallic quartz vein with typical gold-bearing assemblage of 2201 zone mineralization (3.82 g/t Au, 5.5 g/t Ag). (c) Sample AX46-2203.3 ft displaying an example of manto-style massive sulfide mineralization encountered at the contact between the Dixie Valley Formation and overlying limestone of the Favret Formation (0.647 g/t Au, 85.6 g/t Ag). Abbreviations: py = pyrite, carb = carbonate, qtz = quartz, sph = sphalerite, gn = galena, elec = electrum, po = pyrrhotite, aspy = arsenopyrite, sid = siderite, sulf = sulfide

The gold in the 2201 zone is present as electrum with approximately 15 wt % Ag and occurs on the margins of veins associated with coarse quartz crystals or is hosted as inclusions in sulfides such as chalcopyrite or arsenopyrite (Figure 9). Galena can contain 3 - 10 wt % Ag based on EDS spot analyses. In cross- and long-section across the zone (Figure 10c, Figure 11c), visible gold occurrences are enveloped by a pyrrhotite halo found within a larger chalcopyrite zone. Zoning outwards, a larger arsenopyrite halo encompasses the chalcopyrite zone. A large galena-sphalerite zone forms the outermost known halo, the

limits of which have not been constrained by drilling. The galena-sphalerite halo roughly matches zones of illite and illite-sericite zoning outwards to illite-chlorite (Figure 10c).

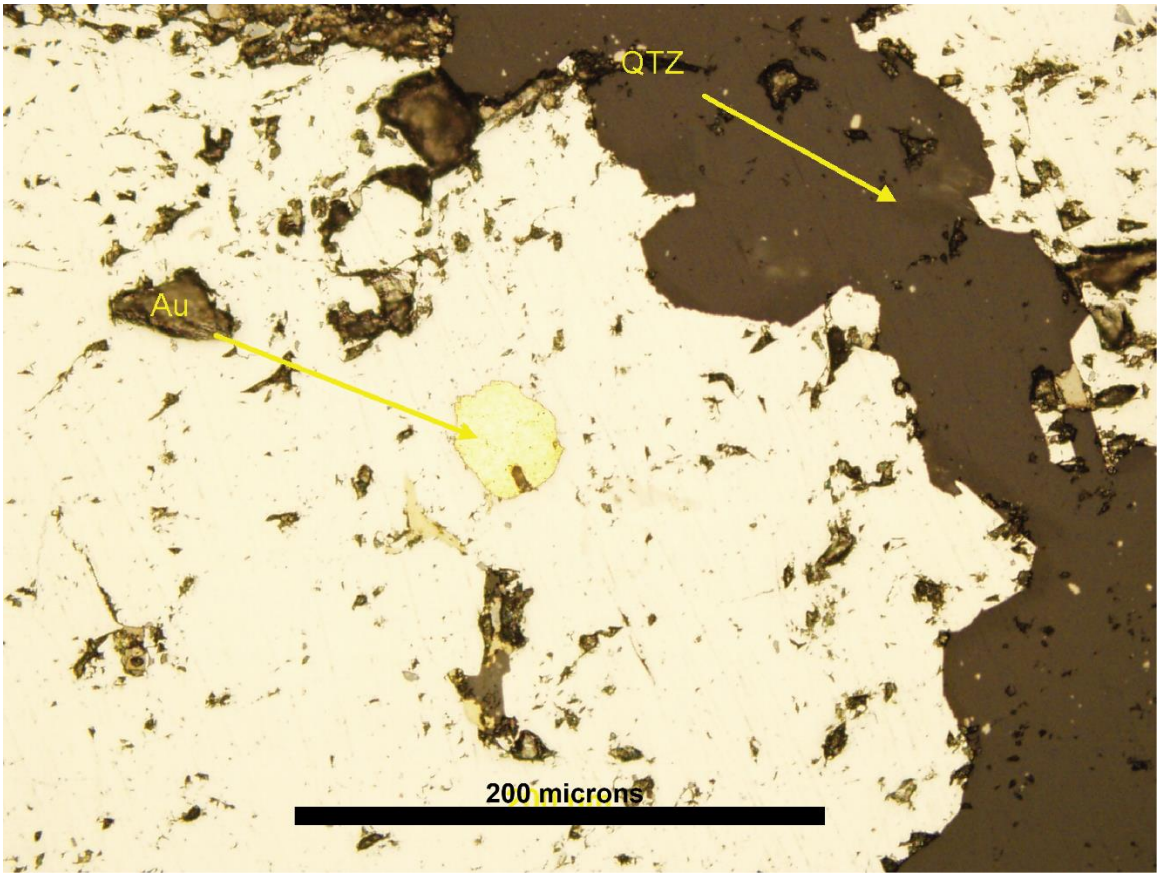

Figure 9. Photomicrograph of PG1410-2654.5 (3.82 g/t Au, 5.5 g/t Ag) in reflected light showing an electrum grain within a chalcopyrite grain hosted in a quartz vein. Scale bar is 200 microns long.

An oriented core hole (PG14-23) provided structural data for the polymetallic vein mineralization. There were no trends for veins grouped by gangue, assay values, mineralogy, or thickness, but when grouped by depth the data show that veins shallower than 530 m generally strike NE-SW with varying dips and veins deeper than 580 m generally strike NW-SE and dip steeply in both directions. In cross- and long-sections, gold contours suggest the gold-bearing veins dip gently to the southwest (Figure 10d, Figure 11d).

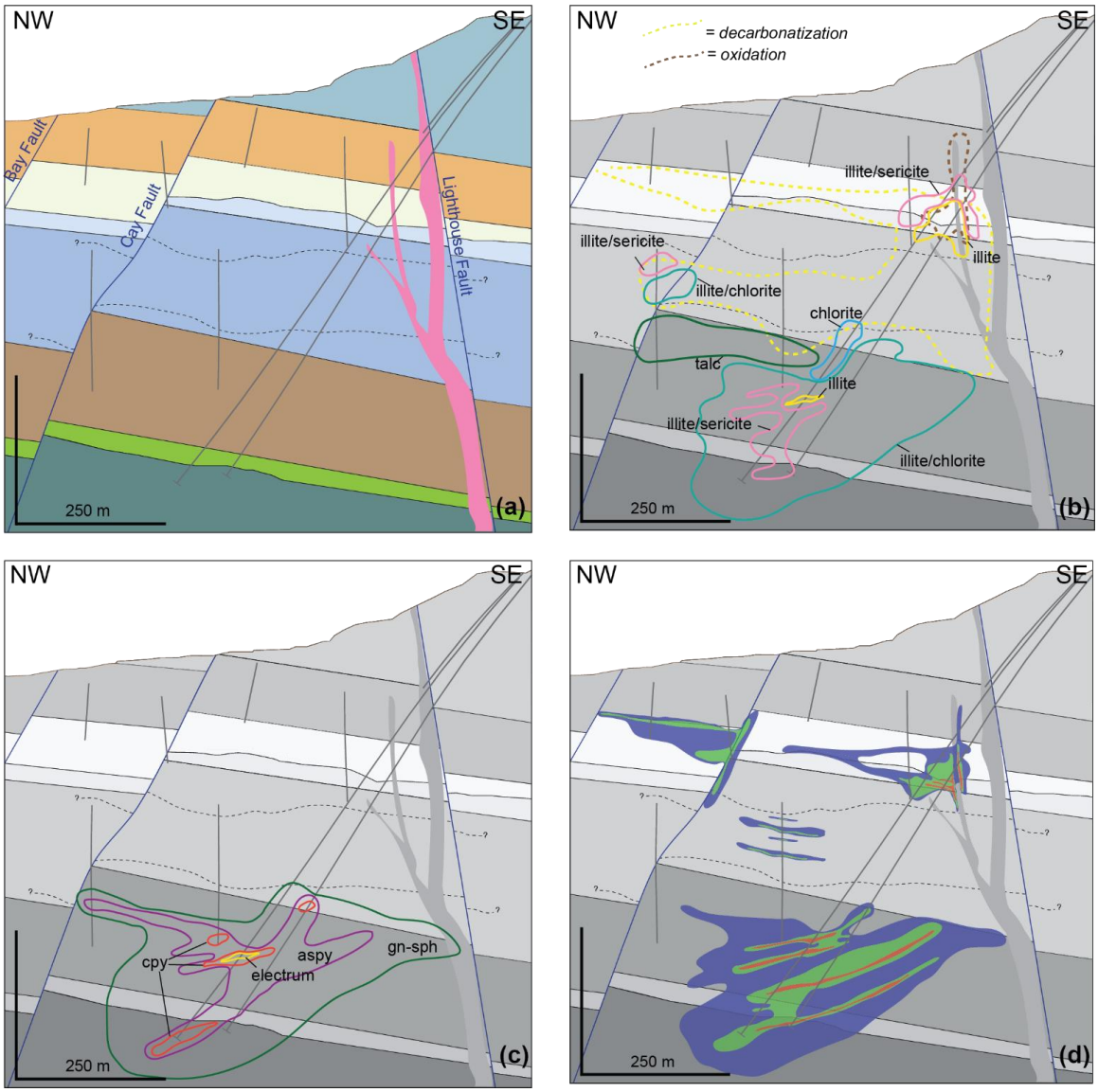

Figure 10. (a) Geologic long section looking NE across 2201 zone and CSD zone displayed at 45 m thick slice. Informal middle Favret unit displayed by dotted lines. (b) Alteration (dashed lines) and clay mineralogy (solid lines) of the 2201 zone and CSD zone. (c) ore mineralogy zonation of the 2201 zone; gn = galena, sph = sphalerite, aspy = arsenopyrite, cpy = chalcopyrite. (d) Gold contours in the 2201 zone and CSD zone. Blue shell = > 0.1 ppm Au, green shell = > 1 ppm Au, red shell = > 5 ppm Au. Formation colors match those in Fig. 2

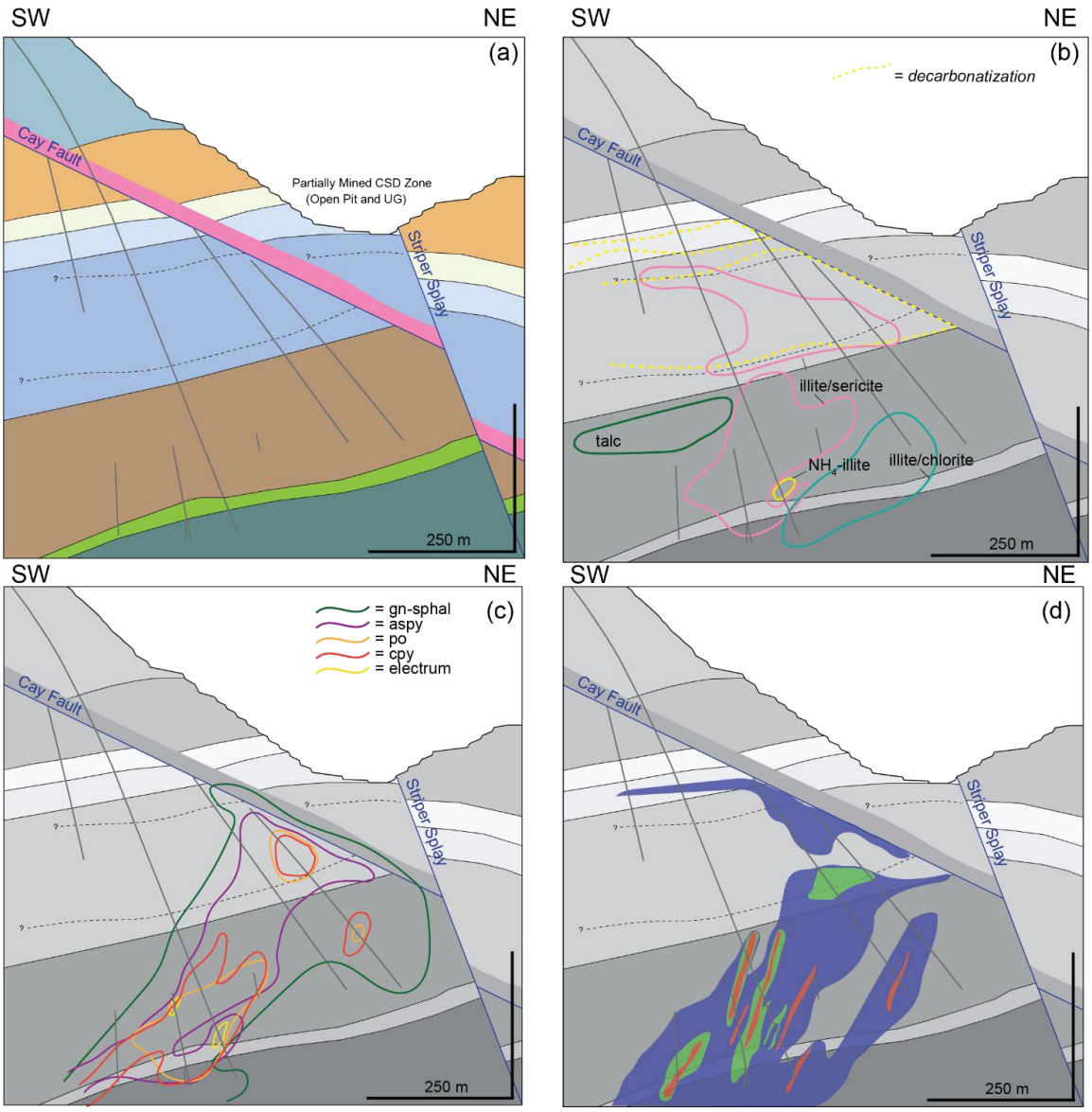

Figure 11. (a) Geologic cross section looking NW across 2201 zone and CSD zone displayed at 45 m thick slice. Informal middle Favret unit displayed by dotted lines. (b) Alteration (dashed lines) and clay mineralogy (solid lines) of the 2201 zone and CSD zone. (c) ore mineralogy zonation of the 2201 zone; gn = galena, sph = sphalerite, aspy = arsenopyrite, cpy = chalcopyrite, po = pyrrhotite. (d) Gold contours in the 2201 zone and CSD zone. Blue shell = > 0.1 ppm Au, green shell = > 1 ppm Au, red shell = > 5 ppm Au. Formation colors match those used in Fig. 2

Manto-style mineralization

In the area of the Cove pit, deep drilling locally intercepts manto-style replacement zones at the contact of the Favret and the Dixie Valley Formations (Figure 8c). These polymetallic manto contain up to 90% sulfides and consist predominantly of pyrite, sphalerite, and galena with lesser chalcopyrite and arsenopyrite

replacing both the basal Favret fossiliferous unit and interbeds of fossiliferous debris flows within the upper Dixie Valley Formation. Gold grades are typically < 5 g/t but silver grades can be several 100's g/t.

Overprinting Relationship

A sample collected from a zone in the informal basal unit of the Favret limestone appeared in hand sample to be Carlin-style alteration overprinting polymetallic mineralization. Nearby polymetallic mineralization within the same drill hole was not altered or mineralized with Carlin-style alteration, supporting the assumption that the early-stage sulfides were related to the same polymetallic event. Both Carlin-overprinted and non-overprinted polymetallic-style mineralization were analyzed using SEM-EDS and microprobe for pyrite textures and pyrite geochemistry. Large pyrite grains (> 30 microns) in Carlin-overprinted mineralization display distinct 10-15 micron As-, Au-, and Ag-bearing "rims" that are "ratty" or digitated on their edges but nonetheless mimic the shape of the earlier pyrite grain related to polymetallic mineralization (Figure 12). These rims are especially high in Ag and As (up to 1.8 wt% Ag and 7.5 wt % As) and only minor gold was detected with microprobe analysis (Figure 13). Comparing bulk drill core assay results of the non-overprinted massive sulfides in PG14-23 to samples that are overprinted with Carlin-style mineralization show Au, As, Ag, Sb, and Hg concentrations more than twice the unaltered massive sulfide samples. The interpretation is that the ratty, outermost pyrite rims represent an overprinting of the polymetallic mineralization by Carlin-style mineralization presumably deposited by sulfidation.

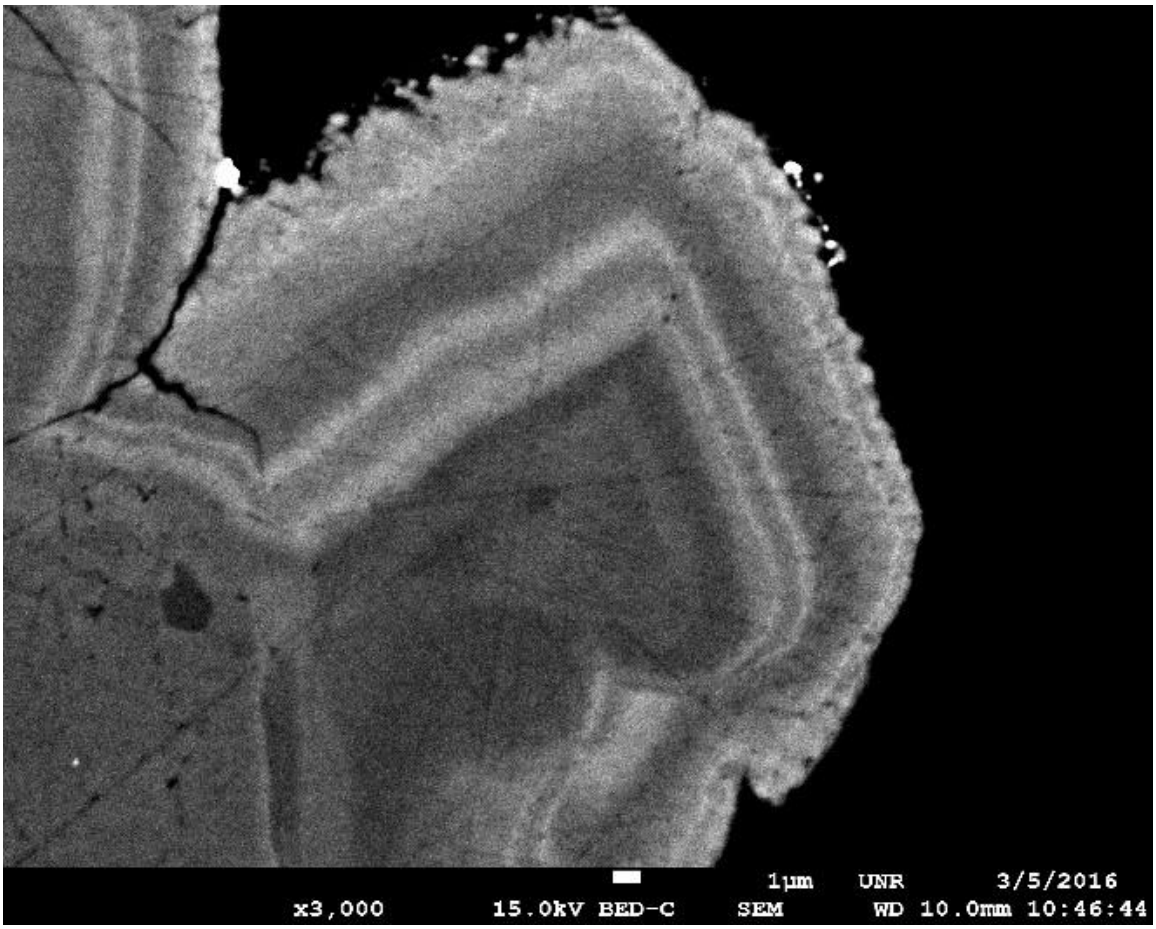

Figure 12. SEM-BSE image of pyrite grain associated with coarse polymetallic sulfide mineralization displaying ratty As- and Ag-bearing rims. Brighter colors represent higher density. Sample PG1423-2464 is from informal basal unit of the Favret. The outermost "ratty" rim is interpreted to be the Carlin-style overprint of the early-stage polymetallic event. Sample assayed 1.0 g/t Au and 524.1 g/t Ag.

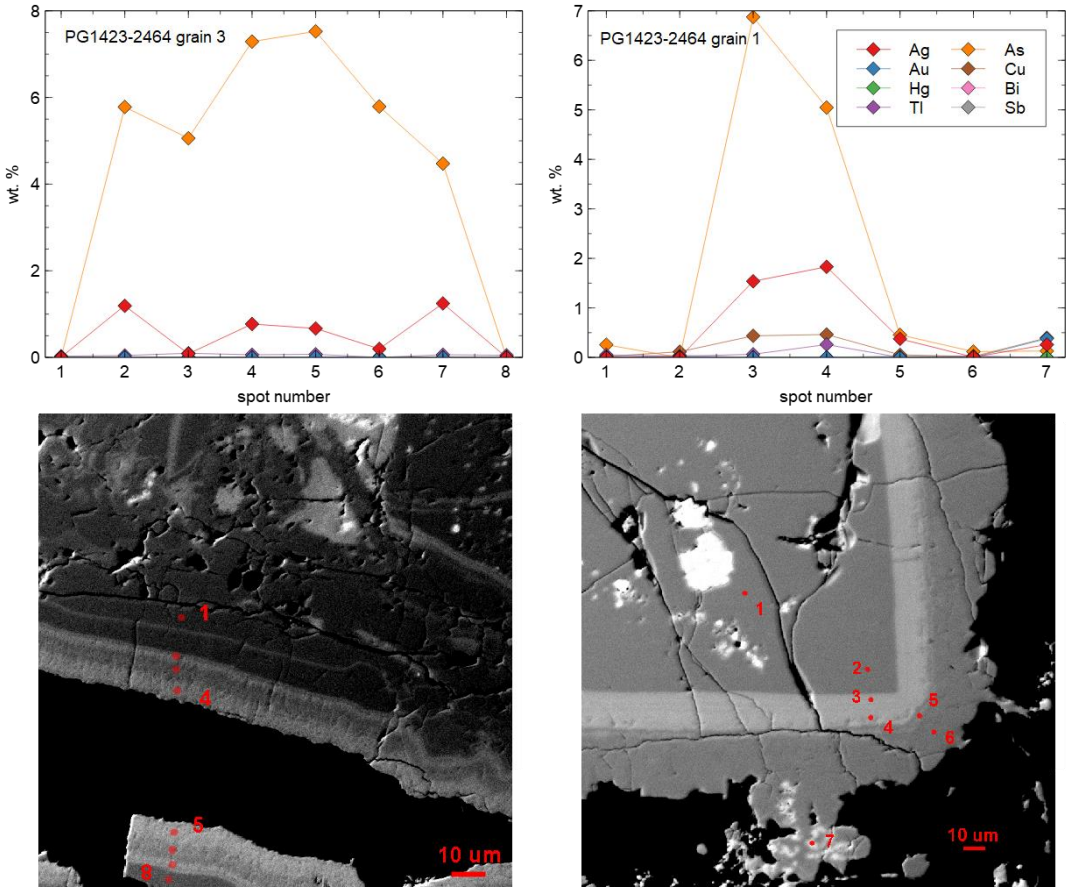

Figure 13. Microprobe results from sample PG1423-2464 shown in Fig. 16. Displays pyrite grain associated with coarse polymetallic sulfide mineralization displaying ratty As- and Ag-bearing rims. Sample PG1423-2464 is from informal basal unit of the Favret and is interpreted to be an example of the two styles of mineralization present at Cove occurring together with the Carlin-style event overprinting the polymetallic event. Note spot 5 on grain 3 (left) contained 0.01 wt.% Au. Sample assayed 1.0 g/t Au and 524.1 g/t Ag.

Cove South Deep (CSD) Zone

The CSD zone occurs above the 2201 zone in the dolostones of the Home Station Member and lower submember of the Panther Canyon (Figure 14). It was partly mined out by Echo Bay in an underground operation called the Omega Dike zone that was active in the final years of production (Johnston, 2003). The deposit occurs in a structural high between the oppositely dipping Lighthouse and Cay faults and gold mineralization is strongly controlled by contacts (lithology, dikes, sills) and faults. The CSD zone is silver-rich relative to other Carlin-style deposits in the district with an average Ag/Au ratio of ~12/1 and it has a

lower gold grade than the peripheral Helen and Gap zones. CSD has an inferred resource of ~100,000 oz at 7 g/t Au (Premier preliminary economic assessment, 2018).

Figure 14. (a) Cut core sample AX46-1268 of CSD mineralization hosted in the Panther Canyon dolomite submember. Sample is HQ core assaying 1.02 g/t Au and 1.5 g/t Ag.

Pyrites from the CSD zone are commonly 10 – 50 microns wide (Chryssoulis et al., 1997; Johnston, 2000) and often display complicated geochemical zonations indicating multiple episodes of precipitation (Figure 15). Based on microprobe results at the CSD zone, these internal zonations are controlled by elevated concentrations of As and Sb ± Cu, Tl, whereas As, Sb, Tl, Hg, and Bi tend to be elevated in the rims (Figure 18). Gold is associated with arsenian pyrite rims, arsenian pyrite, and rims of late stoichiometric arsenopyrite. In well-zoned pyrite grains, gold is locally detected by microprobe in the wider internal rims, though higher concentrations of gold are detected in the outermost rims (Figure 17, Figure 18). Up to 1 wt % silver was detected in Au-bearing arsenian rims but at Ag/Au ratios slightly less than that calculated

from bulk assay results indicating some of the silver is present in other phases. This is supported by observations of late argentiferous galena and sphalerite locally rimming arsenian pyrite rims.

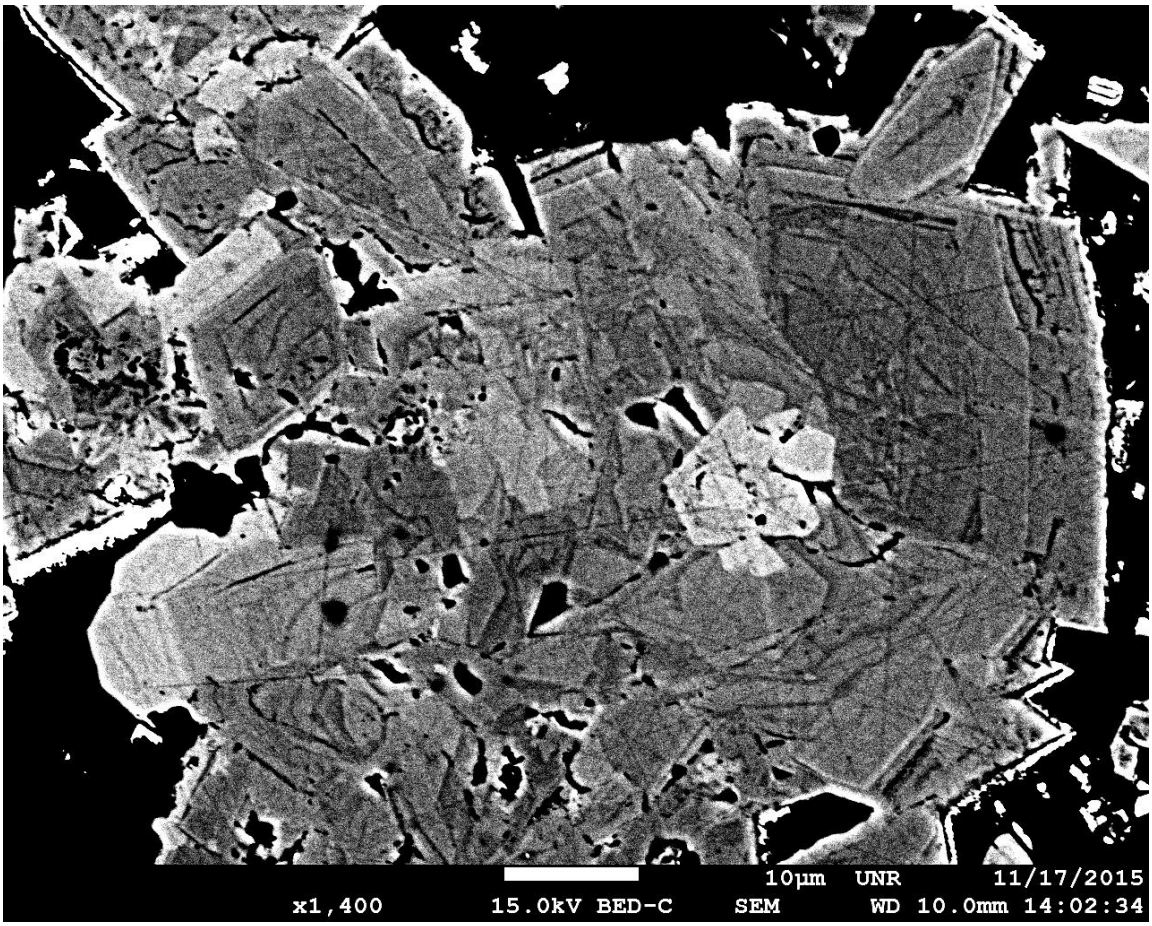

Figure 15. Back scatter electron image of a coarse-grained pyrite displaying multiple generations of growth from sample PG1404-1336.3 (7.92 g/t Au, 2.1 g/t Ag).

Alteration of the Home Station Member and Panther Canyon lower submember consists of decarbonatization (sanding), illitization/sericitization, and late Fe- and Mn-oxidation. Underground mapping of the CSD deposit completed by Echo Bay noted relatively late-stage realgar and lesser orpiment commonly occurring at the Panther Canyon dolomite submember contact with the underlying Home Station dolomite. Realgar and orpiment are absent in other Carlin-style deposits of the district.

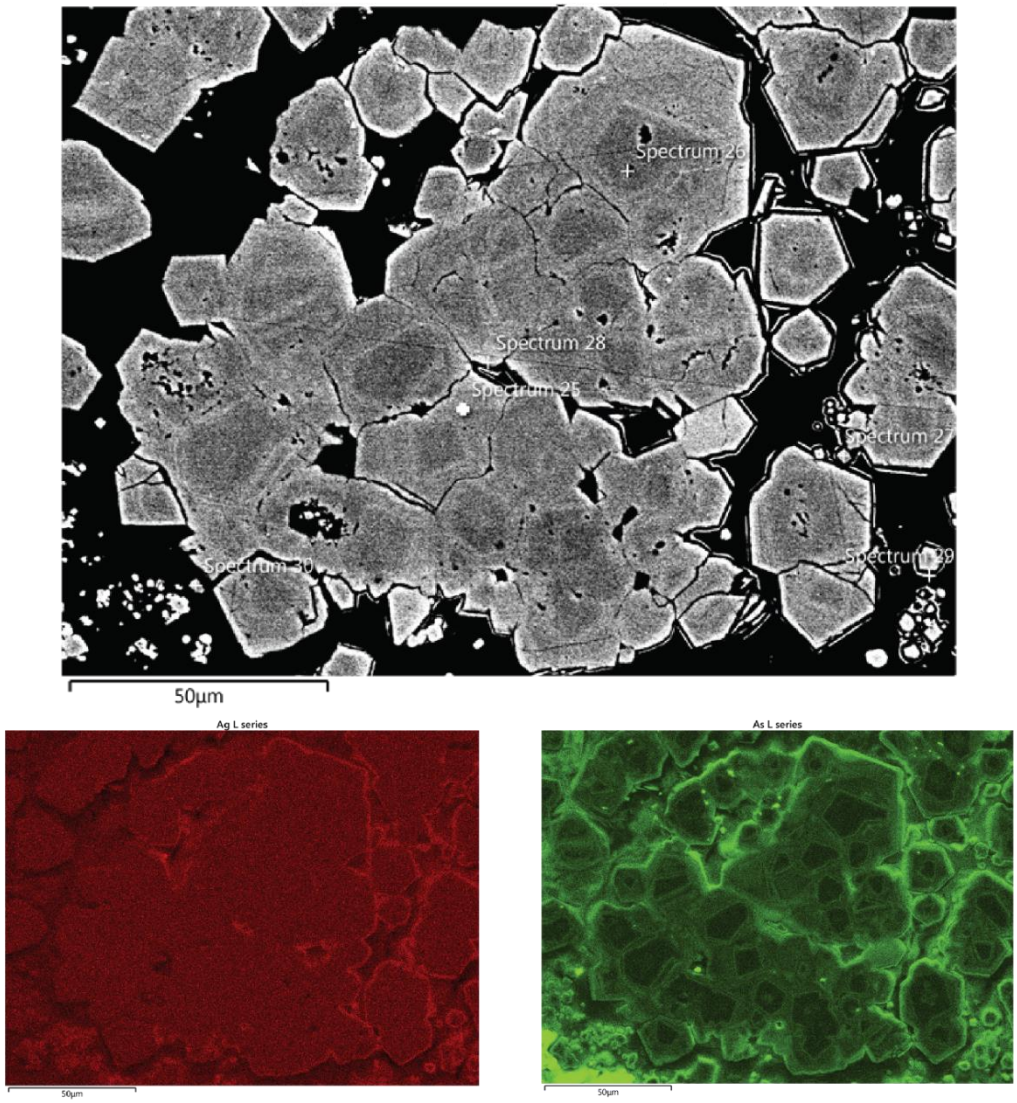

Figure 16. Back scatter electron image of a polyphase pyrite grain from sample PG01-2044 (0.230 g/t Au, 559.4 g/t Ag). Ag and As mineral maps produced by EDS are shown below in red and green, respectively.

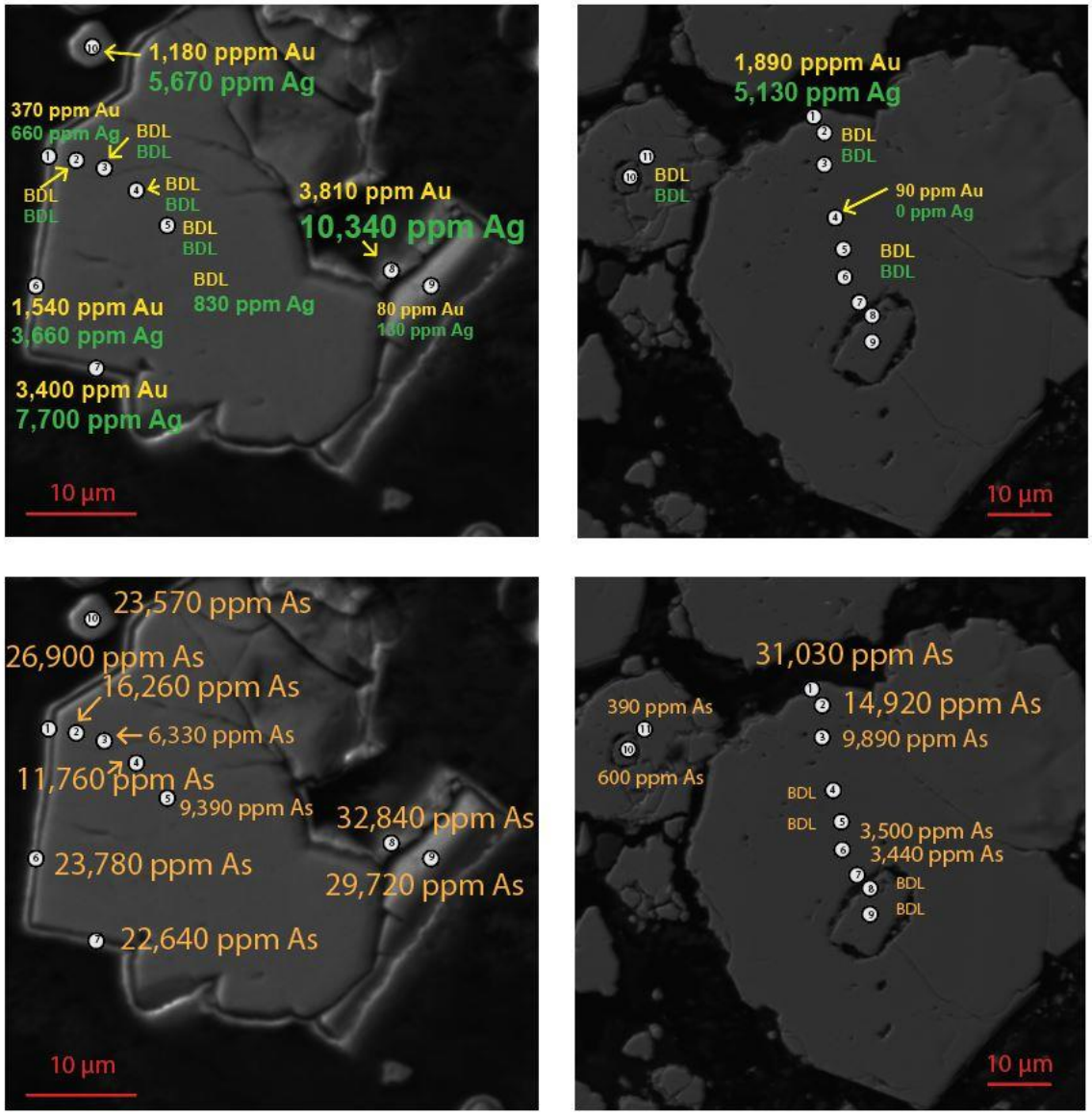

Figure 17. Back scatter electron images of two pyrite grains from sample PG01-2044 (0.230 g/t Au, 559.4 g/t Ag) showing typical CSD pyrite grain sizes and distribution of gold and silver. Note the most significant mineralizing event is the outer rims though minor gold (90 ppm) and significant arsenic concentrations exist in inner rims of the grains. Detection limits for Au = 100 ppm, As = 40 ppm, Ag = 30 ppm

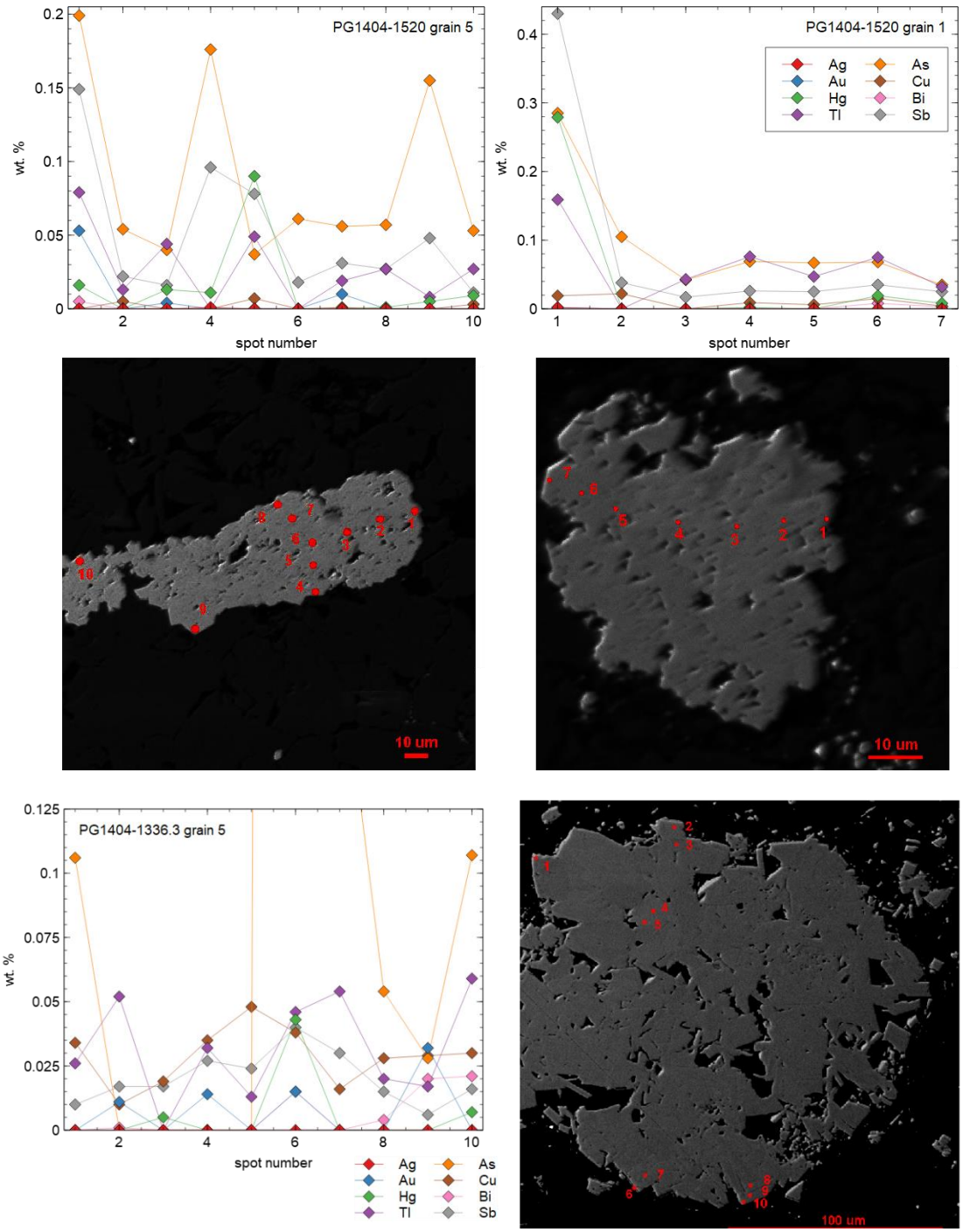

Figure 18. Microprobe results from spot analyses on CSD zone pyrite samples PG1404-1520 (8.33 g/t Au, 12.1 g/t Ag) and PG1404-1336.3 (7.92 g/t Au, 2.1 g/t Ag). Both samples are of mineralization hosted in the Panther Canyon dolomite submember. Scale units are microns.

Cove Pit

Though disseminated polymetallic mineralization occurred in oxide ore associated with clay alteration and Mn oxides in limestones of the Smelser Pass Member, most polymetallic mineralization existed as sulfide ore in the Panther Canyon Member as crustiform sulfides, veins, and open space-filling vugs. Oxide ore in the Smelser Pass Member was largely constrained to the hanging wall of the Lighthouse fault, whereas most sulfide ore occurred between the Bay and Cay faults. The form of the sulfide mineralization was governed by lithology with crustiform sulfides dominating in the coarse-grained conglomerates of the upper Panther Canyon submember and veins occurring in the dolostones of the lower Panther Canyon submember and the Home Station Member. Controls on mineralization included contacts between stratigraphic units, the margins of feldspar porphyry dikes and sills, and structural intersections where high-grade breccias were mined. The mineralization is associated with silicification and/or quartz-illite alteration. Gangue mineralogy is characterized by early quartz-bearing veins and late carbonate- (calcite, dolomite, rhodochrosite) veins (Johnston et al., 2008). Veins are commonly described as having multiple episodes of sulfide precipitation, brecciation, and orientations suggesting a dynamic environment of formation; vein thicknesses up to 25 cm occur in the deepest exposures of the open pit. Vein orientations are not well documented, but most veins mined in the open pit are noted to exist along the axis of the Cove anticline between the Bay and Cay faults (Johnston, 2001).

Johnston et al. (2008) described a vertical zonation to the mineralization and alteration in the Cove pit. The deepest alteration associated with the CSD zone was decarbonatization and quartz-illite-pyrite alteration proximal to dikes and faults. Alteration associated with most of the hypogene ore in the pit was highly variable but included silicification, quartz-illite-pyrite, and decarbonatization. Above the ore body the Smelser Pass limestone contained zones of manganese flooding and carbon enrichment. Jasperoids were the highest alteration type at Cove occurring at the late Eocene surface underneath the tuff of Cove Mine (Johnston, 2008).

Gap Zone

The Gap zone (Figure 2) is hosted by the Home Station Member of the Augusta Mountain Formation and the Favret Formation in the hanging wall of the Bay-110 fault zone and the footwall of the Gold Dome dike. It was discovered on trend of the Helen and CSD zones in 2016 by Premier. Mineralization is strongly controlled by lithology with the most prospective horizons being the contact between the Home Station and the Favret and where basalt and basaltic andesite sills cut the informal middle unit of the Favret. The southwestern extent of the mineralization is controlled by the Fire dike, which appears to have acted as an aquiclude. Polymetallic mineralization occurs predominantly in the dolostone of the Home Station member and Ag/Au ratios of the Carlin-style mineralization based on assays average around 2.5/1. Similar to the mineralization at the Helen zone, economic gold mineralization is present in two stacked zones – an upper, lower-grade but more dispersed zone in the dolomites and at the Home Station Favret contact, and a lower, higher-grade zone present in thinner lenses of middle Favret often subparallel to bedding and sill contacts (Figure 19). Gold grades are higher-grade than the CSD zone with an inferred resource of ~550,000 oz at 11 g/t Au.

Figure 19. Core photo of PG16-02 at the Gap deposit, which is hosted in the informal middle unit of the Favret Formation. This core is part of an intercept of 50.9 m of 7.08 g/t Au. HQ core, units are in feet.

In limited petrographic observations of the Gap zone, highest gold grades are associated with arsenian rims, arsenian pyrite and arsenopyrite (Figure 20). Local late arsenopyrite-stibnite-calcite veins are observed cutting decarbonatized intervals and possibly increase the gold grade as their occurrence is correlative with higher bulk assay gold values.

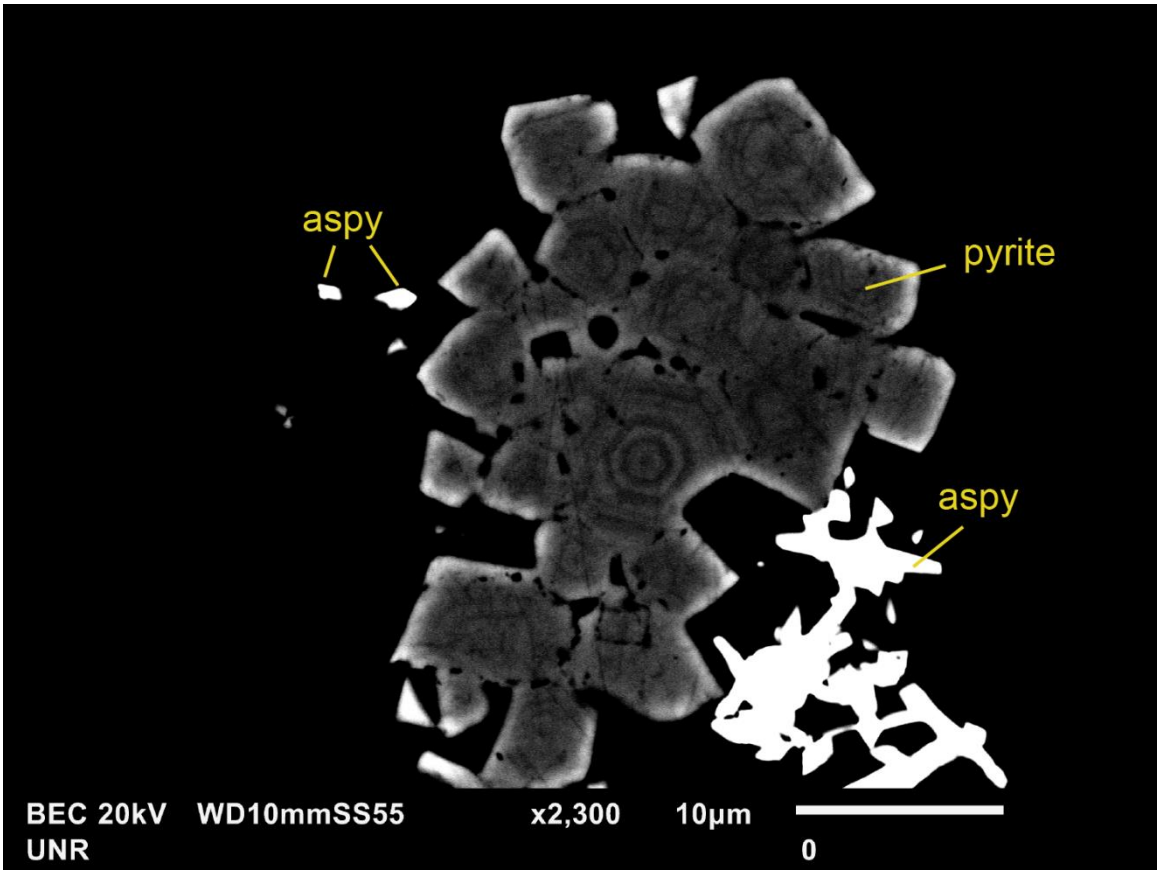

Figure 20. Back scatter electron image of a mineralized sample from the Gap zone. Sample PG1606-2232.5 (29.4 g/t Au, 10 g/t Ag). Apparent late arsenopyrite (+ stibnite) is commonly observed in hand sample and thin section.

Alteration in the Gap zone is characterized by decarbonatization, illitization/sericitization, and local silicification especially in the Favret Formation.

Helen Zone

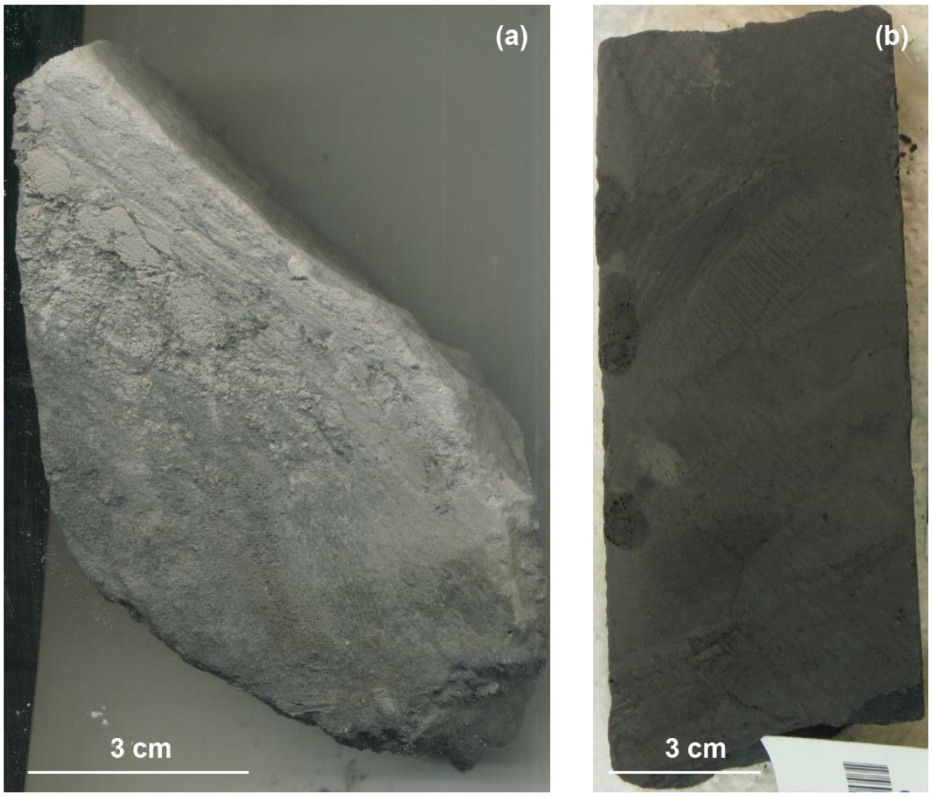

Figure 21. Drill core samples of Helen zone mineralization in dolomite of the Home Station Member (a) and interbedded silty limestones of the informal middle unit of the Favret Formation (b). Sample AX12-1222.6 (a) assayed 2.82 g/t Au and 0.25 g/t Ag and sample AX31-1924.7 (b) assayed 44.33 g/t Au and 12 g/t Ag.

The Helen zone occurs northwest of the Gap zone along the Cove anticline at depths of 385 m to 620 m. It is loosely divided into the upper Helen zone hosted by the dolostones of the Panther Canyon dolomite submember and the Home Station Member of the Augusta Mountain Formation and the higher-grade lower Helen zone hosted in the informal middle unit of the Favret Formation (Figure 21). The deposit occurs in the hanging wall of the Gold Dome fault and the footwall of the Hidden Valley fault, and mineralization is strongly controlled by contacts (lithology, dikes, sills) and north to northeast-striking faults with minor offset including the Clara fault. The Helen zone has an average Ag/Au ratio of ~0.5/1 and contains an inferred resource of ~500,000 oz at 11.5 g/t Au (Premier preliminary economic assessment, 2018).

In all observed samples of the Helen zone, the most frequently observed phase of sulfide was euhedral to subeuhedral grains of pyrite, generally 10 – 50 microns wide, which were observed in all three host rocks for the deposit. Often observable in hand sample, these grains do not display the outer arsenian rims

typically observed in the CSD zone nor does their abundance correlate with grade or degree of alteration. In mineralized samples, a second phase of pyrite is observed in the Helen zone consisting of fine-grained (<10 microns) patchy, anhedral "fuzzy" grains sometimes appearing alongside the first phase (Figure 22). When detected by SEM-EDS, the arsenic distribution within the fuzzy grains appear to be zoned with the only detectable occurrences of arsenic appearing in the outer reaches of the grains (Figure 22, Figure 23) or in < 1 micron grains existing outboard of these fuzzy grains. However, in the same sample, gold was detected by microprobe in both phases of pyrite albeit at higher concentrations on the rims of the more euhedral grains (Figure 24). Microprobe results from analyses of the fuzzy grains is not reported here due to poor total concentrations (<80%) as a result of fine grain size and beam drift (See Appendix D).

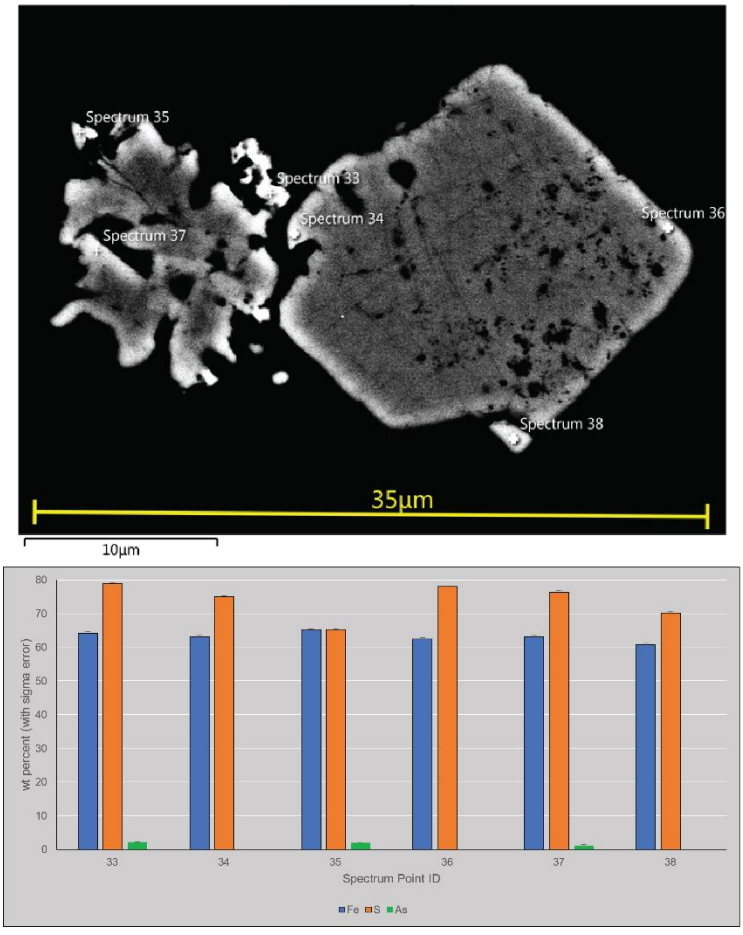

Figure 22. **Helen zone sample AX12-1704 of mineralized (13.69 g/t Au, 0.005 g/t Ag) informal middle unit of Favret formation. Sample appears to show juxtaposed ratty, arsenic-bearing pyrite (left) with euhedral, barren**

pyrite (right). Any brightness on edge of As-devoid grain is explained by edge effects. Wt. percent is estimate based on energy dispersive x-ray spectra acquired by JEOL JSM-6010LA tungsten-filament SEM.

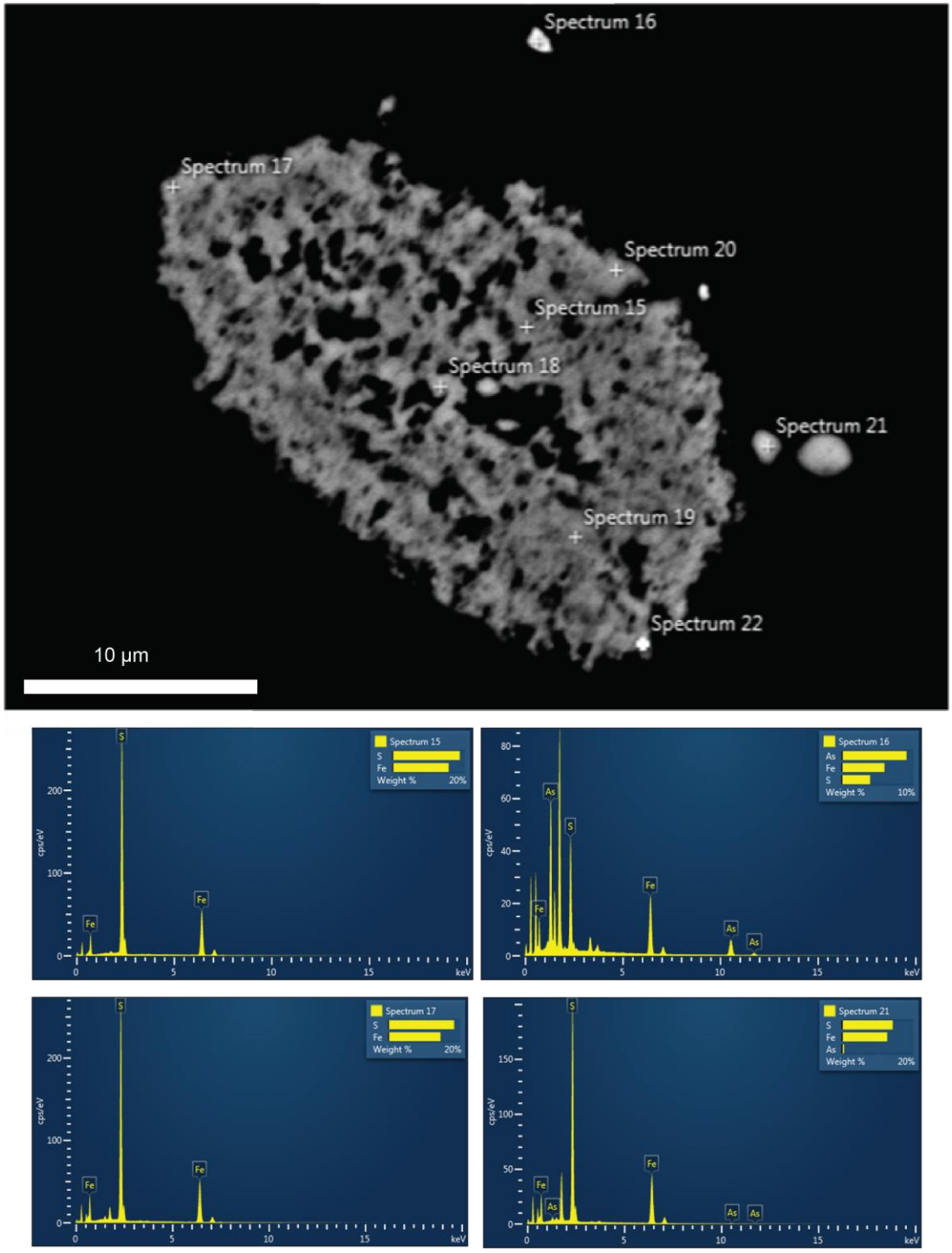

Figure 23. Helen zone sample AX31-1927.8 of mineralized (44.328 g/t Au, 12 g/t Ag) informal middle unit of Favret formation. Ratty pyrite grain containing displaying arsenian-bearing grains outboard of grain itself. Any

brightness on edge of As-devoid grain with is explained by edge effect. Spectrums 18, 19, 20, and 22 displayed similar results as 15 and 17.

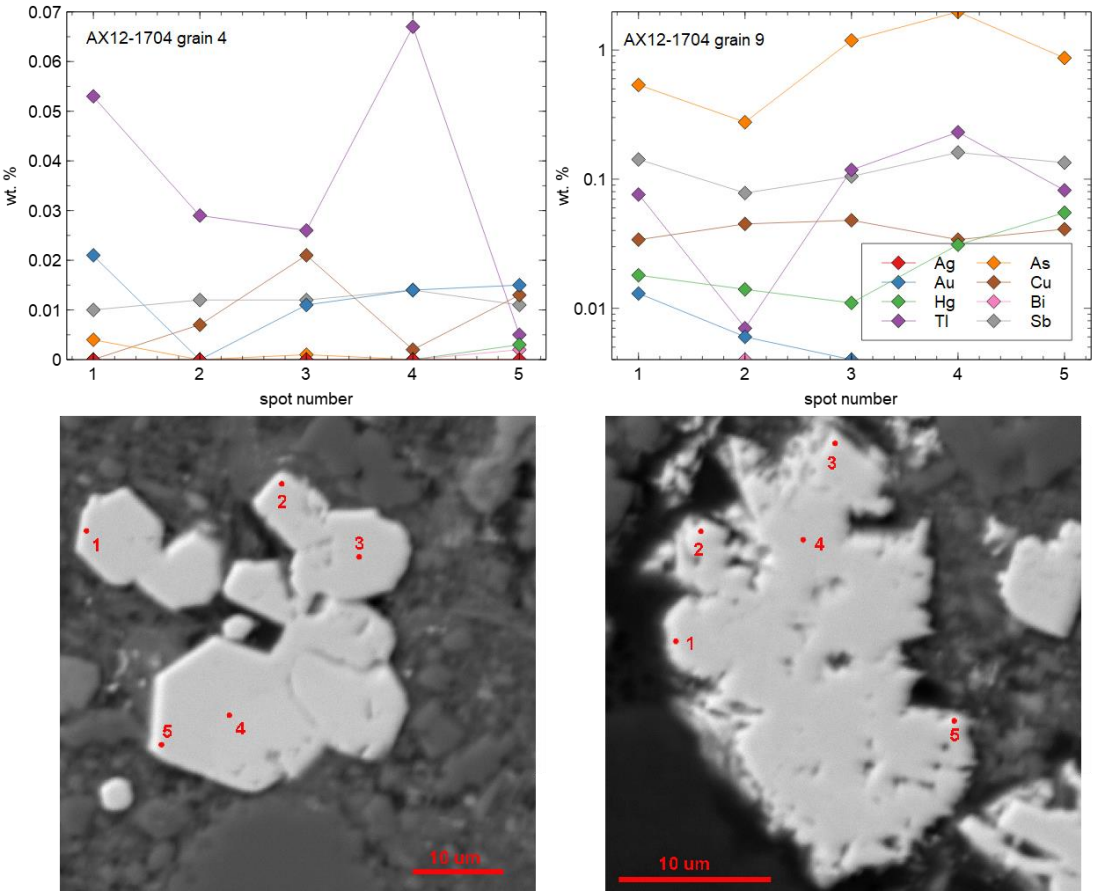

Figure 24. Microprobe results from sample AX12-1704 of mineralized (13.69 g/t Au, 0.005 g/t Ag) informal middle unit of Favret formation in the Helen zone. Gold was detected in both the rims and centers of both euhedral to subhedral grains displayed here, though higher concentrations of gold was consistently detected in the rims. Results from fuzzy pyrite grains did not produce high enough total concentrations of elements to report results. This poor data quality was due to both beam drift and the fine-grained nature of the sulfides analyzed.

Carlin-Style Mineralization Summary

Within the Cove deposit, from the CSD zone to the Helen zone, just northwest of the pit, multiple mineralogic and geochemical trends are observed. Pyrite grain sizes decrease from CSD to Helen zone as well as the complexity of grain precipitation observed in SEM.

Ag/Au ratios decrease across this transect in both bulk sample assay of Carlin-style mineralization and in microprobe analyses of arsenian rims. In samples > 1 g/t Au, in carbonate rocks, and with Ag, Pb, and Zn

values less than 100 ppm, Tl/Au ratios from the Gap deposit to Windy Point, a target located northwest of Helen along the Cove anticline, increase across the Helen zone whereas Sb/Au decrease across this same transect. In an analysis of all samples > 1 g/t Au from carbonate host rocks assayed by the same fusion and digestion methods, Ag/Au ratios increase with greater Pb, Cu, and Zn concentrations and decrease with higher As and Tl concentrations (Figure 26). When the data points are broken down by deposit, the Helen zone and Windy Point prospect display the lowest Ag/Au ratios and base metal concentrations.

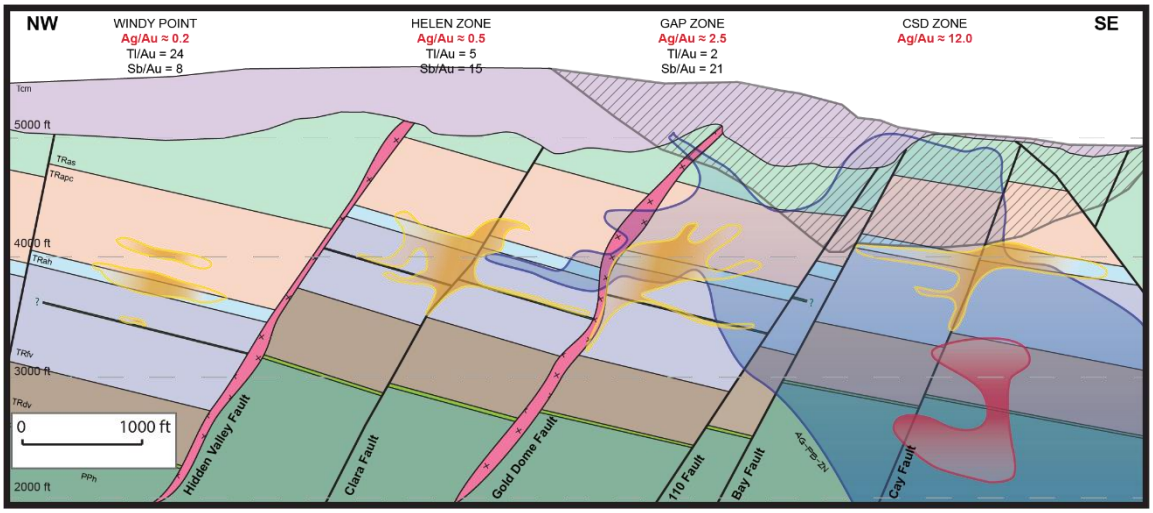

Figure 25. Generalized long section looking northeast showing metal zonation of Cu (> 100 ppm, red), Pb-Zn (> 100 ppm, blue), and As-Sb-Hg (yellow) along the Cove antiform and the trends in metal/gold ratios. Windy Point is a target NW of the Helen zone. Ag/Au decreases to the NW, Tl/Au increases to the NW, Sb/Au decreases to the NW. Not enough samples from the CSD zone were assayed with the same digestion as the Windy Point, Helen, and Gap so only Ag/Au ratios are shown.

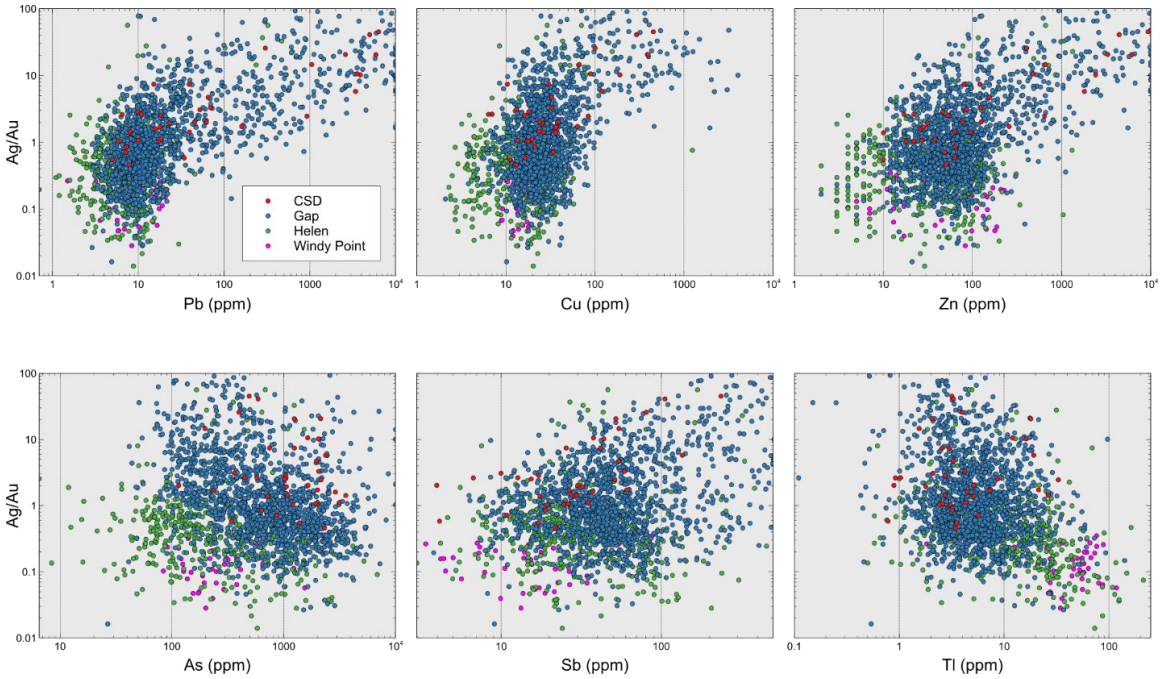

Figure 26. Log/Log Ag/Au vs. Pb, Cu, Zn, As, Sb, and Tl plots using Premier dataset and filtering to samples >= 1 g/t Au hosted in Favret Formation, Home Station Member, or Panther Canyon dolomite submember. Note opposite trends in Sb and Tl and strong correlation of higher Ag/Au ratios with higher Pb, Zn, and Cu concentrations reflecting Ag in different mineralogy.

DISCUSSION

Time Relationships and Source of Ore Fluids

The data presented above indicates the Cove-McCoy district was a dynamic environment in the Eocene marked by periods of diverse magmatism and mineralization. New U/Pb zircon dates of the Brown stock provide a more constrained age range of ~37.4 – 38.8 Ma though its reliability needs to be evaluated given its disagreement with a previously reported $^{40}Ar/^{39}Ar$ age for emplacement of the Bay dike. In either case, the same relative timing reported by previous workers (Brooks, 1994; Emmons and Eng, 1995; Johnston et al., 2008) holds. In evaluating just the U-Pb zircon dataset, the Gold Dome dike (Appendix C) produced a age of 37.6 Ma which matches field and mapping observations that it formed as a part of the polyphase emplacement of the Brown stock (37.4 – 38.8). Other NE-striking, NW-dipping granodiorite dikes are likely of similar ages – emplaced relatively late in the development of the Brown stock. Due to the Gold Dome dike's cross-cutting relationships with both polymetallic quartz veins and Carlin-style mineralization and alteration at Cove, its age may represent a maximum age for Cove mineralization younger than previously

reported by $^{40}Ar/^{39}Ar$ biotite (Johnston et al., 2008) if these data are supported by further work. These new results could provide a more constrained bracket of time available for mineralization in the Cove-McCoy district until the deposition of the 34.45 Ma Tuff of Cove Mine (John et al., 2008).

The highest temperature expression of the Cove-McCoy Eocene magmatic-hydrothermal system is the skarn at McCoy. The northeast-striking dikes, slightly younger than to contemporaneous with the emplacement of the Brown stock, extend from McCoy to Cove. Fluid inclusion analysis from polymetallic veins at Cove produced homogenization temperatures that range from 250º to 370ºC, with most between 275º and 325ºC, and salinities between 2 – 7 wt% NaCl eq (Johnston et al., 2008). δD and $\delta^{18}O$ values from illite at Cove consistent with magmatic water and minor contributions of meteoric water and $\delta^{34}S$ from polymetallic sulfides between 2.2 and 3.3 ‰ (Johnston et al., 2008). Cove ore fluids could thus have been sourced from the Brown stock and cooled laterally along connecting, high-angle structures towards Cove. However, as suggested by Johnston et al. (2008), fluids were more likely sourced from one or more deeper cupola zones.

Although workers in the district traditionally speculated the Brown stock was the source of the mineralization at Cove, the deposits at Cove are within 2-3 kilometers of at least three magnetic highs interpreted or confirmed to be granodioritic intrusions (Figure 27). The Brown stock is definitively Eocene in age, and at least the shallowest possible igneous bodies (sill) of an undrilled, deeper magnetic high under pediment cover at Davenport east of the Cove pit are also Eocene (Emmons and Eng, 1995). Another deep magnetic high possibly representing another Eocene granodioritic intrusion is buried under the tuff of Cove Mine to the NW of the Cove deposits. Any or all of these buried intrusions if confirmed to be Eocene could have contributed ore fluids to the Cove system in a complicated range of times and depths of emplacement and fluid exsolution histories. However, given the clear Ag/Au zoning away from the Cove deposit towards the northwest at Helen and Windy Point and lack of significant alteration between the Brown stock and Cove, the buried intrusion at Davenport to the east of Cove under pediment cover may be the predominant source of magmatic-hydrothermal fluids that formed the Cove deposit.

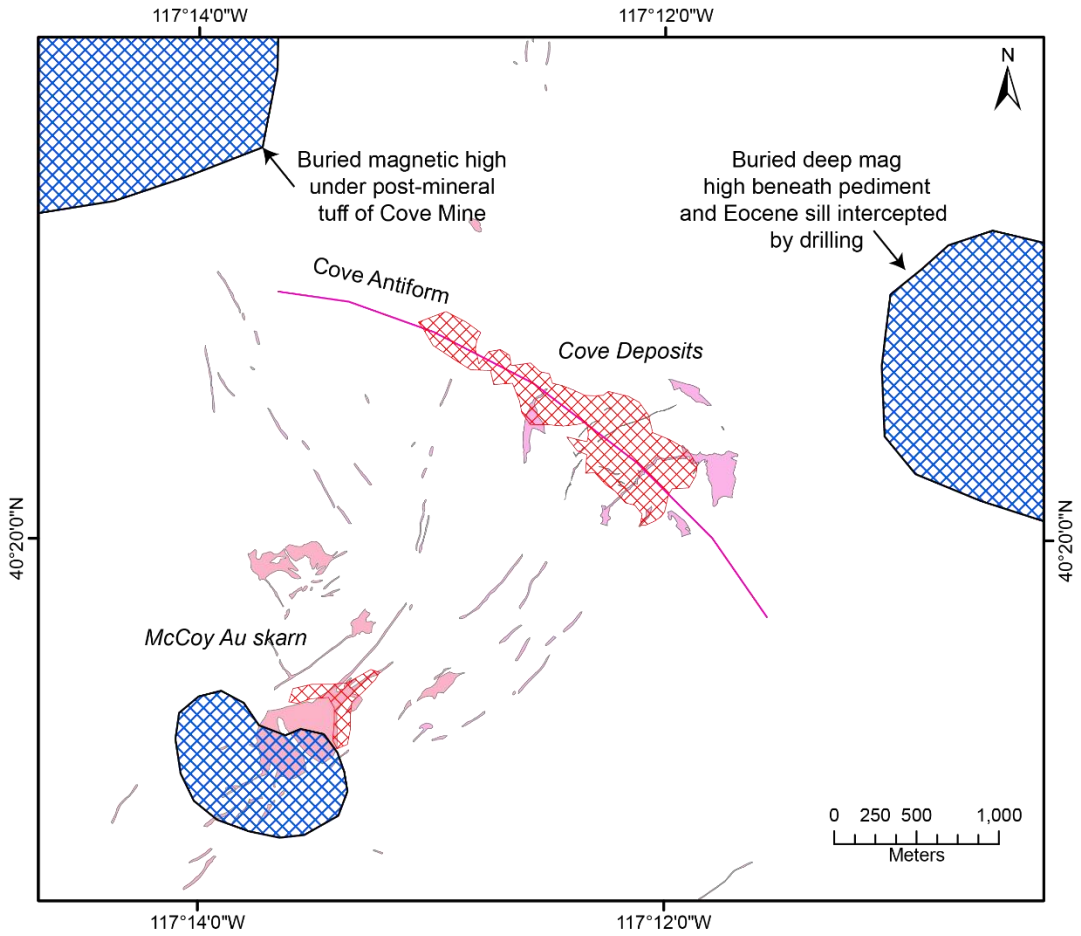

Figure 27. Location of nearby buried or exposed magnetic highs (anomalies that can be tracked to deepest resolutions) interpreted or known to be granodioritic intrusions (blue hatch) depicted with Eocene mineralization (red hatch) and Eocene intrusions (pink polygons). The Brown stock at McCoy and an igneous sill above the deeper magnetic high under pediment cover at Davenport are dated Eocene.

Fluid Evolution and Transitions to Carlin-style Mineralization

Including the proximal, high-temperature prograde and retrograde skarn mineralization at McCoy, most mineralization in the Cove-McCoy district can be explained by an evolving system and transition from metals traveling dominantly as chloride to hydrosulfide complexes. As Ag-Pb-Zn-Au-(Cu)-rich brines were exsolving off these granodioritic intrusions and deeper cupola zones in the Eocene at Cove-McCoy, they traveled vertically up high-angle structures forming veins by hydrofracturing above the brittle-ductile transition, disseminated polymetallic mineralization as a result of adiabatic cooling, and high-grade pods where rapid pH gradients existed due to abrupt change in wall rock (ie. conglomerate to carbonate). For example, the manto-style bodies of massive sulfide encountered above the 2201 zone in the basal Favret

likely formed as a result of rapid pH change as fluids rose through the quartz pebble conglomerates of the Dixie Valley Formation and into the carbonate debris flow breccias at the base of the Favret Formation.

Zonation in the higher temperature polymetallic mineralization can be explained by fluids saturated with chloride metal complexes cooling between ~350º to 250ºC. Observed zonations in mineralogy at the 2201 zone (Figure 10c, Figure 11c) show deeper chalcopyrite, arsenopyrite, pyrrhotite occurrences surrounded outboard by a more dispersed galena-sphalerite zone. Johnston et al. (2008) reported tennantite and tetrahedrite as part of the Cove mineralization paragenesis, though no sulfosalts were identified as part of this study in the deeper polymetallic zones. These relationships can be explained by decreasing temperatures resulting in increased sulfidation state (Einaudi et al., 2003; Figure 28).

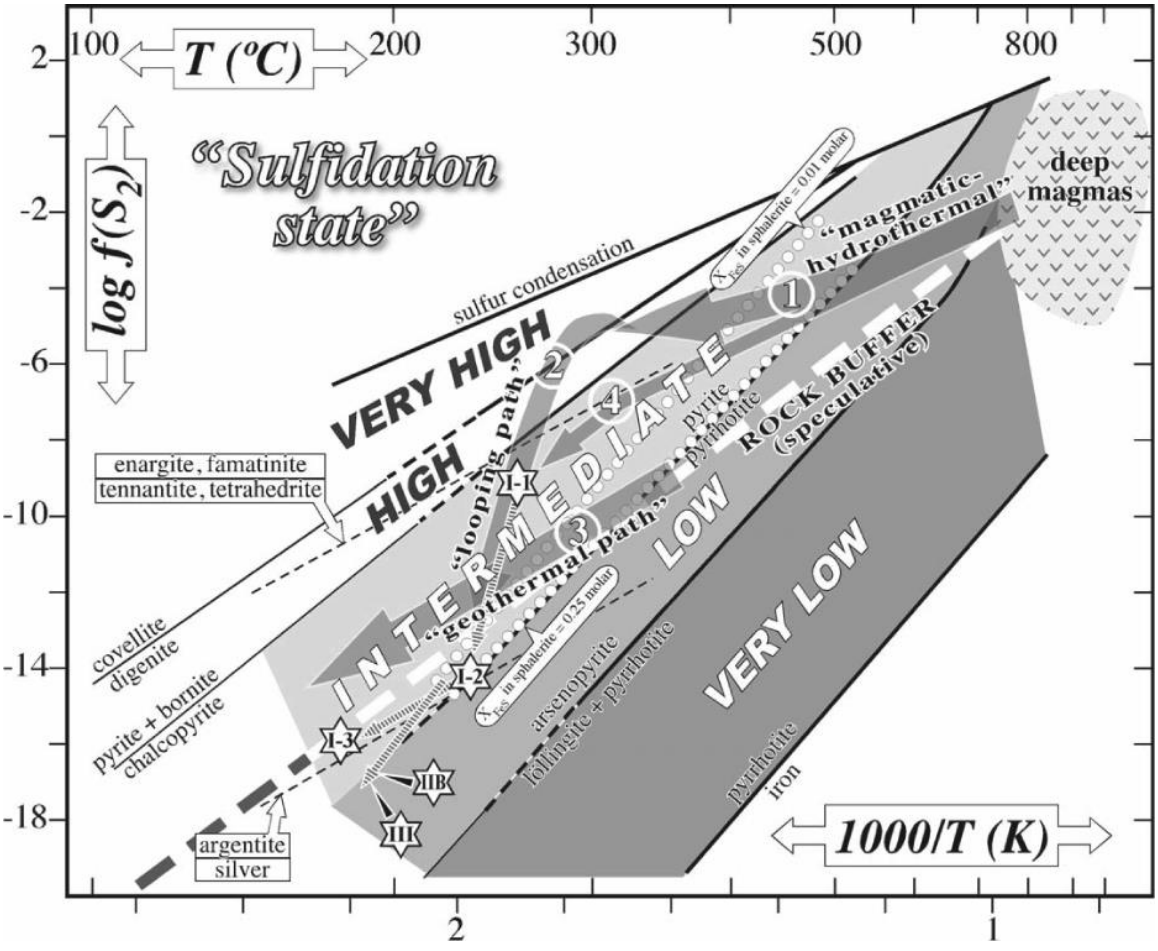

Figure 28. log$f$(S_2) – inverted T plot showing Fe-Cu sulfide phases. From Einaudi et al. 2003. An intermediate sulfidation path, like pathway 3 on the figure, would result in pyrrhotite-arsenopyrite deposition ceding to pyrite-chalcopyrite as temperatures cooled. Pyrite-tennantite-tetrahedrite assemblages would deposit at even lower temperatures matching the vertical zonation observed at the Cove deposit.

Gold would be transported and deposited by this higher temperature fluid as well by chloride complexes dominantly up until ~400ºC and at least in part to ~300ºC (Figure 29). However, by 300ºC, the predominant complexes would become Au(HS) and $Au(HS)_2^-$, which are less susceptible to depositions by decreases in temperature (Figure 29). Under the same conditions, Ag would switch from predominantly Ag-chloride complexes (Figure 30) to hydrosulfide complexes at lower temperatures (~225ºC). Evidence of meteoric fluid input from the stable isotope results of Johnston et al. (2008) implies a dilution of the brine at higher temperatures possibly depressing the solubility of $AgCl_2^-$ and $AuCl_2^-$ and allowing the switch to hydrosulfide complexes at higher temperatures.

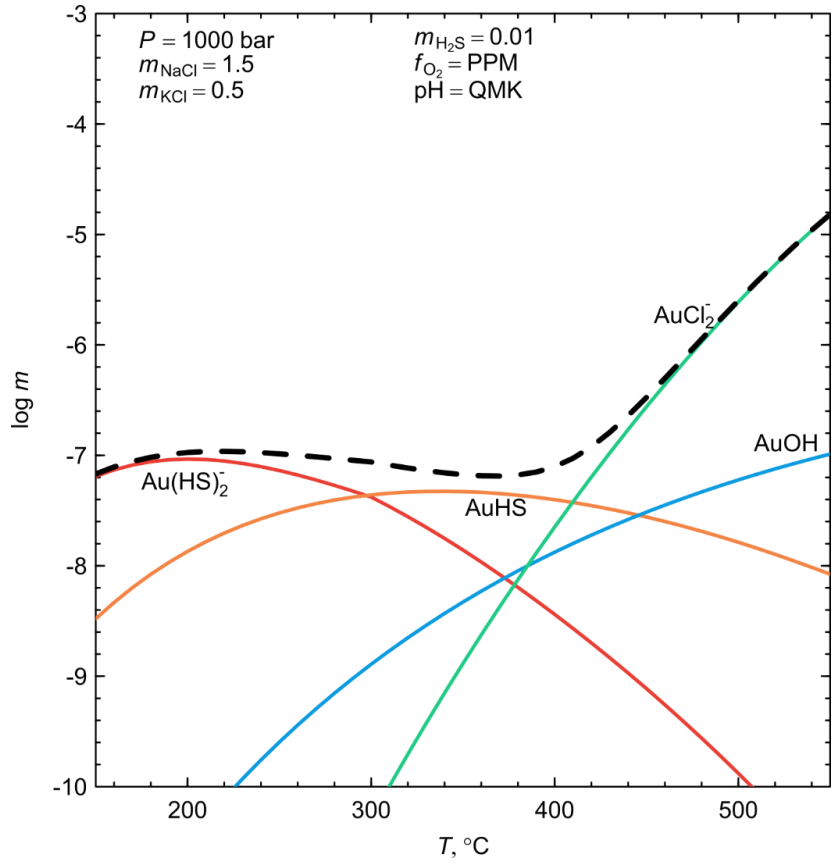

Figure 29. Solubility of Au complexes at pyrite-pyrrhotite-magnetite fO_2 buffer, quartz-muscovite-K-feldspar pH buffer and 1000 bar versus temperature. Dashed black line represents a possible path in the transition from chloride to bisulfide complexation. Note the higher temperature predominance of $AuCl_2^-$ to the overall solubility

of Au versus lower temperature bisulfide predominance. After Williams-Jones et al. (2009), Pokrovski et al. (2014), and demo from CHNOSZ (Dick, 2019).

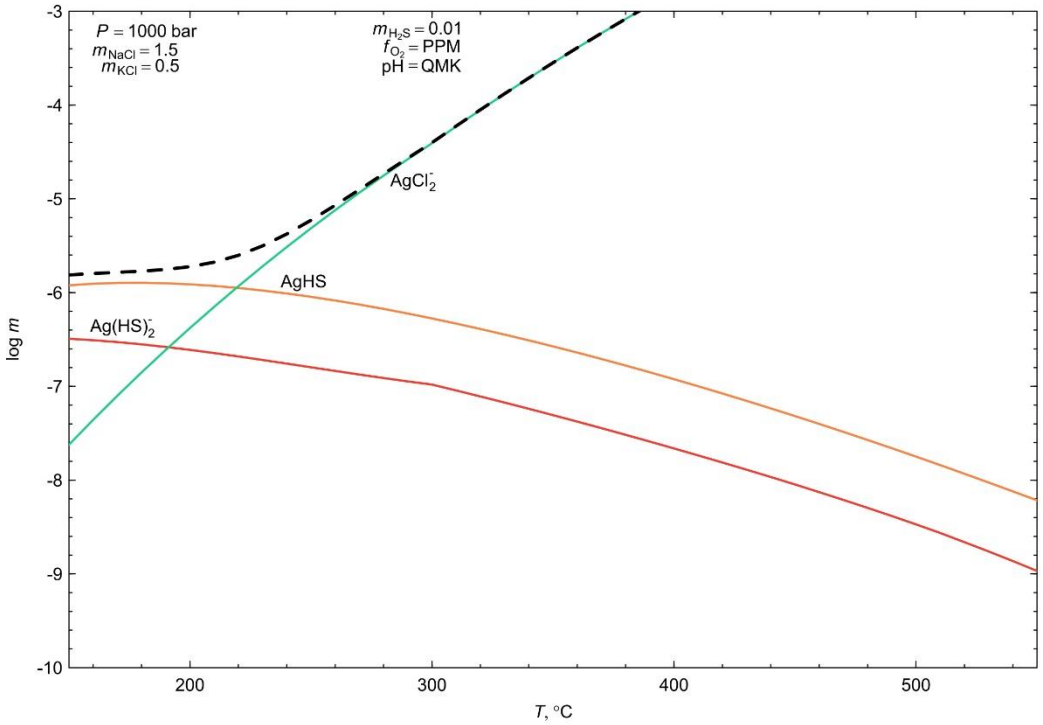

Figure 30. Solubility of Ag complexes at pyrite-pyrrhotite-magnetite fO_2 buffer, quartz-muscovite-K-feldspar pH buffer and 1000 bar versus temperature. Based on demo for Au solubility from CHNOSZ (Dick, 2019).

While Au and Ag become more soluble as hydrosulfide complexes due to cooling or fluid mixing, the fluid, by dissociation of volatiles (i.e..HCl, H_2S, H_2SO_4), would become more acidic. These evolved fluid conditions permit the transport of gold and silver for long distances without deposition by cooling unless the fluid encounters reactive Fe^{2+} either in wall rock or as a result of ferroan carbonate dissolution (Hofstra and Cline, 2000) therefore forming Carlin-style mineralization.

This appears to have been a complicated transition at Cove and pyrite textures and geochemistry in the CSD zone suggest the possibility that the lower temperature Carlin-style mineralization co-existed with some higher temperature polymetallic mineralization at least for some time. However, the two styles of mineralization were strongly restricted to different lithologies – Carlin-style mineralization to reactive carbonate rocks and vein-style mineralization to competent clastic units limiting the possibilities of clear

overprinting relationships outside of the Favret-hosted manto-style mineralization where local overprint is documented by this study.

Predicting Ag-rich Carlin-style Fluid Characteristics and Influence of Wall-Rock Interaction

Among Carlin-style and Carlin-type deposits, Cove is unusual for having very high Ag content in the zones of Carlin-style mineralization. The Ag/Au ratio varies across the Carlin-style mineralization in the Cove area from ~12/1 to a more typical Carlin-type Ag/Au ratio of >1/1 (Hofstra and Cline, 2000). Besides an internal metallurgical report produced for Echo Bay (Chryssoulis et al., 1997), which was later published in part by Johnston (2000), that documents Au and Ag in arsenian pyrite using secondary ion mass spectrometry (SIMS), this work is the first to report significantly high values of Ag concentrations in arsenian rims of Carlin-style mineralization at Cove using ion microprobe analyses. While some of the other metal ratio zonations across the property from CSD to Windy Point in Carlin-style mineralization may be explained by pyrite concentration, degree of sulfidation, or mineralogy, Ag concentrations and Ag/Au ratios are higher in the rims at CSD than Helen. Ag concentrations in rims are highest in the sample that represents an overprint of the pre-existing manto mineralization at the base of the Favret. Significant Ag has not been reported in published analyses of arsenian pyrite rims in Carlin-type deposits.

Below approximately ~225ºC, Ag-hydrosulfide complexes (AgHS and $Ag(HS)_2^-$) become the predominant Ag complexes (Figure 30) at oxygen fugacities above pyrite-pyrrhotite-magnetite buffer with pH controlling speciation between the two (Figure 31). As temperature cools below ~225ºC, or as AgHS complexes become predominant in the low-mid pH range, the solubility curves for the two metals diverge and Ag becomes more soluble than Au (Figure 32). At higher pH's within the $Ag(HS)_2^-$ predominance field, Ag/Au ratios will never be any more than 1:1. However, understanding that the pH of typical mineralizing fluids for Carlin-type gold deposits is ~5 (Hofstra and Cline, 2000) and that most Carlin fluids should therefore be capable of transporting significant Ag as AgHS, most Carlin-type gold deposits are Ag-poor with Ag/Au ratios <1. The high Ag contents at the CSD (and Gap) zones at Cove are therefore most likely due to its closer proximity to source. While most Ag had been deposited prior to sulfur becoming the predominant transporting agent (2201 zone, manto-style mineralization, polymetallic zones in Cove pit), enough Ag

remained in the system for transport by predominantly hydrosulfide complexes before precipitating. With distance from source towards the Helen zone, Ag/Au ratios decrease with overall decreasing Ag in the system.

Where Ag contents are extraordinarily high in arsenian pyrite rims associated with overprinting, there may have been no buffering capacity left in the completely sulfidized wallrock moderating pH to values suitable for extremely high Ag/Au ratios (muscovite-destructive alteration). Lower pH fluids due to sulfidized wallrock and reduced carbonate buffering capacity may also have played a role at the CSD zone and dolomites of the Gap zone where evidence of polymetallic mineralization is found.

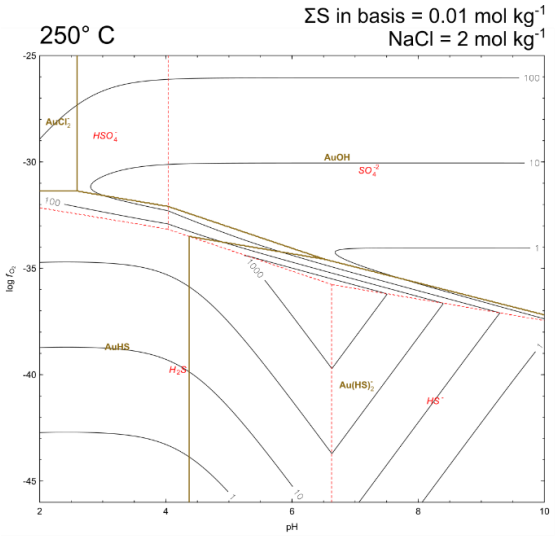
250° C
ΣS in basis = 0.01 mol kg-1
NaCl = 2 mol kg-1
AuCl2-
HSO4-
AuOH
SO4-2
AuHS
H2S
Au(HS)2-
HS-
log fO2
pH

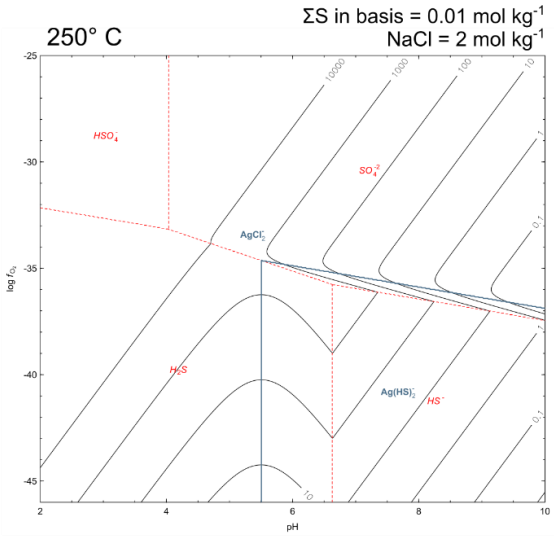
250° C
ΣS in basis = 0.01 mol kg-1
NaCl = 2 mol kg-1
HSO4-
SO4-2
AgCl2-
H2S
Ag(HS)2-
HS-
log fO2
pH

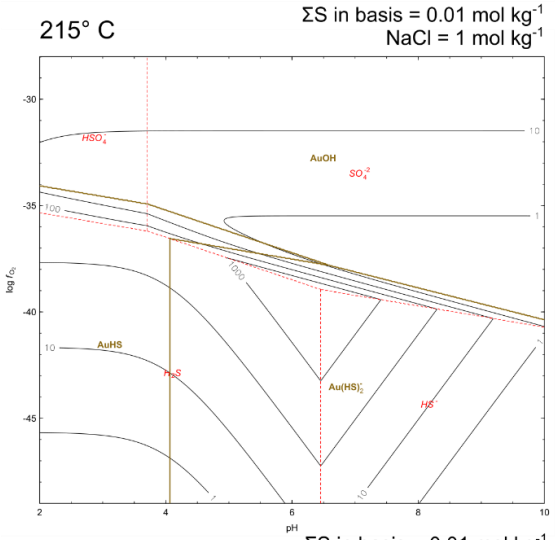
215° C
ΣS in basis = 0.01 mol kg-1
NaCl = 1 mol kg-1
HSO4-
AuOH
SO4-2
AuHS
H2S
Au(HS)2-
HS-
log fO2
pH

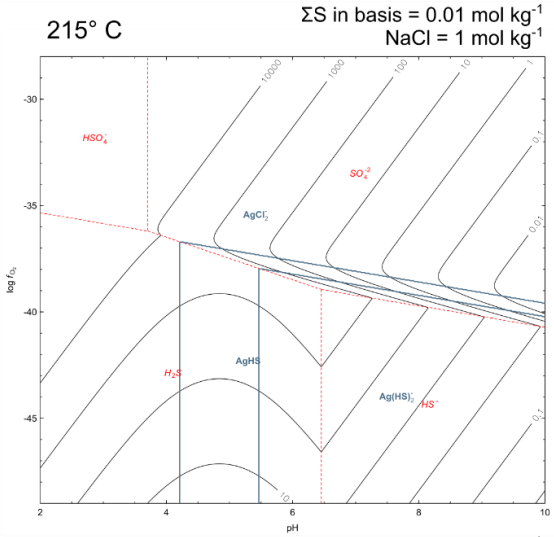
215° C
ΣS in basis = 0.01 mol kg-1
NaCl = 1 mol kg-1
HSO4-
SO4-2
AgCl2-
AgHS
H2S
Ag(HS)2-
HS-
log fO2
pH

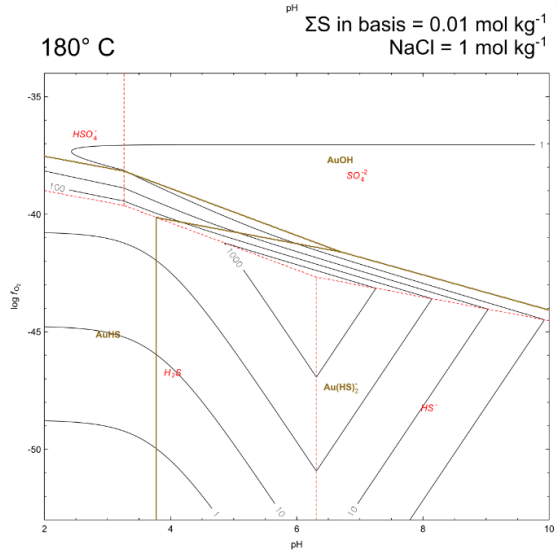
180° C
ΣS in basis = 0.01 mol kg-1
NaCl = 1 mol kg-1
HSO4-
AuOH
SO4-2
AuHS
H2S
Au(HS)2-
HS-
log fO2
pH

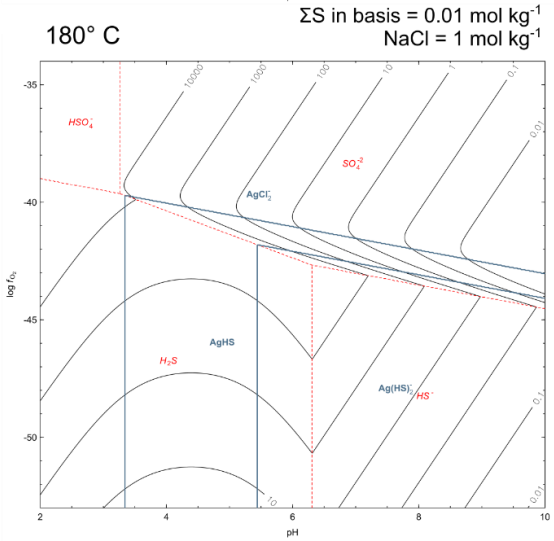
180° C
ΣS in basis = 0.01 mol kg-1
NaCl = 1 mol kg-1
HSO4-
SO4-2
AgCl2-
AgHS
H2S
Ag(HS)2-
HS-
log fO2
pH

Figure 31. Solubility plots for Au and Ag in logfO_2-pH space for 250º, 215º, and 180ºC. Chloride and bisulfide activities are shown above plots. Produced using thermodynamic properties for Ag and Au complexes recommended by Pokrovski et al. (2014). Note that $AgCl^-$ complexes predominate lower pH conditions at higher temperatures. After Williams-Jones et al. (2009) and Liang and Hoshino (2015).

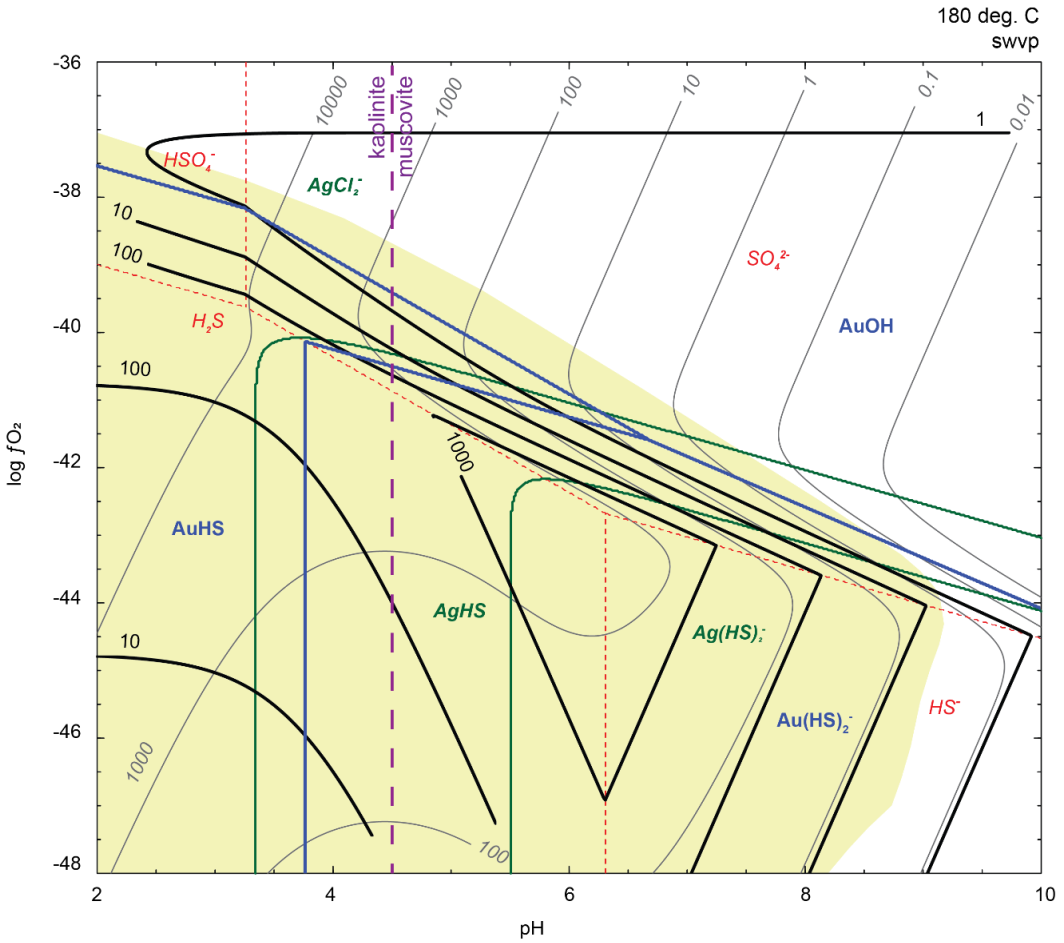

Figure 32. logfO_2 – pH plot at 180 deg. C and saturated water vapor pressure displaying sulfur speciation predominance fields, Au complex predominance fields (blue), Ag complex predominance fields (green), the pyrite field (yellow), kaolinite-muscovite boundary (purple), and solubility curves for Au (bold black) and Ag (gray) in parts per billion. Total S = 0.01 mol kg^{-1} and NaCl = 1 mol kg^{-1}. Ag/Au is highest in the pH range of ~5.5 – 4.5. After Williams-Jones et al. (2009) and Liang and Hoshino (2015).

Telescoping and Uplift History of District

Brooks (1994) reported a minimum pressure estimate of 350 bars from garnet fluid inclusion analysis at McCoy. This pressure estimate places the depth of alteration and mineralization of the McCoy deposit around the Brown stock between approximately 3.6 (hydrostatic load) and 1.3 kilometers (lithostatic load (Brooks, 1994). Using the fluid inclusion data of Johnston et al. (2008) and assuming a homogenization temperature

of 300ºC, a salinity of 5 wt% NaCl eq, no CO_2, and trapping along the liquid-vapor curve, fluid inclusions from the deepest sample at Cove (665 m) had a trapping pressure of 83.2 bars and density of 0.767 g/cm^3 (Haas, 1971; Muntean et al., 2017). The calculated minimum estimated depth at Cove therefore is approximately 1 km. However, no boiling textures are observed in Cove veins and no evidence of boiling was found in fluid inclusions as part of Johnston et al. (2008) possibly supporting a greater depth of formation similar to the depth at McCoy. Based on new U-Pb zircon dates, the crystallization ages of the Brown stock at McCoy and the Gold Dome dike at Cove occurred between 38.6 and 37.4 Ma. By 34.45 Ma, the Tuff of Cove Mine buried the shallowest jasperoids and disseminated oxide parts of the Cove deposit at surface. This requires approximately 2-3 kilometers of uplift over approximately 3 million years during which most of the Cove mineralization occurred given the cross-cutting relationship shared with the older 37.6 Ma Gold Dome dike. If uplift occurred contemporaneously with mineralization, it may have juxtaposed lower temperature mineralization near older, previously deeper, higher temperature mineralization and may help explain in part the close spatial relationship at Cove between polymetallic mineralization and Carlin-style mineralization. Further studies at Cove and other Eocene Carlin-style deposits with telescoping of hydrothermal systems like Kinsley Mountain (Hill, 2016) should use thermochronology, geologic mapping, and fluid inclusion petrography and microthermometry to quantify amount and rate of uplift.

Implications for Carlin-type Gold Deposits

The research presented here at Cove supports the hypothesis of a continuum existing between polymetallic magmatic-hydrothermal systems and Carlin-type gold deposits. While other Carlin-style deposits have been shown to represent distal products of magmatic-hydrothermal systems (Kinsley: Hill, 2016; Lone Tree: Holley et al. 2019), Cove's most distal deposit, the Helen zone, is the most similar in its chemistry, pyrite textures, and alteration to traditional Carlin-type gold deposits in Nevada. Furthermore, this study suggests an overprinting relationship between polymetallic and younger to coeval Carlin-style mineralization that links the two styles of mineralization in one evolving district-scale magmatic-hydrothermal system.

Muntean et al. (2011) pointed out the lack of metal zonations at Carlin-type gold deposits commonly seen in magmatic-hydrothermal mineral deposits (Sillitoe, 2010) and proposed a genetic model where the magmatic

source of hydrothermal fluids was deeper. A deeper magmatic source, consistent with theories of overthickened crust in northern Nevada during the Eocene, would mean greater spatial separation allowing Ag and base metals to precipitate from solution before the fluids cooled to temperatures suitable for transporting gold as bisulfide complexes (~ 300º - 250º C). Any Carlin-type gold deposits that formed as a result of this fluid evolution pathway would be expected to produce deposits with low Ag/Au ratios and no significant polymetallic mineralization. The fact that Cove mineralization has obvious zonations in Ag/Au, Pb, Zn, Cu, Sb, and Tl tells us it could be a telescoped system due to rapid uplift during mineralization or that Eocene distal disseminated deposits in Nevada form from hydrothermal fluids sourced from more shallowly emplaced magmatism.

Further research at Carlin-style or "Carlin-like" deposits in Nevada and elsewhere will continue to inform genetic models for Carlin-type gold deposits where zonations and age constrains are difficult to ascertain. Future work at Cove should build upon this study and Johnston et al. (2008) in quantifying uplift rates, depths of formation, and fluid evolution through fluid inclusion studies and additional geochronology.

REFERENCES

Barth, A. P., and Wooden, J. L., 2010, Coupled elemental and isotopic analyses of polygenetic zircons from granitic rocks by ion microprobe, with implications for melt evolution and the sources of granitic magmas: Chemical Geology, v. 277, p. 149–159.

Black, L. P., Kamo, S., Allen, C. M., Aleinikoff, J., Davis, D. W., Korsch, R., and Foudoulis, C., 2003, TEMORA 1: A new zircon standard for Phanerozoic U-Pb geochronology: Chemical Geology, v. 200, p. 155–170.

Bliss, J. D., 1992, Developments in mineral deposit modeling:, accessed at Bulletin at http://pubs.er.usgs.gov/publication/b2004.

Brooks, J. W., 1994, Petrology and Geochemistry of the McCoy Gold Skarn, Lander County, Nevada: Washington State University.

Brooks, J. W., Meinert, L. D., Kuyper, B. A., and Lane, M. L., 1991, Petrology and Geochemistry of the McCoy Gold Skarn, Lander County, Nevada, in Raines, G. L., Lisle, R. E., Schafer, R. W., and Wilkinson, W. H. eds., Geology and ore deposits of the Great Basin: Reno, Geological Society of Nevada, p. 419–442.

Chryssoulis, S. L., Zhou, Y., Weisener, C., and Kingston, D., 1997, Deportment of gold and silver in testwork products of select McCoy ore zones: p. 59.

Cline, J. S., 2018, Nevada's Carlin-Type Gold Deposits: What We've Learned During the Past 10 to 15 Years (J. L. Muntean, Ed.): Diversity in Carlin-Style Gold Deposits, v. 20, p. 0.

Coble, M. A., Vazquez, J. A., Barth, A. P., Wooden, J., Burns, D., Kylander-Clark, A., Jackson, S., and Vennari, C. E., 2018, Trace Element Characterisation of MAD-559 Zircon Reference Material for Ion Microprobe Analysis: Geostandards and Geoanalytical Research, v. 42, p. 481–497.

Colgan, J. P., Dumitru, T. A., McWilliams, M., and Miller, E. L., 2006a, Timing of Cenozoic volcanism and Basin and Range extension in northwestern Nevada: New constraints from the northern Pine Forest Range: GSA Bulletin, v. 118, p. 126–139.

Colgan, J. P., Dumitru, T. A., Reiners, P. W., Wooden, J. L., and Miller, E. L., 2006b, Cenozoic Tectonic Evolution of the Basin and Range Province in Northwestern Nevada: American Journal of Science, v. 306, p. 616–654.

Cousens, B., Henry, C., Stevens, C., Varve, S., John, D., and Wetmore, S., 2019, Igneous rocks in the Fish Creek Mountains and environs, Battle Mountain area, north-central Nevada: A microcosm of Cenozoic igneous activity in the northern Great Basin, Basin and Range Province, USA: Earth-Science Reviews, v. 192.

Cox, D. P., and Singer, D. A., 1990, Descriptive and grade-tonnage models for distal disseminated Ag-Au deposits; a supplement to U.S. Geological Survey bulletin 1693:, accessed at Open-File Report at http://pubs.er.usgs.gov/publication/ofr90282.

Dick, J. M., 2019, CHNOSZ: Thermodynamic Calculations and Diagrams for Geochemistry: Frontiers in Earth Science, v. 7, p. 180.

Dickinson, W. R., 2006, Geotectonic evolution of the Great Basin: Geosphere, v. 2, p. 353–368.

Einaudi, M. ., Hedenquist, J. W., and Inan, E., 2003, Sulfidation state of hydrothermal fluids: The porphyry-epithermal transition and beyond, in Simmons, S. F. and Graham, I. J. eds., SEG Special Publication 10 - Volcanic geothermal and ore-forming fluids: Rulers and witnesses of processes within the Earth: Society of Economic Geologists and Geochemical Society, p. 285–313.

Emmons, D. L., and Eng, T. L., 1995, Geologic Map of the McCoy Mining District, Lander County, Nevada:, accessed at https://pubs.nbmg.unr.edu/Geol-McCoy-mining-district-p/m103.htm.

Haas, J. L., 1971, The effect of salinity on the maximum thermal gradient of a hydrothermal system at hydrostatic pressure: Economic Geology, v. 66, p. 940–946.

Hill, T., 2016,Time-Space Relationships between Sediment-Hosted Gold Mineralization and Intrusion-Related Polymetallic Mineralization at Kinsley Mountain, NV: University of Nevada, Reno: 200 p.

Hofstra, A., and Cline, J., 2000, Characteristics and models for Carlin-type gold deposits: Reviews in Economic Geology, v. 13, p. 163–220.

Holley, E. A., Lowe, J. A., Johnson, C. A., and Pribil, M. J., 2019, Magmatic-Hydrothermal Gold Mineralization at the Lone Tree Mine, Battle Mountain District, Nevada: Economic Geology, v. 114, p. 811–856.

Humphreys, E., 1995, Post-Laramide removal of the Farallon slab, western United States: Geology, v. 23.

Ilchik, R. P., and Barton, M. D., 1997, An Amagmatic Origin for Carlin-Type Gold Deposits (P. Vikre, T. B. Thompson, K. Bettles, O. Christensen, & R. Parratt, Eds.): Carlin-Type Gold Deposits Field Conference, v. 28, p. 0.

Janousek, V., Farrow, C., and Erban, V., 2006, Interpretation of Whole-rock Geochemical Data in Igneous Geochemistry: Introducing Geochemical Data Toolkit (GCDkit): Journal of Petrology, v. 47, p. 1255–1259.

John, D., Henry, C., and P. Colgan, J., 2008, Magmatic and tectonic evolution of the Caetano caldera, north-central Nevada: A tilted, mid-Tertiary eruptive center and source of the Caetano Tuff: Geosphere, v. 4.

Johnston, M. K., 2000, Hypogene alteration and ore characteristics at the Cove gold silver deposit, Lander County, Nevada, in Price, J. K., Struhsacker, E. M., Hardyman, R. F., and Morris, C. L. eds., Geology and ore deposits 2000: The Great Basin and Beyond: Reno, NV, Geological Society of Nevada, p. 621–641.

Johnston, M. K., 2001, Structural and temporal setting of the McCoy-Cove system, Lander County, Nevada: Geological Society of Nevada, accessed at Geological Society of Nevada Special Publication 33.

Johnston, M. K., 2003,Geology of the Cove Mine, Lander County, Nevada, and a Genetic Model for the McCoy-Cove Magmatic-Hydrothermal System: University of Nevada, Reno: 376 p.

Johnston, M. K., Thompson, T. B., Emmons, D. L., and Jones, K., 2008, Geology of the cove mine, Lander County, Nevada, and a genetic model for the McCoy-Cove hydrothermal system: Economic Geology, v. 103, p. 759–782.

King, C., 2017,Igneous Petrology, Geochronology, Alteration, and Mineralization Associated with Hydrothermal Systems in the Battle Mountain District, Nevada: University of Arizona: 707 p.

Kuyper, B. A., Mach, L. E., Streiff, R. E., and Brown, W. A., 1991, Geology of the Cove gold-silver deposit, in Preprint no. 91-125: Society for Mining, Metallurgy, and Exploration, p. 19.

Large, R., Bull, S., and Maslennikov, V., 2011, A Carbonaceous Sedimentary Source-Rock Model for Carlin-Type and Orogenic Gold Deposits: Economic Geology, v. 106, p. 331–358.

Liang, Y., and Hoshino, K., 2015, Thermodynamic calculations of AuxAg1−x – Fluid equilibria and their applications for ore-forming conditions: Applied Geochemistry, v. 52, p. 109–117.

Miller, B. W., and Silberman, M. L., 1977, Cretaceous K-Ar age of hydrothermal alteration at the North Fish Creek porphyry copper prospect, Fish Creek Mountains, Lander County, Nevada: Isochron/West, p. 7.

Muntean, J., and Taufen, P., 2011, Geochemical exploration for gold through transported alluvial cover in Nevada: Examples from the cortez mine: Economic Geology, v. 106, p. 809–833.

Muntean, J., Bonner, W., and Hill, T., 2017, Carlin-style gold-silver mineralization at the Cove deposit in Nevada, USA: possible missing link between Carlin-type gold deposits and magmatic-hydrothermal systems, in Society for Geology Applied to Mineral Deposits Conference Proceedings.:

Nakamura, N., 1974, Determination of REE, Ba, Fe, Mg, Na and K in carbonaceous and ordinary chondrites: Geochimica et Cosmochimica Acta, v. 38, p. 757–775.

Nichols, K. M., and Silberling, N. J., 1977, Stratigraphy and Depositional History of the Star Peak Group (Triassic), Northwestern Nevada, in Nichols, K. M. and Silberling, N. J. eds., Stratigraphy and Depositional History of the Star Peak Group (Triassic), Northwestern Nevada: Geological Society of America, p. 0.

Oldow, J. S., 1983, Tectonic implications of a late Mesozoic fold and thrust belt in northwestern Nevada: Geology, v. 11, p. 542–546.

Pearce, J. A., 1982, Trace element characteristics of lavas from destructive plate boundaries, in Thorpe, R. S. ed., Andesites: Orogenic Andesites and Related Rocks: Chichester, John Wiley & Sons, p. 525–548.

Pearce, J. A., 1996, A user's guide to basalt discrimination diagrams, in Wyman, D. A. ed., Trace Element Geochemistry of Volcanic Rocks: Applications for Massive Sulphide Exploration. Short Course Notes 12: Geological Association of Canada, p. 79–113.

Pokrovski, G., Akinfiev, N., Borisova, A., Zotov, A., and Kouzmanov, K., 2014, Gold speciation and transport in geological fluids: Insights from experiments and physical-chemical modelling, in Geological Society, London, Special Publications.

Practical Mining LLC, 2013, Prepared for Premier Gold Mines, Limited, NI 43-101 Technical Report Cove Exploraiton Project, Lander County, Nevada: Technical Report dated September 30, 2013

Practical Mining LLC, 2018, Prepared for Premier Gold Mines, Limited, NI 43-101, Preliminary Economic Assessment of Cove Project, Lander County, Nevada: Technical Report dated March 31, 2018

Seedorff, E., 1991, Magmatism, extension, and ore deposits of Eocene to Holocene age in the Great Basin; mutal effects and prelimiary proposed genetic relationships, in Raines, G. L., Lisle, R. E., Schafer, R. W., and Wilkinson, W. H. eds., Geology and ore deposits of the Great Basin: Reno, Geological Society of Nevada, p. 133–178.

Silberling, N. J., and Roberts, R. J., 1962, Pre-Tertiary Stratigraphy and Structure of Northwestern Nevada, in Silberling, N. J. and Roberts, R. J. eds., Pre-Tertiary Stratigraphy and Structure of Northwestern Nevada: Geological Society of America, p. 0.

Silberman, M. L., and McKee, E., 1971, K-Ar Ages of plutons in north-central Nevada: Isochron/West, v. 71, p. 15–32.

Sillitoe, R. H., 2010, Porphyry Copper Systems: Ecoonomic Geology, v. 105, p. 3–41.
Sillitoe, R. H., and Bonham, Jr., H. F., 1990, Sediment-hosted gold deposits: Distal products of magmatic-hydrothermal systems: Geology, v. 18, p. 157.
Stewart, J., McKee, E., and Stager, H., 1977, Geology and Mineral Deposits of Lander County, Nevada: Nevada Bureau of Mines Bulletin 88; Part I and II, Nevada Bureau of Mines and Geology.
Theodore, T. G., 2000, Geology of pluton-related gold mineralization at Battle Mountain, Nevada:, accessed at https://pubs.nbmg.unr.edu/Geology-of-pluton-related-gold-p/cmr.htm.
Tosdal, R. M., ed., 1998, Contributions to the gold metallogeny of northern Nevada:, accessed at Open-File Report at http://pubs.er.usgs.gov/publication/ofr98338B.
Vermeesch, P., 2018, IsoplotR: A free and open toolbox for geochronology: Geoscience Frontiers, v. 9, p. 1479–1493.
Wallace, A. R., Ludington, S., Mihalasky, M. J., Peters, S. G., Theodore, T. G., Ponce, D. A., John, D. A., and Berger, B. R., Zientek, M. L., Sidder, G. B., and Zierenberg, R. A., 2004, Assessment of metallic mineral resources in the Humboldt River Basin, Northern Nevada, with a section on Platinum-Group-Element (PGE) Potential of the Humboldt Mafic Complex:, accessed at Bulletin at http://pubs.er.usgs.gov/publication/b2218.
Wyld, S. J., 2000, Triassic evolution of the arc and backarc of northwestern Nevada, and evidence for extensional tectonism, in Special Paper 347: Paleozoic and Triassic paleogeography and tectonics of western Nevada and Northern California: Geological Society of America, p. 185–207.

Appendix A.
Whole Rock Geochemistry of Select Igneous Units at Cove-McCoy Mining District, Lander County, NV

SampleID	Al2O3_pct	BaO_pct	CaO_pct	Cr2O3_pct	Fe2O3_pct	K2O_pct	MgO_pct	MnO_pct	Na2O_pct	P2O5_pct	SiO2_pct	SrO_pct	TiO2_pct	LOI 1000_pct	Total_pct
PG16-02 1600	14.62	0.06	7.7	0.07	7.94	2.43	2.63	0.14	0.22	0.28	48.78	0.02	0.95	10.96	100.85
PG16-10 1745	16.28	0.12	7.04	0.07	7.39	4.21	1.41	0.14	0.1	0.34	50.06	0.02	1.11	8.38	103.45
PG16-11 2123	18.12	0.06	4.23	0.09	15.38	1.92	4.17	0.07	1.34	0.54	43.26	0.02	1.74	8.42	99.78
PG16-14 2840	13.26	0.08	8.34	0.06	9.79	1.54	9.01	0.14	2.03	0.4	41.65	0.06	1.28	11.93	99.72
PG16-15 1394	16.03	0.06	5.38	0.01	4.16	2.43	1.44	0.09	0.15	0.19	59.78	0.03	0.62	9.07	99.87
PG16-15 1413	15.8	0.09	5.96	0.01	4.16	2.95	1.46	0.1	0.08	0.19	59.08	0.04	0.61	8.16	99.39
PG16-15 1487	18.22	0.04	0.41	<0.01	5.79	4.74	0.59	0.02	0.05	0.22	63.22	0.01	0.7	5.76	108.7
HV Basalt 1	15.06	0.09	8.66	0.06	9.7	2	6.79	0.14	2.87	0.48	50.16	0.1	1.38	1.52	99.16
HV Basalt 2	15.98	0.16	6.31	0.07	10.31	2.43	5.1	0.17	1.82	0.56	50.21	0.08	1.48	4.78	99.64
HV Basalt 3	15.11	0.09	8.61	0.06	9.79	1.89	7.41	0.14	2.77	0.48	50.33	0.1	1.37	1.77	100.05
HV Basalt 4	13.62	0.14	7.75	0.06	8.64	2.86	5	0.13	1.35	0.43	50.47	0.17	1.22	7.49	99.47
WPI - 1	16.26	0.01	0.49	<0.01	2.38	0.82	0.41	0.02	7.3	0.14	69.46	0.03	0.41	1.32	99.14
PG16-14 2871	26.24	0.03	2.19	0.12	7.26	0.37	2.27	0.02	0.11	0.76	46.02	0.02	2.42	11.7	100.4
PG17-18 2082	11.86	0.15	7.26	0.04	7.9	4.28	4.6	0.36	0.08	0.32	46.34	0.02	1.24	13.34	>110
PG14-05 2562	12.95	0.63	2.29	0.03	12.08	4.74	5.1	0.2	0.14	0.35	49.68	0.01	1.24	9.95	>110
PG16-24 1906	12.73	0.15	7.99	0.03	7.91	2.26	5.24	0.09	1.7	0.34	48.69	0.07	1.21	9.09	99.18
AX-22 1311	15.71	0.06	5.55	0.04	3.49	2.59	3.69	0.11	0.06	0.44	54.76	0.02	1.5	9.87	101.45
AX39-2106.5	16.48	0.13	3.95	<0.01	5.52	3.15	1.42	0.07	0.53	0.2	59.9	0.02	0.63	8.06	105.25
AX32-1959	18.89	0.06	6.73	0.09	10.1	1.98	1.81	0.11	1.32	0.56	45.04	0.02	1.84	10.18	99.5
AX39-2045	14.98	0.07	9.62	0.08	13.36	1.74	3.92	0.13	1.95	0.44	42.98	0.05	1.5	8.59	99.58
AX25-1970	15.67	0.27	7.85	0.08	13.29	1.92	2.01	0.21	1.56	0.47	41.98	0.04	1.54	12.14	99.69
AX35-1337.8	11.71	0.04	10.85	0.07	4.95	2.82	7.38	0.09	0.06	0.29	44.69	0.02	0.78	14.3	104.25
AX18-2072	15.85	0.05	2.78	0.01	4.25	3.66	1.5	0.06	0.07	0.19	62.89	0.02	0.61	6.41	103.35
PG1601-1992	16	0.12	3.31	0.07	7.37	4.48	2.6	0.11	0.05	0.32	54.81	0.01	1.06	8.12	107.6
AX14-1952	19.97	0.08	2.14	0.09	13.04	2.37	2.25	0.02	1.48	0.58	48.86	0.04	1.9	6.68	100.1
PG1619-177.5	18.78	0.07	2.16	0.01	6.87	1.55	3.54	0.1	0.32	0.23	56.13	0.02	0.84	8.88	99.65
PG1618-782	15.6	0.1	5.28	<0.01	4.14	2.54	2.21	0.04	1.9	0.19	61.01	0.04	0.6	5.41	99.12
AX39-2100	14.38	0.08	11.8	0.08	10.16	1.74	4.66	0.16	2.43	0.43	44.84	0.07	1.42	7.55	99.98
AX8A-1955	22.1	0.07	3.05	0.12	11.06	2.13	1.92	0.07	1.44	0.63	47.29	0.02	2.19	7.94	100.5
AX18-1938.5	29.62	0.08	1.56	0.16	3.02	2.08	0.74	0.01	0.85	0.75	46.96	0.02	2.94	10.41	102.9
AX8A-1961	16.26	0.05	0.35	<0.01	3.68	3.8	0.71	<0.01	0.06	0.18	69	0.01	0.64	4.6	105.05
AX39-2045	14.98	0.07	9.62	0.08	13.36	1.74	3.92	0.13	1.95	0.44	42.98	0.05	1.5	8.59	99.58
AX39-2100	14.38	0.08	11.8	0.08	10.16	1.74	4.66	0.16	2.43	0.43	44.84	0.07	1.42	7.55	99.98
AX32-1959	18.89	0.06	6.73	0.09	10.1	1.98	1.81	0.11	1.32	0.56	45.04	0.02	1.84	10.18	99.5
AX18-1938.5	29.62	0.08	1.56	0.16	3.02	2.08	0.74	0.01	0.85	0.75	46.96	0.02	2.94	10.41	102.9
AX8A-1955	22.1	0.07	3.05	0.12	11.06	2.13	1.92	0.07	1.44	0.63	47.29	0.02	2.19	7.94	100.5
AX8A-1961	16.26	0.05	0.35	<0.01	3.68	3.8	0.71	<0.01	0.06	0.18	69	0.01	0.64	4.6	105.05
CHV-2	16.56	0.12	4.22	<0.01	4.65	2.79	1.88	0.07	2.77	0.21	64.35	0.06	0.61	1.38	99.75
NW-2	16.61	0.13	4.56	<0.01	4.47	2.42	1.94	0.09	3.27	0.21	63.65	0.07	0.5	1.78	99.77
NS-2	15.53	0.11	2.55	<0.01	3.65	2.74	1.97	0.07	4.09	0.17	64.82	0.04	0.59	3.19	99.59

SampleID	Ba_ppm	Ce_ppm	Cr_ppm	Cs_ppm	Dy_ppm	Er_ppm	Eu_ppm	Ga_ppm	Gd_ppm	Ge_ppm	Hf_ppm	Ho_ppm	La_ppm	Lu_ppm	Nb_ppm
PG16-02 1600	513	70.5	540	11.1	4.07	2.35	1.55	16.7	4.76	<5	4	0.85	36	0.31	13.8
PG16-10 1745	1125	80	530	38.2	3.89	2.17	1.29	17.6	4.51	<5	4.6	0.67	40.8	0.36	16
PG16-11 2123	564	63.5	640	2	4.45	2.08	1.89	22.2	5.85	<5	4.1	0.82	29.1	0.26	13.5
PG16-14 2840	741	46	420	5.96	3.38	1.64	1.53	16.8	4.45	<5	3	0.59	21.2	0.22	10.2
PG16-15 1394	582	51.7	40	14.25	2.68	1.34	1.03	19.4	3.51	<5	4.3	0.5	25.5	0.2	8.4
PG16-15 1413	818	51.1	30	10.65	2.62	1.45	1.15	19.8	3.48	<5	3.9	0.5	26.2	0.23	8.1
PG16-15 1487	318	58.5	30	8.89	2.42	1.34	0.75	22.9	3.92	<5	4.8	0.46	29.5	0.19	9.3
HV Basalt 1	890	57.8	470	1.87	4.2	2.23	1.85	19.9	5.89	<5	4	0.82	28.8	0.26	13.5
HV Basalt 2	1600	62	490	0.71	4.63	2.28	2.01	21.1	6.15	<5	4.2	0.86	33.2	0.27	14.3
HV Basalt 3	869	57.9	470	1.32	4.03	2.04	1.73	19.9	5.33	<5	4.1	0.79	27.6	0.24	13.6
HV Basalt 4	1395	52.5	410	1.35	3.57	1.8	1.52	16.9	4.59	<5	3.6	0.69	23.1	0.21	12.2
WPI - 1	116.5	46.7	30	0.75	2.15	1.22	0.7	16.7	2.56	<5	4.2	0.41	24.5	0.17	10.1
PG16-14 2871	290	101	810	2.86	8.42	4.25	3.48	32.4	10.85	14	6.5	1.54	47.2	0.44	20.1
PG17-18 2082	1330	166.5	250	7.04	4.68	2.29	2.58	16.6	7.49	<5	4.2	0.86	90.5	0.3	13.1
PG14-05 2562	5580	187.5	200	1.71	4.69	2.42	3.36	18.8	7.55	<5	4.5	0.88	104	0.31	14.8
PG16-24 1906	1420	180.5	210	2.37	4.52	2.28	2.65	17	7.23	<5	4.5	0.82	98.5	0.29	14.4
AX-22 1311	553	228	260	17.55	5.87	2.8	3.52	19.9	9.15	<5	5.7	1.07	122	0.37	18.1
AX39-2106.5	1140	52.7	30	7.43	2.12	1.19	0.89	19.4	2.77	<5	4.7	0.44	26.7	0.19	8.2
AX32-1959	551	67.3	640	2.5	4.23	2.28	1.94	24.2	6.13	<5	4.2	0.85	30.9	0.28	13.7
AX39-2045	713	53.7	560	5.04	3.75	1.87	1.7	20.2	5.59	<5	3.5	0.79	24.2	0.24	10.3
AX25-1970	2490	56.2	510	8.67	4.15	2.28	1.8	20.3	6.13	<5	3.7	0.82	25.7	0.26	10.9
AX35-1337.8	254	50.6	480	7.36	3.05	1.79	1.13	12.3	3.67	<5	3.7	0.67	26	0.27	10.3
AX18-2072	424	53.7	20	8.32	2.46	1.47	1.04	19.7	3.54	<5	4.5	0.53	27.1	0.2	8.2
PG1601-1992	1090	77.1	440	13.25	3.54	2.15	1.18	17.8	4.65	<5	4.7	0.8	38.8	0.34	16.2
AX14-1952	743	67.2	600	3.1	4.07	2.15	1.86	25.2	6.27	<5	4.3	0.86	30.1	0.25	13.6
PG1619-177.5	586	64.2	60	10.3	3.62	2.05	1.2	19.2	4.9	<5	5.3	0.72	26.5	0.28	12
PG1618-782	886	53.1	20	3.43	2.64	1.45	1.07	19.5	3.38	<5	4.3	0.56	27.5	0.21	7.9
AX39-2100	779	53.9	540	4.16	3.6	1.92	1.75	19.1	5.36	<5	3.4	0.71	24.4	0.2	10.3
AX8A-1955	617	72.2	780	2.9	4.42	2.07	2.04	29.3	6.55	16	5.2	0.83	32.5	0.28	15.1
AX18-1938.5	741	95.8	1110	2.18	5.81	2.89	2.64	37.3	8.51	43	7	1.15	43.8	0.36	20.8
AX8A-1961	419	55.9	30	13.4	2.52	1.56	0.89	18.4	2.93	<5	4.7	0.56	29.5	0.28	12.9
AX39-2045	713	53.7	560	5.04	3.75	1.87	1.7	20.2	5.59	<5	3.5	0.79	24.2	0.24	10.3
AX39-2100	779	53.9	540	4.16	3.6	1.92	1.75	19.1	5.36	<5	3.4	0.71	24.4	0.2	10.3
AX32-1959	551	67.3	640	2.5	4.23	2.28	1.94	24.2	6.13	<5	4.2	0.85	30.9	0.28	13.7
AX18-1938.5	741	95.8	1110	2.18	5.81	2.89	2.64	37.3	8.51	43	7	1.15	43.8	0.36	20.8
AX8A-1955	617	72.2	780	2.9	4.42	2.07	2.04	29.3	6.55	16	5.2	0.83	32.5	0.28	15.1
AX8A-1961	419	55.9	30	13.4	2.52	1.56	0.89	18.4	2.93	<5	4.7	0.56	29.5	0.28	12.9
CHV-2	1110	59.9	10	2.76	3.35	1.56	1.17	21.1	4.29	<5	5.5	0.59	30.7	0.26	12.4
NW-2	1170	52.1	10	1.36	2.84	1.38	1.2	20.8	3.59	<5	4.1	0.51	26.7	0.19	8.7
NS-2	924	51.8	30	1.91	3.22	1.69	1.1	18	3.54	<5	4.4	0.56	26.3	0.21	12.5

SampleID	Nd_ppm	Pr_ppm	Rb_ppm	Sm_ppm	Sn_ppm	Sr_ppm	Ta_ppm	Tb_ppm	Th_ppm	Tm_ppm	U_ppm	V_ppm	W_ppm	Y_ppm	Yb_ppm
PG16-02 1600	32.9	8.26	101	6.43	1	114	0.7	0.71	7.29	0.37	2.53	166	2	22.5	1.95
PG16-10 1745	35.3	9.15	148.5	5.94	3	129	0.9	0.64	8.48	0.32	9.56	193	9	20.2	2.17
PG16-11 2123	35.7	8.16	43.3	7.71	2	174.5	0.7	0.79	4	0.26	1.19	340	6	21.6	1.93
PG16-14 2840	26.9	5.9	27.8	5.48	1	471	0.5	0.63	2.93	0.23	0.78	250	1	16.3	1.6
PG16-15 1394	24.1	6.02	87.5	4.3	2	238	0.6	0.46	8.01	0.18	2.16	86	1	14	1.3
PG16-15 1413	24.3	5.97	101	4.52	1	305	0.6	0.55	7.77	0.21	2.27	84	1	14.7	1.5
PG16-15 1487	26.4	6.76	141	4.74	9	19.5	0.6	0.49	8.55	0.16	3.27	96	7	12.1	1.22
HV Basalt 1	33.1	7.9	43.9	6.9	1	850	0.6	0.8	3.89	0.32	1.1	275	<1	21.6	1.83
HV Basalt 2	37.2	9.19	43.4	7.58	1	642	0.7	0.86	4.14	0.3	1.37	232	<1	22.7	1.89
HV Basalt 3	31.2	7.47	40.8	6.45	1	821	0.7	0.74	3.84	0.27	0.99	265	<1	20.5	1.72
HV Basalt 4	27	6.61	47.4	5.82	1	1535	0.6	0.66	3.48	0.24	0.88	190	2	17.9	1.55
WPI - 1	18.5	5.18	28	3.41	1	222	0.7	0.37	10.5	0.17	3.13	78	1	11.7	1.07
PG16-14 2871	59.4	14.05	12.5	12.55	2	208	1	1.49	5.92	0.52	6.41	473	29	46.3	3.11
PG17-18 2082	70.8	18.55	126.5	10.9	1	178.5	0.9	0.98	19.5	0.33	10.1	199	2	23.4	1.96
PG14-05 2562	78.5	20.9	109	12	15	118.5	0.9	0.99	22	0.32	5.15	196	9	25.4	2.03
PG16-24 1906	75.6	20.1	41.8	11.55	1	606	1	0.91	22.1	0.31	4.72	192	1	22.6	1.91
AX-22 1311	96	25.5	111	15	2	175	1.2	1.23	28.2	0.4	15.05	233	14	29.5	2.59
AX39-2106.5	23.8	6.02	82	3.97	1	120.5	0.5	0.4	8.5	0.18	3.17	77	2	10.4	1.15
AX32-1959	38.8	8.84	40	8	2	163	0.7	0.89	4.17	0.3	0.84	366	6	21	1.94
AX39-2045	32.5	7.02	34.8	6.98	1	431	0.5	0.71	3.17	0.25	0.89	307	<1	19.1	1.63
AX25-1970	34.2	7.68	41.1	7.29	2	307	0.5	0.81	3.47	0.3	1.37	309	1	22.4	1.75
AX35-1337.8	24.1	6.02	77.6	4.45	1	153	0.5	0.54	5.53	0.26	6.89	132	3	17.1	1.83
AX18-2072	25	6.31	131	4.76	2	125.5	0.6	0.47	7.83	0.18	2.6	77	2	13.5	1.27
PG1601-1992	35.8	8.98	134.5	6.1	2	39.9	0.9	0.68	9.17	0.34	2.62	168	4	20.1	2.13
AX14-1952	38.8	8.7	42.8	7.81	2	291	0.8	0.84	4.44	0.28	1.94	362	12	19.6	1.88
PG1619-177.5	30.7	7.4	91.3	6.07	2	136.5	0.8	0.69	11.8	0.3	1.91	116	1	19.8	1.81
PG1618-782	25.9	6.27	73.6	4.9	1	337	0.5	0.44	8.02	0.19	2.45	75	1	13.8	1.21
AX39-2100	32.8	7.12	32.3	6.57	1	621	0.6	0.72	3.14	0.23	0.9	293	<1	18.3	1.63
AX8A-1955	41.9	9.43	46.9	8.77	2	196	0.8	0.84	4.8	0.26	1.32	440	12	19.8	1.81
AX18-1938.5	56.5	12.65	40.1	11.3	3	178.5	1.2	1.18	6.51	0.39	3.5	579	108	28.8	2.51
AX8A-1961	23.9	6.23	135	4	4	33.9	1.2	0.43	8.91	0.23	4.95	72	4	14.6	1.53
AX39-2045	32.5	7.02	34.8	6.98	1	431	0.5	0.71	3.17	0.25	0.89	307	<1	19.1	1.63
AX39-2100	32.8	7.12	32.3	6.57	1	621	0.6	0.72	3.14	0.23	0.9	293	<1	18.3	1.63
AX32-1959	38.8	8.84	40	8	2	163	0.7	0.89	4.17	0.3	0.84	366	6	21	1.94
AX18-1938.5	56.5	12.65	40.1	11.3	3	178.5	1.2	1.18	6.51	0.39	3.5	579	108	28.8	2.51
AX8A-1955	41.9	9.43	46.9	8.77	2	196	0.8	0.84	4.8	0.26	1.32	440	12	19.8	1.81
AX8A-1961	23.9	6.23	135	4	4	33.9	1.2	0.43	8.91	0.23	4.95	72	4	14.6	1.53
CHV-2	28.3	7	84.3	4.78	2	552	0.8	0.56	9.59	0.26	1.9	92	1	15.2	1.54
NW-2	25	6.2	69.7	4.21	1	596	0.6	0.47	7.55	0.17	1.51	65	1	13	1.28
NS-2	23.6	6.02	80.2	4.32	3	363	1.1	0.59	8.44	0.24	3.51	62	2	15.8	1.7

SampleID	Zr_ppm	Ag_ppm	Cd_ppm	Co_ppm	Cu_ppm	Li_ppm	Mo_ppm	Ni_ppm	Pb_ppm	Sc_ppm	Zn_ppm	As_ppm	Bi_ppm	Hg_ppm	In_ppm
PG16-02 1600	173	<0.5	<0.5	34	42	30	1	213	7	23	87	208	0.04	0.534	0.051
PG16-10 1745	201	4.6	0.5	35	42	<10	1	218	16	17	72	>250	0.07	11.35	0.049
PG16-11 2123	164	<0.5	<0.5	45	59	30	2	187	5	26	146	81.8	0.05	0.18	0.076
PG16-14 2840	116	<0.5	<0.5	38	43	20	<1	145	3	22	86	2.3	0.04	0.01	0.029
PG16-15 1394	173	<0.5	<0.5	8	7	50	<1	7	11	7	72	2.2	0.05	0.126	0.028
PG16-15 1413	155	0.5	<0.5	8	2	30	1	4	10	8	66	2.2	0.07	0.215	0.022
PG16-15 1487	189	9.9	<0.5	9	64	10	1	7	56	8	42	>250	0.89	1.495	0.026
HV Basalt 1	143	<0.5	0.6	34	61	20	3	155	16	20	131	2.9	0.04	0.023	0.017
HV Basalt 2	155	<0.5	<0.5	37	34	20	<1	141	8	25	107	2.8	0.06	0.021	0.03
HV Basalt 3	146	<0.5	<0.5	32	38	20	<1	153	6	22	106	1	0.01	0.015	0.015
HV Basalt 4	130	<0.5	<0.5	31	34	10	<1	101	2	20	83	1.7	0.02	0.021	0.026
WPI - 1	151	<0.5	<0.5	6	7	20	<1	11	<2	6	3	46	0.23	0.024	0.014
PG16-14 2871	237	<0.5	<0.5	56	81	110	<1	204	11	34	32	5.6	0.1	0.072	0.083
PG17-18 2082	163	8	<0.5	30	59	<10	1	92	15	26	136	225	0.1	0.506	0.053
PG14-05 2562	181	13.1	22.3	58	447	20	1	77	1405	22	2160	108	5.2	0.066	0.324
PG16-24 1906	176	<0.5	<0.5	34	49	50	2	83	14	22	72	12.9	0.09	0.025	0.06
AX-22 1311	224	<0.5	<0.5	36	21	20	2	95	18	28	78	>250	0.32	2.99	0.073
AX39-2106.5	178	<0.5	<0.5	12	9	90	2	16	17	7	74	185	0.09	0.079	0.033
AX32-1959	155	<0.5	<0.5	45	63	30	2	177	10	28	106	>250	0.05	0.012	0.072
AX39-2045	138	<0.5	<0.5	27	52	10	1	121	7	24	97	5.3	0.03	0.011	0.056
AX25-1970	134	<0.5	0.5	54	55	20	2	216	12	28	99	20.4	0.04	0.018	0.074
AX35-1337.8	149	<0.5	<0.5	38	14	10	2	187	10	17	84	>250	0.08	0.888	0.04
AX18-2072	177	<0.5	<0.5	9	13	30	1	6	14	8	67	25.8	0.13	0.106	0.032
PG1601-1992	207	10.5	<0.5	38	41	<10	1	253	14	19	61	>250	0.04	1.39	0.038
AX14-1952	144	<0.5	0.5	46	62	30	1	177	8	33	170	26.2	0.04	0.037	0.083
PG1619-177.5	199	<0.5	<0.5	13	34	60	1	33	26	14	398	12.2	0.32	0.463	0.058
PG1618-782	164	<0.5	<0.5	7	4	30	1	3	16	8	69	1.5	0.02	0.014	0.029
AX39-2100	130	<0.5	<0.5	37	52	10	1	152	8	24	108	2.7	0.04	0.013	0.04
AX8A-1955	193	<0.5	<0.5	47	74	90	1	190	8	30	111	71.3	0.04	0.699	0.095
AX18-1938.5	261	0.5	<0.5	48	102	300	2	212	11	37	252	84.9	0.1	0.024	0.114
AX8A-1961	178	1.4	<0.5	10	5	40	1	14	2	7	43	>250	0.29	8.64	0.016
AX39-2045	138	<0.5	<0.5	27	52	10	1	121	7	24	97	5.3	0.03	0.011	0.056
AX39-2100	130	<0.5	<0.5	37	52	10	1	152	8	24	108	2.7	0.04	0.013	0.04
AX32-1959	155	<0.5	<0.5	45	63	30	2	177	10	28	106	>250	0.05	0.012	0.072
AX18-1938.5	261	0.5	<0.5	48	102	300	2	212	11	37	252	84.9	0.1	0.024	0.114
AX8A-1955	193	<0.5	<0.5	47	74	90	1	190	8	30	111	71.3	0.04	0.699	0.095
AX8A-1961	178	1.4	<0.5	10	5	40	1	14	2	7	43	>250	0.29	8.64	0.016
CHV-2	225	<0.5	<0.5	8	2	30	1	<1	15	10	76	0.6	0.03	0.021	0.023
NW-2	160	<0.5	<0.5	7	3	30	1	<1	14	7	87	0.4	0.01	0.01	0.024
NS-2	184	<0.5	<0.5	9	3	40	<1	13	8	8	38	0.3	0.02	0.019	0.021

SampleID	Re_ppm	Sb_ppm	Sc_ppm	Se_ppm	Te_ppm	Tl_ppm	S_pct	C_pct	Lab Used	Rock Type
PG16-02 1600	0.001	1.9	8.7	<0.2	<0.01	2.89	5.49	2.01	ALS	basaltic andesite
PG16-10 1745	0.001	22.4	3.4	0.2	0.01	15.7	5.41	1.57	ALS	basaltic andesite
PG16-11 2123	<0.001	37	24.1	0.2	0.01	0.41	0.06	0.57	ALS	basalt sill
PG16-14 2840	<0.001	2.06	3.3	<0.2	<0.01	0.06	0.02	2.62	ALS	basalt sill
PG16-15 1394	0.001	0.2	3.4	<0.2	<0.01	0.32	0.09	1.55	ALS	Eocene granodiorite
PG16-15 1413	<0.001	0.43	2.7	<0.2	<0.01	0.13	0.22	1.47	ALS	Eocene granodiorite
PG16-15 1487	<0.001	26.9	0.4	0.8	0.03	2.92	3.95	0.02	ALS	Eocene granodiorite
HV Basalt 1	<0.001	0.25	3.6	<0.2	<0.01	0.08	0.01	0.02	ALS	Hidden Valley basalt
HV Basalt 2	<0.001	0.27	7.9	<0.2	0.01	0.13	0.02	0.03	ALS	Hidden Valley basalt
HV Basalt 3	<0.001	0.27	3.4	<0.2	<0.01	0.04	0.01	0.03	ALS	Hidden Valley basalt
HV Basalt 4	<0.001	0.11	6.2	<0.2	<0.01	0.08	0.02	0.45	ALS	Hidden Valley basalt
WPI - 1	<0.001	0.36	3.4	<0.2	<0.01	0.47	0.02	0.02	ALS	Eocene granodiorite
PG16-14 2871	<0.001	12	27.8	<0.2	<0.01	0.19	0.27	0.06	ALS	basalt sill
PG17-18 2082	0.001	14.3	12.4	0.2	<0.01	0.67	6.04	2.79	ALS	Fire dike
PG14-05 2562	<0.001	10	9.4	5.6	0.34	0.28	5.6	1.34	ALS	Fire dike
PG16-24 1906	<0.001	1.72	15.3	<0.2	0.01	0.09	0.62	1.8	ALS	Fire dike
AX-22 1311	<0.001	7.4	16.6	<0.2	0.01	15.7	1.35	2.11	ALS	Fire dike
AX39-2106.5	0.001	2.41	3	<0.2	<0.01	0.12	2.11	0.75	ALS	Eocene granodiorite
AX32-1959	0.001	4.1	19.4	0.2	<0.01	0.11	0.21	1.13	ALS	basalt sill
AX39-2045	0.001	14.1	14.1	<0.2	<0.01	0.04	0.02	1.29	ALS	basalt sill
AX25-1970	0.002	3.83	18.1	0.4	<0.01	0.26	0.16	2.25	ALS	basalt sill
AX35-1337.8	0.003	9.17	10.8	0.7	0.01	9.16	2.49	4.25	ALS	basaltic andesite
AX18-2072	<0.001	2.78	4.8	<0.2	<0.01	0.34	2.04	0.99	ALS	Eocene granodiorite
PG1601-1992	<0.001	27.8	3.8	0.2	<0.01	8.09	5.23	1.03	ALS	basaltic andesite
AX14-1952	0.001	21.4	18.9	<0.2	<0.01	0.38	0.15	0.07	ALS	basalt sill
PG1619-177.5	0.001	0.35	12.5	<0.2	0.03	1.48	0.01	0.05	ALS	Unk
PG1618-782	<0.001	0.06	5.5	<0.2	<0.01	0.18	<0.01	0.83	ALS	Eocene granodiorite
AX39-2100	0.001	7.77	5.7	0.2	<0.01	0.06	0.01	1.6	ALS	basalt sill
AX8A-1955	<0.001	16.05	24.3	0.2	<0.01	0.88	0.08	0.31	ALS	basalt sill
AX18-1938.5	0.001	112	18.7	0.4	<0.01	0.26	1.29	0.06	ALS	basalt sill
AX8A-1961	0.001	17.25	0.8	0.7	<0.01	14.05	2.12	0.02	ALS	Eocene granodiorite
AX39-2045	0.001	14.1	14.1	<0.2	<0.01	0.04	0.02	1.29	ALS	basalt sill
AX39-2100	0.001	7.77	5.7	0.2	<0.01	0.06	0.01	1.6	ALS	basalt sill
AX32-1959	0.001	4.1	19.4	0.2	<0.01	0.11	0.21	1.13	ALS	basalt sill
AX18-1938.5	0.001	112	18.7	0.4	<0.01	0.26	1.29	0.06	ALS	basalt sill
AX8A-1955	<0.001	16.05	24.3	0.2	<0.01	0.88	0.08	0.31	ALS	basalt sill
AX8A-1961	0.001	17.25	0.8	0.7	<0.01	14.05	2.12	0.02	ALS	Eocene granodiorite
CHV-2	<0.001	0.07	4.2	<0.2	0.01	0.09	0.01	0.01	ALS	Hidden Valley GD
NW-2	<0.001	<0.05	3.7	0.2	0.02	0.07	<0.01	0.15	ALS	NW Intrusion
NS-2	<0.001	0.05	3.7	<0.2	0.04	0.05	0.01	0.4	ALS	North Star Dike

Appendix B.
Interpreted Mineralogy from SWIR Hyperspectral Imaging

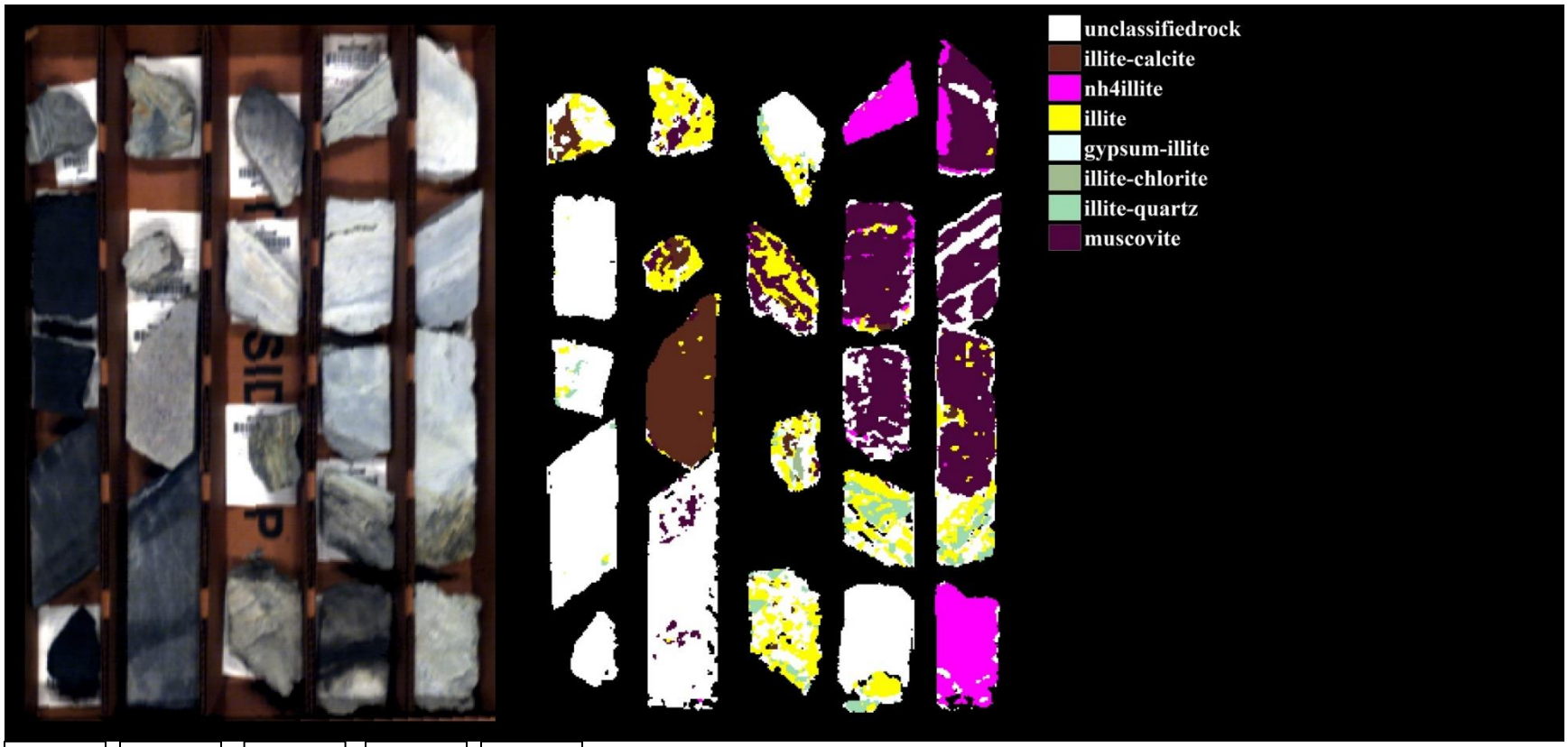

AX12-1163 AX12-1717.7 AX12-1713 AX12-1708.3 AX12-1704	AX12-1174.8 AX12-1170.2 AX12-1145.5 AX12-1751	AX12-1222.6 AX12-1198 AX12-1188 AX12-1178	AX12-1236 AX12-1234.8 AX12-1223 AX12-1228.6 AX12-1224	AX12-1251.4 AX12-1249.6 AX12-1244 AX12-1239.7

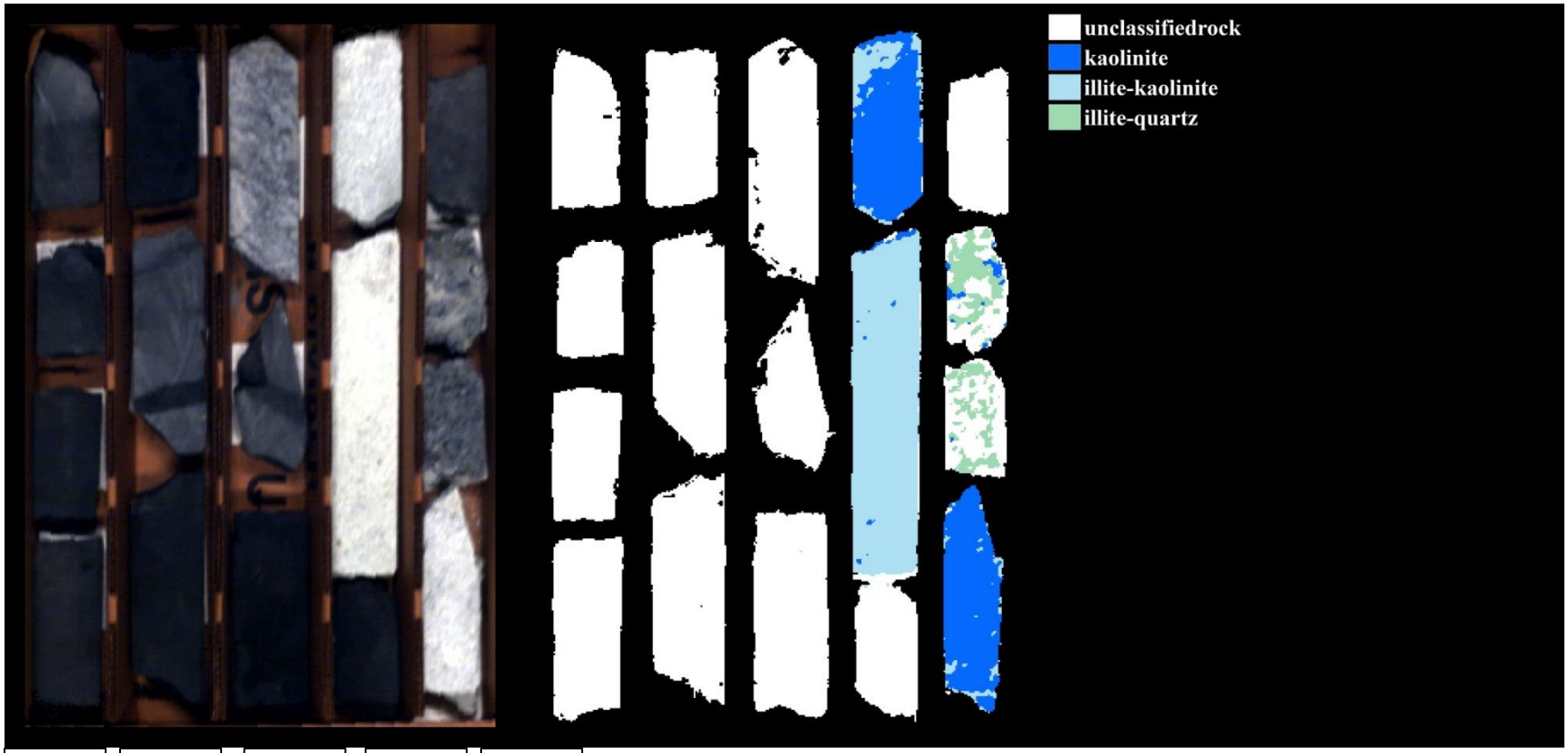

AX31-1931 AX31-1930 AX31-1928.5 AX31-1927.8	AX31-1946 AX31-1936 AX31-1932.7	AX31-2112.4 AX31-1948.3 AX31-1942	AX31-2144 AX31-2138.5 AX31-2128.3	AX31-2154 AX31-2148.3 AX31-2147.5 AX31-2143

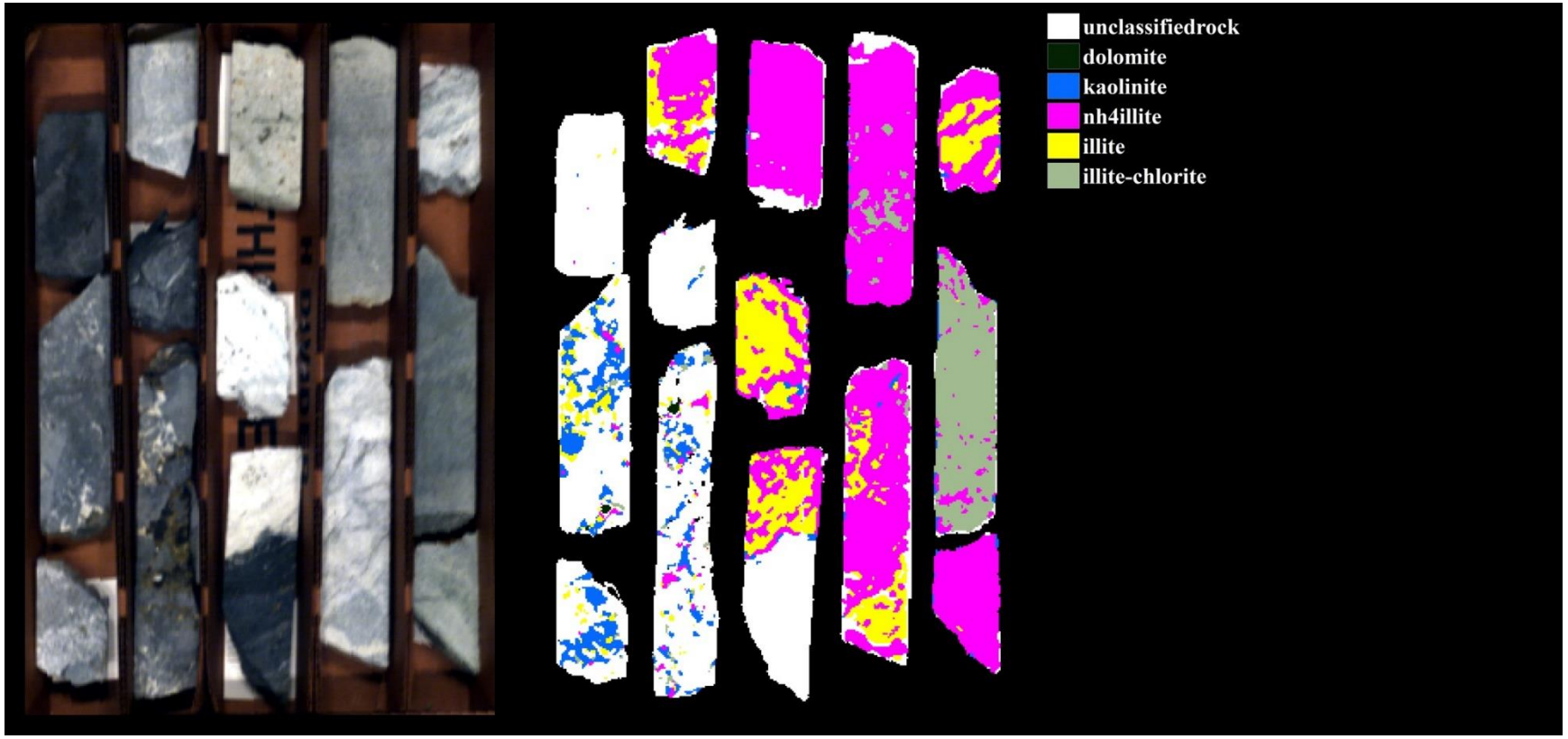

AX53-2424 AX53-2409.5 AX53-2404	AX53-2458.2 AX53-2430.5 AX53-2410.5	AX53-2467 AX53-2455 AX53-2454	AX53-2460 AX53-2457.5	AX53-2483 AX53-2481 AX53-2477.4

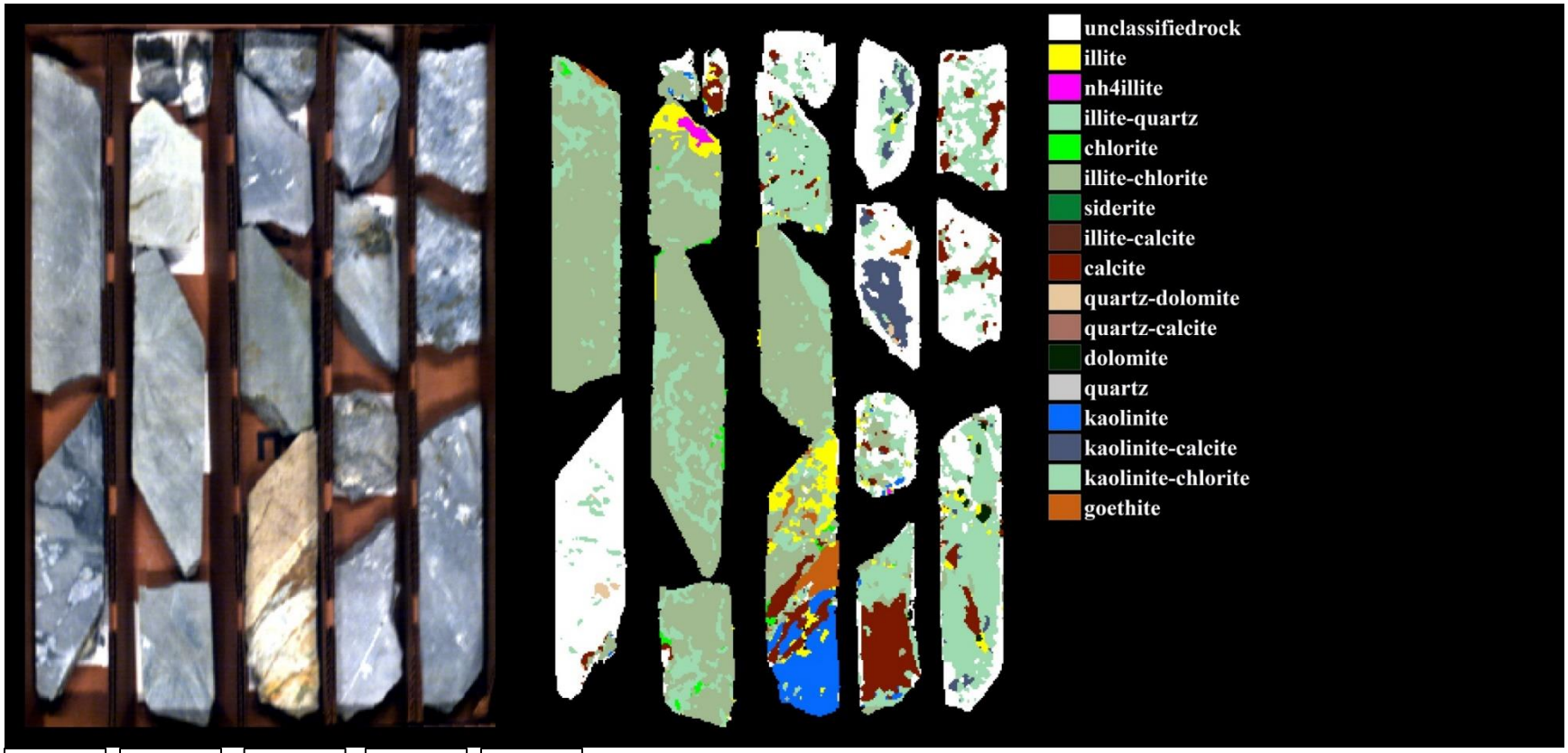

AX53-1920 AX53-1918	AX53-2386.5 AX53-1938.3 AX53-1926 AX53-1924.8	AX53-2393 AX53-2363.7 AX53-1947 AX53-1943	AX53-2378 AX53-2376 AX53-2373 AX53-2367	AX53-2396.3 AX53-2393.9 AX53-2383

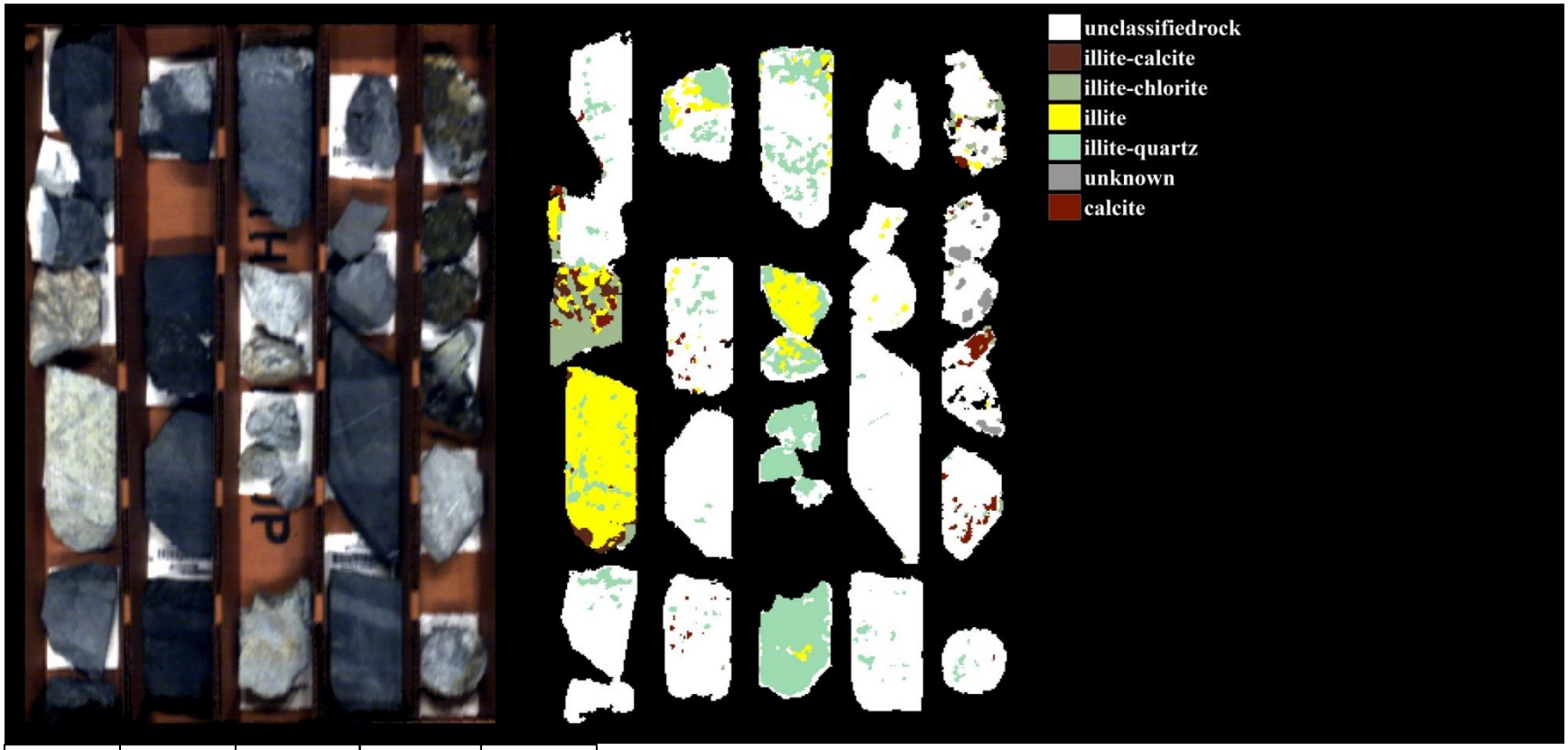

PG1415-1887 PG1415-1882 PG1415-1881.3 PG1415-1876 PG1415-1872	PG1415-1717.9 PG1415-1717 PG1415-1714 PG1415-1893.3	PG1415-1730.6 PG1415-1728.6 PG1415-1722 PG1415-1718.3	PG1423-2156.5 PG1423-2150.5 PG1423-1742 PG1423-1734.8	PG1423-2240.1 PG1423-2233 PG1423-2192 PG1423-2168 PG1423-2157.2

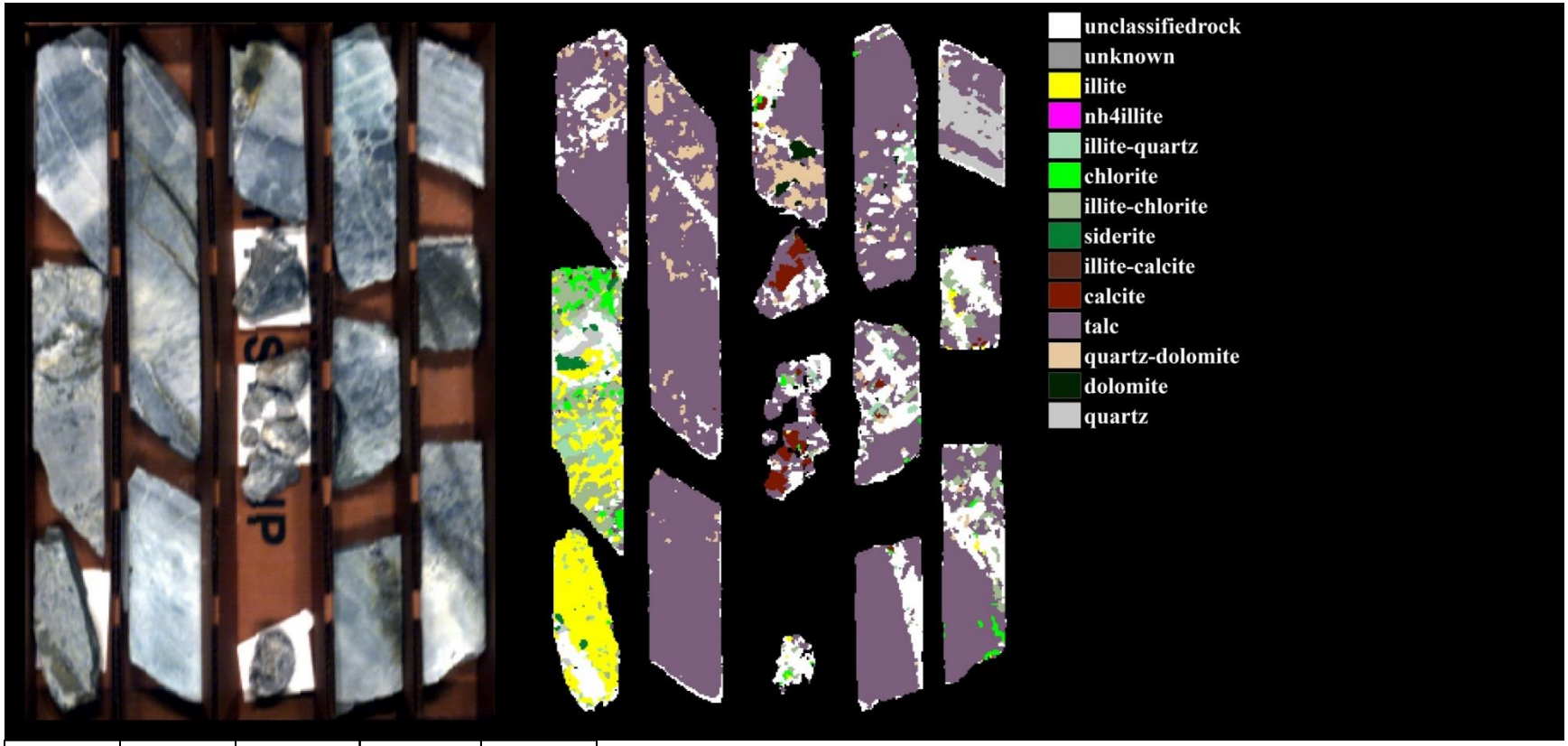

PG1415-2179.5 PG1415-2616.5 PG1415-2609	PG1415-2044 PG1415-2184	PG1415-2235.5 PG1415-2234 PG1415-2244 PG1415-2218.5	PG1415-2242 PG1415-2240.7 PG1415-2236	PG1415-2257.3 PG1415-2244 PG1415-2243.5

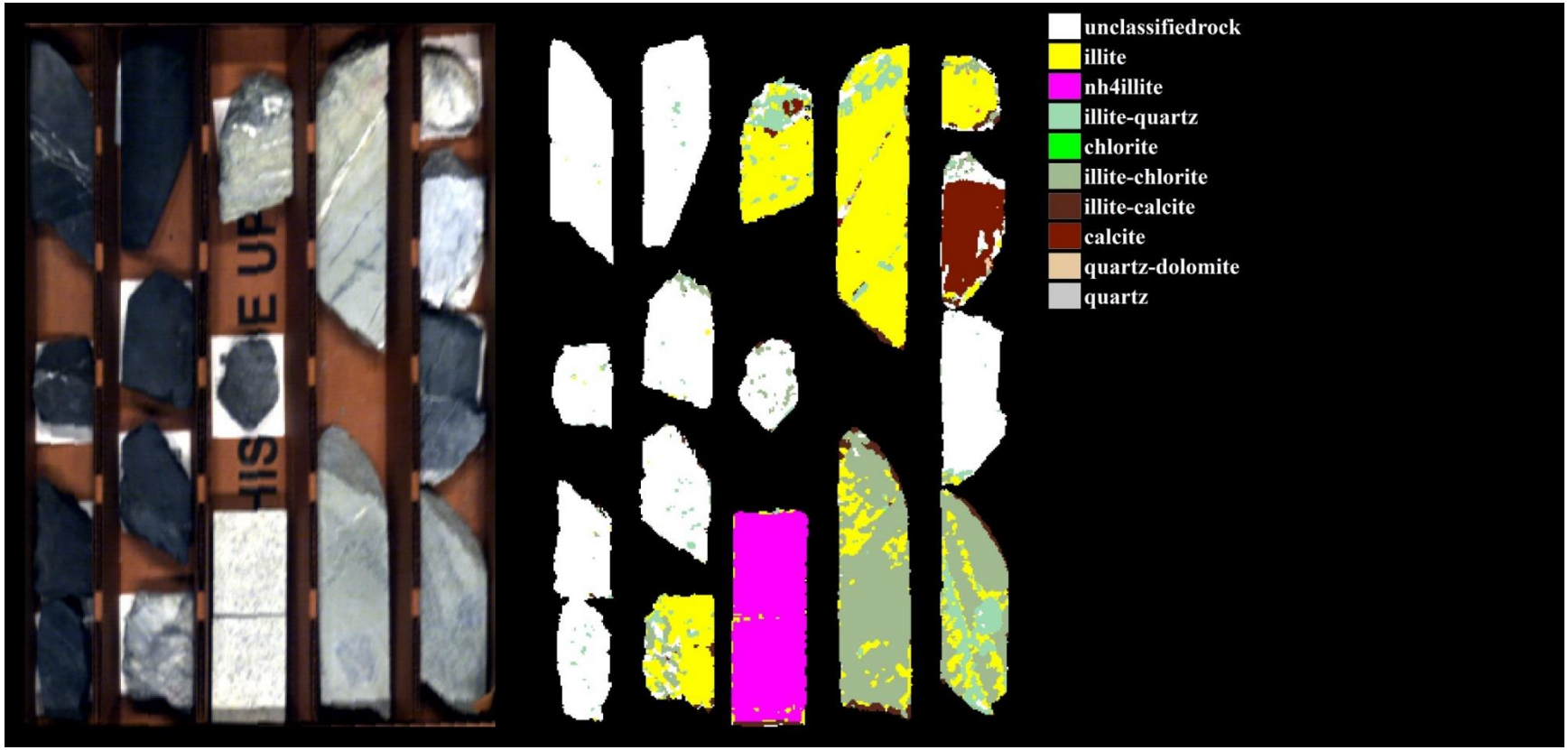

PG1415-1862.7 PG1415-1863 PG1415-1864.2 PG1415-1865.7	PG1415-1855 PG1415-1859.3 PG1415-1860 PG1415-1861.1	PG1415-1949.7 PG1415-1980.5 PG1415-3084	PG1415-1944 PG1415-1947.5	PG1415-1935.4 PG1415-1940.4 PG1415-1943.6 PG1415-1948.5

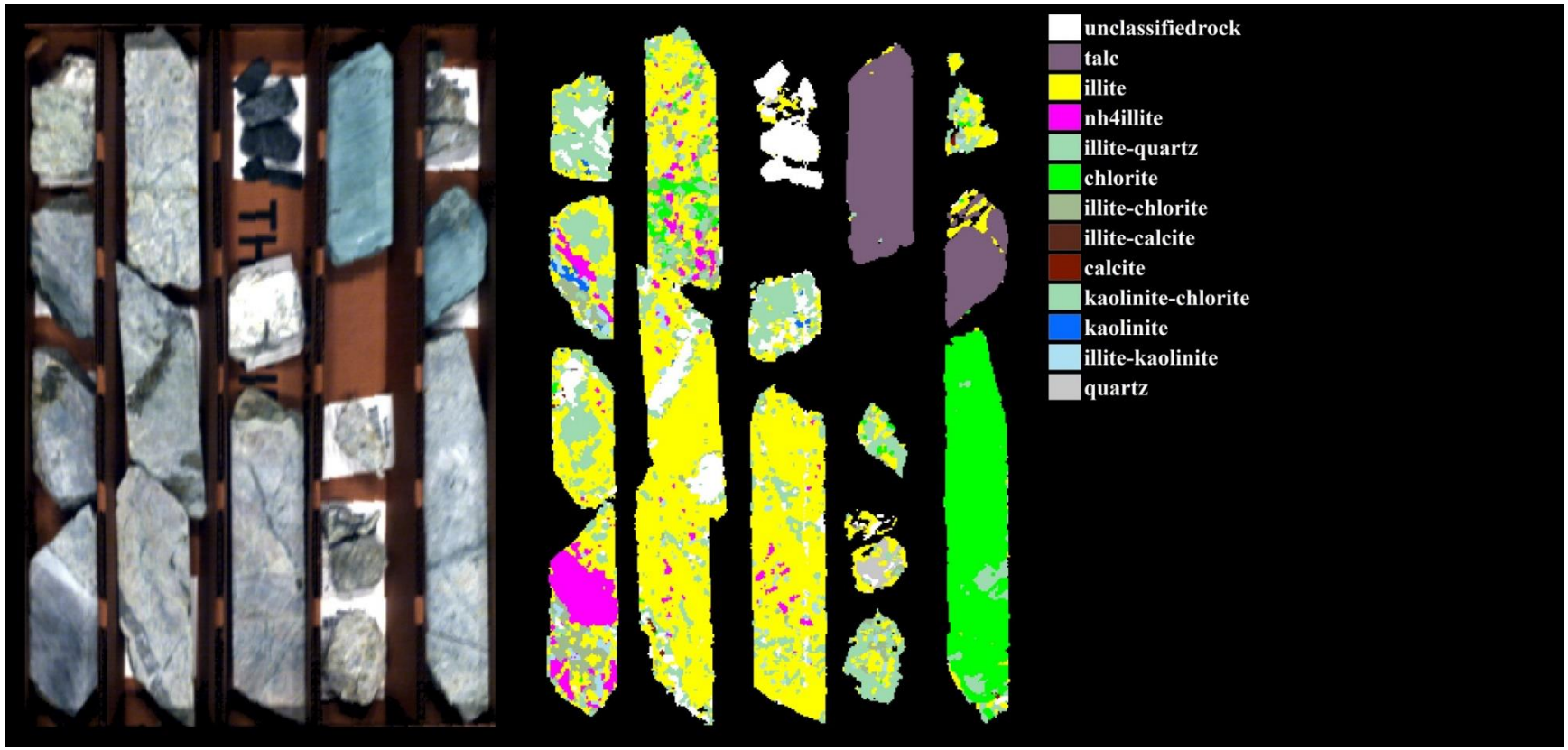

PG1415-3012.8 PG1415-3381.8 PG1415-3374.2 PG1415-3369.7	PG1415-3000.7 PG1415-3383.4 PG1415-3382.7	PG1415-3015.4 PG1415-3012 PG1415-3385.5	PG1415-2422.5 PG1415-3024 PG1415-3022.8 PG1415-3020.7	PG1415-2456.5 PG1415-2422.7 PG1415-2417

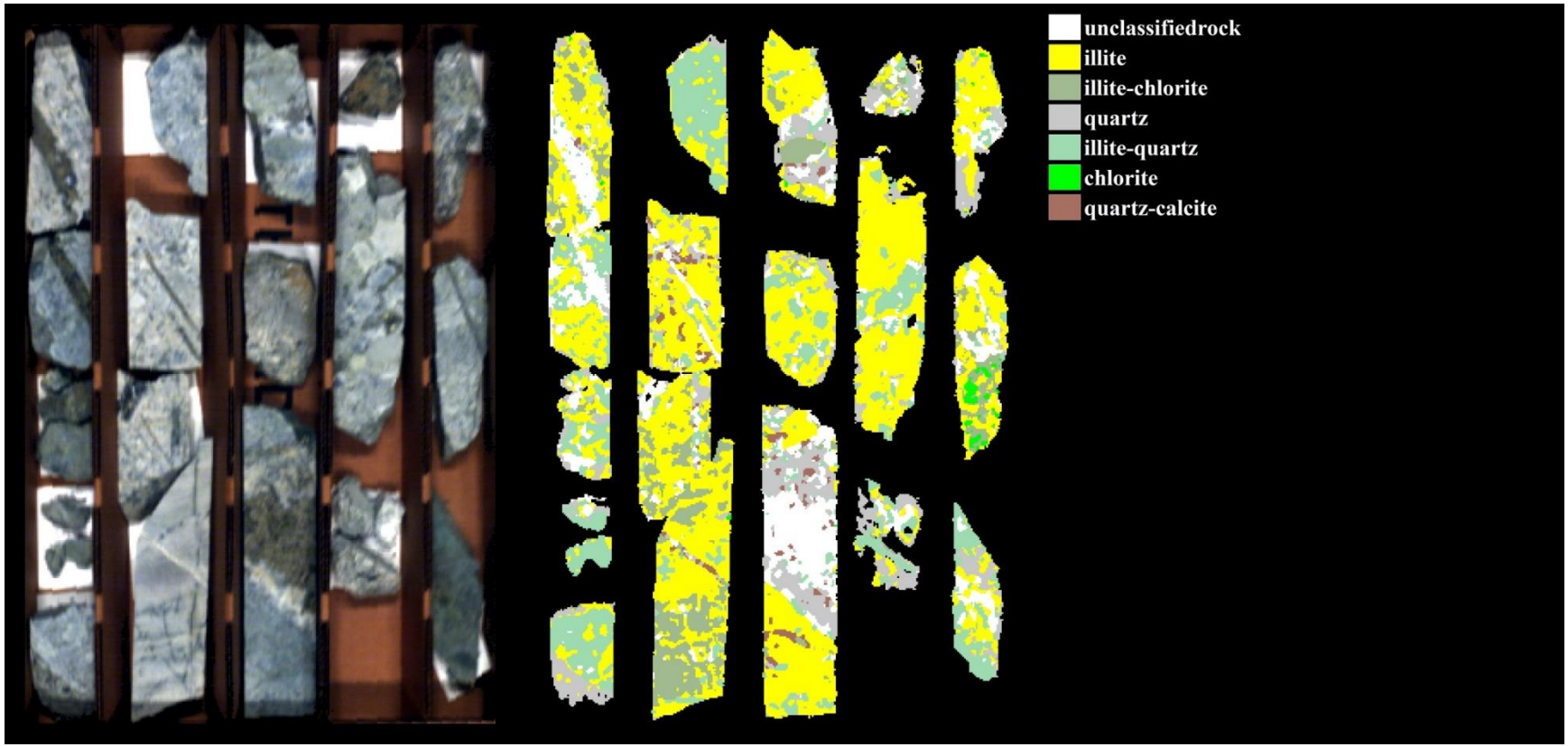

PG1415-2491 PG1415-2463.3 PG1415-2462 PG1415-2460.5 PG1415-2459	PG1415-2519.5 PG1415-2492 PG1415-2487.4 PG1415-2486.5	PG1415-2557 PG1415-2530 PG1415-2513.6	PG1415-2599.3 PG1415-2542.5 PG1415-2530.6	PG1415-2608.5 PG1415-2587.4 PG1415-2573.3

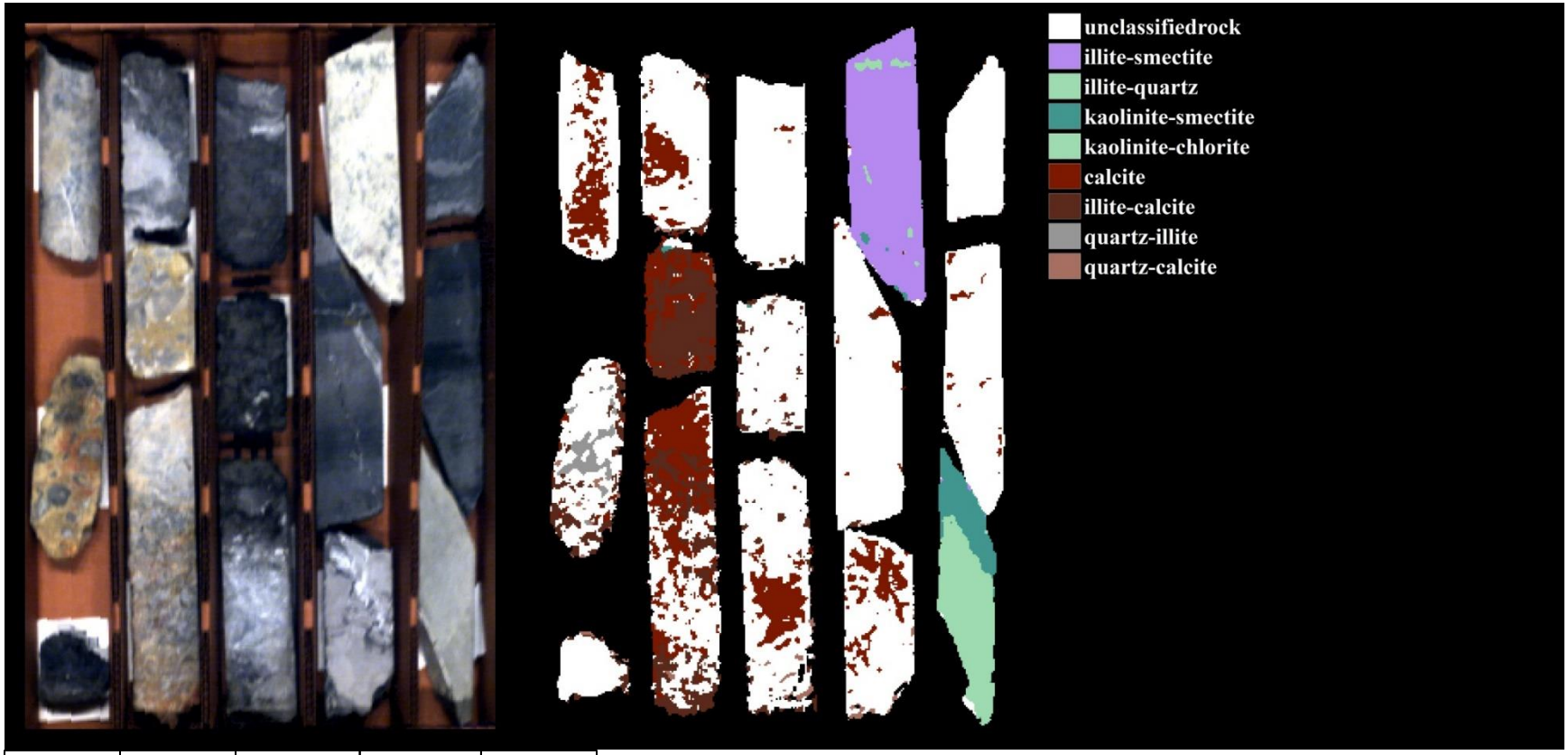

AX35-1560.5 AX35-1543.7 AX35-1521.4	AX35-1578 AX35-1562.2 AX35-1555.5	AX35-1588.3 AX35-1583 AX35-1570	AX35-1790.5 AX35-1780 AX35-1591.2	AX35-1958.5 AX35-1800 AX35-1792.7

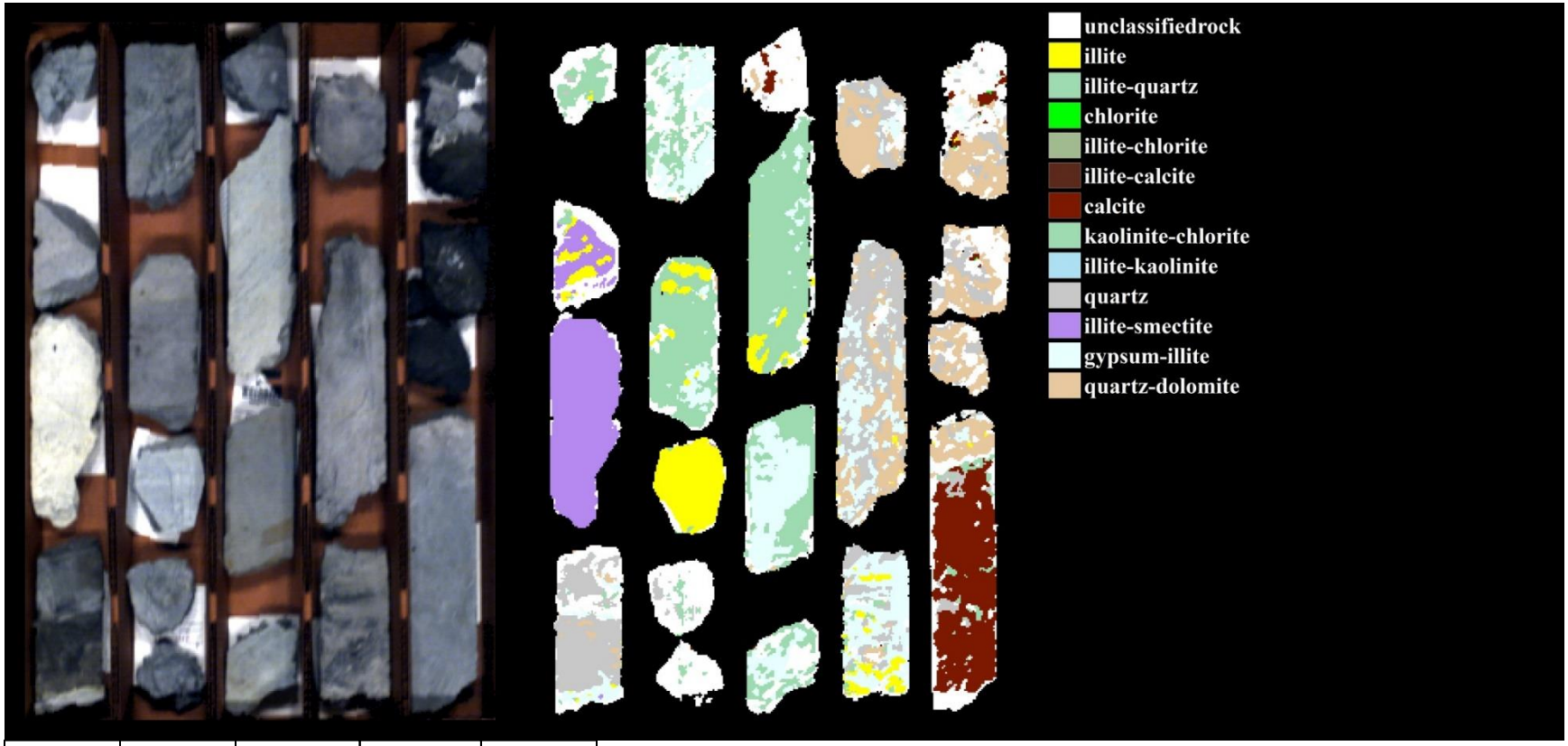

AX35-1375	AX35-1388.5	AX35-1494	AX35-1508	AX35-1519.6
AX35-1362.1	AX35-1385.5	AX35-1408.5	AX35-1426.7	AX35-1518.6
AX35-1371.6	AX35-1366	AX35-1404	AX35-1411.5	AX35-1430.5
AX35-1360.8	AX35-1379	AX35-1393.2		

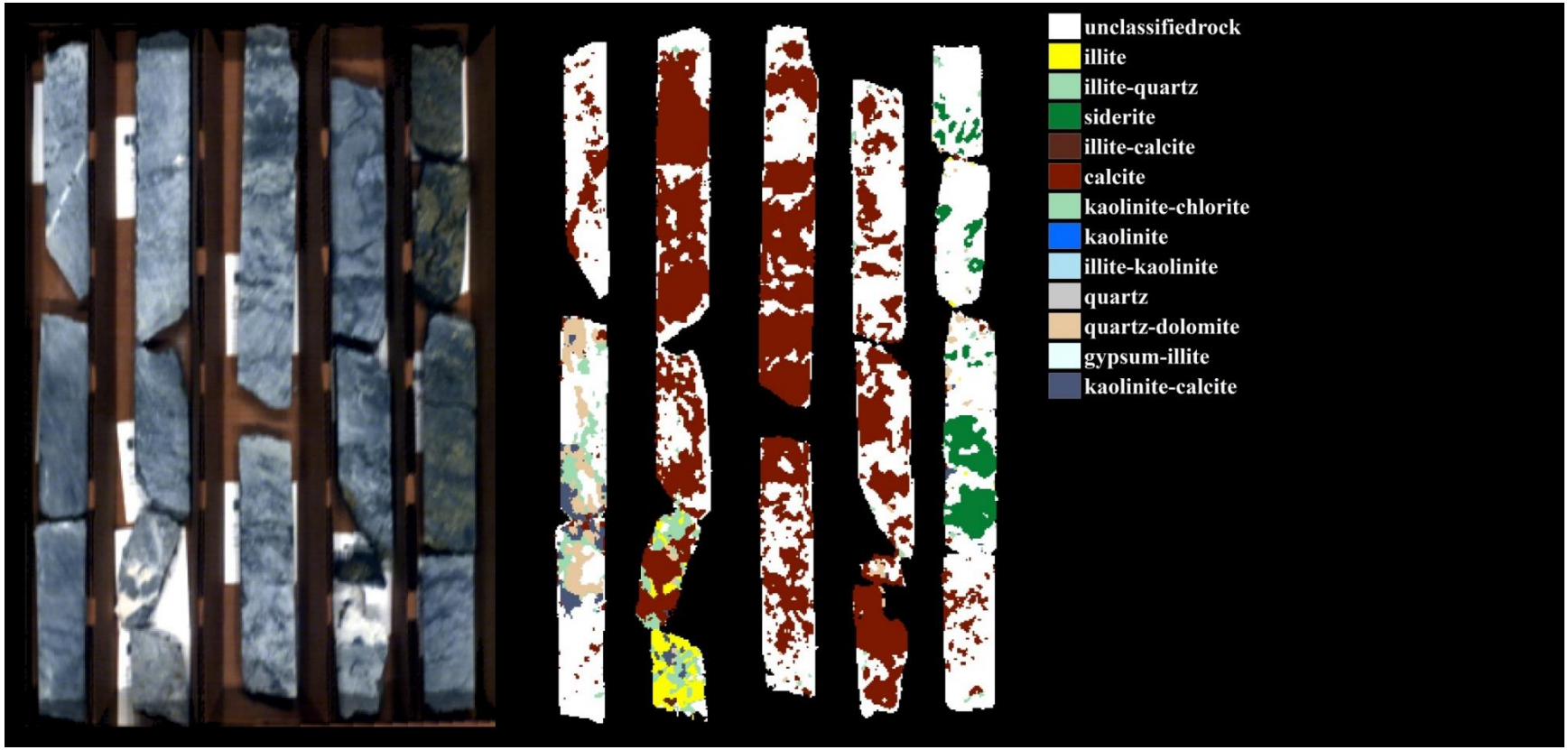

AX46-2110.5 AX46-2102.5 AX46-2101.8	AX46-2140.5 AX46-2134.9 AX46-2130.3 AX46-2119.5	AX46-2173 AX46-2153.5	AX46-2192 AX46-2182 AX46-2178	AX46-2204.2 AX46-2203.3 AX46-2202.2 AX46-2198

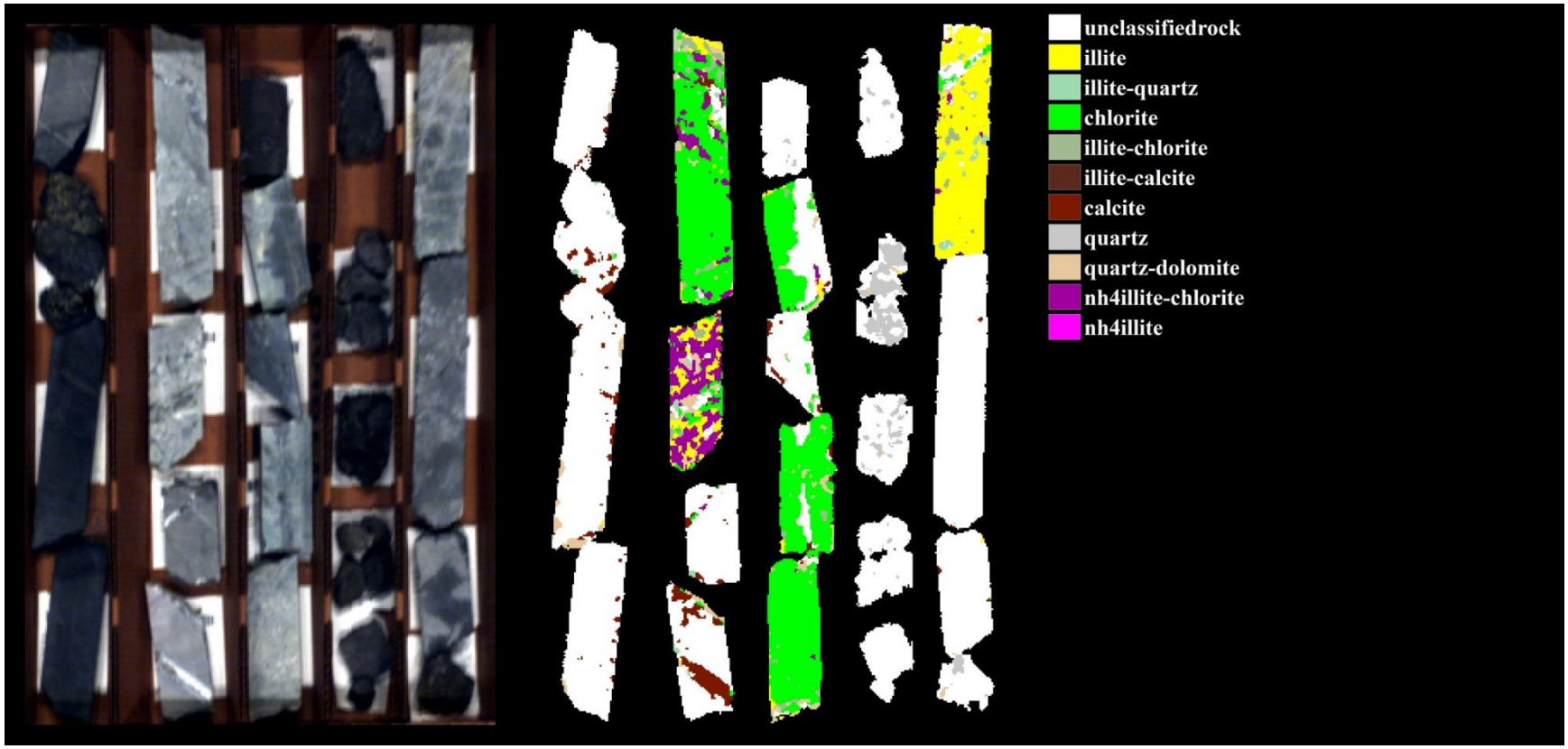

PG1405-1967.5 PG1405-1957 PG1405-1919.5 PG1405-1908.7	PG1405-2292 PG1405-2279 PG1405-1993 PG1405-1989.3	PG1405-1417 PG1405-2296.5 PG1405-2294.3 PG1405-2294 PG1405-2293.8	PG1405-1438.5 PG1405-1437 PG1405-1431.5 PG1405-1425 PG1405-1420	AX46-2888 PG1405-1475 PG1405-1445 PG1405-1439

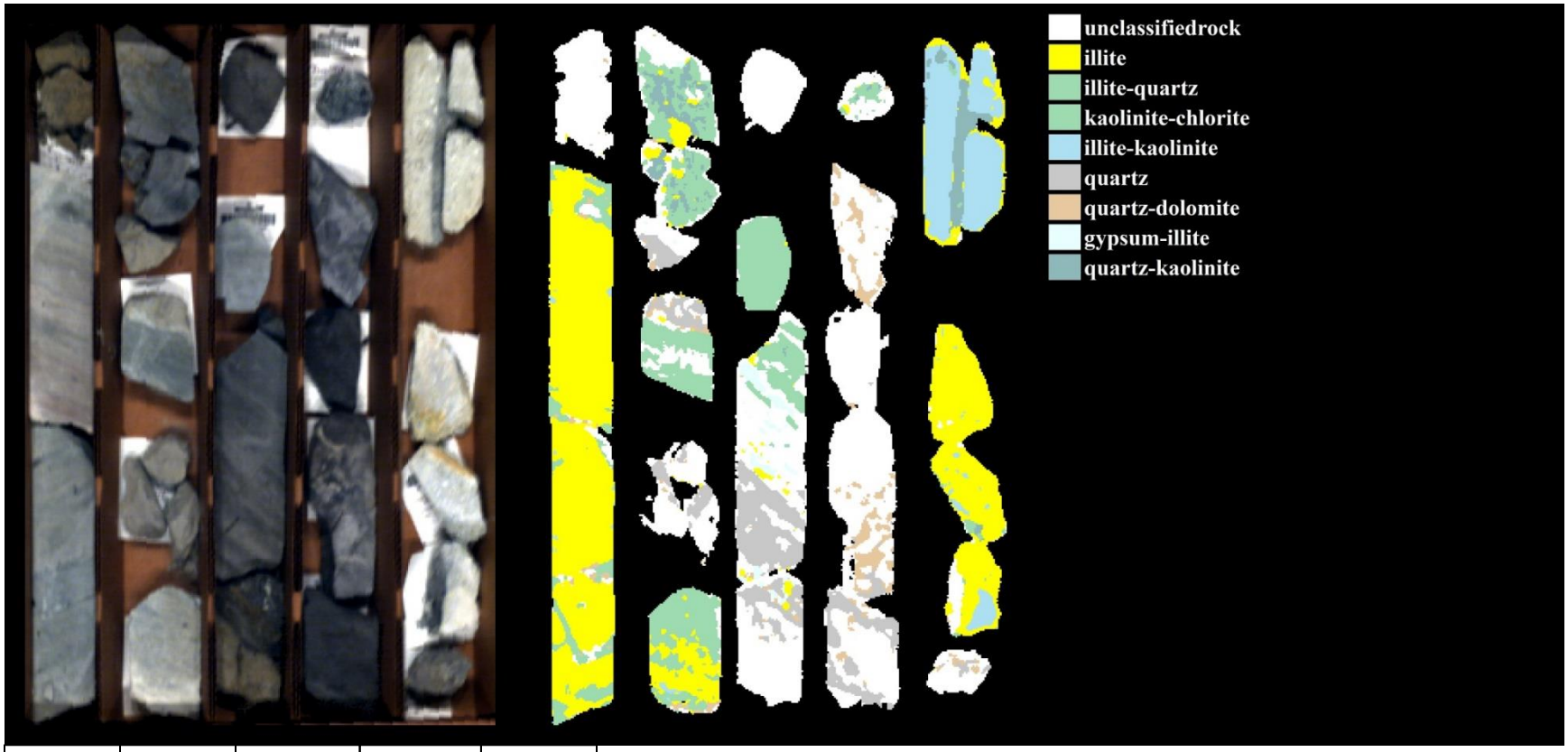

AX46-1252	AX46-1272.5	AX46-1312	AX46-1328	AX46-1354
AX46-1236	AX46-1268	AX46-1303.4	AX46-1320.8	AX46-1335.8
AX46-1238	AX46-1267	AX46-1298	AX46-1315.5	AX46-1334.5
	AX46-1262.3	AX46-1280	AX46-1314.1	AX46-1329.5
			AX46-1312.8	AX46-1326.2

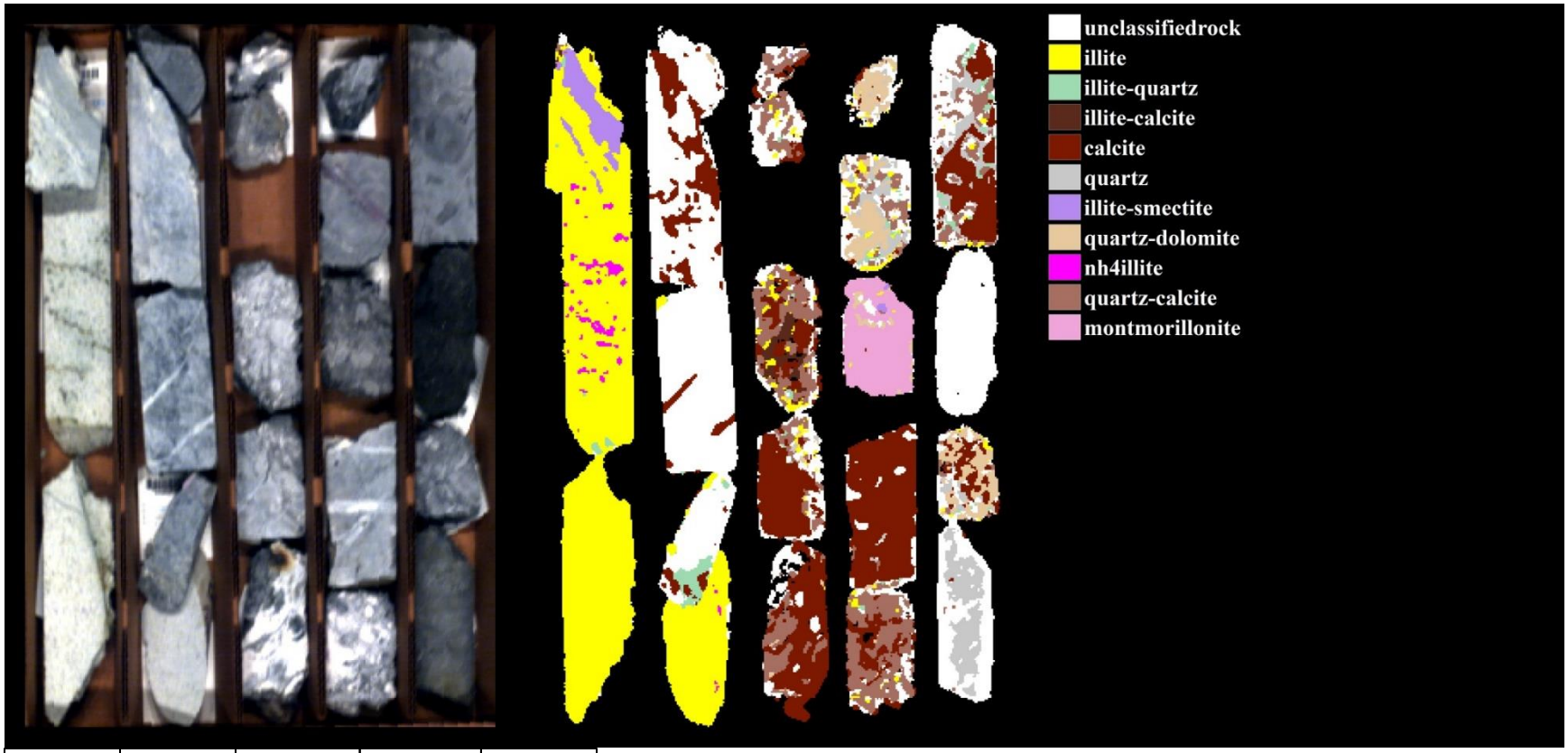

PG1403-2830.2 PG1403-2818.3 PG1403-2808	PG1403-2041.5 PG1403-2858.7 PG1403-2855 PG1403-2846.5 PG1403-2838	PG01-2526.3 PG01-2525 PG01-2523.5 PG01-2522.8	PG01-2023 PG01-2016 PG01-2013 PG01-2529.4 PG01-2527	PG01-2064.5 PG01-2044 PG01-2043 PG01-2034.5

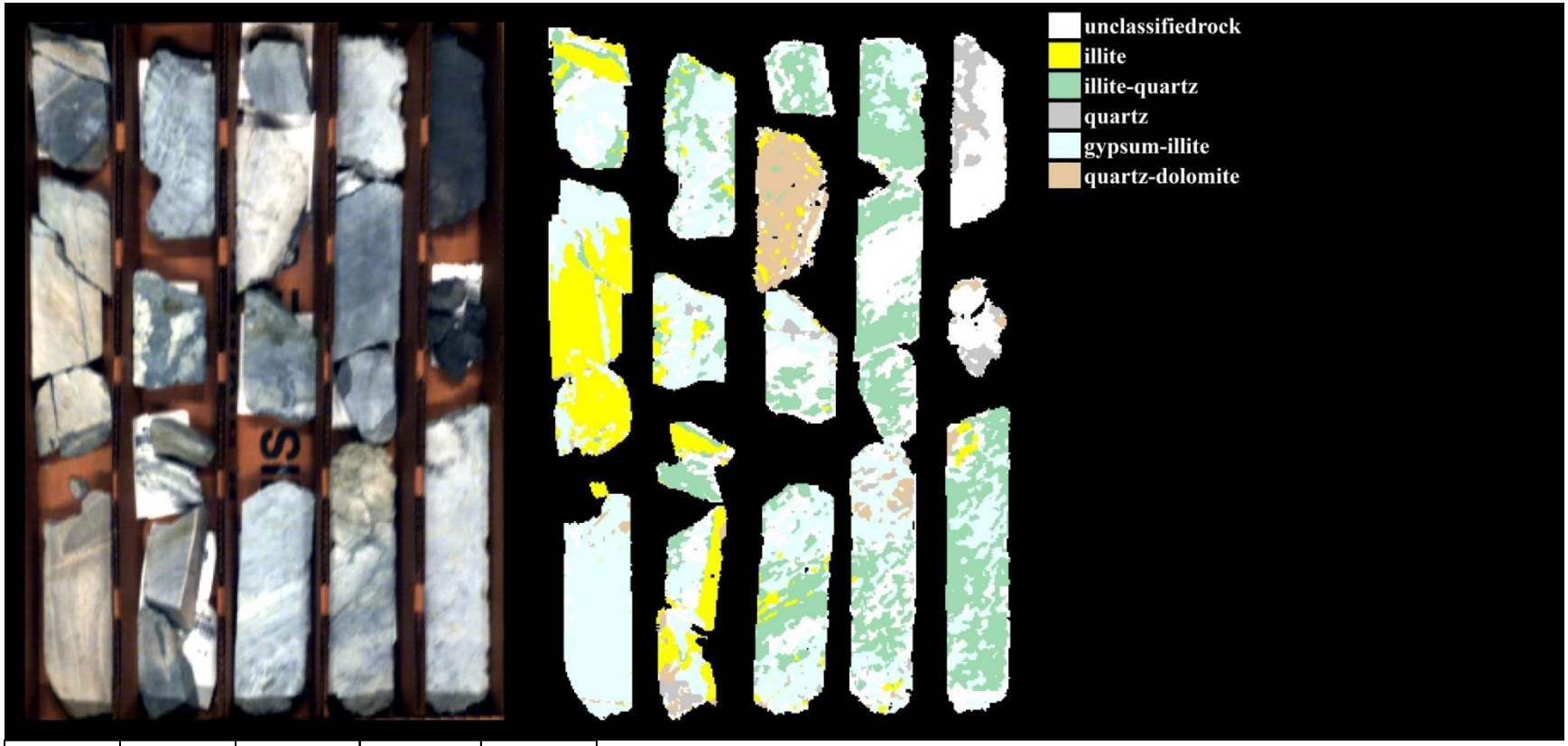

PG1404-1284 PG1404-1283 PG1404-1279 PG1404-1251	PG1404-1328.8 PG1404-1321 PG1404-1302.5 PG1404-1296.5 PG1404-1285.8	PG1404-1459.8 PG1404-1455.5 PG1404-1336.3 PG1404-1326.5	PG1404-1494.5 PG1404-1464 PG1404-1462 PG1404-1337	PG1404-1518.5 PG1404-1520 PG1404-1493.5

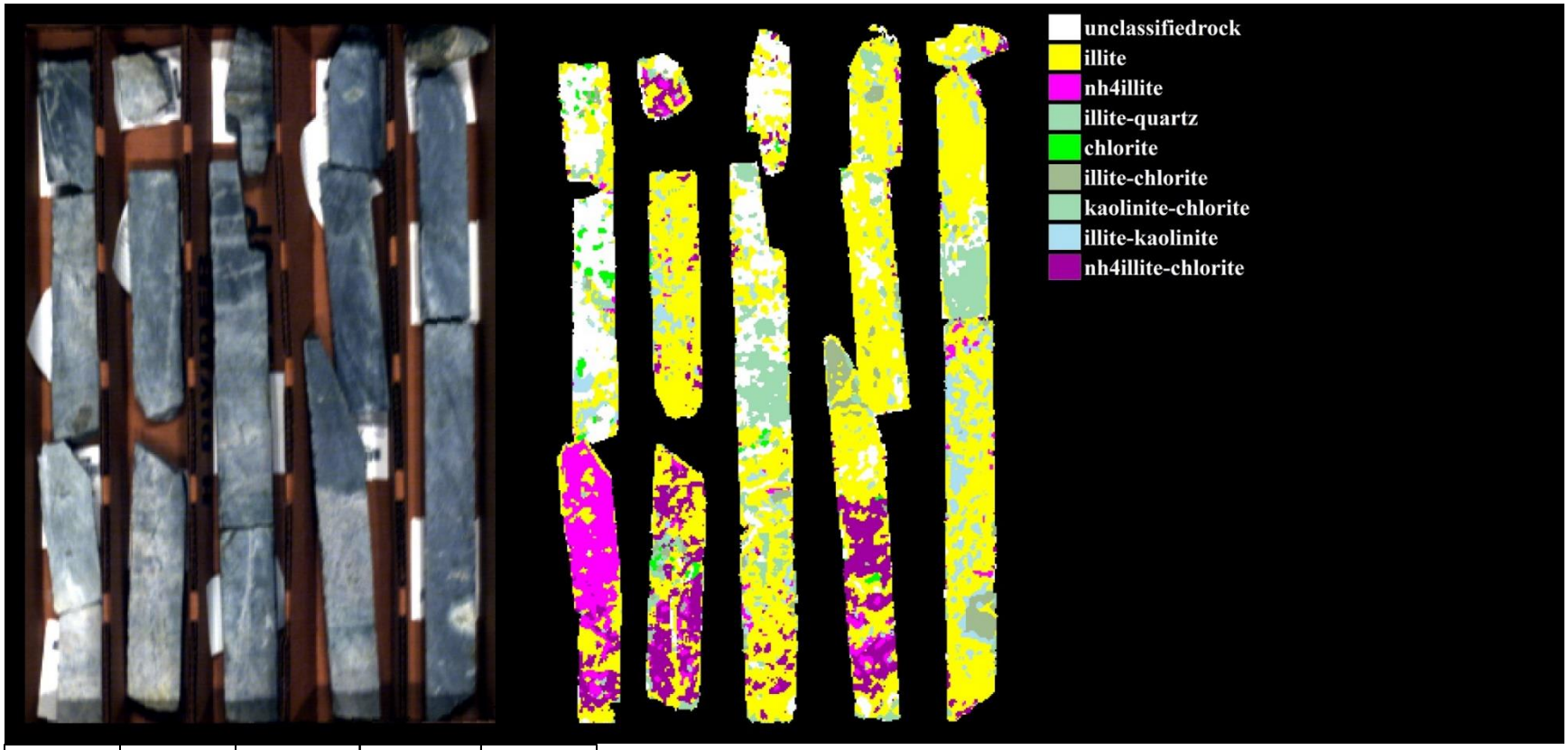

AX46-2889.7 AX46-2883 AX46-2881.5 AX46-2879	AX46-2943.5 AX46-2894.7 AX46-2894	AX46-2240.3 AX46-2900.2 AX46-2895.3	AX46-2926.5 AX46-2920.5 AX46-2899	AX46-2985 AX46-2925.5 AX46-2915.5

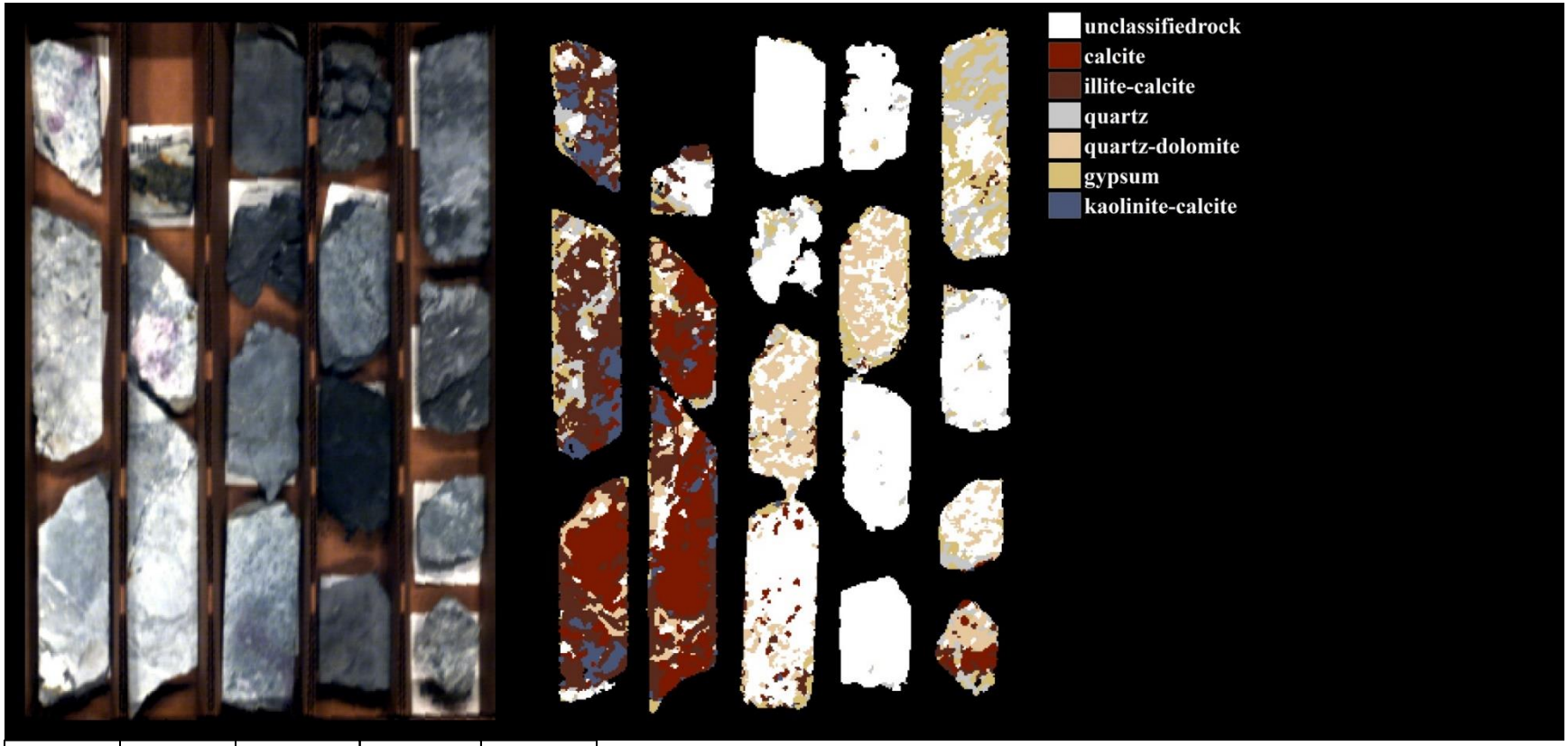

PG1414-2436 PG1414-2417.6 PG1414-2414.5	PG1414-2440 PG1414-2406 PG1414-2428.5	PG01-2081 PG01-2079 PG01-2074 PG1414-2442.5	PG01-2096.7 PG01-2094 PG01-2091.5 PG01-2003	PG01-2114.5 PG01-2108.7 PG01-2103.3 PG01-2100

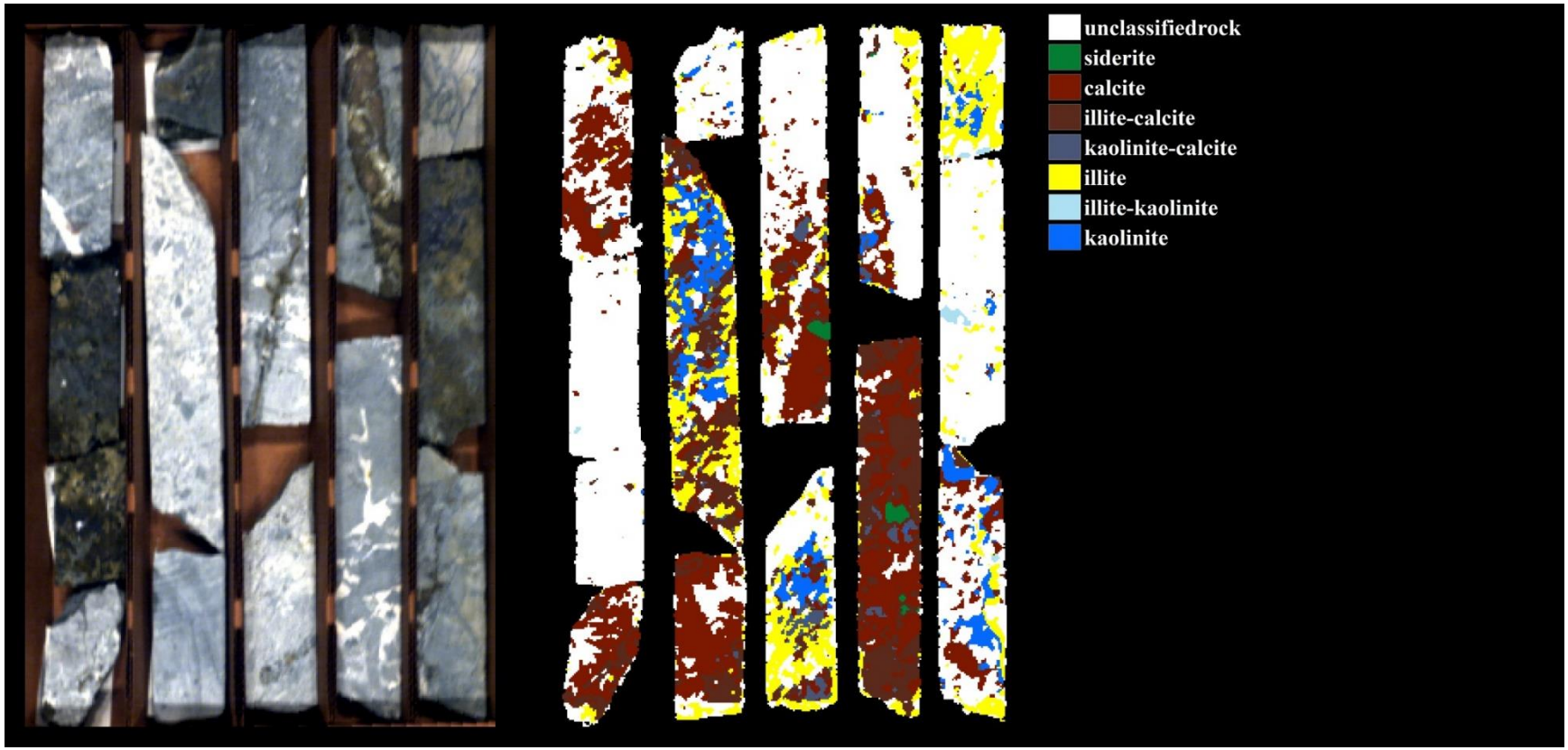

PG02-2105 PG02-2100.5 PG02-2099.5 PG02-2091.5	PG02-2181.2 PG02-2136.5 PG02-2119	PG02-2147.5 PG02-2143.7	PG02-2065.8 PG02-2161.5	PG02-2183 PG02-2186 PG02-2065.2

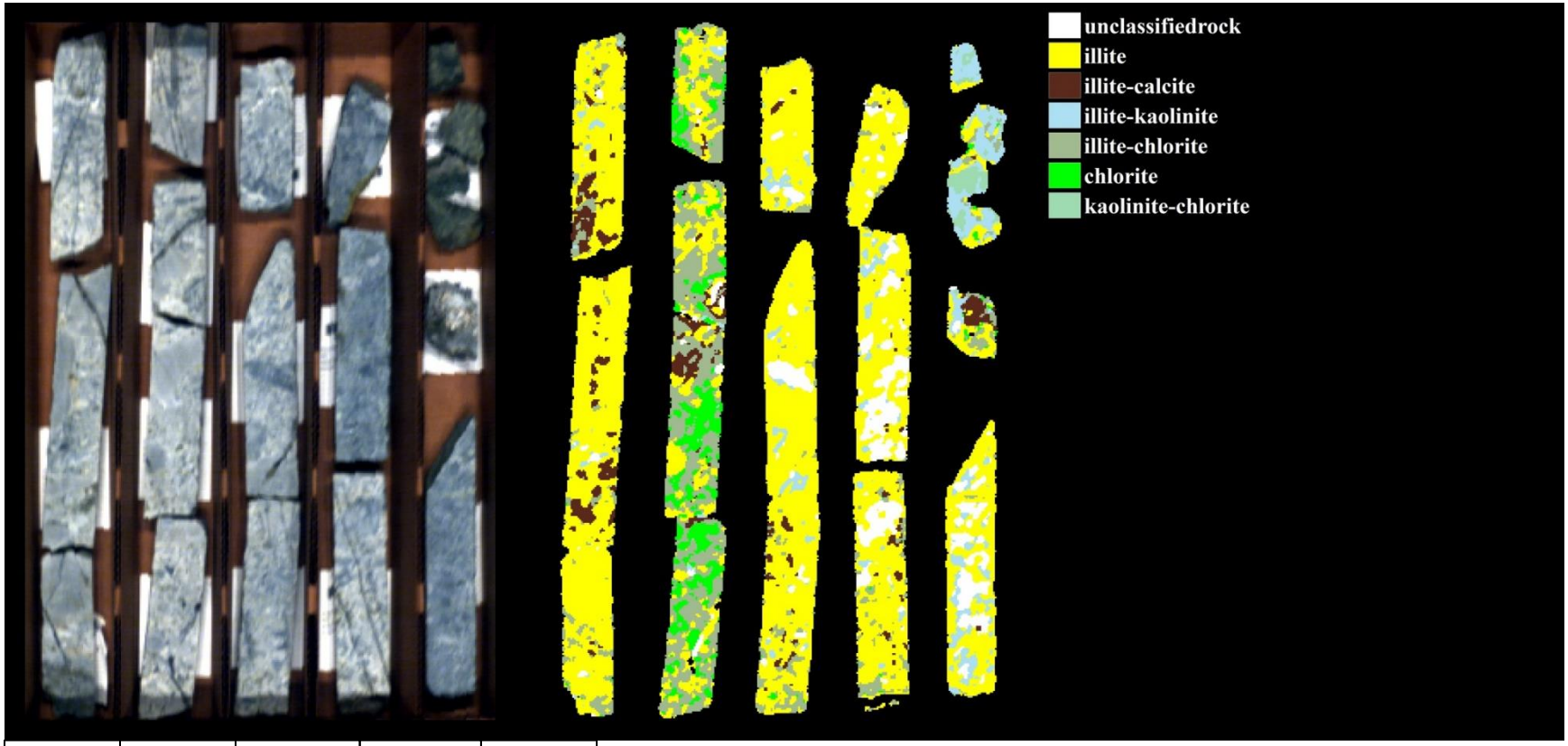

AX46-2684 AX46-2646.8 AX46-2642.3	AX46-2666.5 AX46-2675.5 AX46-2672.2 AX46-2665.7	AX46-2704.8 AX46-2700 AX46-2697.6	AX46-2750.7 AX46-2746.3 AX46-2710.8	AX46-2974 AX46-2851 AX46-2762.5

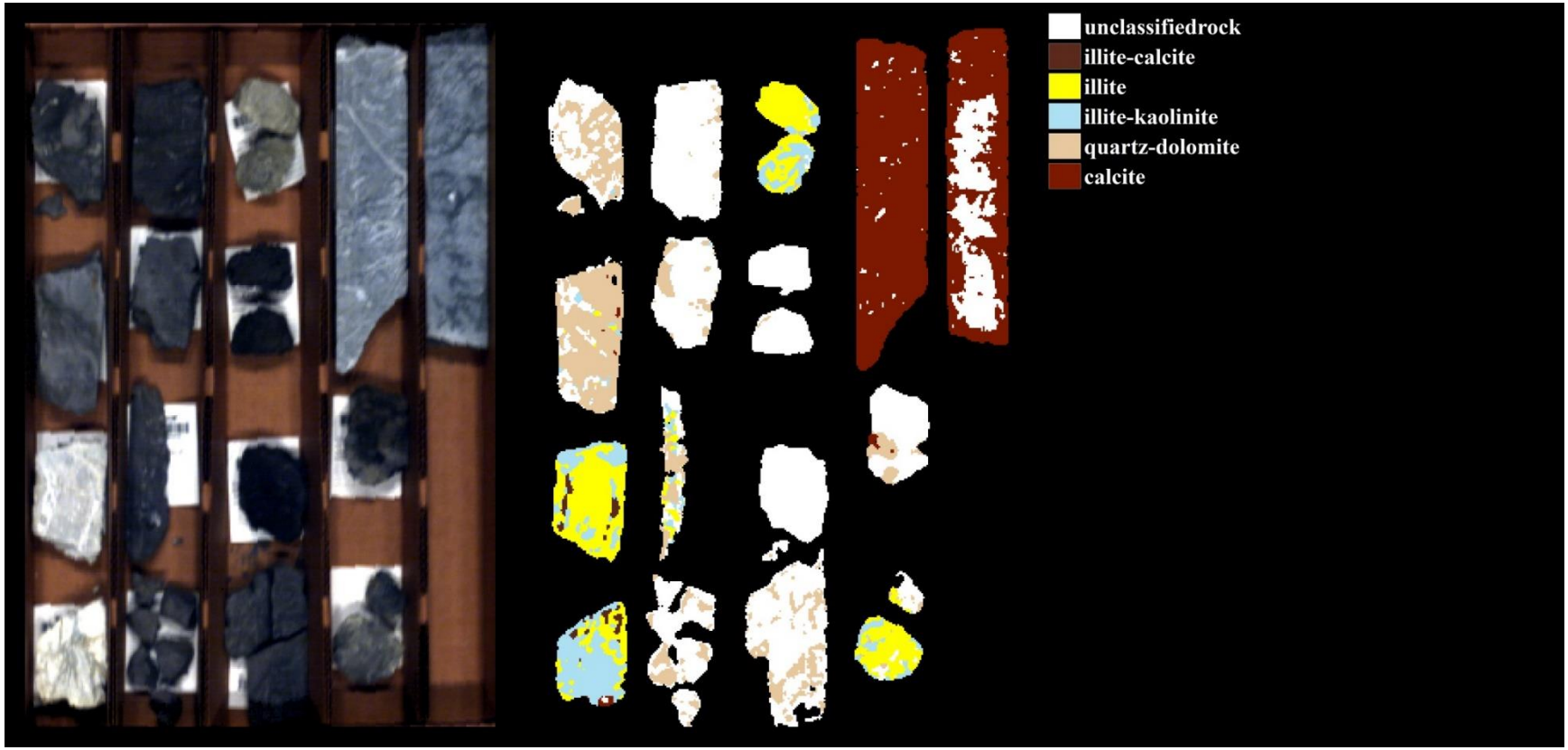

AX46-1383 AX46-1373.8 AX46-1361.5 AX46-1357.8	AX46-1416.2 AX46-1399.5 AX46-1391.5 AX46-1385	AX46-1445 AX46-1427 AX46-1426 AX46-1423	AX46-1480 AX46-1450 AX46-1446.5	AX46-1511

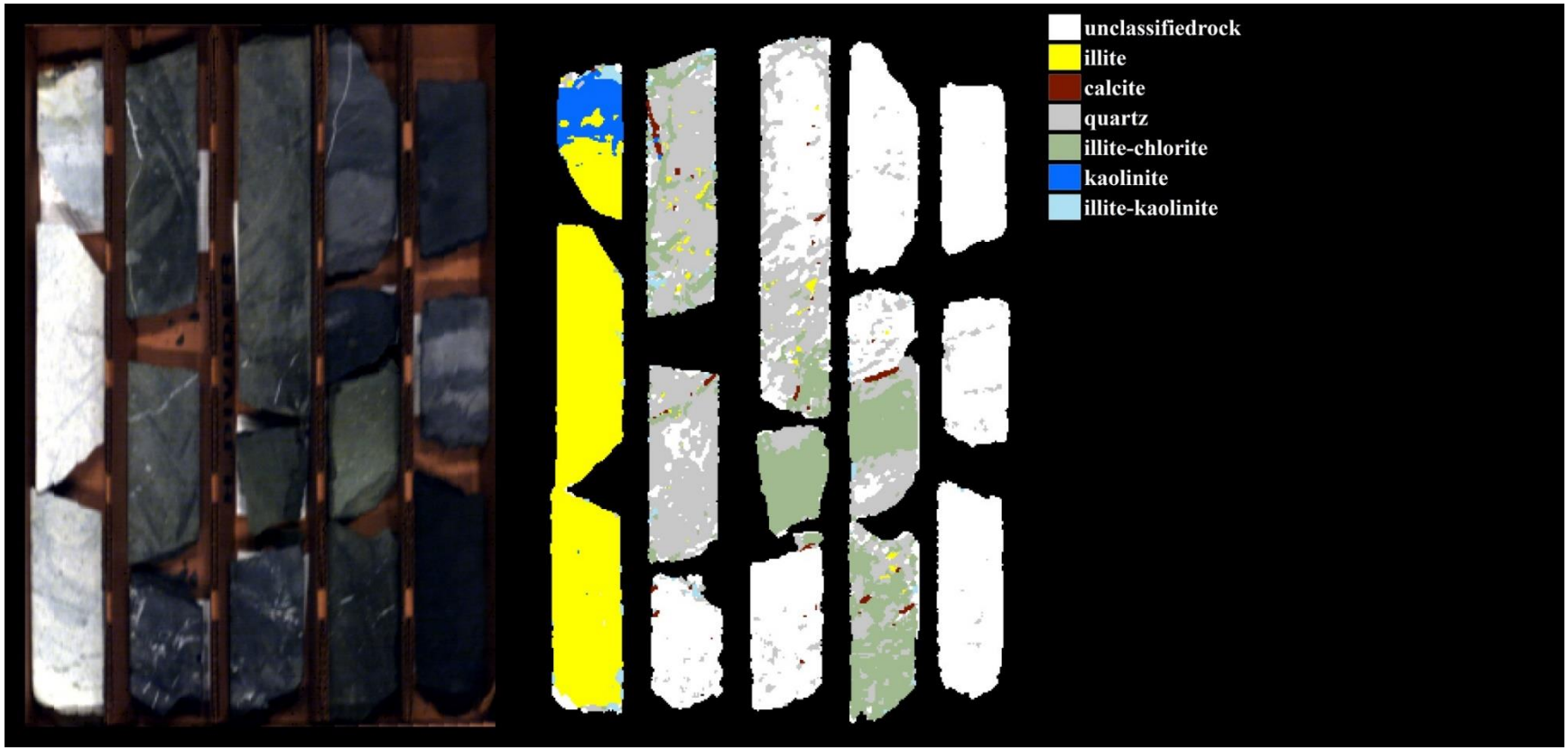

AX53-2502.5 AX53-2496 AX53-2490	AX31-1785.5 (two samples) AX31-1783.5	AX31-1870.5 AX31-1866.5 AX31-1855.7	AX31-1920 AX31-1878.5 AX31-1877.5 AX31-1871.7	AX31-1924.7 AX31-1922.2 AX31-1887

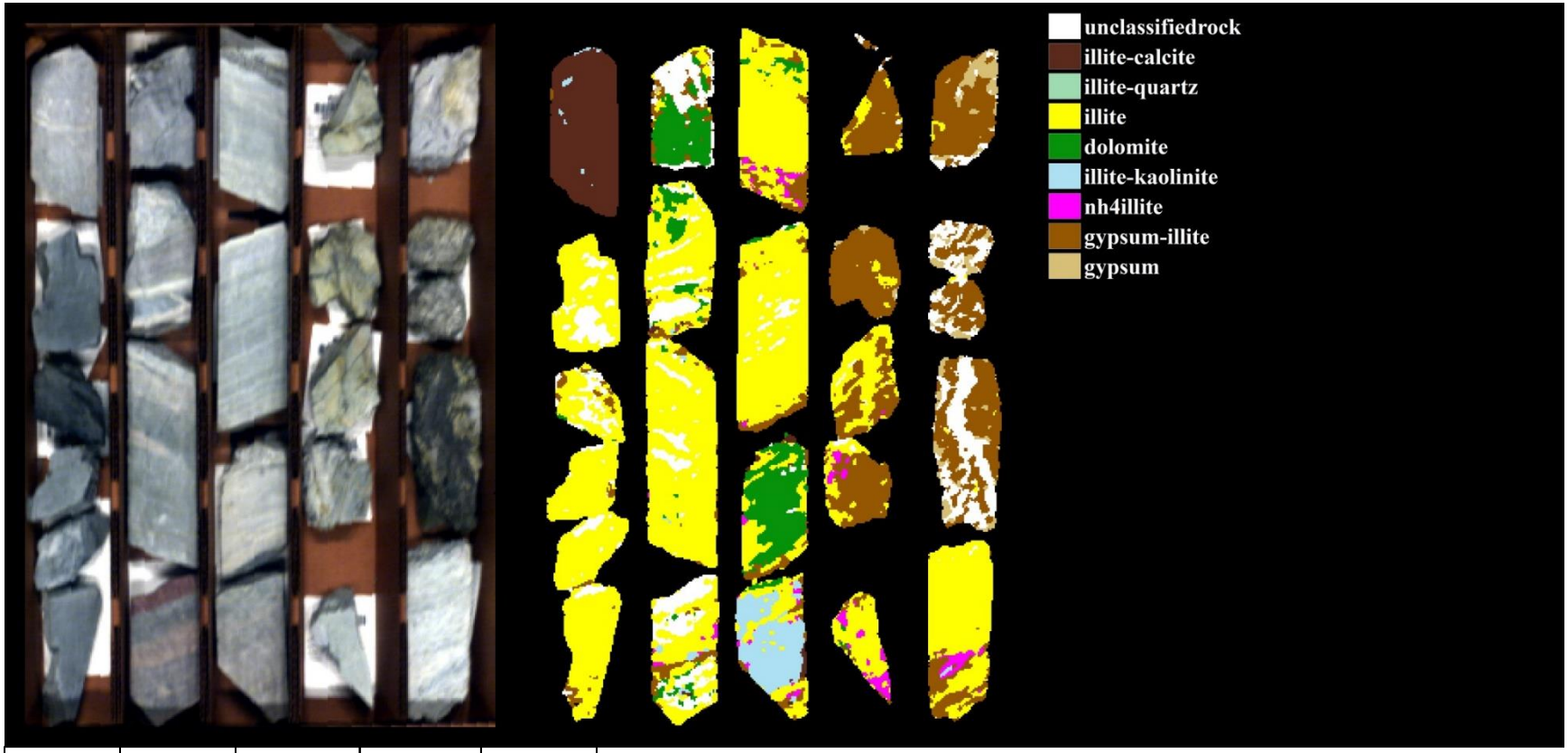

AX35-1270.5 AX31-2176.2 AX31-2173 AX31-2170 AX31-2165.2 AX31-2168	AX35-1307.3 AX35-1304.5 AX35-1299.5 AX35-1273.5	AX35-1330 AX35-1327.9 AX35-1324 AX35-1320.8	AX35-1347.8 AX35-1347.2 AX35-1344.7 AX35-1339.3 AX35-1337.8	AX35-1359 AX35-1355 AX35-1357.5 AX35-1354.3

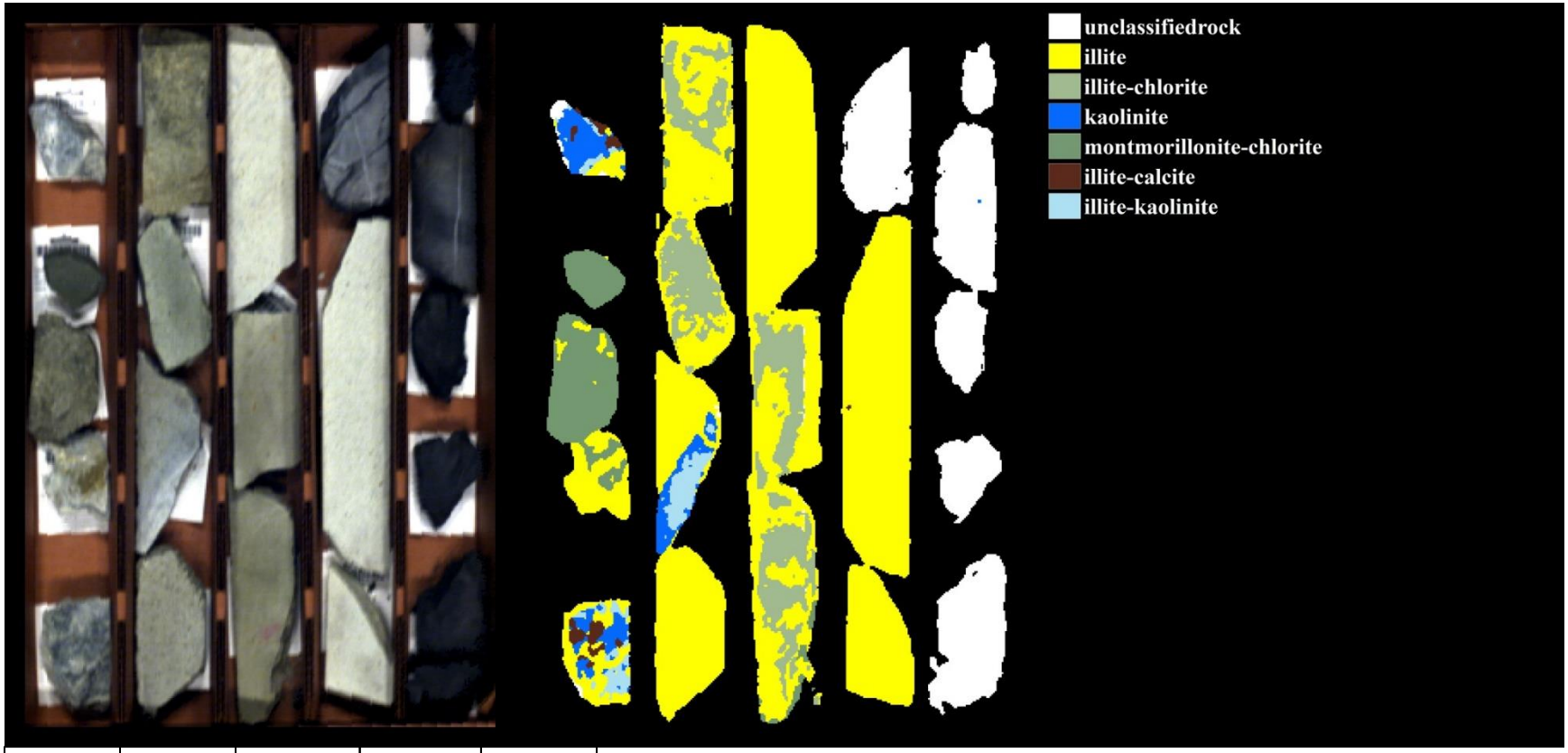

AX35-1977.1 AX35-1970 AX35-1968.6 AX35-1967 AX35-1962	AX35-1996 AX35-1983.5 AX35-1977.8 AX35-1926	AX35-2008.1 AX35-2003.5 AX35-1994	AX12-1684.7 AX35-2030 AX35-2018.4	AX12-1702.4 AX12-1700 AX12-1693.7 AX12-1691 AX12-1685.2

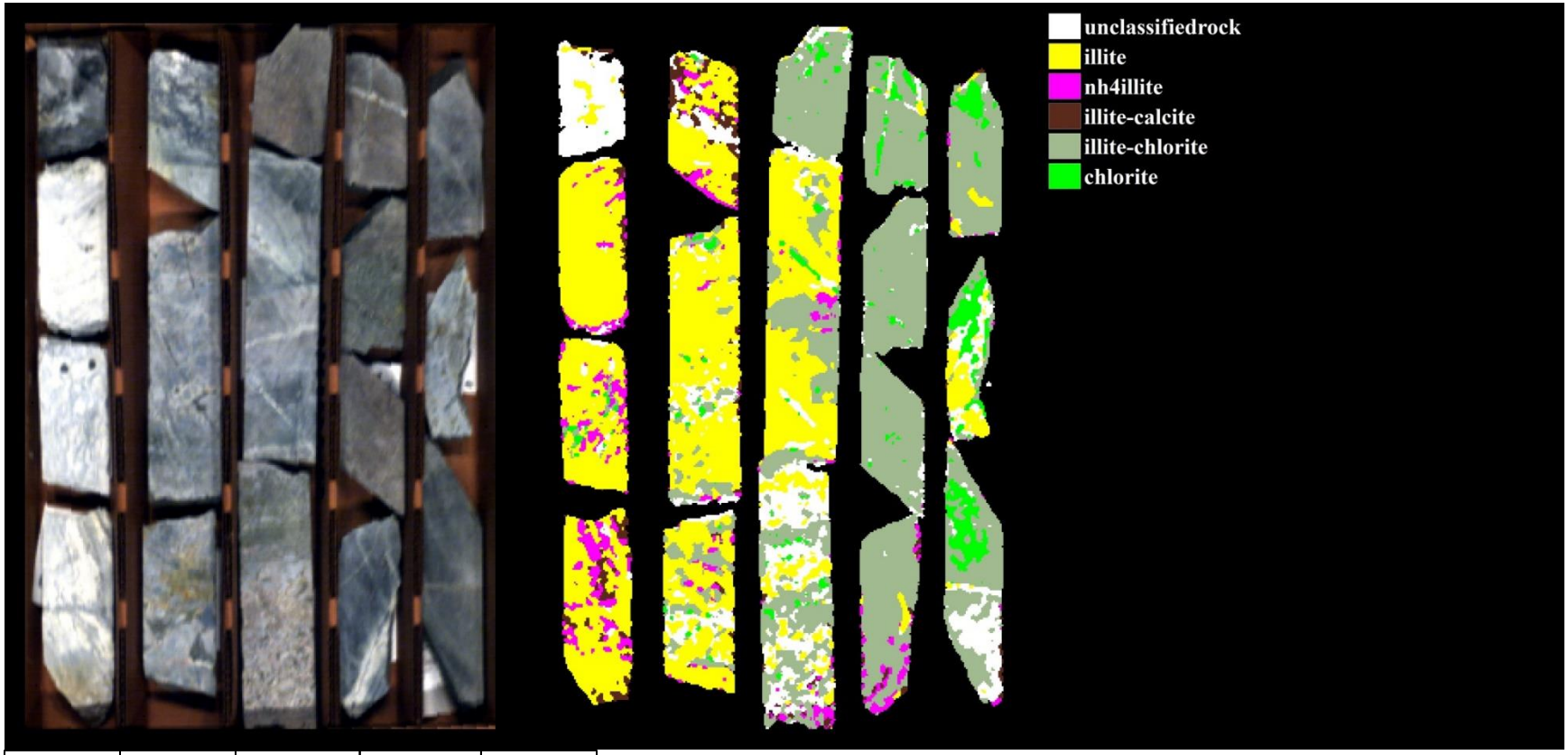

AX12-1266 AX12-1262.3 AX12-1259.5 AX12-1253	PG1415-3323 PG1415-3315.6 PG1415-3310.7	PG1415-3335.3 PG1415-3322 PG1415-3320.7	PG1415-3352.2 PG1415-3340.7 PG1415-3338 PG1415-3331	PG1415-3365 PG1415-3354 PG1415-3346.4

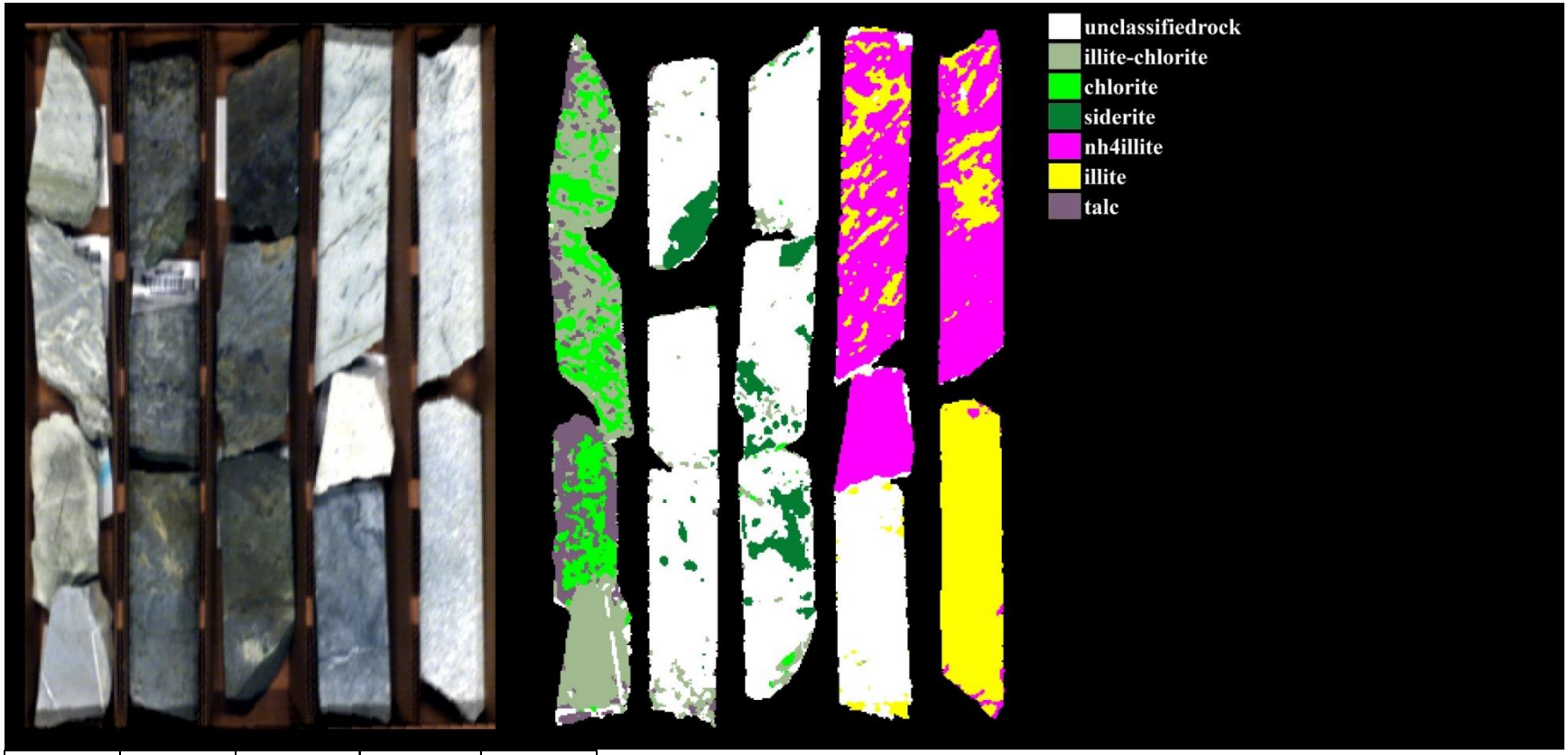

PG1403-2733 PG1403-2727.5 PG1403-2721.5 PG1403-2714.3	PG1403-2747.3 PG1403-2745 PG1403-2743.5	PG1403-2759 PG1403-2757 PG1403-2751	PG1403-2771.5 PG1403-2765.5 PG1403-2761.8	PG1403-2794.5 PG1403-2782

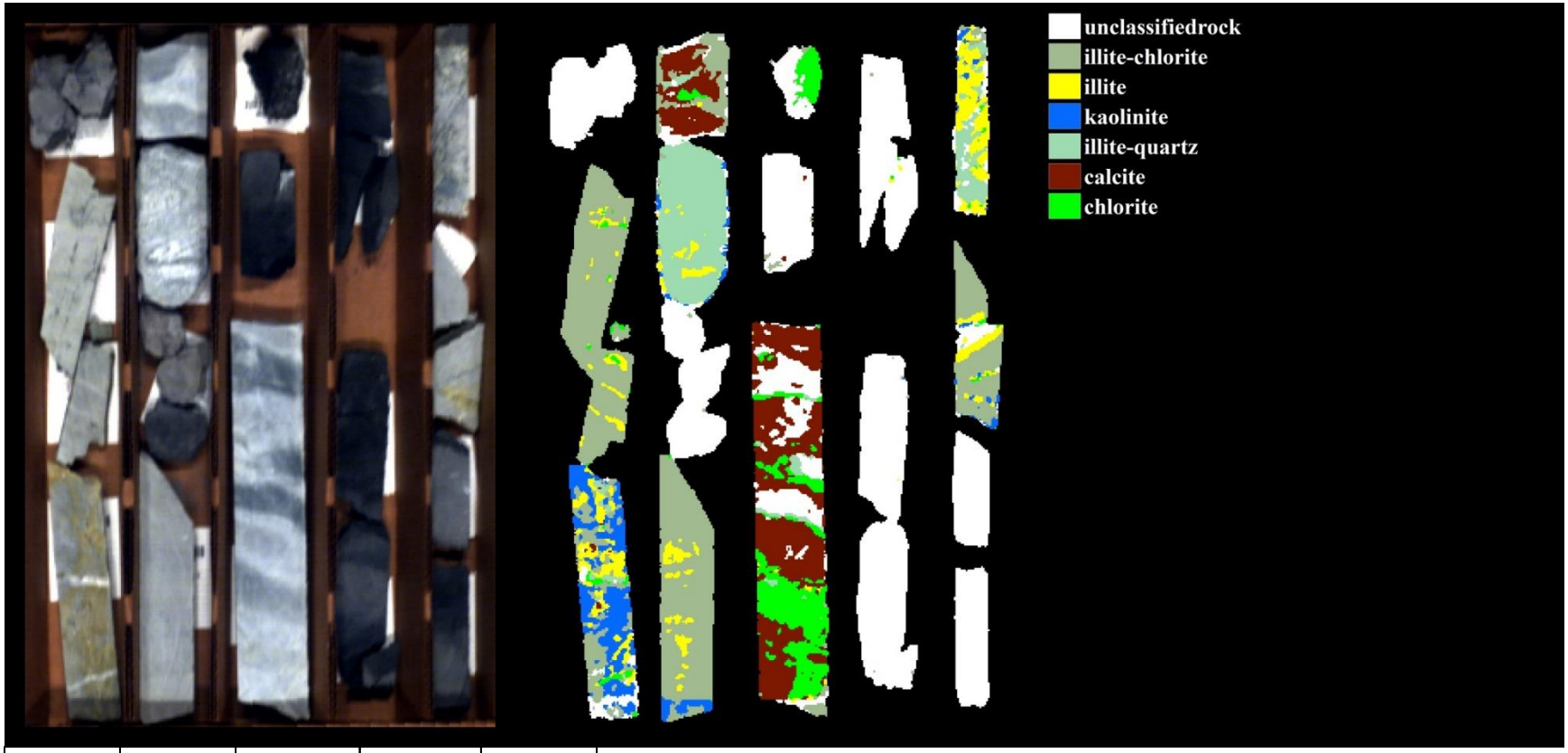

AX46-1545.5 AX46-2222 AX46-2222.7 AX46-2114	AX46-1551.3 AX46-1549.7 AX46-1549 AX46-2236.5	AX46-1940.4 AX46-1937.5 AX46-1554	AX46-1951.5 AX46-1951 AX46-1948.5	AX46-2638.8 AX46-2236.5 AX46-2237.3 AX46-1987.3 AX46-1957.2

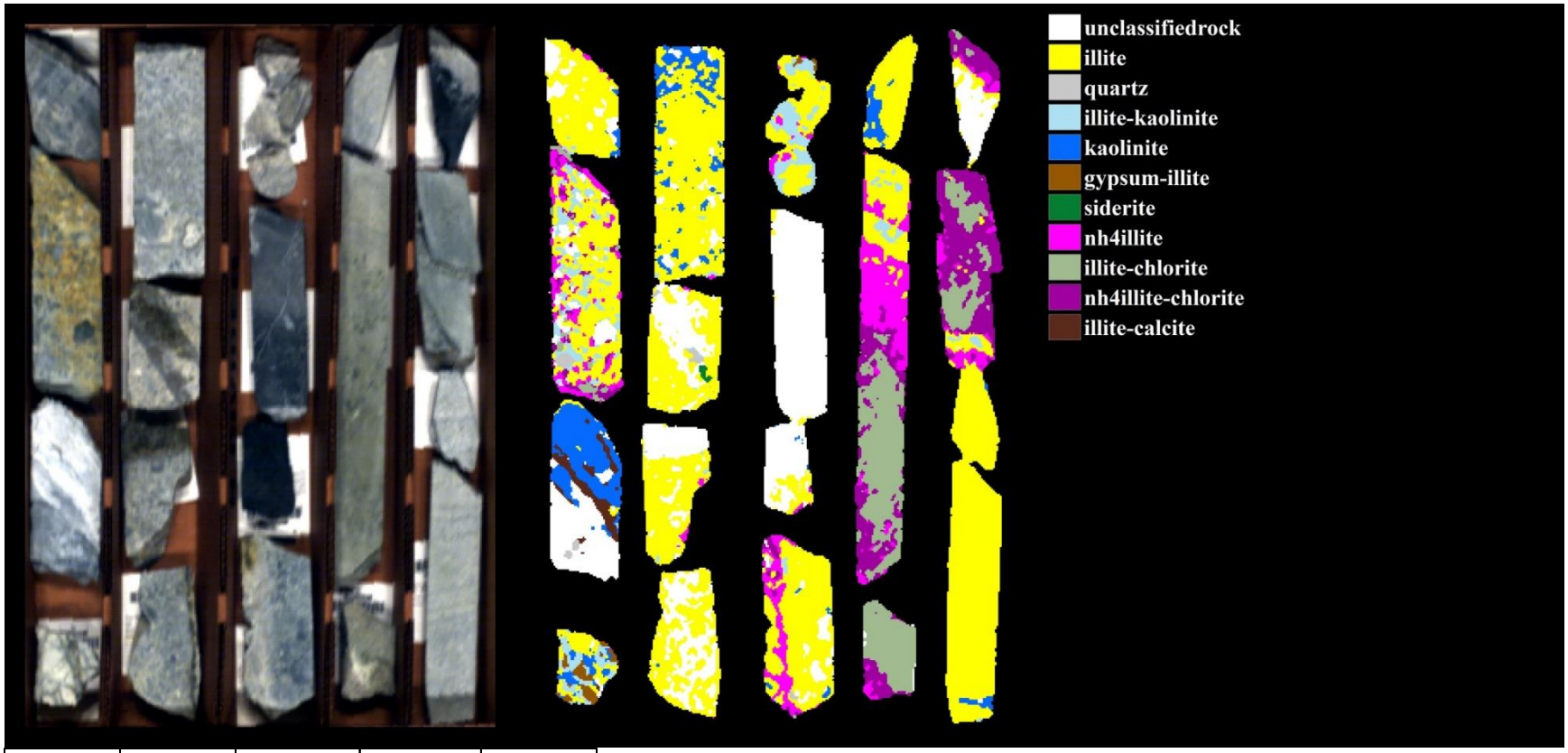

PG1410-2606 PG1410-2596.5 PG1410-1516.3 PG1410-1512	PG1410-2661 PG1410-2654.5 PG1410-2652.5 PG1410-2652	PG1405-1870 PG1405-1869 PG1405-1867.5 PG1410-2614	PG1405-1885.5 PG1405-1880 PG1405-1871.5	PG1405-1908 PG1405-1907 PG1405-1890.5 PG1405-1887.5

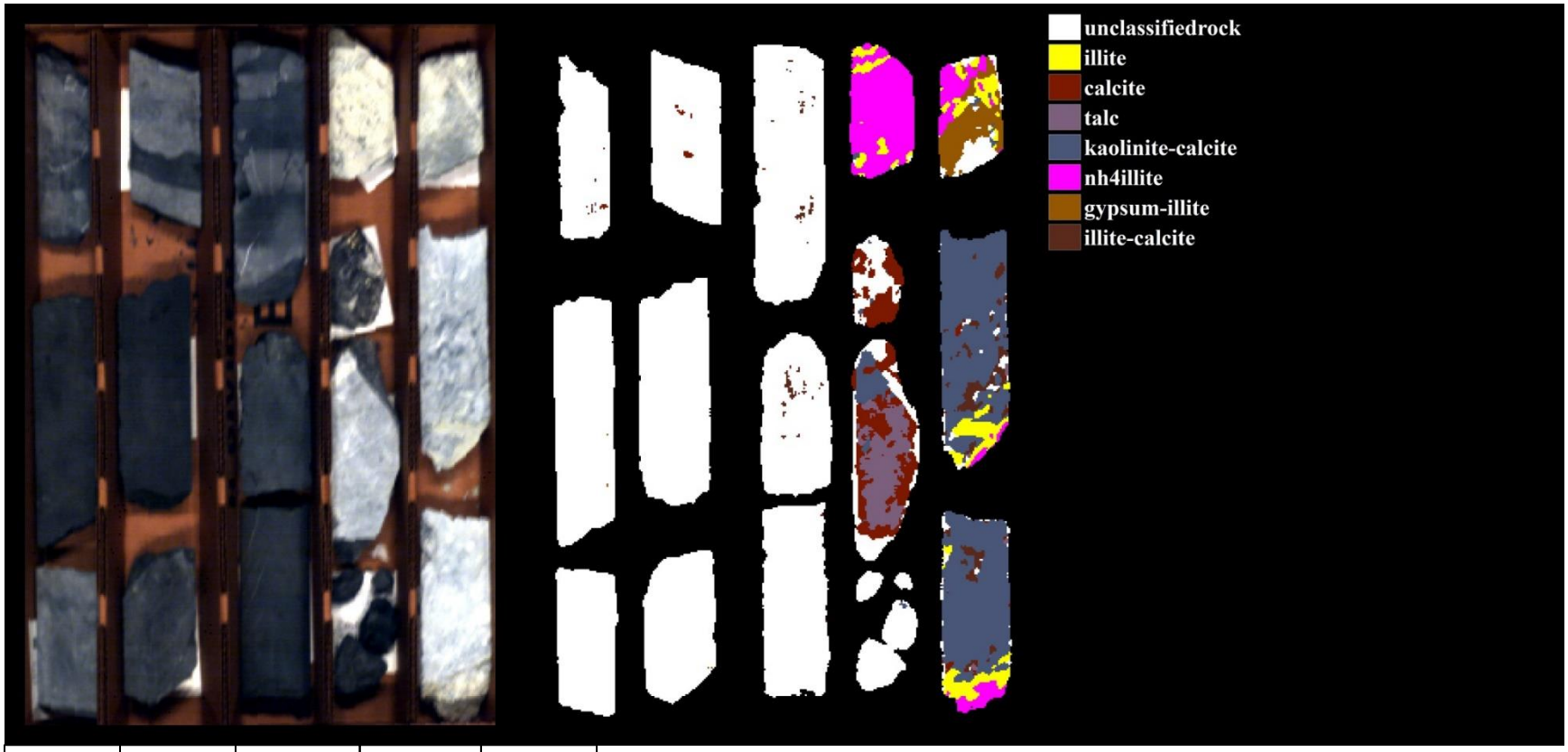

PG1404-1792 PG1404-1489.5 PG1404-1781.5	PG1404-1801 PG1404-1798 PG1404-1794	PG1404-2100 PG1404-2102.7 PG1404-2075	PG1410-1500.5 PG1404-2296 PG1404-2297 PG1404-2102	PG1410-1513 PG1410-1506 PG1410-1505

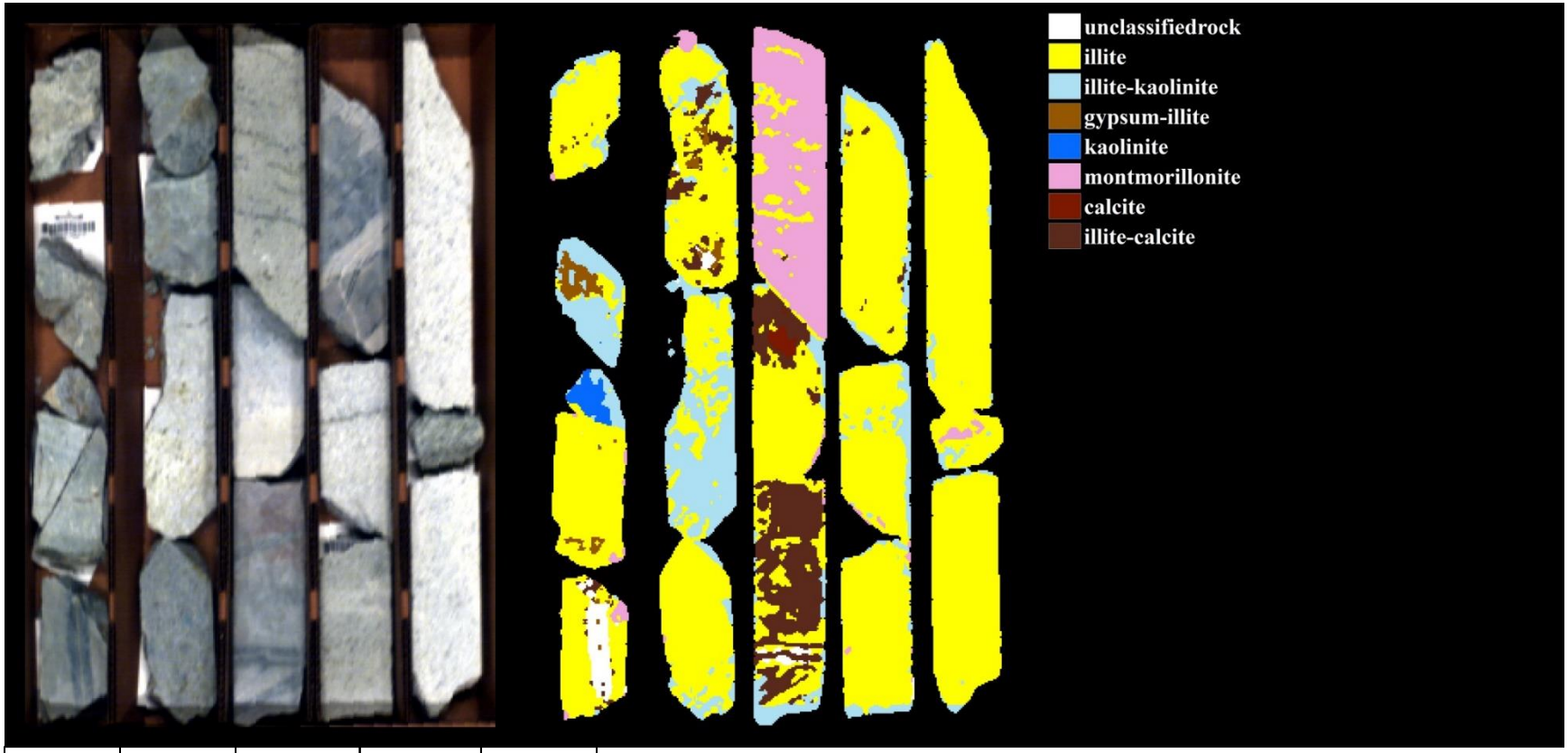

AX53-1241 AX53-1239.7 AX53-1238.7 (two samples) AX53-1237	AX53-1257.5 AX53-1354.5 AX53-1246.7	AX46-1326 AX46-1322 AX46-1320.5	AX53-1358.5 AX53-1331.5 (two samples)	AX53-1340 AX53-1255 AX53-1341.7

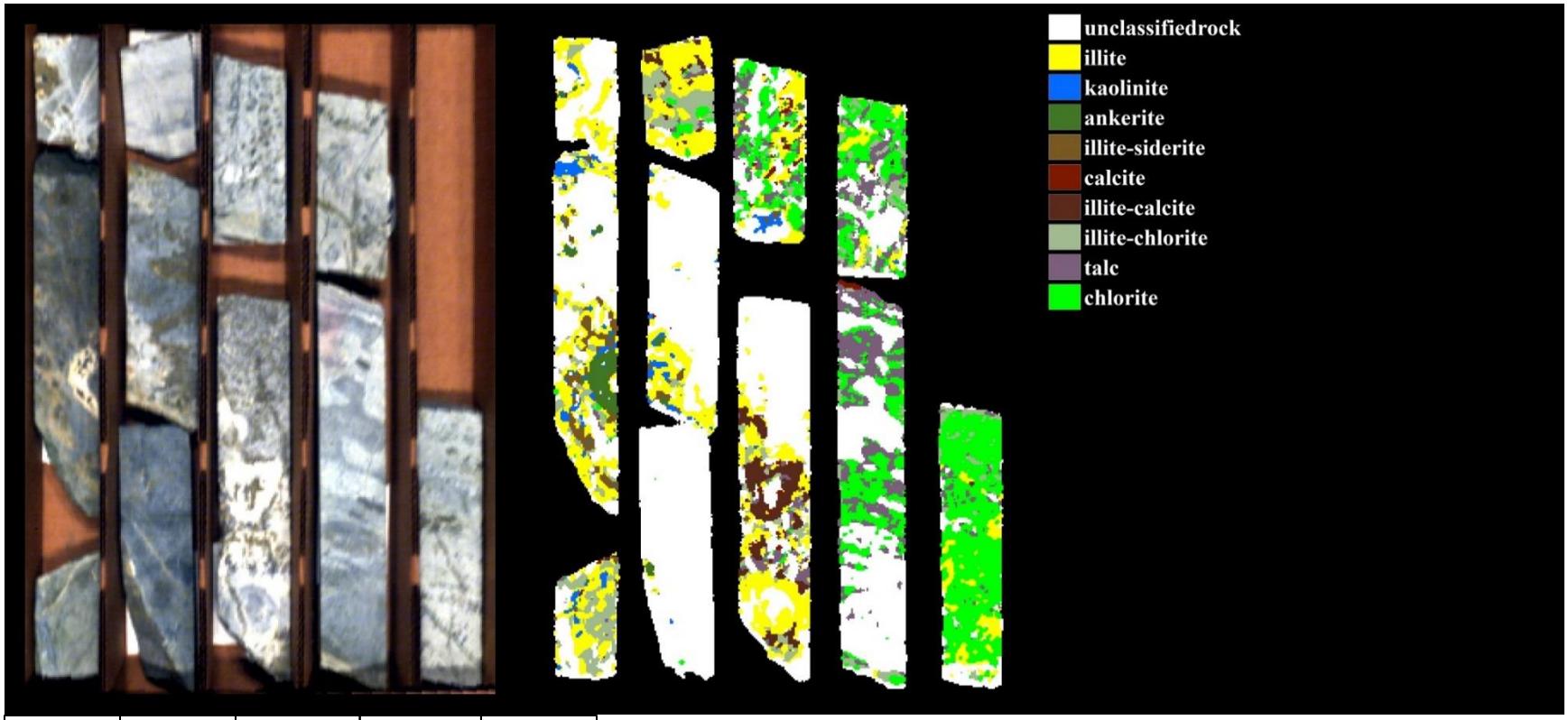

PG02-2232.2 PG02-2194.5 PG02-2182.8	PG02-2299.2 PG02-2118.3 PG02-2200.8	PG02-2288.8 PG02-2234	PG02-2294.8 PG02-2246	PG02-2301.8

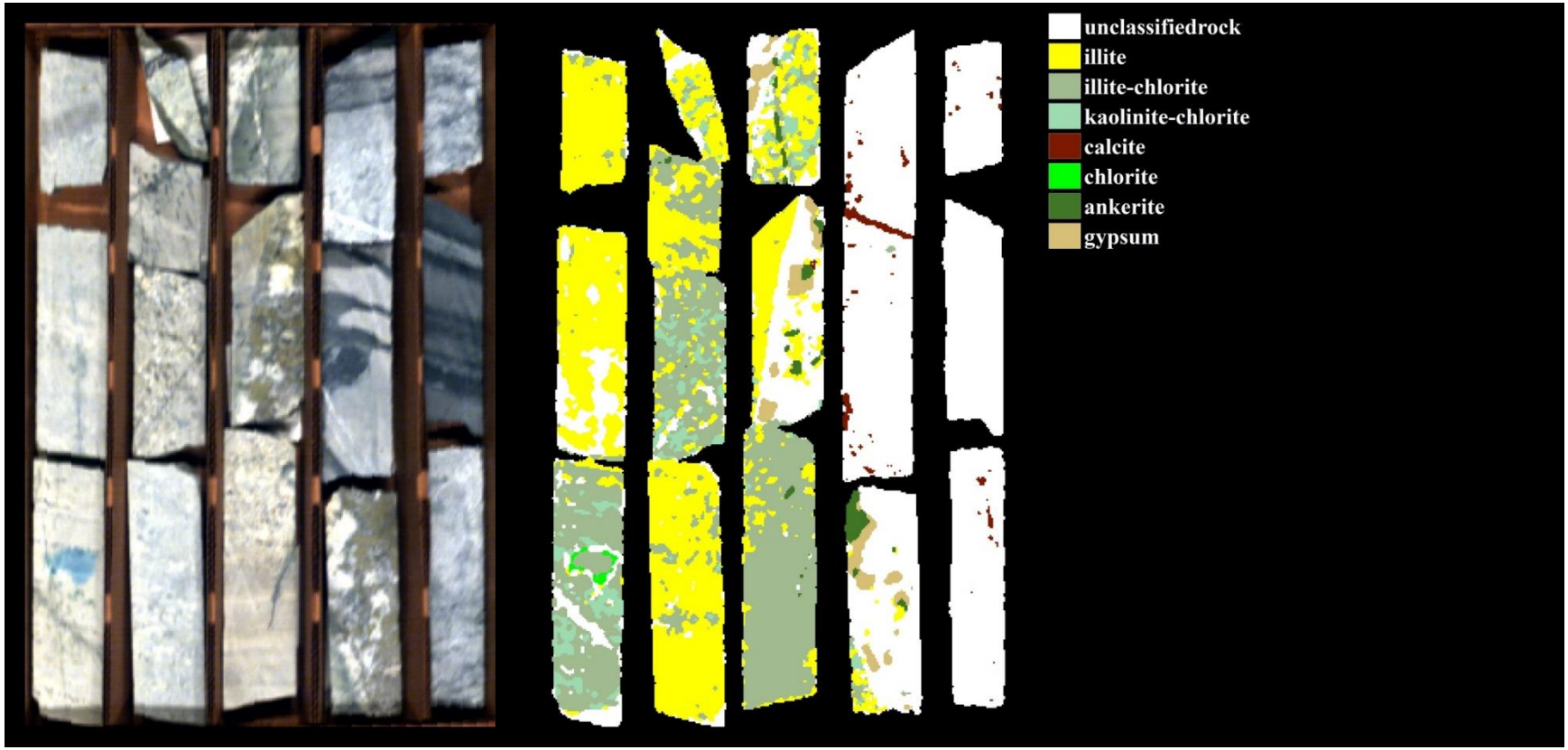

PG02-2517.2 PG02-2512 PG02-2510	AX51-2867.5 PG02-2534.9 PG02-2529.5 PG02-2515.5	PG02-2536.7 PG02-2535.5 PG02-2532	PG02-2067.8 PG02-2065.5 PG02-2536	PG02-2089.5 PG02-2080.5 PG02-2068.5

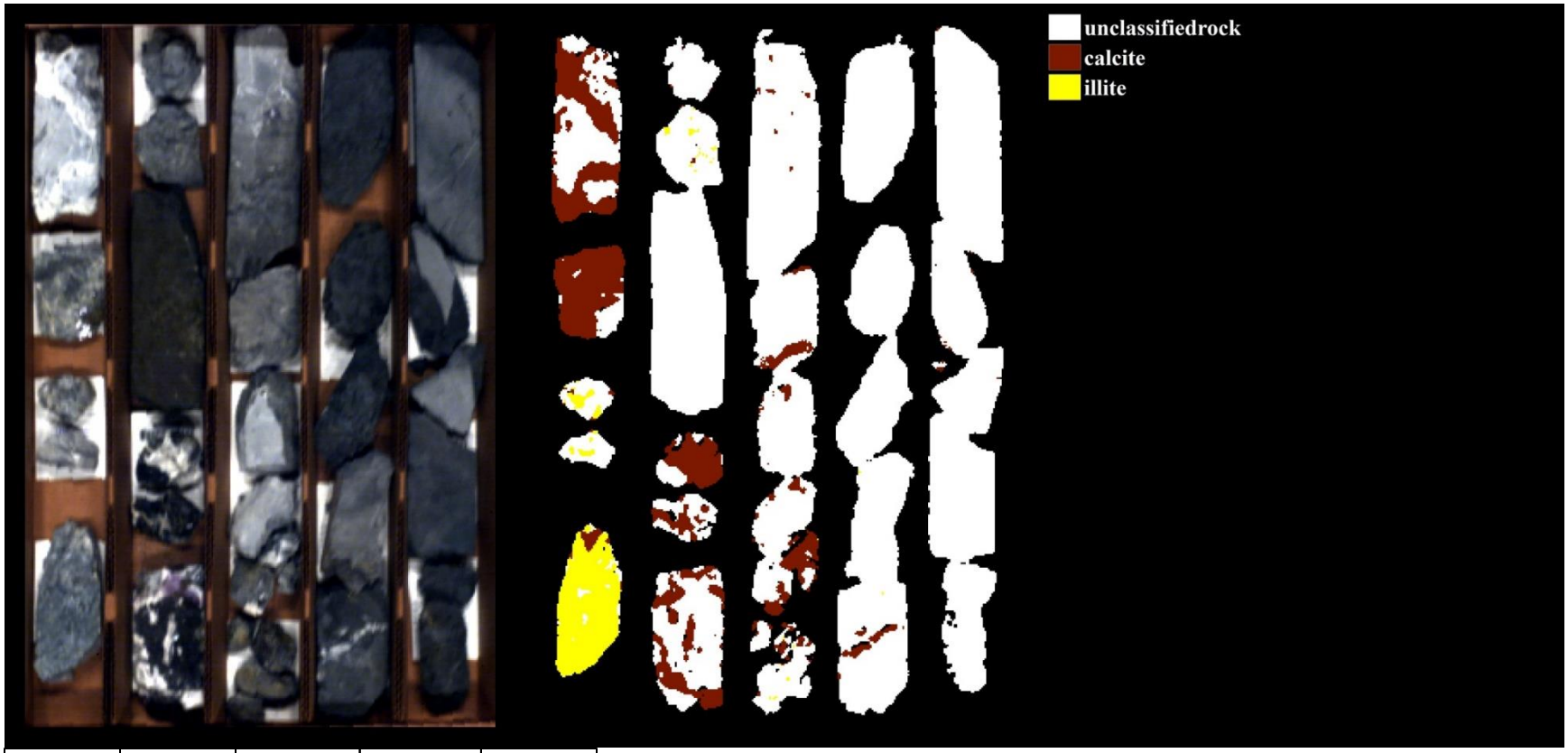

PG1414-2308.5 PG1414-2351 PG1414-2391 PG1414-2410.8	PG1414-2279 PG1414-2282.5 PG1414-2283.2 PG1414-2308	PG1414-2255 PG1414-2259 PG1414-2262.5 PG1414-2272 PG1414-2268.5	PG1414-2221.5 PG1414-2218 PG1414-2238.3 PG1414-2247	PG1414-2203.7 PG1414-2210.5 PG1414-2209.4 PG1414-2212.5 PG1414-2216

AX51-1500 AX51-1480 AX51-1478.5 AX51-1477.3	AX51-1511.7 AX51-1504-1509 AX51-1485.5 AX51-1485	AX51-1555 AX51-1538 AX51-1529 AX51-1521.5	AX51-1571.5 AX51-1570 AX51-1541.5 AX51-1538.5	? AX51-1574.8 AX51-1572.5 AX51-1572

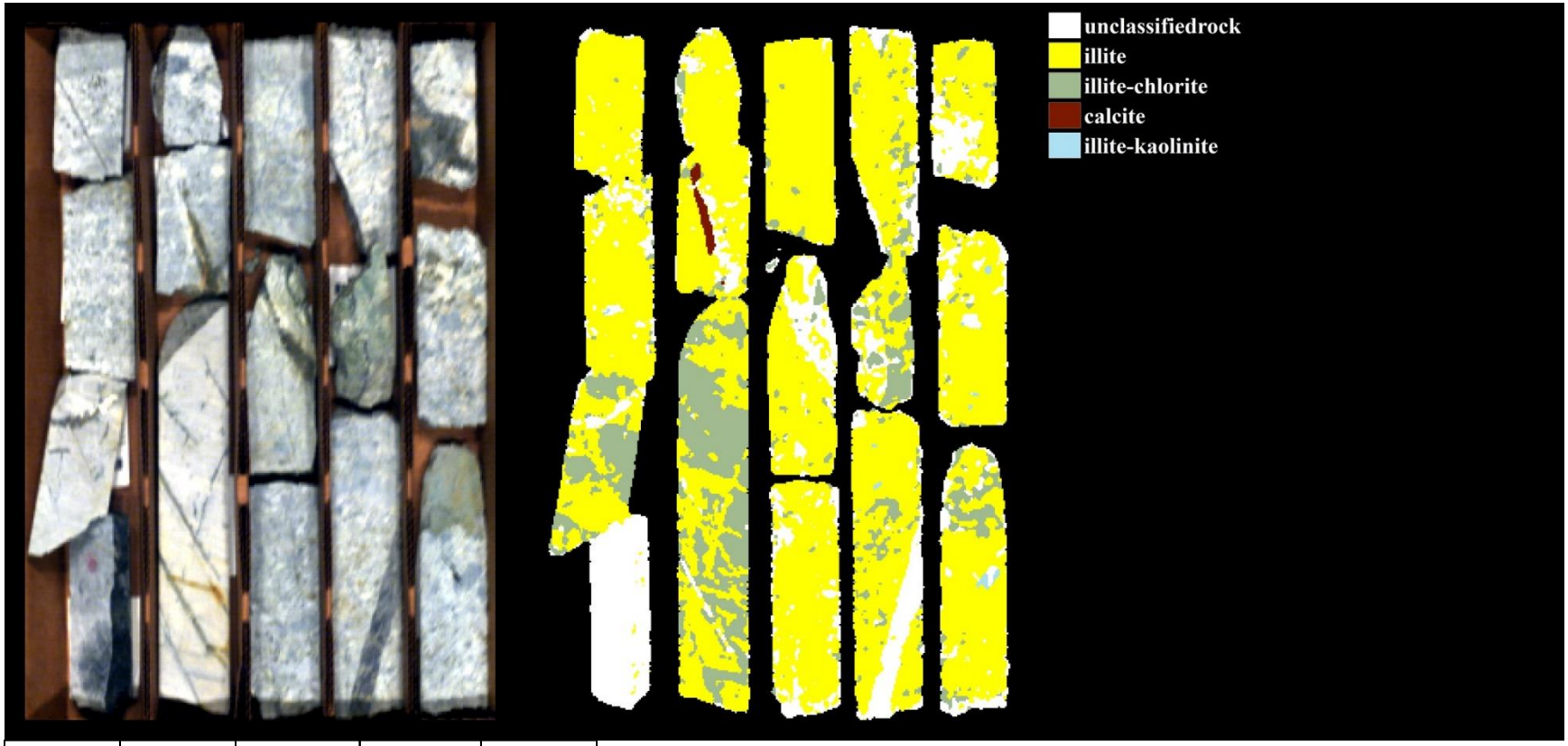

AX51-2600 AX51-2599.2 AX51-2591.8 AX51-2203.8	AX51-2615.5 AX51-2605.2 AX51-2591	AX51-2857.8 AX51-2622.7 AX51-2611.8	AX51-2898 AX51-2872.8 AX51-2848.5	AX51-2888 AX51-2883 AX51-2876.5

Appendix C1.
U-Pb Zircon SHRIMP Isotopic Ratios

Cathodoluminescence images of zircon grains and analyzed spots shown per sample following trace element data in Appendix C2.

Errors are 1σ unless otherwise specified																																				
																									---------- 204 corrected ----------											
			204corr		207corr		208corr		204corr		204corr		%																								
			206Pb		206Pb		206Pb		207Pb		208Pb		Dis-	7corr		4corr		8corr		Total		Total		4corr		4corr		4corr		4corr					
	ppm	ppm	/238U	1σ	/238U	1σ	/238U	1σ	/206Pb	1σ	/232Th	1σ	cor-	206*	%	208*	%	206*	%	238	%	207	%	238	%	207*	%	207*	%	206*	%	err				
Spot Name	U	Th	Age	err	Age	err	Age	err	Age	err	Age	err	dant	/238	err	/232	err	/238	err	/206	err	/206	err	/206*	err	/206*	err	/235	err	/238	err	corr				
BS-1-7.1	239	69	37.2	0.7	36.5	0.6	-1339	83	692	239	16665	610	+95	0.00567	0.54	1.28	5.4	.0058	1.8	174	1.6	0.0565	6.5	173	1.8	0.063	11	0.050	11	0.00579	1.8	0.2				
BS-1-8.1	157	57	41.4	1	37.4	0.4	-2003	171	2019	294	17917	838	+98	0.00581	0.34	1.43	7.1	.0064	2.9	169	0.9	0.0626	7.9	155	2.9	0.124	17	0.111	17	0.00645	2.9	0.2				
BS-1-2.1	239	82	36.7	0.9	37.7	0.8	-1176	76			13442	557		0.00587	0.68	0.94	5.7	.0057	2.4	171	2.1	0.0427	6.2	175	2.4	0.024	40	0.019	40	0.00571	2.4	0.1				
BS-1-9.1	318	142	38.2	0.8	38.4	0.8	-733	30	-145	580	7848	234	+127	0.00598	0.65	0.47	3.6	.0060	2.1	165	1.9	0.0588	10.7	168	2.1	0.043	23	0.036	23	0.00595	2.1	0.1				
BS-1-10.1	121	56	39.6	0.8	39.4	0.9	-2273	82	271	231	16009	321	+86	0.00613	0.71	1.21	2.9	.0062	2.1	162	2.1	0.0517	10.1	162	2.1	0.052	10	0.044	10	0.00616	2.1	0.2				
BS-1-4.1	153	60	42.6	0.8	~~40.6~~	~~0.4~~	-1566	56	1325	306	14591	316	+97	0.00631	0.28	1.06	3.0	.0066	1.9	158	0.8	0.0490	6.8	151	1.9	0.085	16	0.078	16	0.00664	1.9	0.1				
BS-1-5.1	92	36	39.4	1	~~40.7~~	~~0.9~~	-3857	155			23112	389		0.00634	0.69	2.14	2.8	.0061	3.0	158	2.1	0.0445	10.0	163	3.0	0.021	83	0.018	83	0.00614	3.0	0.0				
BS-1-6.1	776	255	60.0	2	~~59.7~~	~~2~~	-328	54	263	132	5966	687	+78	0.00930	1.11	0.34	13.3	.0094	3.5	108	3.5	0.0466	3.5	107	3.5	0.052	6	0.066	7	0.00935	3.5	0.5				
BS-1-3.1	1210	11	92.5	1	~~92.5~~	~~1~~	-105	18	101	38	41347	1594	+9	0.01445	0.42	6.73	9.1	.0145	1.3	69	1.3	0.0481	1.6	69	1.3	0.048	2	0.096	2	0.01446	1.3	0.6				

Errors are 1σ unless otherwise specified																																				
																									---------- 204 corrected ----------											
			204corr		207corr		208corr		204corr		204corr		%																								
			206Pb		206Pb		206Pb		207Pb		208Pb		Dis-	7corr		4corr		8corr		Total		Total		4corr		4corr		4corr		4corr					
	ppm	ppm	/238U	1σ	/238U	1σ	/238U	1σ	/206Pb	1σ	/232Th	1σ	cor-	206*	%	208*	%	206*	%	238	%	207	%	238	%	207*	%	207*	%	206*	%	err				
Spot Name	U	Th	Age	err	Age	err	Age	err	Age	err	Age	err	dant	/238	err	/232	err	/238	err	/206	err	/206	err	/206*	err	/206*	err	/235	err	/238	err	corr				
BS-2-3.1	165	43	39.2	0.7	38.1	0.6	-1889	49	875	324	21550	289	+96	0.00593	0.48	1.90	2.2	.0061	1.8	168	1.3	0.0522	11.1	164	1.8	0.068	16	0.057	16	0.00609	1.8	0.1				
BS-2-6.1	274	81	38.3	0.3	38.1	0.3	-961	18	190	198	13323	159	+80	0.00593	0.24	0.93	1.6	.0060	0.8	167	0.7	0.0533	4.9	168	0.8	0.050	9	0.041	9	0.00595	0.8	0.1				
BS-2-8.1	163	51	36.9	0.7	38.2	0.3	-2097	43			20030	216		0.00595	0.28	1.69	1.7	.0057	2.0	167	0.8	0.0537	6.3	174	2.0	0.019	82	0.015	82	0.00574	2.0	0.0				
BS-2-4.1	207	69	39.5	0.7	39.3	0.7	-1428	45	218	309	15589	296	+82	0.00612	0.53	1.16	2.7	.0062	1.8	164	1.6	0.0417	6.6	163	1.8	0.051	13	0.043	13	0.00615	1.8	0.1				
BS-2-1.1	420	184	40.3	0.7	39.5	0.7	-546	14	731	136	6417	120	+95	0.00614	0.57	0.37	2.2	.0063	1.8	161	1.8	0.0576	3.7	159	1.8	0.064	6	0.055	7	0.00627	1.8	0.3				
BS-2-7.1	270	109	38.1	0.8	39.5	0.7	-965	22			10392	160		0.00615	0.55	0.67	2.0	.0059	2.2	162	1.7	0.0522	5.1	169	2.2	0.016	75	0.013	75	0.00592	2.2	0.0				
BS-2-5.1	110	38	39.9	1	39.6	1	-3002	203	279	504	22502	699	+86	0.00616	1.13	2.04	5.1	.0062	3.5	163	3.4	0.0440	19.3	161	3.5	0.052	22	0.044	22	0.00620	3.5	0.2				
BS-2-2.1	195	68	39.5	1	40.2	1	-1289	62	-873	728	14237	427	+105	0.00625	0.91	1.02	4.2	.0061	3.0	160	2.8	0.0463	6.2	163	3.0	0.033	25	0.028	25	0.00614	3.0	0.1				

Errors are 1σ unless otherwise specified

Spot Name	ppm U	ppm Th	204corr 206Pb /238U Age	1σ err	207corr 206Pb /238U Age	1σ err	208corr 206Pb /238U Age	1σ err	204corr 207Pb /206Pb Age	1σ err	204corr 208Pb /232Th Age	1σ err	% Dis-cor-dant	7corr 206* /238	% err	4corr 208* /232	% err	8corr 206* /238	% err	Total 238 /206	% err	Total 207 /206	% err	4corr 238 /206*	% err	4corr 207* /206*	% err	4corr 207* /235	% err	4corr 206* /238	% err	err corr
BS-3-1.1	395	155	37.2	0.8	36.5	0.8	-635	31	673	310	7876	282	+95	0.00568	0.69	0.48	4.3	.0058	2.2	175	2.0	0.0503	12.2	173	2.2	0.062	14	0.050	15	0.00579	2.2	0.1
BS-3-3.1	517	221	36.3	0.5	36.7	0.5	-524	31	-579	454	6292	282	+107	0.00572	0.42	0.37	5.2	.0056	1.5	175	1.3	0.0480	4.7	177	1.5	0.037	17	0.029	17	0.00564	1.5	0.1
BS-3-2.1	333	194	37.1	0.3	37.1	0.3	-747	11	67.3	255	6208	72	+45	0.00577	0.24	0.36	1.3	.0058	0.8	172	0.7	0.0515	5.6	173	0.8	0.047	11	0.038	11	0.00577	0.8	0.1
BS-3-10.1	155	56	39.6	0.9	37.7	0.3	-2196	75	1313	366	18747	338	+97	0.00587	0.29	1.53	2.8	.0062	2.2	170	0.8	0.0484	8.0	162	2.2	0.085	19	0.072	19	0.00616	2.2	0.1
BS-3-9.1	307	116	37.8	0.3	37.9	0.3	-924	16	-33	369	10612	127	+215	0.00589	0.29	0.69	1.5	.0059	0.9	171	0.7	0.0407	12.6	170	0.9	0.045	15	0.037	15	0.00588	0.9	0.1
BS-3-6.1	286	105	37.1	0.6	37.9	0.4	-943	18			11016	139		0.00590	0.34	0.72	1.6	.0058	1.7	168	1.0	0.0531	5.9	173	1.7	0.029	39	0.023	39	0.00577	1.7	0.0
BS-3-12.1	210	69	39.6	1	38.4	0.9	-1225	65	935	305	14366	479	+96	0.00597	0.74	1.04	4.7	.0062	2.6	166	2.3	0.0529	6.8	162	2.6	0.070	15	0.060	15	0.00616	2.6	0.2
BS-3-11.1	357	183	38.3	0.6	38.7	0.6	-655	20	-366	467	6350	144	+111	0.00601	0.49	0.37	2.6	.0060	1.5	166	1.4	0.0467	11.0	168	1.5	0.040	18	0.033	18	0.00596	1.5	0.1
BS-3-8.1	175	68	35.5	1	39.2	0.8	-1397	41	-648	559	13578	248	+106	0.00610	0.64	0.96	2.5	.0055	3.9	162	2.0	0.0543	6.9	181	3.9	0.036	20	0.027	21	0.00552	3.9	0.2
BS-3-7.1	377	180	39.7	0.5	~~39.5~~	~~0.6~~	-594	13	289	252	6286	108	+86	0.00614	0.46	0.36	2.0	.0062	1.4	161	1.3	0.0554	8.4	162	1.4	0.052	11	0.044	11	0.00618	1.4	0.1
BS-3-4.1	278	94	37.3	1	39.5	1.0	-891	44			11398	378		0.00615	0.81	0.76	4.3	.0058	3.2	162	2.5	0.0491	10.0	173	3.2	0.001	1227	0.001	1227	0.00580	3.2	0.0
BS-3-5.1	365	140	39.6	0.3	~~39.6~~	~~0.3~~	-655	9	-20	127	8253	85	+302	0.00616	0.22	0.50	1.3	.0062	0.6	162	0.6	0.0457	5.3	162	0.6	0.046	5	0.039	5	0.00616	0.6	0.1

Errors are 1σ unless otherwise specified

Spot Name	ppm U	ppm Th	204corr 206Pb /238U Age	1σ err	207corr 206Pb /238U Age	1σ err	208corr 206Pb /238U Age	1σ err	204corr 207Pb /206Pb Age	1σ err	204corr 208Pb /232Th Age	1σ err	% Dis-cor-dant	7corr 206* /238	% err	4corr 208* /232	% err	8corr 206* /238	% err	Total 238 /206	% err	Total 207 /206	% err	4corr 238 /206*	% err	4corr 207* /206*	% err	4corr 207* /235	% err	4corr 206* /238	% err	err corr
BS4bt-1.1	93	37	35.0	2	37.1	2	-3503	257			22199	719		0.00578	1.33	2.00	5.3	.0054	5.6	167	4.0	0.0728	13.7	184	5.6	0.002	1472	0.002	1472	0.00544	5.6	0.0
BS4bt-6.1	98	41	38.6	1	37.4	1	-3000	127	973	435	19938	407	+96	0.00582	0.98	1.68	3.2	.0060	3.0	169	2.7	0.0612	18.7	166	3.0	0.072	21	0.059	22	0.00601	3.0	0.1
BS4bt-4.1	228	71	36.8	0.8	37.8	0.7	-943	26			12600	228		0.00588	0.60	0.87	2.4	.0057	2.3	169	1.8	0.0505	10.2	175	2.3	0.025	51	0.020	51	0.00572	2.3	0.0
BS4bt-10.1	125	69	38.9	1	37.8	1	-1867	258	881	438	12338	1061	+96	0.00588	0.94	0.84	11.5	.0060	3.4	170	2.9	0.0485	9.8	165	3.4	0.068	21	0.057	21	0.00605	3.4	0.2
BS4bt-3.1	138	87	36.8	1	38.1	0.9	-2236	116			12422	386		0.00593	0.77	0.85	4.2	.0057	3.1	168	2.4	0.0488	7.9	175	3.1	0.017	98	0.014	99	0.00572	3.1	0.0
BS4bt-7.1	218	73	38.5	1	38.2	1	-901	40	264	301	11603	349	+86	0.00595	0.98	0.78	4.0	.0060	3.0	167	3.0	0.0515	13.1	167	3.0	0.052	13	0.043	13	0.00599	3.0	0.2
BS4bt-5.1	152	77	38.6	1	39.0	1.0	-1798	127	-378	531	12968	566	+111	0.00607	0.80	0.90	5.9	.0060	2.6	165	2.5	0.0467	7.9	166	2.6	0.040	20	0.033	21	0.00601	2.6	0.1
BS4bt-8.1	192	97	35.7	4	38.9	3	-1281	106			10434	576		0.00606	2.42	0.68	7.1	.0056	9.9	109	5.6	0.3147	8.4	180	9.9	0.025	298	0.019	298	0.00555	9.9	0.0
BS4bt-6.1…dup1	132	71	40.1	2	40.4	1	-2451	608	-283	577	14828	2063	+114	0.00628	1.18	1.08	19.6	.0062	3.8	159	3.6	0.0493	8.5	160	3.8	0.041	23	0.035	23	0.00623	3.8	0.2
BS4bt-2.1	175	181	86.4	1	~~87.5~~	~~1~~	-1642	323	-498	387	6561	883	+118	0.01367	0.39	0.38	15.8	.0135	1.3	73	1.2	0.0477	4.7	74	1.3	0.038	15	0.070	15	0.01350	1.3	0.1
BS4bt-9.1	50	15	1397	24	~~1246~~	~~23~~	-3534	184	2681	21	34633	381	+53	0.21314	0.66	4.55	2.3	.2420	1.9	4	1.9	0.1803	1.1	4	1.9	0.183	1	6.112	2	0.24201	1.9	0.8

Errors are 1σ unless otherwise specified

Spot Name	ppm U	ppm Th	204corr 206Pb /238U Age	1σ err	207corr 206Pb /238U Age	1σ err	208corr 206Pb /238U Age	1σ err	204corr 207Pb /206Pb Age	1σ err	204corr 208Pb /232Th Age	1σ err	% Dis-cor-dant	7corr 206* /238	% err	4corr 208* /232	% err	8corr 206* /238	% err	Total 238 /206	% err	Total 207 /206	% err	4corr 238 /206*	% err	4corr 207* /206*	% err	4corr 207* /235	% err	4corr 206* /238	% err	err corr
BS-5-1.1	178	65	36.5	0.7	37.1	0.6	-1490	39	-774	906	14920	239	+105	0.00576	0.49	1.09	2.3	.0057	2.0	172	1.5	0.0518	6.7	176	2.0	0.034	32	0.027	32	0.00567	2.0	0.1
BS-5-11.1	149	53	39.2	1	37.7	0.9	-1787	59	1117	481	16948	316	+97	0.00587	0.75	1.31	2.8	.0061	2.9	170	2.0	0.0485	20.7	164	2.9	0.077	24	0.065	24	0.00610	2.9	0.1
BS-5-7.1	89	37	39.4	0.8	37.8	0.5	-3876	125	1182	386	22314	307	+97	0.00588	0.41	2.02	2.3	.0061	2.1	166	1.0	0.0650	10.0	163	2.1	0.079	20	0.067	20	0.00613	2.1	0.1
BS-5-6.1	281	100	35.6	0.9	38.0	0.3	-859	17			10594	145		0.00591	0.27	0.69	1.8	.0055	2.4	167	0.7	0.0595	6.1	180	2.4	0.005	321	0.004	321	0.00554	2.4	0.0
BS-5-8.1	294	110	37.2	0.8	38.3	0.7	-907	34			10627	274		0.00595	0.56	0.69	3.3	.0058	2.3	167	1.7	0.0527	6.0	173	2.3	0.023	56	0.018	56	0.00578	2.3	0.0
BS-5-2.1	1044	464	39.2	1	38.8	1.0	-209	14	415	160	3012	152	+91	0.00604	0.82	0.16	5.4	.0061	2.6	166	2.6	0.0452	5.5	164	2.6	0.055	7	0.046	8	0.00610	2.6	0.3
BS-5-4.1	83	35	39.1	2	39.3	2	-3964	246	-147	1020	22179	582	+127	0.00611	1.28	2.00	4.3	.0061	4.5	160	3.9	0.0666	8.3	164	4.5	0.043	41	0.036	41	0.00608	4.5	0.1
BS-5-10.1	370	184	36.9	1	39.5	1	-692	59			6779	436		0.00615	0.83	0.40	7.6	.0057	3.1	163	2.5	0.0455	12.5	174	3.1	0.009	131	0.007	131	0.00574	3.1	0.0
BS-5-3.1	358	165	41.2	1	41.2	1	-604	54	57.9	247	6632	443	+29	0.00642	1.09	0.39	7.8	.0064	3.4	154	3.4	0.0546	4.2	156	3.4	0.047	10	0.042	11	0.00642	3.4	0.3
BS-5-9.1	247	148	39.0	2	41.4	2	-1068	108			7919	579		0.00644	1.46	0.48	8.8	.0061	5.0	155	4.5	0.0460	6.9	165	5.0	0.001	2273	0.001	2273	0.00608	5.0	0.0
BS-5-5.1	397	13	85.4	2	~~85.8~~	~~2~~	-508	27	-82	130	38012	726	+206	0.01340	0.85	5.56	4.2	.0133	2.7	75	2.7	0.0478	2.9	75	2.7	0.045	5	0.082	6	0.01334	2.7	0.4

Errors are 1σ unless otherwise specified																															---------- 204 corrected ----------									
Spot Name	ppm U	ppm Th	204corr 206Pb /238U Age	1σ err	207corr 206Pb /238U Age	1σ err	208corr 206Pb /238U Age	1σ err	204corr 207Pb /206Pb Age	1σ err	204corr 208Pb /232Th Age	1σ err	% Dis-cor-dant	7corr 206* /238	% err	4corr 208* /232	% err	8corr 206* /238	% err	Total 238 /206	% err	Total 207 /206	% err	4corr 238 /206*	% err	4corr 207* /206*	% err	4corr 207* /235	% err	4corr 206* /238	% err	err corr
AX35-1.1	215	76	37.0	6	35.7	6	-988	235	1078	498	11812	1886	+97	0.00555	4.95	0.79	21.1	.0058	15.5	181	15.4	0.0433	30.4	174	15.5	0.075	25	0.060	29	0.00576	15.5	0.5
AX35-8.1	627	259	36.3	1	36.2	1	-440	27	135	210	5697	267	+73	0.00563	0.90	0.33	5.4	.0056	2.8	176	2.8	0.0522	6.9	177	2.8	0.049	9	0.038	9	0.00564	2.8	0.3
AX35-4.1	424	168	35.3	0.9	36.4	0.9	-542	18			6915	176		0.00566	0.78	0.41	3.0	.0055	2.6	177	2.4	0.0469	4.4	182	2.6	0.022	38	0.017	38	0.00549	2.6	0.1
AX35-3.1	195	103	37.3	1	37.1	1	-1273	88	284	379	9993	473	+87	0.00577	0.99	0.64	6.0	.0058	3.0	173	3.0	0.0472	15.3	172	3.0	0.052	17	0.042	17	0.00581	3.0	0.2
AX35-10.1	124	60	38.2	1	37.2	1	-2692	185	881	277	16862	610	+96	0.00578	1.13	1.30	5.3	.0059	3.6	170	3.5	0.0604	7.6	168	3.6	0.068	13	0.056	14	0.00594	3.6	0.3
AX35-6.1	323	128	38.2	0.9	37.5	0.8	-741	41	605	286	8767	352	+94	0.00584	0.72	0.54	5.0	.0059	2.4	165	2.2	0.0775	4.0	168	2.4	0.060	13	0.049	13	0.00594	2.4	0.2
AX35-7.1	111	44	39.0	1	38.3	1	-2486	101	603	323	18851	395	+94	0.00596	0.90	1.54	3.2	.0061	2.6	165	2.6	0.0600	14.9	165	2.6	0.060	15	0.050	15	0.00607	2.6	0.2
AX35-9.1	307	131	38.7	0.8	38.9	0.8	-784	46	-211	320	8531	361	+119	0.00606	0.69	0.53	5.2	.0060	2.1	165	2.1	0.0456	9.3	166	2.1	0.042	13	0.035	13	0.00602	2.1	0.2
AX35-5.1	291	126	40.5	0.7	40.2	0.7	-846	28	337	166	8915	211	+88	0.00626	0.56	0.55	2.9	.0063	1.8	159	1.7	0.0502	4.9	158	1.8	0.053	7	0.046	8	0.00631	1.8	0.2
AX35-11.1	266	122	40.3	0.6	~~40.9~~	~~0.5~~	-801	23	-672	449	8158	167	+106	0.00637	0.42	0.50	2.5	.0063	1.5	157	1.3	0.0445	5.1	159	1.5	0.035	16	0.031	16	0.00628	1.5	0.1
AX35-2.1	299	36	122	2	~~121~~	~~2~~	-641	52	446	81	21124	832	+73	0.01896	0.62	1.84	6.4	.0191	1.9	52	1.9	0.0585	2.4	52	1.9	0.056	4	0.147	4	0.01914	1.9	0.5

Appendix C2.
U-Pb Zircon SHRIMP Trace Element Geochemistry

Fe ppm values in red denote possible contamination by an inclusion.

Spot Name	Fe (ppm)	Y (ppm)	La (ppm)	Ce (ppm)	Nd (ppm)	Sm (ppm)	Eu (ppm)	Gd (ppm)	Dy (ppm)	Er (ppm)	Yb (ppm)	Hf (ppm)	Eu (star)	Yb/Gd	La (ch)	Ce (ch)	Nd (ch)	Sm (ch)	Eu (ch)	Gd (ch)	Dy (chn)	Y (ch)	Er (ch)	Yb (ch)
BS-1-7.1	0.3	447	0.010	11.9	0.22	0.61	0.44	7.6	34	79	200	12874	0.623	26.5	0.044	19.4	0.49	4.1	7.8	38	137	284	493	1245
BS-1-8.1	0.1	386	0.014	10.8	0.28	0.81	0.40	7.6	31	68	169	12396	0.492	22.4	0.058	17.7	0.61	5.4	7.1	38	125	246	427	1052
BS-1-2.1	0.1	505	0.009	11.6	0.31	1.06	0.52	10.8	42	90	214	11326	0.466	19.8	0.037	18.9	0.69	7.2	9.2	54	171	322	560	1329
BS-1-9.1	0.8	792	0.017	17.7	0.60	1.36	0.74	15.4	67	140	311	10713	0.492	20.1	0.073	28.9	1.32	9.2	13.1	78	272	504	873	1930
BS-1-10.1	0.5	562	0.077	12.4	0.46	1.22	0.57	10.0	49	105	235	10526	0.500	23.4	0.326	20.3	1.00	8.3	10.2	50	198	358	658	1460
BS-1-4.1	0.1	436	0.005	11.6	0.22	0.90	0.47	8.7	38	79	169	10664	0.507	19.5	0.021	19.0	0.49	6.1	8.3	44	153	278	492	1051
BS-1-5.1	0.6	237	0.017	10.6	0.24	0.48	0.32	4.0	18	42	110	11242	0.709	27.2	0.070	17.3	0.53	3.2	5.8	20	75	151	263	682
BS-1-6.1	1.7	840	0.040	19.5	0.40	1.60	0.62	18.3	71	125	235	12174	0.349	12.9	0.168	31.8	0.88	10.8	11.0	92	290	535	778	1461
BS-1-3.1	8.7	388	0.010	1.8	0.04	0.21	0.16	4.3	25	68	212	11713	0.522	49.0	0.041	3.0	0.09	1.4	2.9	22	103	247	427	1315

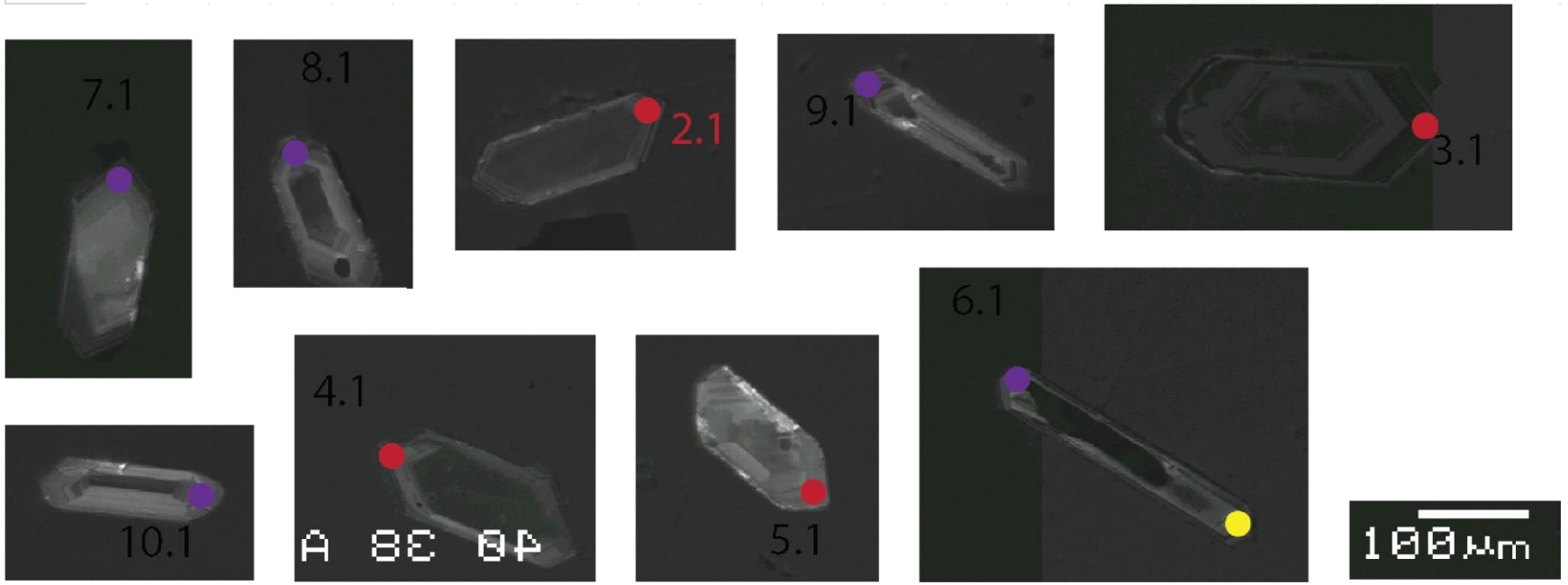

Spot Name	Fe (ppm)	Y (ppm)	La (ppm)	Ce (ppm)	Nd (ppm)	Sm (ppm)	Eu (ppm)	Gd (ppm)	Dy (ppm)	Er (ppm)	Yb (ppm)	Hf (ppm)	Eu (star)	Yb/Gd	La (ch)	Ce (ch)	Nd (ch)	Sm (ch)	Eu (ch)	Gd (ch)	Dy (chn)	Y (ch)	Er (ch)	Yb (ch)
BS-2-3.1	0.3	352	0.017	9.0	0.16	0.46	0.29	5.1	25	65	173	12550	0.584	34.1	0.074	14.7	0.35	3.1	5.2	26	102	224	405	1075
BS-2-6.1	0.1	558	0.004	14.0	0.35	1.02	0.49	10.2	45	99	240	11205	0.468	23.6	0.017	22.8	0.77	6.9	8.8	51	182	356	620	1492
BS-2-8.1	0.2	307	0.003	5.4	0.11	0.30	0.18	3.6	24	57	147	13020	0.530	40.8	0.011	8.7	0.25	2.0	3.2	18	98	195	355	912
BS-2-4.1	0.1	330	0.004	15.4	0.21	0.58	0.36	5.9	26	60	149	11984	0.594	25.2	0.017	25.1	0.46	3.9	6.4	30	104	210	378	924
BS-2-1.1	0.1	983	0.011	22.6	0.70	2.14	1.04	18.3	83	177	400	10331	0.507	21.9	0.045	36.9	1.54	14.4	18.5	92	336	626	1106	2487
BS-2-7.1	0.7	372	0.081	11.2	0.30	0.87	0.44	7.1	29	64	156	9302	0.536	21.9	0.342	18.2	0.66	5.9	7.8	36	119	237	401	967
BS-2-5.1	0.2	182	0.021	8.6	0.13	0.35	0.22	2.9	14	33	86	11514	0.654	29.6	0.087	14.1	0.29	2.3	3.8	15	56	116	207	537
BS-2-2.1	1.6	338	0.063	9.8	0.22	0.65	0.34	6.2	28	58	139	10561	0.518	22.5	0.265	16.0	0.47	4.4	6.1	31	113	215	364	866

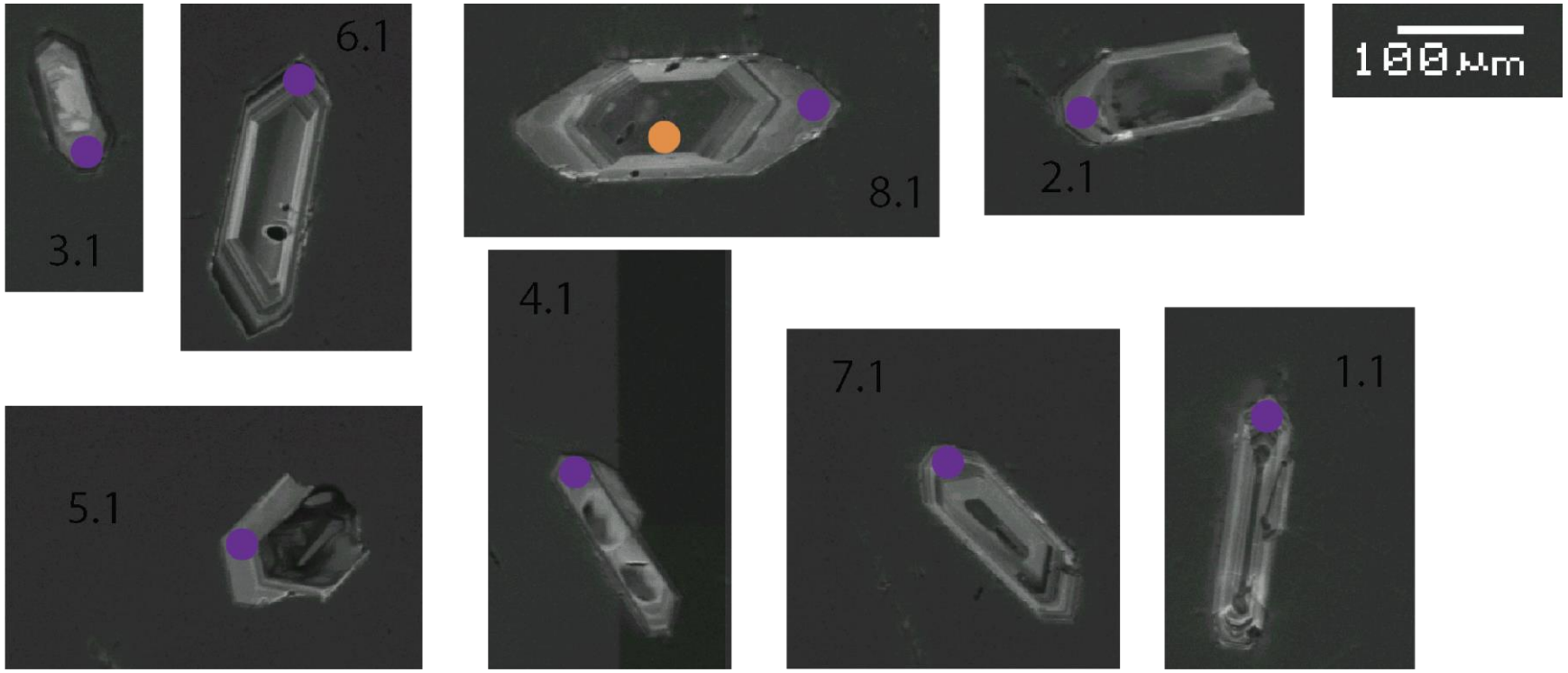

Spot Name	Fe (ppm)	Y (ppm)	La (ppm)	Ce (ppm)	Nd (ppm)	Sm (ppm)	Eu (ppm)	Gd (ppm)	Dy (ppm)	Er (ppm)	Yb (ppm)	Hf (ppm)	Eu (star)	Yb/Gd	La (ch)	Ce (ch)	Nd (ch)	Sm (ch)	Eu (ch)	Gd (ch)	Dy (chn)	Y (ch)	Er (ch)	Yb (ch)
BS-5-1.1	0.1	478	0.008	9.3	0.31	1.08	0.38	8.7	37	81	191	9573	0.373	21.9	0.034	15.2	0.67	7.3	6.7	44	152	304	504	1184
BS-5-11.1	0.3	453	0.010	7.6	0.29	1.12	0.53	9.2	35	81	190	10326	0.508	20.7	0.044	12.4	0.64	7.6	9.5	46	144	289	503	1179
BS-5-7.1	0.5	326	0.012	10.3	0.24	0.62	0.24	6.3	27	61	136	11720	0.370	21.7	0.050	16.8	0.52	4.2	4.3	32	112	208	384	846
BS-5-6.1	21.0	656	0.015	6.6	0.33	0.89	0.45	9.9	53	116	279	10211	0.466	28.2	0.065	10.7	0.73	6.0	8.1	50	215	418	726	1732
BS-5-8.1	19.9	632	0.067	16.0	0.51	1.08	0.63	11.8	47	112	258	11484	0.535	21.9	0.282	26.1	1.11	7.3	11.1	59	192	402	699	1603
BS-5-2.1	0.3	2005	0.010	48.7	0.95	3.57	1.36	38.4	169	355	708	11055	0.354	18.4	0.044	79.5	2.09	24.1	24.2	193	688	1277	2218	4400
BS-5-4.1	0.1	300	0.010	11.2	0.27	0.64	0.36	5.4	24	52	132	10448	0.586	24.7	0.043	18.3	0.59	4.3	6.3	27	96	191	325	823
BS-5-10.1	4.1	881	0.021	20.6	0.78	2.39	1.37	19.5	75	151	307	11387	0.612	15.7	0.088	33.6	1.71	16.2	24.4	98	304	561	942	1909
BS-5-3.1	0.5	891	0.008	12.3	0.49	1.49	0.61	15.6	77	160	347	9755	0.386	22.3	0.033	20.1	1.06	10.1	10.8	78	314	568	1001	2155
BS-5-9.1	10.1	735	0.054	16.1	0.86	1.85	1.06	16.1	61	127	272	9806	0.596	17.0	0.228	26.2	1.87	12.5	18.9	81	250	468	794	1692
BS-5-5.1	0.3	311	0.006	3.3	0.02	0.17	0.16	3.4	23	57	141	11476	0.653	41.4	0.027	5.3	0.05	1.1	2.9	17	95	198	358	875

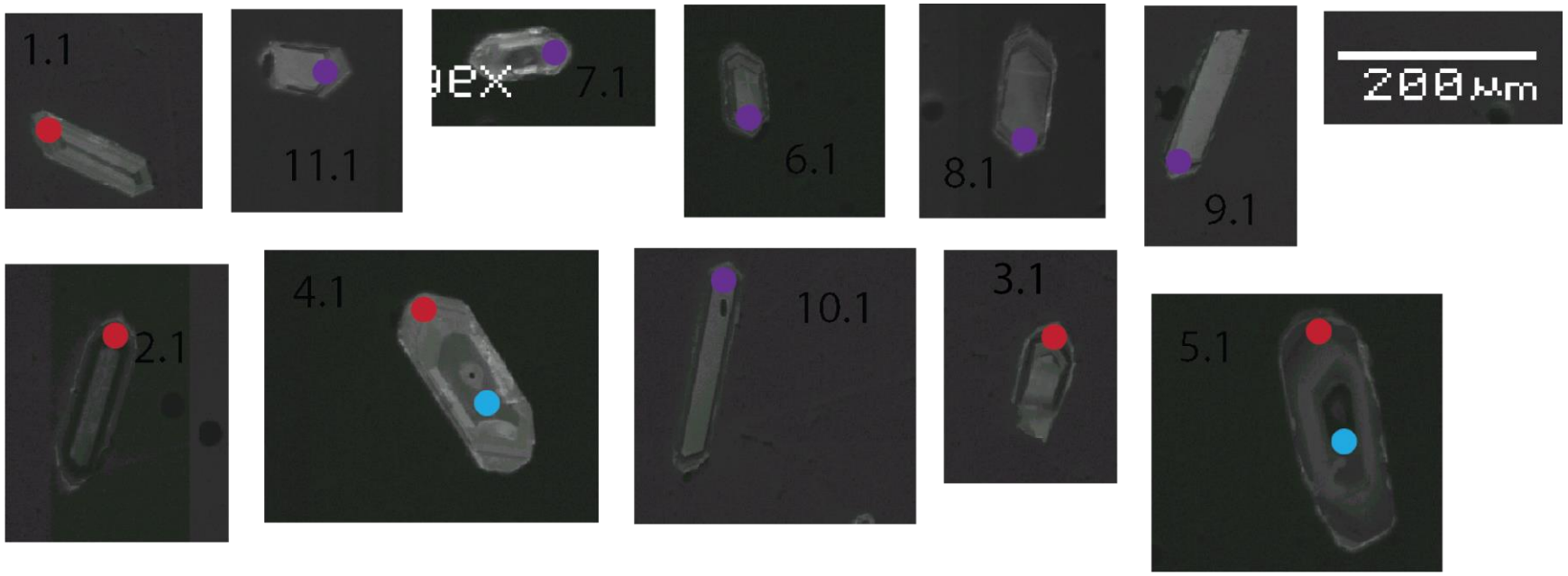

Spot Name	Fe (ppm)	Y (ppm)	La (ppm)	Ce (ppm)	Nd (ppm)	Sm (ppm)	Eu (ppm)	Gd (ppm)	Dy (ppm)	Er (ppm)	Yb (ppm)	Hf (ppm)	Eu (star)	Yb/Gd	La (ch)	Ce (ch)	Nd (ch)	Sm (ch)	Eu (ch)	Gd (ch)	Dy (chn)	Y (ch)	Er (ch)	Yb (ch)
BS4bt-1.1	0.1	361	0.014	8.7	0.26	0.69	0.29	7.2	31	64	150	9251	0.404	21.0	0.058	14.1	0.57	4.7	5.2	36	125	230	403	933
BS4bt-6.1	0.5	440	0.014	11.2	0.37	0.91	0.43	8.9	37	83	196	10349	0.462	22.0	0.058	18.2	0.80	6.2	7.7	45	152	280	520	1216
BS4bt-4.1	4.0	579	0.041	7.2	0.54	1.41	0.66	12.3	47	101	214	8112	0.480	17.5	0.172	11.8	1.18	9.5	11.6	62	192	369	629	1329
BS4bt-10.1	1.4	604	0.071	14.8	0.67	1.49	0.70	11.7	51	111	247	9450	0.513	21.1	0.300	24.2	1.46	10.1	12.5	59	207	385	692	1535
BS4bt-3.1	0.4	527	0.023	15.0	0.53	1.32	0.79	11.9	45	90	206	10511	0.609	17.3	0.095	24.6	1.15	8.9	14.1	60	182	336	562	1281
BS4bt-7.1	8.5	788	0.024	8.2	0.76	1.77	0.83	15.6	65	141	302	8476	0.479	19.3	0.101	13.4	1.67	12.0	14.7	79	265	502	880	1878
BS4bt-5.1	0.7	731	0.012	19.0	0.69	1.60	0.65	12.9	59	135	293	10144	0.434	22.7	0.049	30.9	1.51	10.8	11.5	65	242	466	845	1823
BS4bt-8.1	575.3	670	0.070	14.4	0.56	1.38	0.55	12.1	56	115	239	8469	0.411	19.8	0.294	23.5	1.22	9.3	9.8	61	228	427	716	1484
BS4bt-6.1…dup1	0.2	418	0.029	11.2	0.55	1.32	0.51	10.7	39	82	188	11523	0.411	17.5	0.124	18.2	1.21	8.9	9.0	54	158	266	511	1165
BS4bt-2.1	3.0	643	0.032	36.2	2.09	5.48	2.59	39.3	77	93	131	9538	0.539	3.3	0.135	59.1	4.57	37.0	46.1	198	313	410	578	817
BS4bt-9.1	16.3	276	0.022	3.7	0.20	0.58	0.18	5.7	25	49	91	9101	0.306	15.9	0.091	6.1	0.44	3.9	3.2	29	100	176	309	567

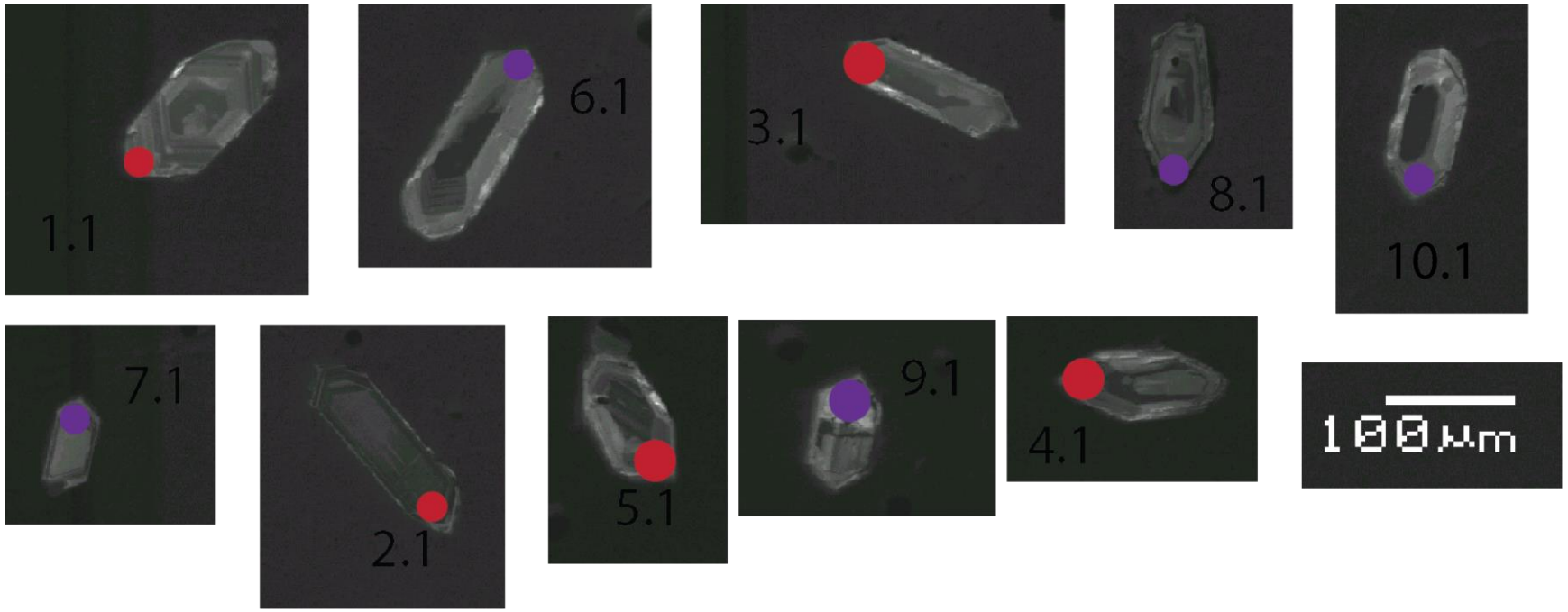

Spot Name	Fe (ppm)	Y (ppm)	La (ppm)	Ce (ppm)	Nd (ppm)	Sm (ppm)	Eu (ppm)	Gd (ppm)	Dy (ppm)	Er (ppm)	Yb (ppm)	Hf (ppm)	Eu (star)	Yb/Gd	La (ch)	Ce (ch)	Nd (ch)	Sm (ch)	Eu (ch)	Gd (ch)	Dy (chn)	Y (ch)	Er (ch)	Yb (ch)
AX35-1.1	0.2	630	0.016	16.9	0.35	1.16	0.56	10.9	52	124	290	12754	0.480	26.6	0.067	27.6	0.77	7.9	10.0	55	213	401	778	1802
AX35-8.1	2.0	1168	0.195	31.5	0.59	1.36	0.84	18.8	89	198	415	9878	0.504	22.1	0.822	51.4	1.29	9.2	14.9	95	363	744	1237	2578
AX35-4.1	3.3	813	0.328	17.7	0.87	1.57	0.92	16.3	65	141	288	8611	0.553	17.7	1.385	28.8	1.91	10.6	16.3	82	264	518	884	1787
AX35-3.1	1.8	521	0.480	13.6	0.84	1.55	0.72	12.1	45	92	190	8837	0.505	15.8	2.024	22.2	1.83	10.5	12.7	61	183	332	577	1181
AX35-10.1	2.1	352	0.064	12.3	0.43	0.85	0.49	6.7	28	62	148	10876	0.623	22.0	0.269	20.1	0.95	5.7	8.7	34	114	224	385	919
AX35-6.1	0.5	787	0.413	18.5	0.70	1.55	0.75	14.4	66	144	327	10232	0.482	22.7	1.742	30.2	1.53	10.5	13.3	72	267	501	902	2030
AX35-7.1	4.5	397	0.130	10.0	0.29	0.94	0.48	7.8	34	72	165	9855	0.539	21.2	0.550	16.3	0.64	6.4	8.5	39	138	253	449	1024
AX35-9.1	3.0	665	0.181	14.7	0.75	1.42	0.85	13.4	52	117	265	9619	0.592	19.8	0.764	24.0	1.65	9.6	15.0	67	212	423	730	1644
AX35-5.1	19.6	486	0.012	11.5	0.50	1.19	0.65	11.4	41	83	185	10407	0.541	16.2	0.051	18.7	1.10	8.0	11.6	58	165	309	517	1151
AX35-11.1	-0.1	469	0.461	14.6	0.56	1.12	0.61	10.1	41	85	188	8962	0.554	18.6	1.947	23.7	1.22	7.5	10.8	51	169	299	531	1165
AX35-2.1	2.5	526	0.014	7.9	0.24	0.85	0.36	9.1	46	111	293	11488	0.393	32.3	0.060	12.9	0.52	5.7	6.4	46	185	335	695	1820

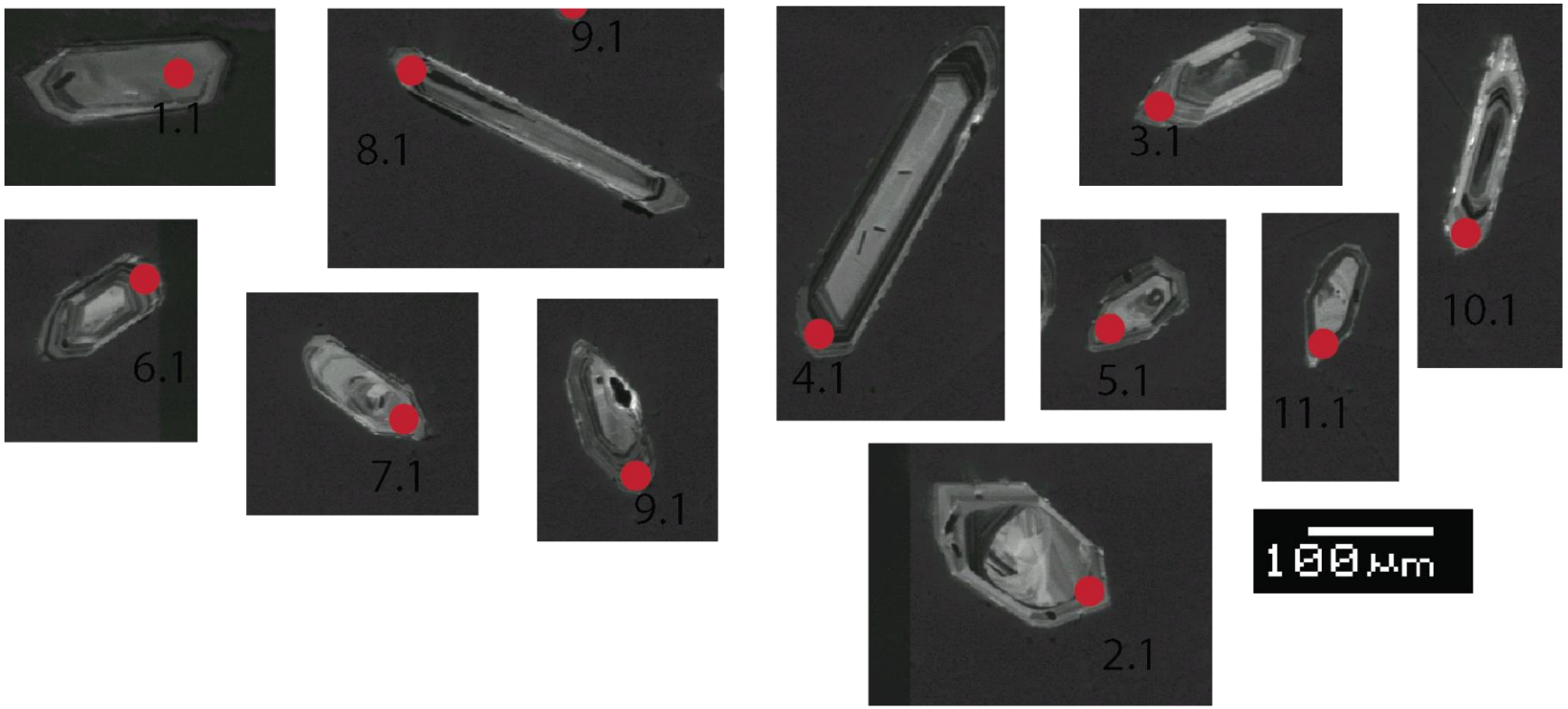

Spot Name	Fe (ppm)	Y (ppm)	La (ppm)	Ce (ppm)	Nd (ppm)	Sm (ppm)	Eu (ppm)	Gd (ppm)	Dy (ppm)	Er (ppm)	Yb (ppm)	Hf (ppm)	Eu (star)	Yb/Gd	La (ch)	Ce (ch)	Nd (ch)	Sm (ch)	Eu (ch)	Gd (ch)	Dy (chn)	Y (ch)	Er (ch)	Yb (ch)
BS-3-1.1	4.5	918	0.012	17.7	0.87	1.93	0.71	16.8	72	165	367	10736	0.382	21.9	0.049	28.8	1.90	13.1	12.7	84	292	585	1034	2282
BS-3-3.1	3.2	1007	0.093	26.1	0.49	1.65	0.99	19.0	85	179	392	11704	0.539	20.6	0.394	42.6	1.07	11.1	17.6	96	345	641	1116	2433
BS-3-2.1	0.4	1225	0.011	31.4	1.03	2.61	1.32	23.1	102	222	487	10996	0.520	21.1	0.048	51.2	2.26	17.6	23.5	116	415	780	1386	3023
BS-3-10.1	1.6	238	0.015	10.0	0.17	0.59	0.32	4.9	18	42	106	11438	0.583	21.8	0.064	16.3	0.38	4.0	5.7	24	75	151	261	659
BS-3-9.1	9.0	422	0.108	12.0	0.41	0.87	0.47	8.9	33	71	162	10212	0.513	18.2	0.457	19.7	0.90	5.9	8.3	45	135	269	446	1008
BS-3-6.1	0.3	694	0.015	13.4	0.52	1.47	0.61	13.8	55	125	285	10865	0.415	20.6	0.065	21.8	1.13	9.9	10.9	70	223	442	778	1767
BS-3-12.1	0.2	456	0.287	11.0	0.61	0.96	0.43	8.3	35	80	194	10714	0.466	23.3	1.211	17.9	1.33	6.5	7.7	42	142	290	497	1202
BS-3-11.1	2.8	1006	0.041	21.8	1.05	2.77	1.65	25.8	89	170	357	10173	0.596	13.9	0.171	35.5	2.29	18.7	29.3	130	363	641	1061	2219
BS-3-8.1	1.7	471	0.031	12.3	0.43	1.10	0.55	9.0	39	89	208	10422	0.533	23.0	0.130	20.0	0.94	7.4	9.8	45	160	300	554	1289
BS-3-7.1	0.6	803	0.021	14.1	0.63	1.78	0.82	16.5	69	144	316	9992	0.459	19.1	0.088	22.9	1.39	12.1	14.5	83	281	511	901	1964
BS-3-4.1	4.4	538	0.135	11.5	0.48	0.90	0.58	10.1	41	97	236	9519	0.588	23.2	0.568	18.7	1.06	6.1	10.3	51	168	342	607	1464
BS-3-5.1	0.3	831	0.011	15.9	0.49	1.79	0.65	16.4	66	149	337	10727	0.364	20.5	0.045	26.0	1.08	12.1	11.5	82	268	529	932	2090

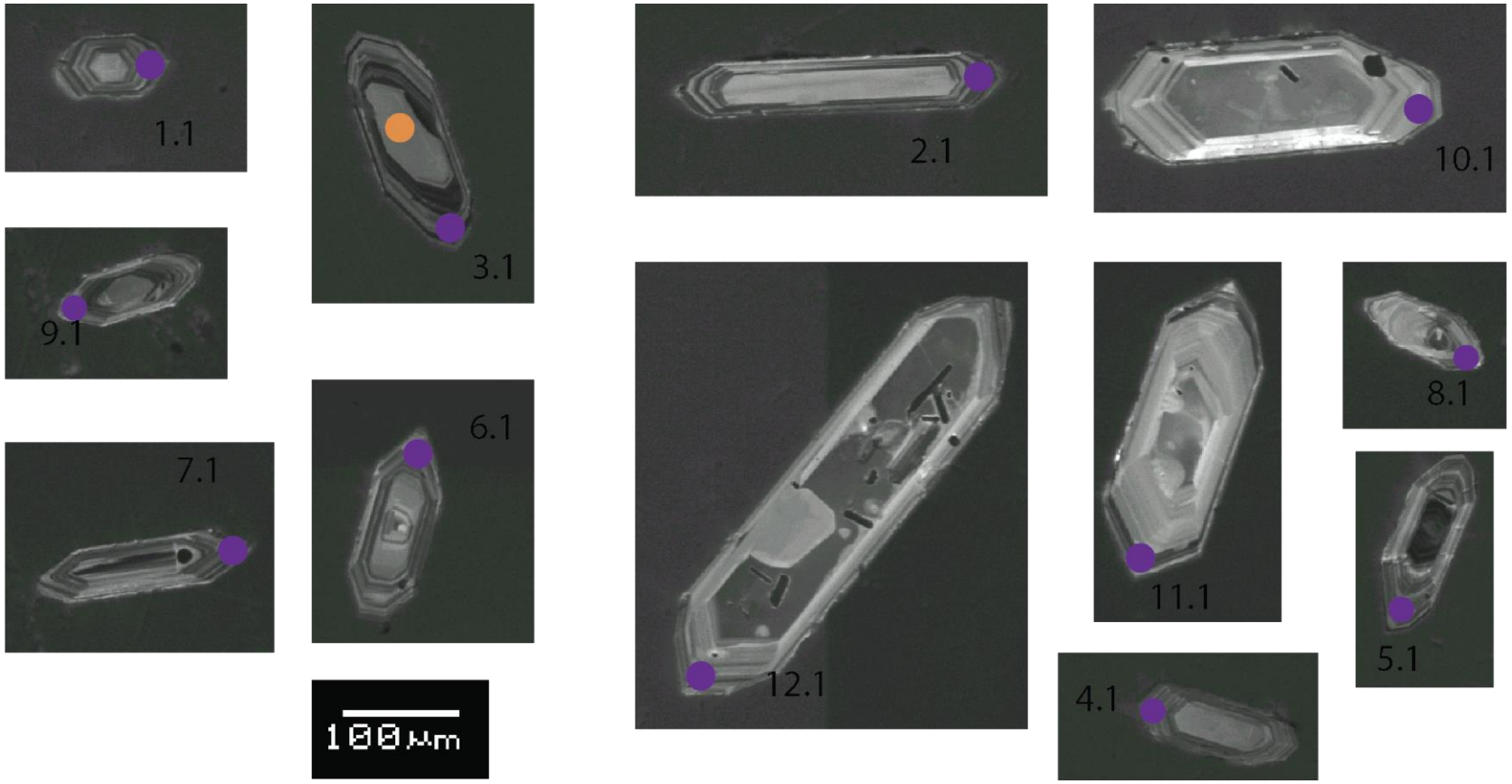

Appendix D.
Microprobe Analyses on Carlin-style Mineralization

AX43-1314.1 Grain 1
CSD Zone

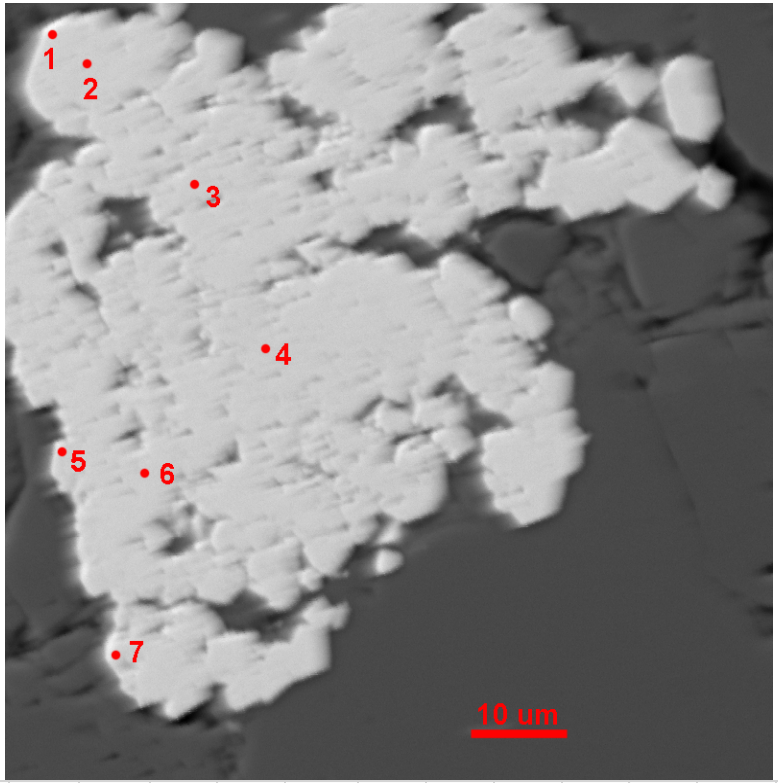

No.	Ag	Au	Na	Hg	Tl	As	Pb	Cu	Se	Bi	Co	Zn	W	Ni	Si	Te	Fe	Al	Sb	Ti	Sn	Mo	S	Ca	Total
1	0	0	0	0	0.075	0.019	0	0	0.009	0.007	0.063	0	0	0.001	0.06	0	45.475	0.024	0.023	0	0.015	0.655	53.61	0.253	100.289
2	0	0	0.009	0	0.032	0.042	0	0	0	0.003	0.048	0	0.008	0	0.019	0	45.598	0.003	0.024	0.025	0.028	0.652	53.757	0.096	100.344
3	0	0	0	0.002	0.017	0.062	0	0	0.002	0	0.054	0.007	0	0.006	0.003	0	42.201	0	0.029	0.014	0.016	0.633	49.699	1.772	94.517
4	0	0	0	0	0.023	0.02	0	0.001	0	0	0.063	0.019	0	0	0.071	0	45.635	0.029	0.016	0	0.023	0.66	53.859	0	100.419
5	0	0	0.005	0	0	0.034	0	0.008	0.008	0.003	0.044	0	0.012	0	0.028	0	45.347	0.004	0.008	0.002	0.017	0.691	53.664	0.156	100.031
6	0	0	0	0.001	0.011	0.076	0	0	0.001	0	0.054	0	0	0	0.017	0	45.564	0	0.031	0.02	0.021	0.656	54.191	0.02	100.663
7	0	0.006	0.016	0	0.026	0.016	0	0.001	0	0	0.063	0.008	0.012	0	0.037	0	45.358	0.006	0.013	0	0.015	0.612	52.306	0.276	98.771

**0 indicates below detection limit. See Hill (2016) for detection limits per element.*

AX43-1314.1 Grain 2
CSD Zone

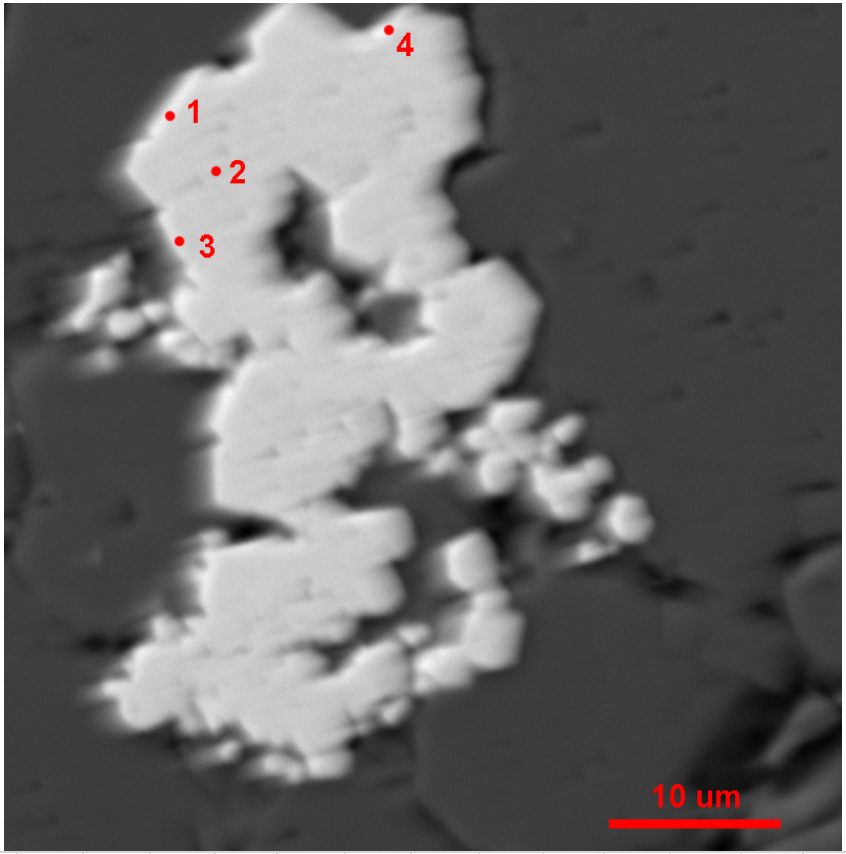

No.	Ag	Au	Na	Hg	Tl	As	Pb	Cu	Se	Bi	Co	Zn	W	Ni	Si	Te	Fe	Al	Sb	Ti	Sn	Mo	S	Ca	Total
1	0	0	0.017	0	0.034	0.05	0	0	0.003	0	0.047	0	0.001	0.003	0.202	0	44.773	0.043	0.012	0	0.015	0.634	53.453	0.212	99.499
2	0	0	0.008	0.008	0.062	0.076	0	0	0.001	0	0.053	0.02	0.009	0.011	0.057	0	45.298	0.02	0.02	0.018	0.024	0.647	53.728	0.134	100.194
3	0	0.009	0.023	0	0.031	0.098	0	0	0	0	0.048	0.028	0	0	0.077	0	44.78	0.04	0.035	0.011	0.02	0.648	53.497	0.123	99.468
4	0	0	0.026	0	0	0.003	0	0.018	0	0	0.063	0.027	0.019	0	0.175	0	44.802	0.062	0.013	0.006	0.019	0.664	53.395	0.321	99.613

AX43-1314.1 Grain 3
CSD Zone

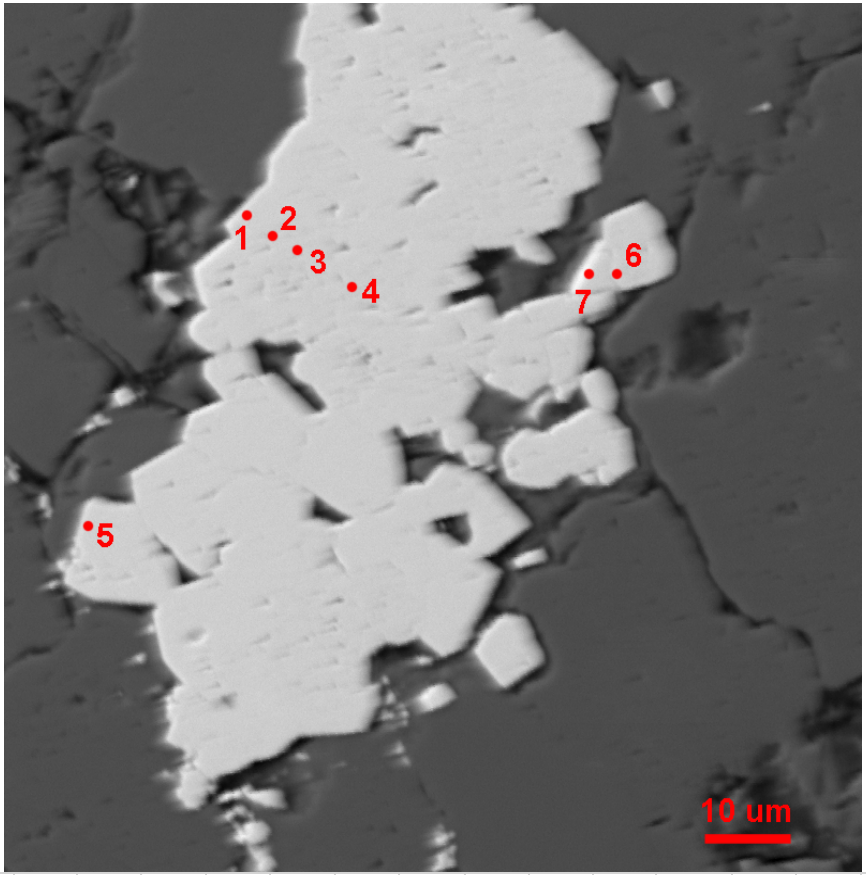

No.	Ag	Au	Na	Hg	Tl	As	Pb	Cu	Se	Bi	Co	Zn	W	Ni	Si	Te	Fe	Al	Sb	Ti	Sn	Mo	S	Ca	Total
1	0	0	0	0	0	0.173	0	0.004	0.002	0.006	0.076	0	0.005	0.153	0.05	0	45.159	0.016	0	0.016	0.021	0.661	53.618	0.091	100.051
2	0	0.002	0.023	0.004	0.065	0.002	0	0.003	0	0	0.062	0.033	0.008	0.009	0.151	0	45.142	0.033	0.012	0	0.019	0.651	53.587	0.032	99.838
3	0	0	0.002	0	0.021	0	0	0.014	0	0	0.048	0	0.003	0.009	0.106	0	45.488	0.035	0.02	0	0.024	0.659	53.793	0	100.222
4	0	0.002	0	0.001	0.066	0.005	0	0.012	0.017	0	0.068	0.039	0	0	0.032	0	45.206	0.004	0.014	0	0.017	0.645	52.574	0	98.702
5	0	0	0	0.009	0	0.023	0	0	0.011	0	0.032	0	0.024	0	0.004	0	45.152	0	0.018	0.01	0.009	0.647	53.825	0.322	100.086
6	0	0	0.008	0	0	0.243	0	0.002	0	0.001	0.011	0	0	0	0.148	0	5.042	0.06	0.124	0.002	0	0.065	5.945	18.319	29.97
7	0.008	0.008	0.046	0.001	0.073	0.614	0	0.003	0	0	0.06	0	0.003	0	0.367	0	39.285	0.241	0.136	0	0.006	0.617	50.017	1.246	92.731

AX43-1314.1 Grain 4
CSD Zone

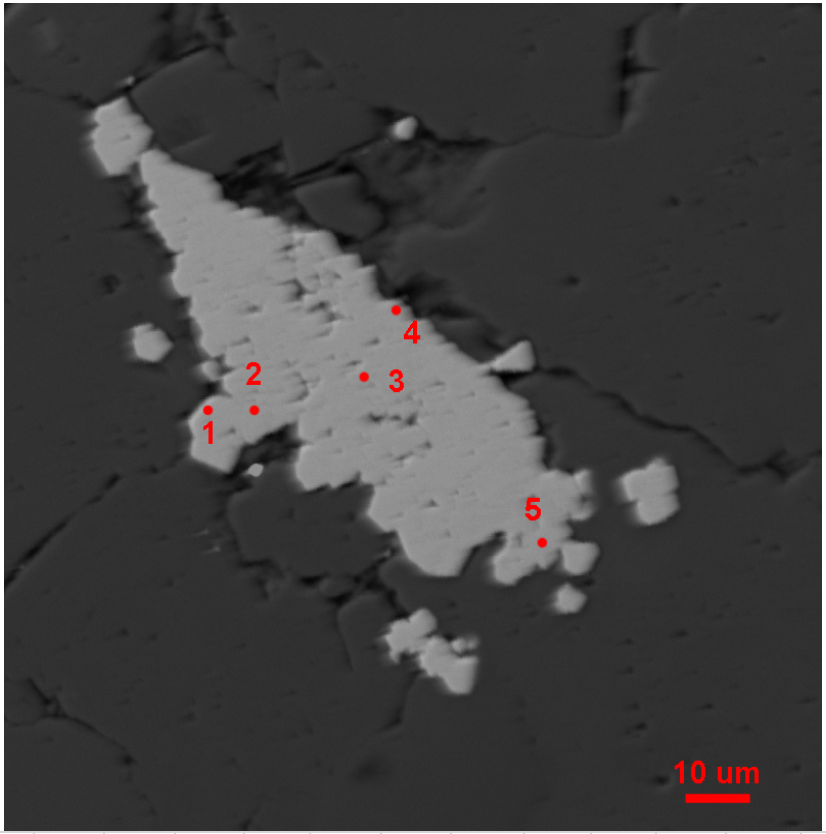

No.	Ag	Au	Na	Hg	Tl	As	Pb	Cu	Se	Bi	Co	Zn	W	Ni	Si	Te	Fe	Al	Sb	Ti	Sn	Mo	S	Ca	Total
1	0	0.03	0.014	0	0.049	0.028	0	0.009	0	0	0.05	0.013	0	0.006	0.971	0	42.192	0.928	0.035	0	0.014	0.632	50.125	0.287	95.383
2	**0**	**0**	**0.056**	**0**	**0**	**0.103**	**0.28**	**0.003**	**0**	**0**	**0.008**	**0.004**	**0**	**0.004**	**0.783**	**0.022**	**1.197**	**0.408**	**0.044**	**0.473**	**0**	**0.01**	**0.874**	**20.268**	**24.537**
3	0	0	0.025	0	0.089	0.12	0	0.014	0	0	0.068	0	0.007	0.006	0.079	0	45.064	0.031	0.017	0.004	0.012	0.695	53.476	0.08	99.787
4	0	0.008	0	0	0.033	0.193	0	0.017	0	0	0.061	0	0.007	0.009	0.064	0	45.029	0.011	0.03	0.008	0.025	0.724	53.877	0.278	100.374
5	**0**	**0.019**	**0**	**0.015**	**0**	**0.188**	**0**	**0**	**0**	**0**	**0.029**	**0**	**0.02**	**0.01**	**0.017**	**0.004**	**14.743**	**0.013**	**0.036**	**0**	**0**	**0.19**	**15.787**	**13.457**	**44.528**

AX43-1314.1 Grain 5
CSD Zone

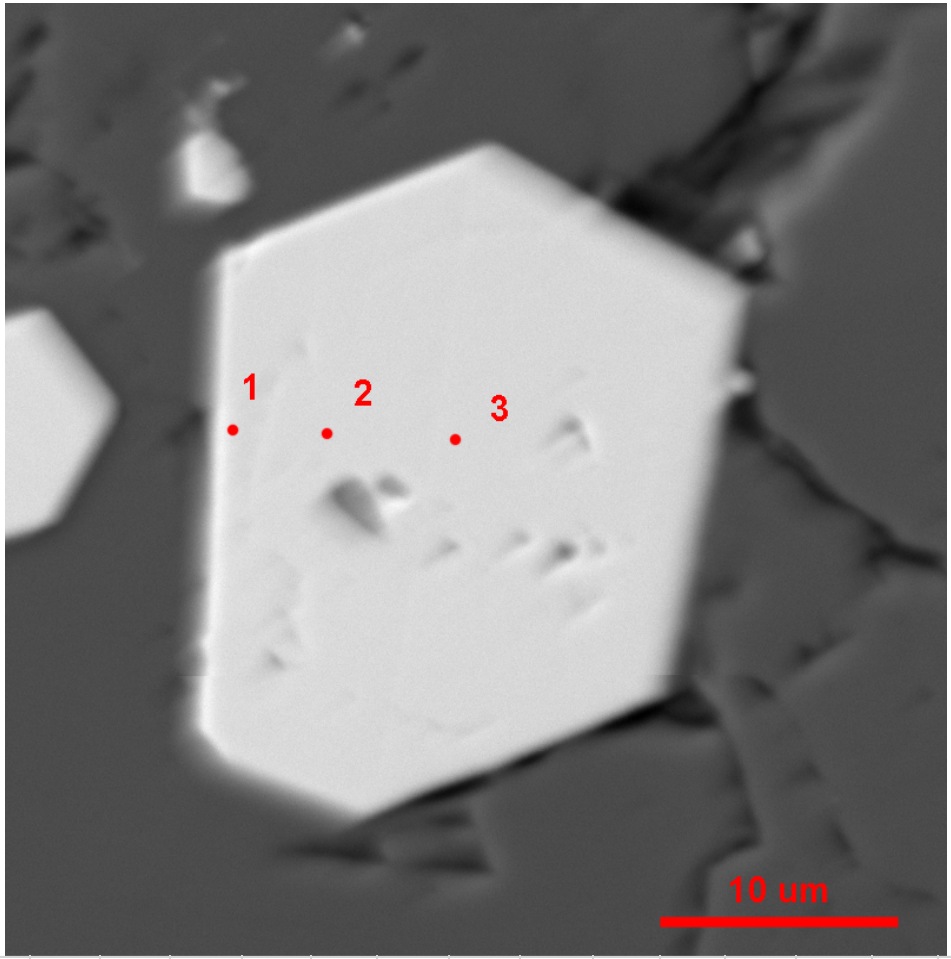

No.	Ag	Au	Na	Hg	Tl	As	Pb	Cu	Se	Bi	Co	Zn	W	Ni	Si	Te	Fe	Al	Sb	Ti	Sn	Mo	S	Ca	Total
1	0	0.067	0.084	0.009	0.073	0	0	0.008	0	0	0.033	0.594	0.013	0.014	0.043	0.001	27.406	0	0.043	0.019	0	0.378	31.771	14.836	75.392
2	0	0	0	0.001	0.055	0	0	0.003	0	0	0.063	0	0	0	0.024	0	45.835	0	0.01	0.022	0.028	0.666	54.314	0.036	101.057
3	0	0	0.021	0	0.048	0	0	0.008	0.005	0	0.074	0.023	0	0	0.156	0	44.681	0.039	0.012	0	0.03	0.66	53.791	0.096	99.644

PG02-2099.5 Grain 1
CSD Zone

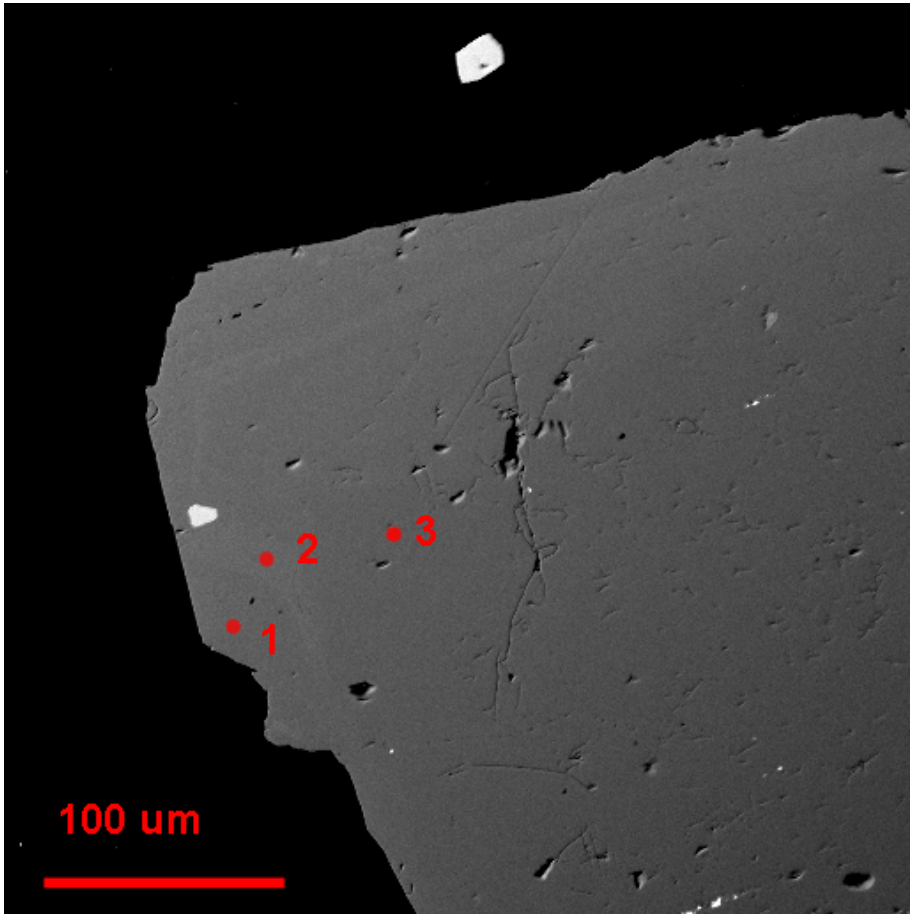

No.	Ag	Au	Na	Hg	Tl	As	Pb	Cu	Se	Bi	Co	Zn	W	Ni	Si	Te	Fe	Al	Sb	Ti	Sn	Mo	S	Ca	Total
1	0	0.001	0.005	0.002	0.053	0.3	0	0	0	0	0.054	0.014	0.012	0	0	0	45.498	0.001	0.013	0	0.019	0.643	53.97	0.124	100.709
2	0	0	0.007	0	0.061	1.485	0	0.011	0	0	0.07	0	0.022	0	0	0	45.357	0.001	0.008	0.01	0.013	0.65	53.112	0	100.807
3	0	0	0	0	0.034	0.016	0	0	0	0	0.062	0.018	0.033	0	0	0	45.808	0	0.007	0.002	0.018	0.657	54.476	0	101.131

PG02-2099.5 Grain 2
CSD Zone

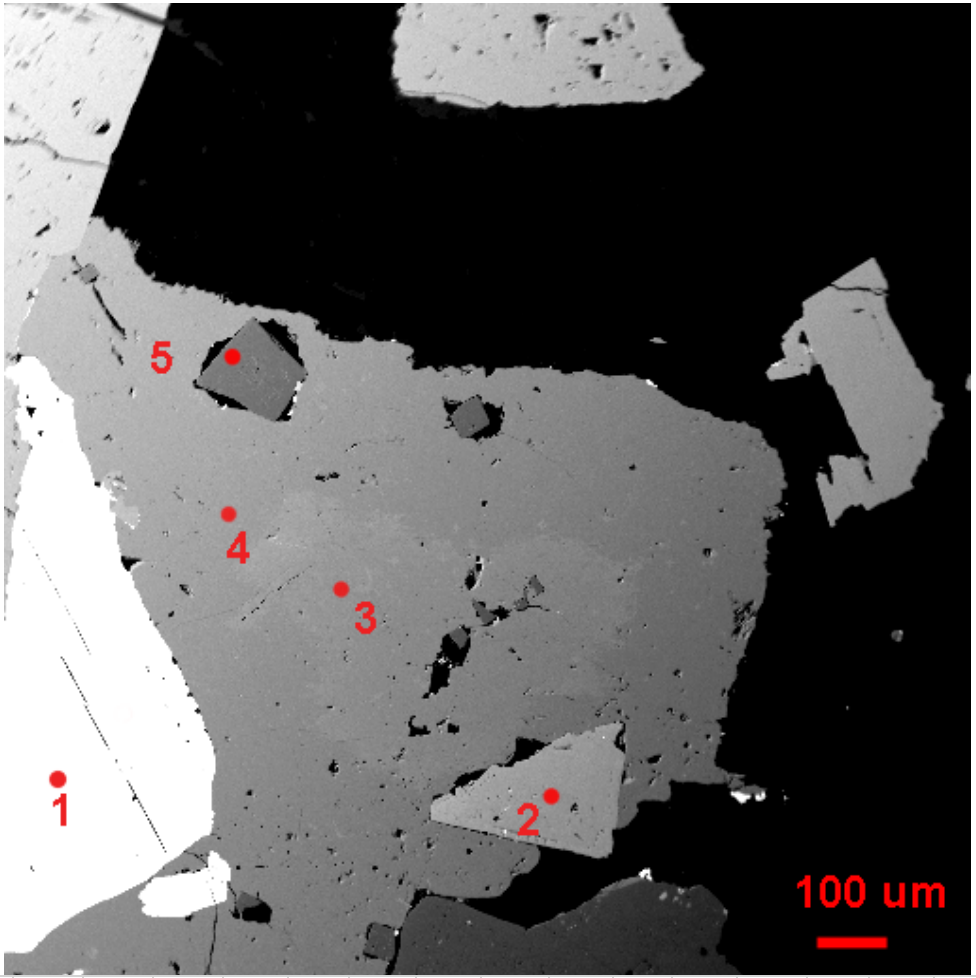

No.	Ag	Au	Na	Hg	Tl	As	Pb	Cu	Se	Bi	Co	Zn	W	Ni	Si	Te	Fe	Al	Sb	Ti	Sn	Mo	S	Ca	Total
1	0.174	0	0.004	0	0.119	0	64.633	0	0.066	0	0	0	0	0	0	0.032	0.019	0	0.252	0.008	0.057	0	13.929	0	79.293
2	0	0	0	0.006	0.114	40.102	0	0.006	0	0	0.065	0	0	0	0	0	35.69	0	0.025	0	0.025	0.276	23.147	0	99.456
3	1.585	0	0.012	0	0.001	0	0	33.107	0	0	0.024	0.106	0.041	0	0	0	28.84	0	0	0	0.239	0.425	35.095	0	99.475
4	0.107	0	0.01	0	0	0	0	33.93	0	0	0.038	0.123	0	0	0	0	29.766	0	0	0	0.588	0.443	35.641	0	100.706
5	0	0	0	0	0	0	0	0.079	0	0	0.066	0.007	0.005	0	0	0	45.743	0.004	0.005	0.004	0.013	0.651	54.331	0	100.908

PG1404-1336.3 Grain 3
CSD Zone

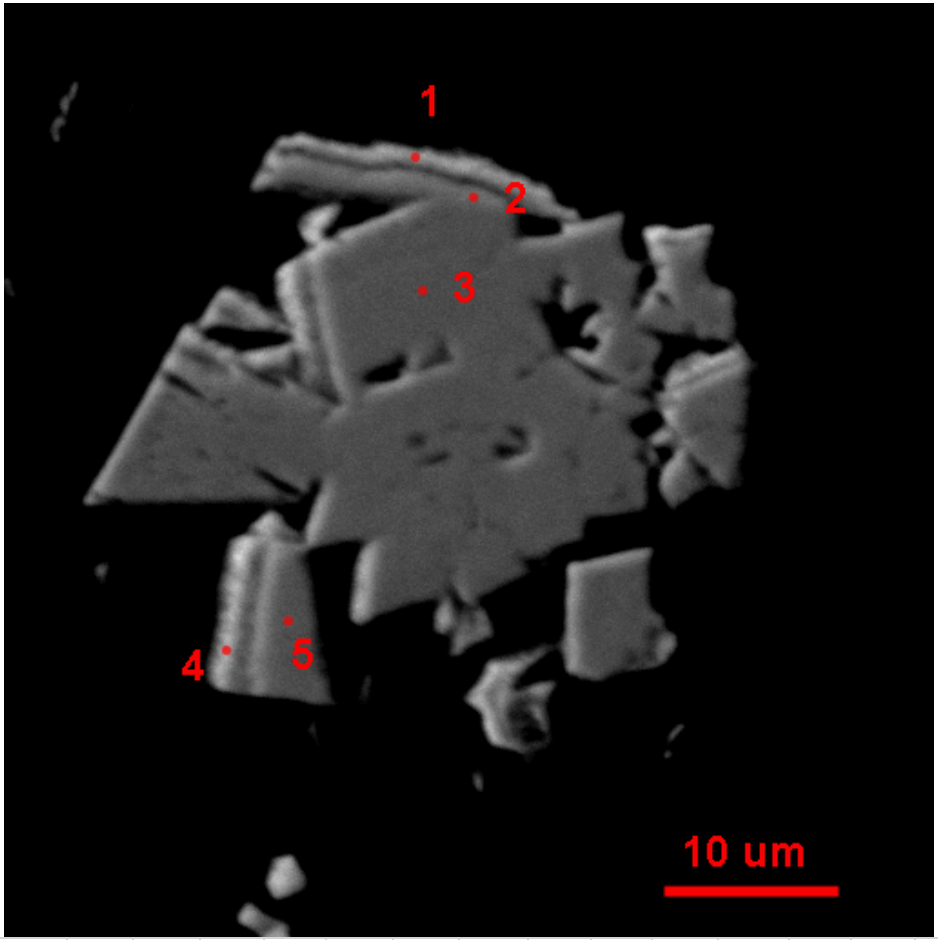

No.	Ag	Au	Na	Hg	Tl	As	Pb	Cu	Se	Bi	Co	Zn	W	Ni	Si	Te	Fe	Al	Sb	Ti	Sn	Mo	S	Ca	Total
1	0	0.022	0.064	0.026	0.043	4.105	0	0.051	0	0	0.062	0	0	0	0.15	0	43.381	0.078	0.047	0.021	0.014	0.626	50.505	0	99.195
2	0	0.029	0.012	0.004	0.019	0.05	0	0.062	0	0.021	0.052	0	0	0	0.045	0	44.95	0.015	0.01	0.007	0.028	0.65	54.113	0	100.067
3	0	0	0	0.02	0.012	0.036	0	0.028	0	0	0.068	0.009	0.019	0	0.023	0	45.691	0.005	0.009	0.004	0.02	0.669	54.748	0	101.361
4	0	0	0.132	0.042	0.089	23.284	0	0.045	0	0.02	0.046	0	0	0	1.271	0	36.919	0.647	0.112	0.007	0.021	0.402	33.497	0.104	96.638
5	0	0	0.013	0.02	0.023	0.317	0	0.049	0	0	0.066	0.013	0.002	0	0.114	0	44.764	0.025	0.006	0.001	0.021	0.646	53.298	0	99.378

PG1404-1336.3 Grain 4
CSD Zone

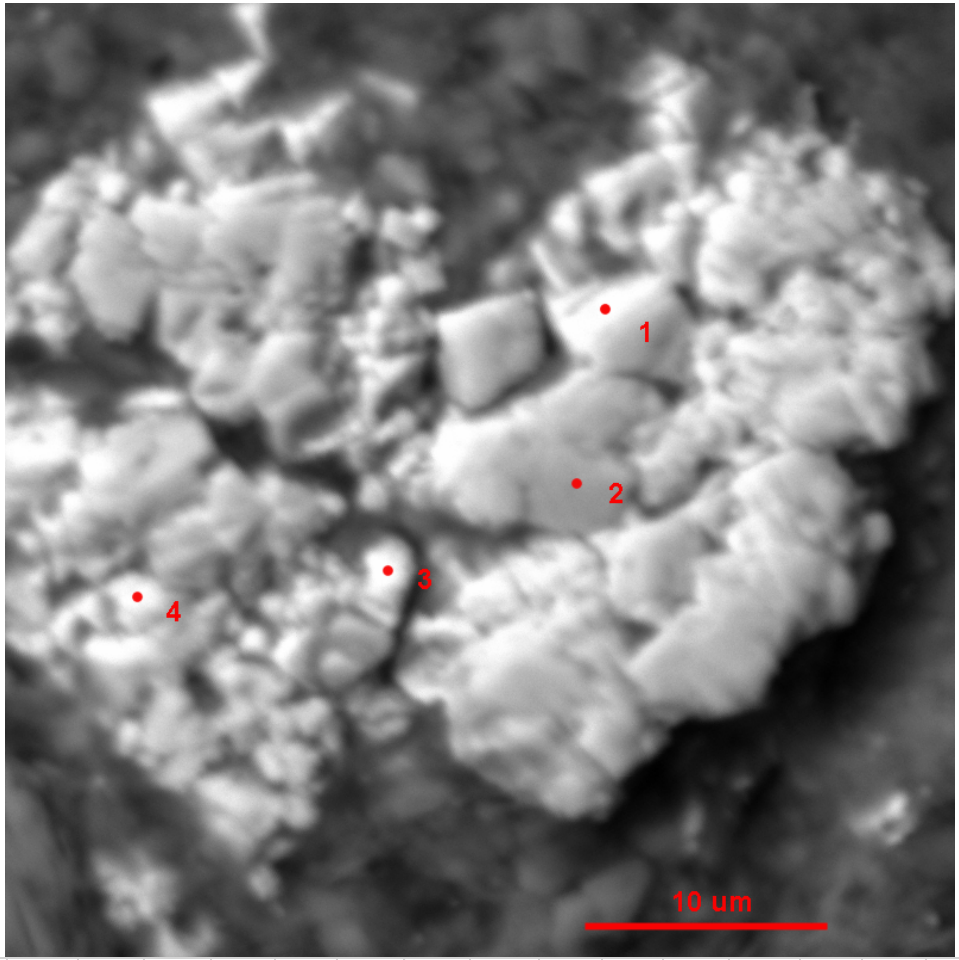

No.	Ag	Au	Na	Hg	Tl	As	Pb	Cu	Se	Bi	Co	Zn	W	Ni	Si	Te	Fe	Al	Sb	Ti	Sn	Mo	S	Ca	Total
1	0	0.047	0.11	0.11	0.133	27.765	0	0.089	0	0.025	0.046	0	0	0	0.457	0	37.918	0.224	0.068	0.01	0.018	0.476	38.992	0.113	106.601
2	0	0	0.051	0.067	0.029	2.738	0	0.058	0	0	0.063	0.004	0	0	0.35	0	43.794	0.18	0.029	0.01	0.016	0.619	51.475	0	99.483
3	0	0.023	0.108	0.108	0.062	26.605	0	0.122	0	0	0.05	0.009	0	0	1.403	0	33.288	0.95	0.085	0.017	0.019	0.34	28.64	0.153	91.982
4	0	0.072	0.066	0.097	0.157	21.53	0	0.102	0	0	0.057	0.037	0	0.01	0.745	0	36.03	0.494	0.073	0	0.023	0.368	31.413	0.141	91.415

PG1404-1336.3 Grain 5
CSD Zone

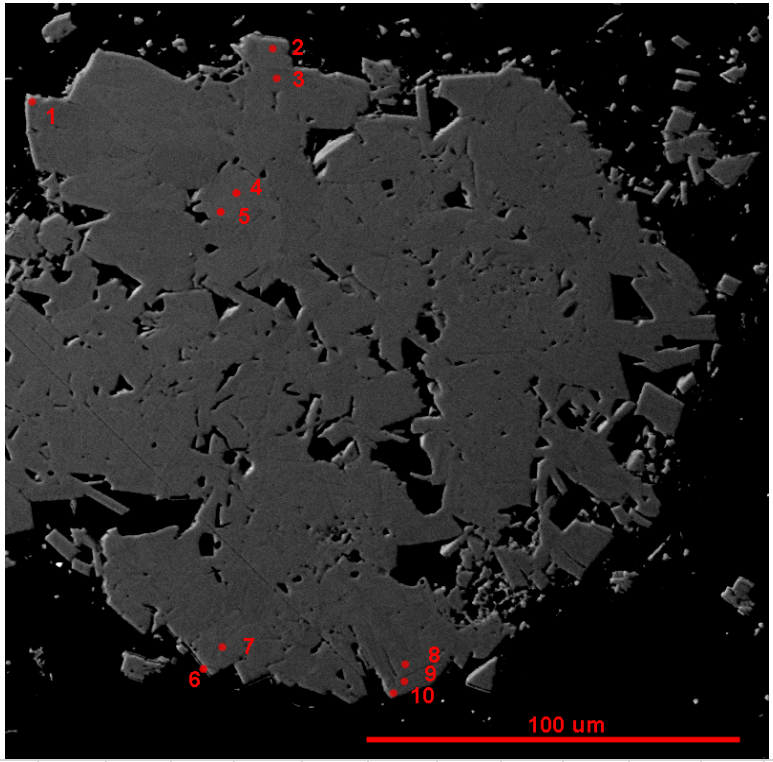

No.	Ag	Au	Na	Hg	Tl	As	Pb	Cu	Se	Bi	Co	Zn	W	Ni	Si	Te	Fe	Al	Sb	Ti	Sn	Mo	S	Ca	Total
1	0	0	0	0	0.026	0.106	0	0.034	0	0	0.065	0.005	0.013	0	0.108	0	44.797	0.034	0.01	0.01	0.013	0.637	53.742	0	99.6
2	0	0.011	0	0	0.052	0	0	0.01	0	0.001	0.064	0.015	0	0	0.054	0	45.181	0.012	0.017	0.027	0.018	0.655	54.536	0	100.653
3	0	0	0.014	0.005	0	0	0	0.019	0	0	0.063	0.011	0.012	0	0.021	0	45.188	0.003	0.017	0.013	0.016	0.663	55.03	0	101.075
4	0	0.014	0	0	0.032	0	0	0.035	0	0	0.053	0	0.004	0	0.001	0	45.219	0.008	0.027	0.011	0.016	0.646	54.632	0	100.698
5	0	0	0.002	0	0.013	0	0	0.048	0	0	0.059	0	0.023	0	0.002	0	45.486	0.001	0.024	0	0.028	0.671	54.821	0	101.178
6	0	0.015	0.044	0.043	0.046	4.814	0	0.038	0	0.015	0.059	0	0	0	0.811	0	41.137	0.579	0.04	0.077	0.011	0.558	45.202	0.008	93.497
7	0	0	0	0	0.054	0.192	0	0.016	0	0	0.054	0.029	0.004	0.001	0.082	0	44.382	0.029	0.03	0.018	0.027	0.655	53.657	0	99.23
8	0	0	0	0	0.02	0.054	0	0.028	0	0.004	0.066	0.006	0	0.007	0.032	0	45.292	0.009	0.015	0.019	0.032	0.661	54.554	0	100.799
9	0	0.032	0.009	0	0.017	0.028	0	0.029	0.005	0.02	0.053	0.003	0.01	0	0.048	0	44.343	0.008	0.006	0	0.021	0.661	54.238	0	99.531
10	0	0	0	0.007	0.059	0.107	0	0.03	0	0.021	0.065	0.014	0	0	0.133	0	44.78	0.041	0.016	0.004	0.021	0.666	53.939	0	99.903

PG1404-1520 Grain 1
CSD Zone

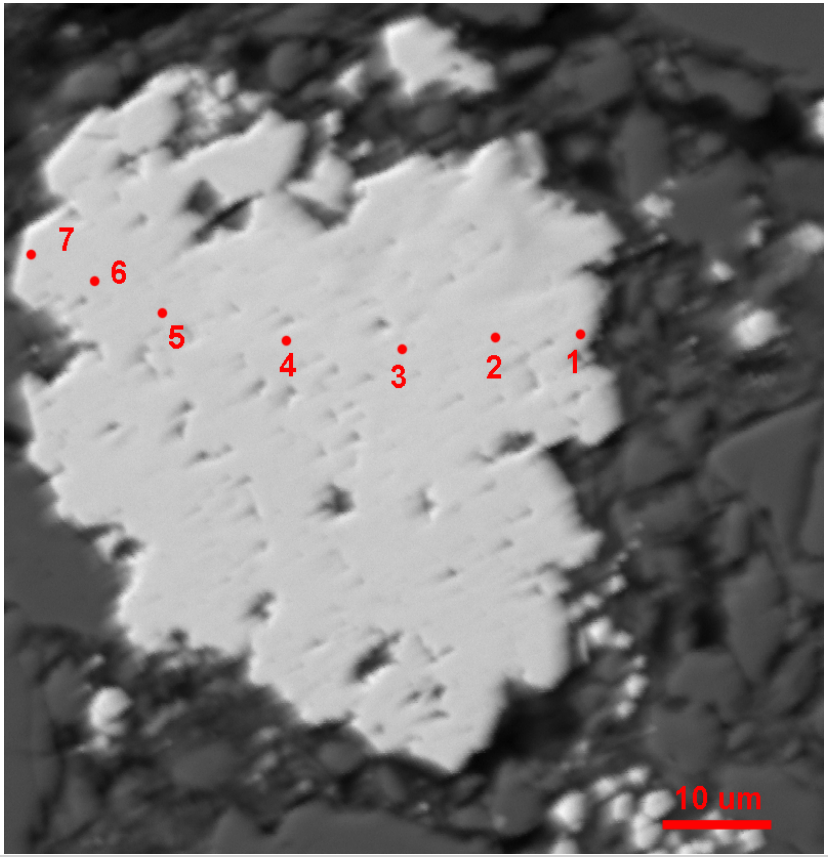

No.	Ag	Au	Na	Hg	Tl	As	Pb	Cu	Se	Bi	Co	Zn	W	Ni	Si	Te	Fe	Al	Sb	Ti	Sn	Mo	S	Ca	Total
1	**0.002**	**0**	**0.145**	**0.279**	**0.159**	**0.285**	**0**	**0.019**	**0**	**0**	**0.032**	**0.018**	**0**	**0**	**12**	**0**	**15.828**	**2.783**	**0.43**	**0.044**	**0**	**0.263**	**20.527**	**0.934**	**53.748**
2	0	0.013	0.004	0	0	0.105	0	0.022	0	0	0.061	0	0	0.018	0.193	0	44.503	0.053	0.038	0.024	0.02	0.714	53.085	0	98.853
3	0	0	0.034	0	0.043	0.042	0	0	0	0	0.047	0	0.009	0.001	0.188	0	45.423	0.055	0.017	0.001	0.014	0.673	53.541	0	100.088
4	0	0	0.016	0.002	0.076	0.069	0	0.009	0	0	0.075	0.012	0.032	0.015	0.052	0	45.177	0.016	0.026	0	0.02	0.671	51.225	0	97.493
5	0	0	0.018	0	0.047	0.067	0	0.006	0.002	0	0.059	0.004	0.012	0	0.094	0	45.899	0.037	0.025	0.006	0.031	0.692	54.091	0	101.09
6	0	0.003	0.02	0.019	0.075	0.068	0	0.015	0	0.008	0.066	0.002	0	0.007	0.037	0	44.751	0.011	0.035	0.006	0.02	0.676	52.18	0	97.999
7	0	0.003	0.181	0.008	0.032	0.035	0	0.004	0	0.003	0.044	0	0	0.003	1.108	0	44.015	0.256	0.025	0.034	0.018	0.645	52.516	0	98.93

PG1404-1520 Grain 2
CSD Zone

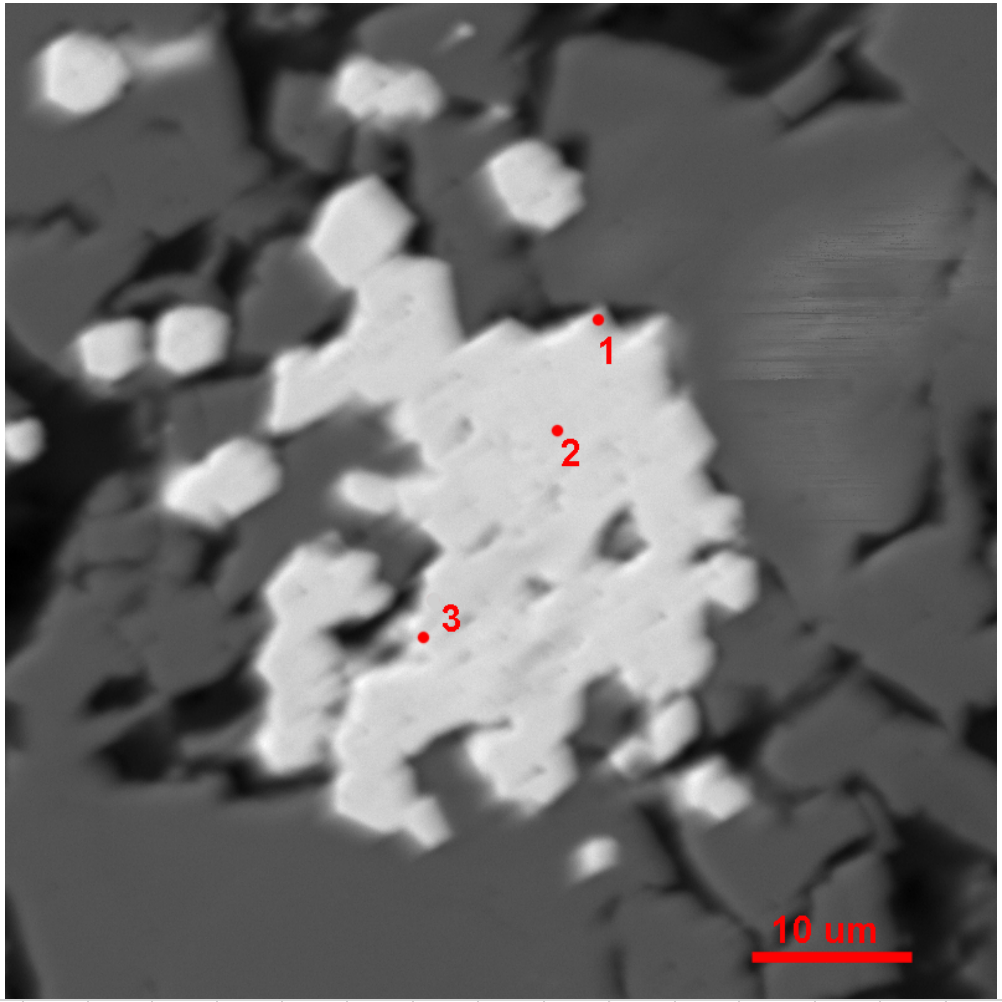

No.	Ag	Au	Na	Hg	Tl	As	Pb	Cu	Se	Bi	Co	Zn	W	Ni	Si	Te	Fe	Al	Sb	Ti	Sn	Mo	S	Ca	Total
1	0	0	0.002	0.011	0	0.158	0	0.019	0.007	0	0.093	0.001	0	0.092	0.18	0	44.911	0.078	0.03	0	0.022	0.66	53.725	0.171	100.16
2	0	0.022	0	0.016	0.049	0.276	0	0.014	0	0.009	0.057	0.018	0	0.081	0.075	0	41.299	0.011	0.352	0.012	0.011	0.598	44.015	0.46	87.375
3	0	0.002	0	0.008	0.038	0.127	0	0.016	0	0	0.061	0.003	0	0.071	0.024	0	45.076	0.002	0.079	0.062	0.016	0.666	52.951	0.124	99.326

PG1404-1520 Grain 4
CSD Zone

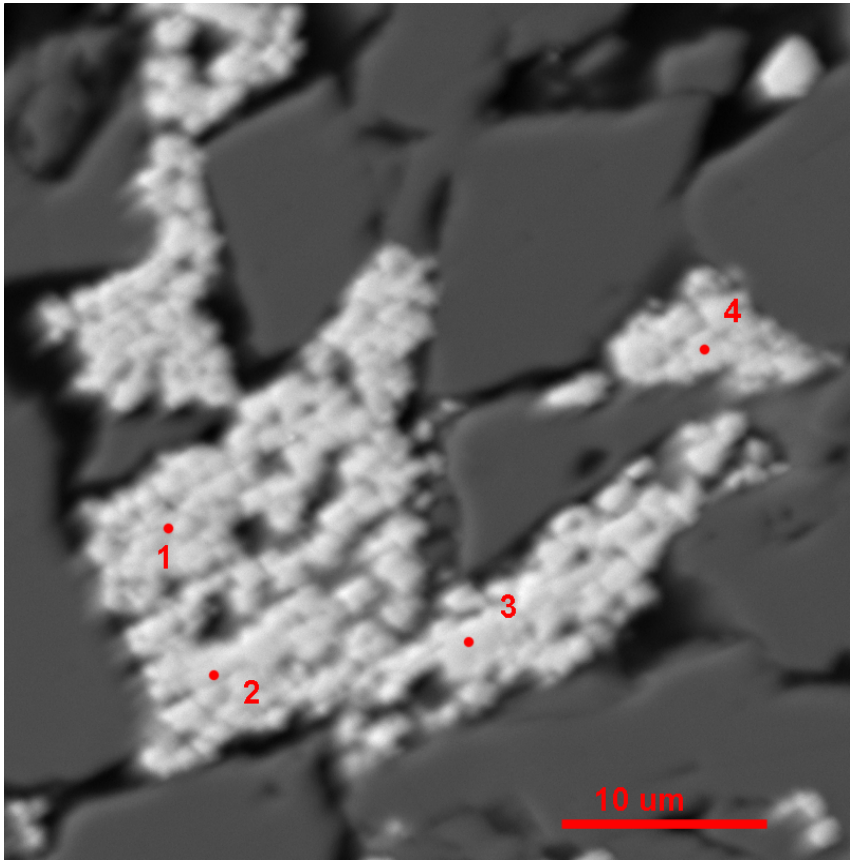

No.	Ag	Au	Na	Hg	Tl	As	Pb	Cu	Se	Bi	Co	Zn	W	Ni	Si	Te	Fe	Al	Sb	Ti	Sn	Mo	S	Ca	Total
1	0.023	0	0.016	0.069	0.33	0.912	0	0	0	0.001	0.054	0.014	0.007	0.046	0.076	0	40.762	0	1.099	0	0	0.515	33.446	1.903	79.273
2	0	0	0.022	0.021	0.041	0.095	0	0	0	0.004	0.018	0.01	0	0.009	0.02	0	17.114	0.007	0.462	0.002	0	0.267	18.331	7.744	44.167
3	0.008	0	0.018	0.088	0.183	0.366	0	0.001	0	0	0.041	0	0	0.013	0.079	0	20.746	0.01	0.917	0.004	0	0.284	16.921	9.191	48.87
4	0	0	0	0.015	0.044	0.192	0	0	0	0.002	0.001	0.006	0	0.009	7.18	0	7.048	0.057	0.227	0	0	0.145	9.529	16.174	40.629

PG1404-1520 Grain 5
CSD Zone

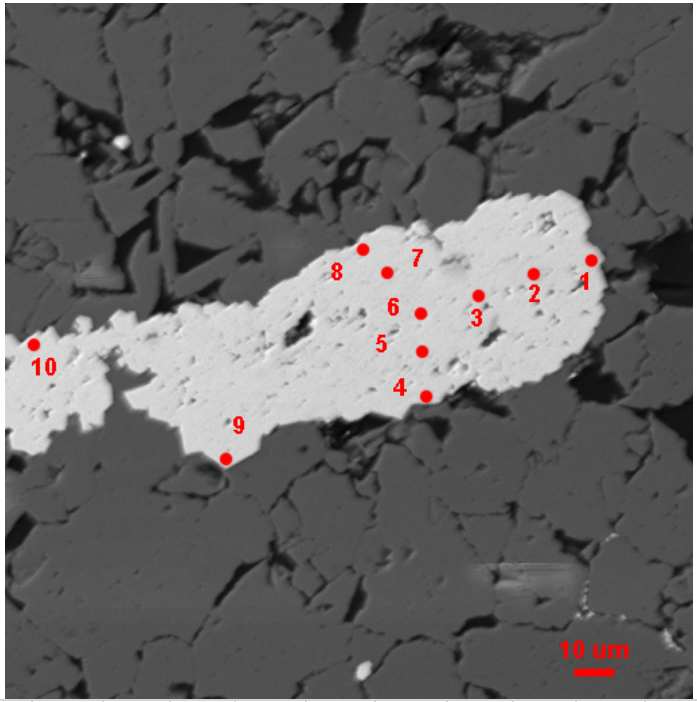

No.	Ag	Au	Na	Hg	Tl	As	Pb	Cu	Se	Bi	Co	Zn	W	Ni	Si	Te	Fe	Al	Sb	Ti	Sn	Mo	S	Ca	Total
1	0	0.053	0.022	0.016	0.079	0.199	0	0	0	0.005	0.049	0.021	0	0.127	0.044	0	32.889	0.019	0.149	0	0.014	0.473	38.518	5.349	78.026
2	0	0	0.024	0	0.013	0.054	0	0.005	0	0	0.053	0.03	0	0	0.477	0	43.864	0.277	0.022	0.011	0.018	0.641	51.695	0.023	97.207
3	0	0.004	0.006	0.013	0.044	0.04	0	0	0.003	0	0.056	0	0.02	0	0.034	0	44.9	0.014	0.016	0	0.021	0.644	53.645	0.003	99.463
4	**0.001**	**0**	**0.017**	**0.011**	**0**	**0.176**	**0**	**0**	**0**	**0**	**0.002**	**0**	**0**	**0.005**	**0.431**	**0.01**	**2.043**	**0.037**	**0.096**	**0.028**	**0**	**0.026**	**1.865**	**21.081**	**25.829**
5	0	0	0.024	0.09	0.049	0.037	0	0.007	0	0	0.04	0.002	0	0.025	4.108	0	35.712	4.038	0.078	0.02	0.012	0.516	42.227	0.076	87.061
6	0	0	0.005	0	0	0.061	0	0	0.001	0	0.049	0	0	0.009	0.006	0	45.487	0.001	0.018	0	0.025	0.674	54.38	0.007	100.723
7	0	0.01	0.023	0	0.019	0.056	0	0.001	0.003	0	0.078	0.014	0.004	0	0.055	0	44.804	0.018	0.031	0.014	0.014	0.679	53.67	0.1	99.593
8	0	0	0.013	0.001	0.027	0.057	0	0	0	0	0.063	0	0.017	0	0.088	0	45.502	0.01	0.027	0.005	0.027	0.683	54.158	0.051	100.729
9	**0**	**0**	**0.002**	**0.005**	**0.008**	**0.155**	**0**	**0**	**0**	**0**	**0.004**	**0**	**0**	**0**	**0.022**	**0.018**	**0.278**	**0.024**	**0.048**	**0.011**	**0**	**0**	**0.102**	**20.883**	**21.56**
10	0	0	0.001	0.009	0.027	0.053	0	0.003	0	0	0.046	0	0.009	0	0.164	0	44.888	0.034	0.011	0.004	0.028	0.674	53.788	0.075	99.814

PG1423-2456a Grain 1
Manto

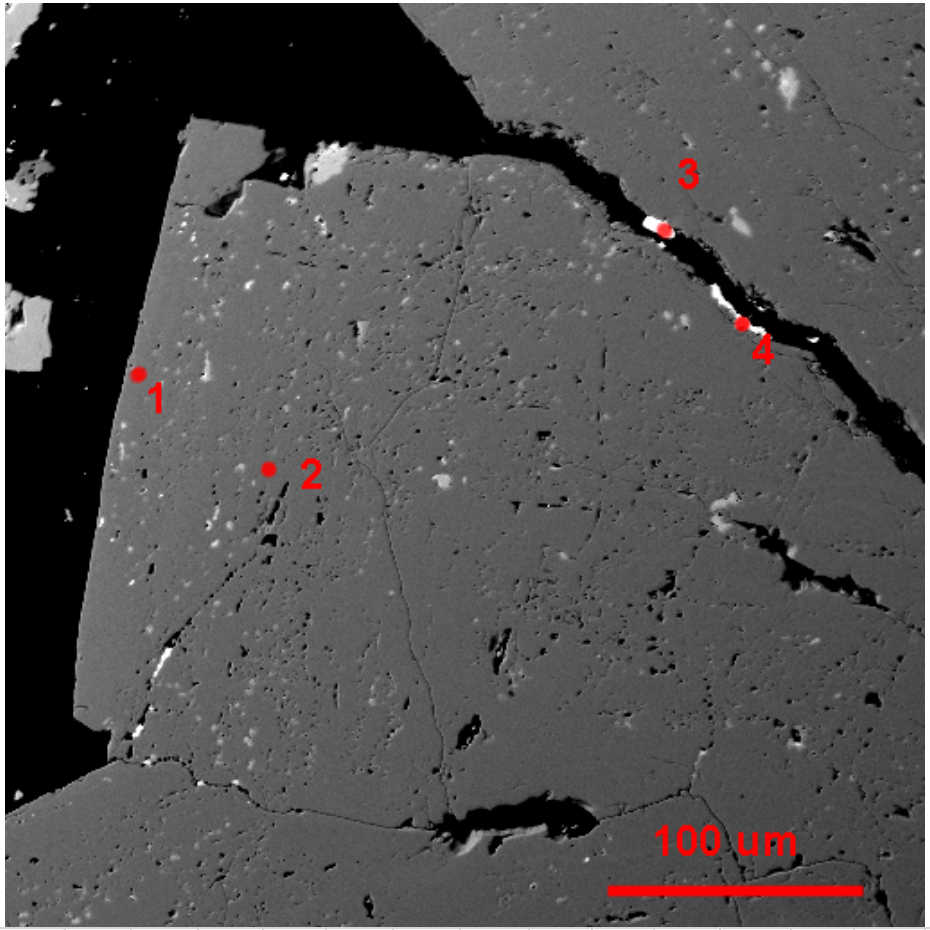

No.	Ag	Au	Na	Hg	Tl	As	Pb	Cu	Se	Bi	Co	Zn	W	Ni	Si	Te	Fe	Al	Sb	Ti	Sn	Mo	S	Ca	Total
1	0	0	0	0	0.016	0.723	0	0.017	0	0.003	0.06	0.009	0.015	0	0	0	45.518	0	0.012	0.003	0.032	0.666	53.642	0.029	100.745
2	0	0	0.003	0	0	0.289	0	0.012	0	0	0.053	0.003	0	0	0	0	45.932	0	0.005	0.006	0.028	0.662	54.223	0	101.216
3	64.6	0	0	0.017	0.04	0.045	0.013	1.172	0.007	0.015	0	0	0	0	0.023	0	1.765	0.06	10.411	0	0	0.158	13.493	0	91.819
4	59.468	0.036	0	0	0.096	0.084	0	0.9	0.032	0	0.02	0.112	0.017	0.002	0.014	0	9.886	0.062	9.744	0	0	0.291	23.434	0	104.198

PG1423-2456a Grain 2
Manto

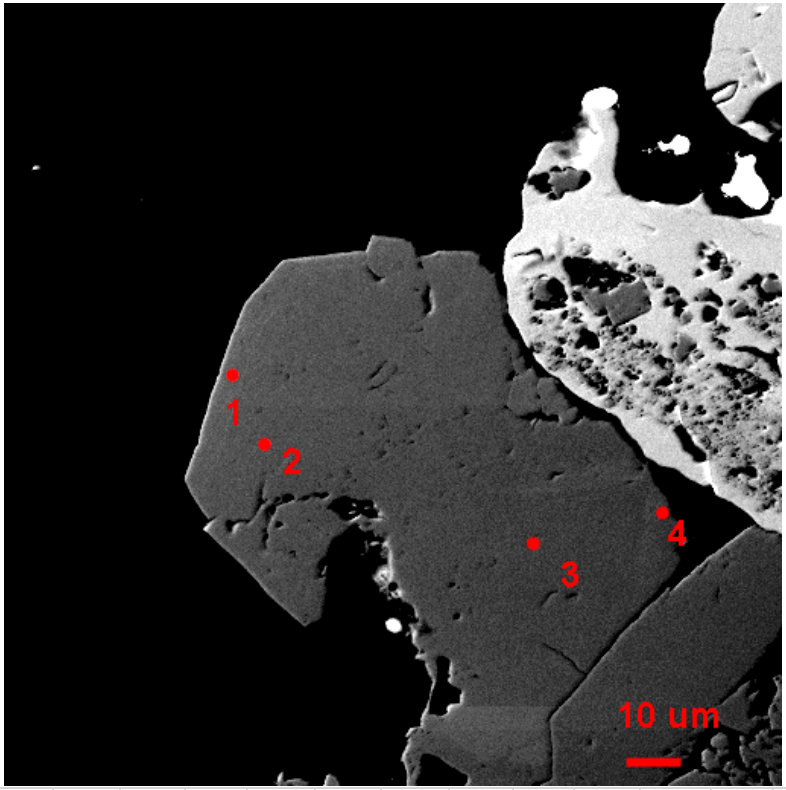

No.	Ag	Au	Na	Hg	Tl	As	Pb	Cu	Se	Bi	Co	Zn	W	Ni	Si	Te	Fe	Al	Sb	Ti	Sn	Mo	S	Ca	Total
1	0	0.002	0.005	0	0.04	0.189	0	0.001	0	0	0.053	0.005	0	0	0.002	0	45.624	0.005	0.015	0	0.018	0.649	53.908	0.085	100.601
2	0	0	0.006	0	0.018	0	0	0	0	0	0.07	0.008	0.022	0	0	0	45.981	0	0.015	0	0.031	0.648	54.364	0	101.163
3	0	0	0	0	0.003	0	0	0.002	0	0	0.065	0.027	0.012	0.001	0.014	0	45.732	0.011	0.013	0	0.028	0.653	54.51	0	101.071
4	0.02	0	0	0.002	0.051	0.006	0	0.097	0	0	0.06	0	0.008	0	0.036	0	45.954	0.024	0.031	0	0.015	0.631	54.838	0	101.773

PG1423-2456a Grain 3
Manto

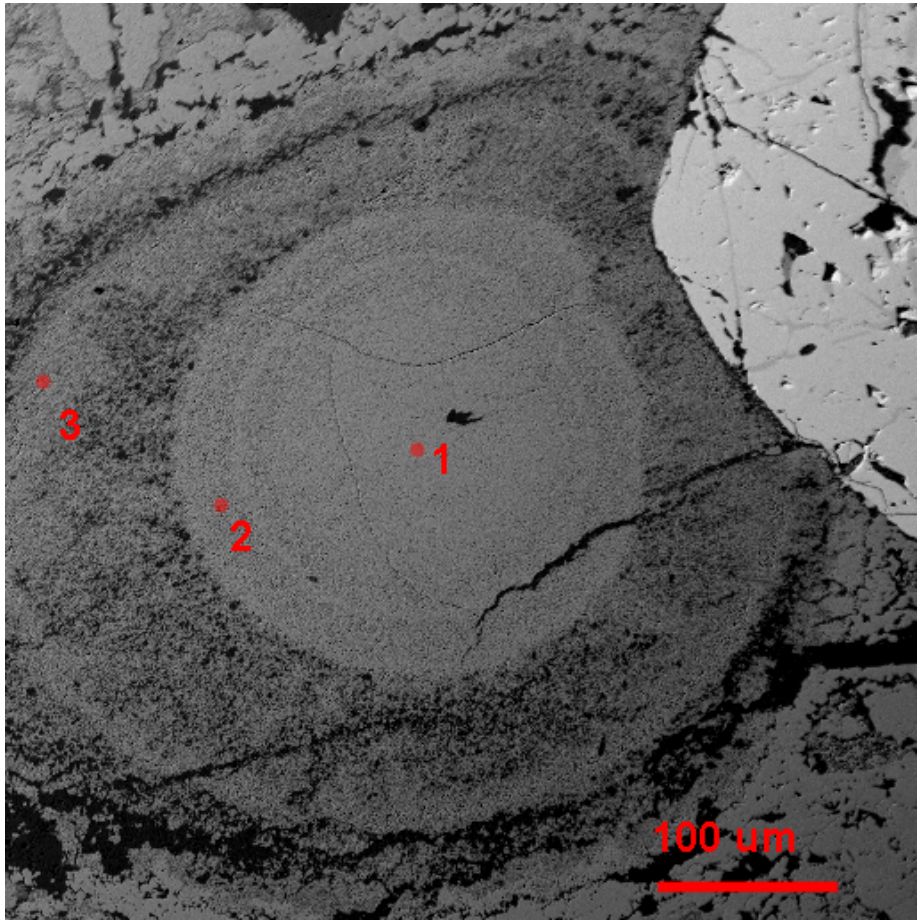

No.	Ag	Au	Na	Hg	Tl	As	Pb	Cu	Se	Bi	Co	Zn	W	Ni	Si	Te	Fe	Al	Sb	Ti	Sn	Mo	S	Ca	Total
1	0.033	0	0	0	0.036	0.033	0.04	0.059	0	0	0.06	0	0.007	0	0	0	45.099	0	0.096	0.013	0.026	0.644	53.813	0	99.959
2	0.044	0.002	0.021	0	0.021	0.024	0.154	0.071	0	0	0.057	0.009	0.004	0	0.009	0	45.028	0.006	0.104	0	0.026	0.629	52.456	0	98.665
3	0.009	0.002	0.001	0	0.005	0.022	0.143	0.094	0	0	0.068	0.012	0.019	0	0	0	46.04	0	0.087	0.004	0.023	0.457	38.68	0	85.666

PG1423-2456a Grain 4
Manto

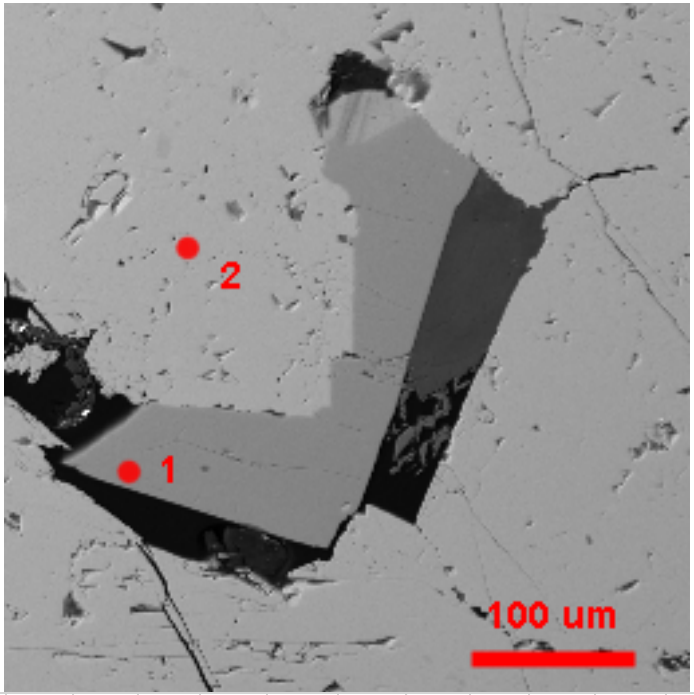

No.	Ag	Au	Na	Hg	Tl	As	Pb	Cu	Se	Bi	Co	Zn	W	Ni	Si	Te	Fe	Al	Sb	Ti	Sn	Mo	S	Ca	Total
1	0	0	0	0.003	0	0.671	0	0.03	0	0	0.056	0	0	0	0	0	45.573	0.002	0.015	0	0.018	0.651	53.642	0	100.661
2	0	1.029	2.876	0	0	0	0	0.953	0	0.01	0.027	46.935	0	0.006	0	0	11.776	0	0.017	0	0.027	0.48	34.596	0	98.732

PG1423-2456 Grain 1
Manto

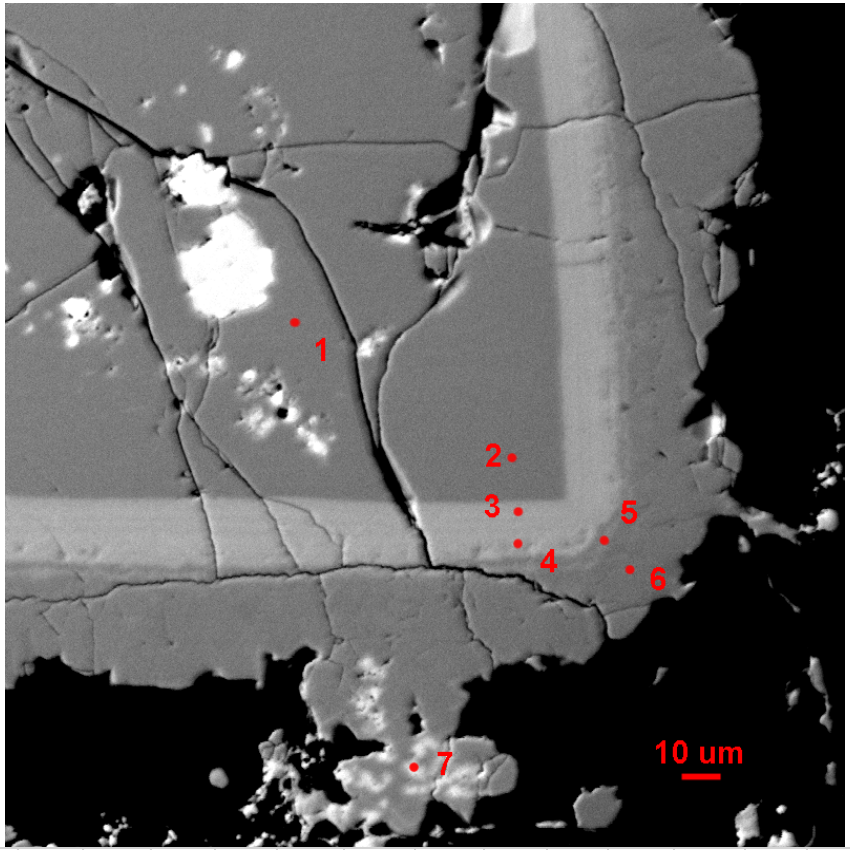

No.	Ag	Au	Na	Hg	Tl	As	Pb	Cu	Se	Bi	Co	Zn	W	Ni	Si	Te	Fe	Al	Sb	Ti	Sn	Mo	S	Ca	Total
1	0	0.013	0.001	0	0.051	0.256	0	0.017	0	0	0.062	0	0	0	0.003	0	46.037	0.002	0.008	0	0.023	0.625	54.646	0	101.744
2	0	0.004	0	0	0.024	0	0	0.115	0	0	0.061	0.021	0.015	0	0	0	46.235	0	0.042	0.007	0.021	0.609	54.829	0	101.983
3	1.537	0	0.002	0	0.063	6.875	0	0.436	0	0	0.04	0	0	0	0	0	41.117	0	0	0.009	0.272	0.569	49.006	0	99.926
4	1.83	0	0.003	0	0.26	5.046	0	0.463	0	0.003	0.064	0.005	0.03	0	0.001	0	41.723	0	0.001	0.018	0.06	0.6	50.667	0	100.54
5	0.374	0	0.004	0	0	0.455	0	0.052	0	0	0.06	0	0.014	0	0	0	45.313	0	0.03	0	0.029	0.627	54.259	0	101.217
6	0.006	0	0.002	0	0.026	0.117	0	0.018	0	0	0.071	0.003	0	0	0	0	45.767	0	0.022	0.008	0.018	0.637	52.787	0	99.485
7	0.258	0.379	1.024	0	0	0.13	0	0.395	0	0	0.045	25.217	0.018	0	0	0	33.304	0	0	0.03	0.344	0.612	48.876	0	110.632

PG1423-2456 Grain 3
Manto

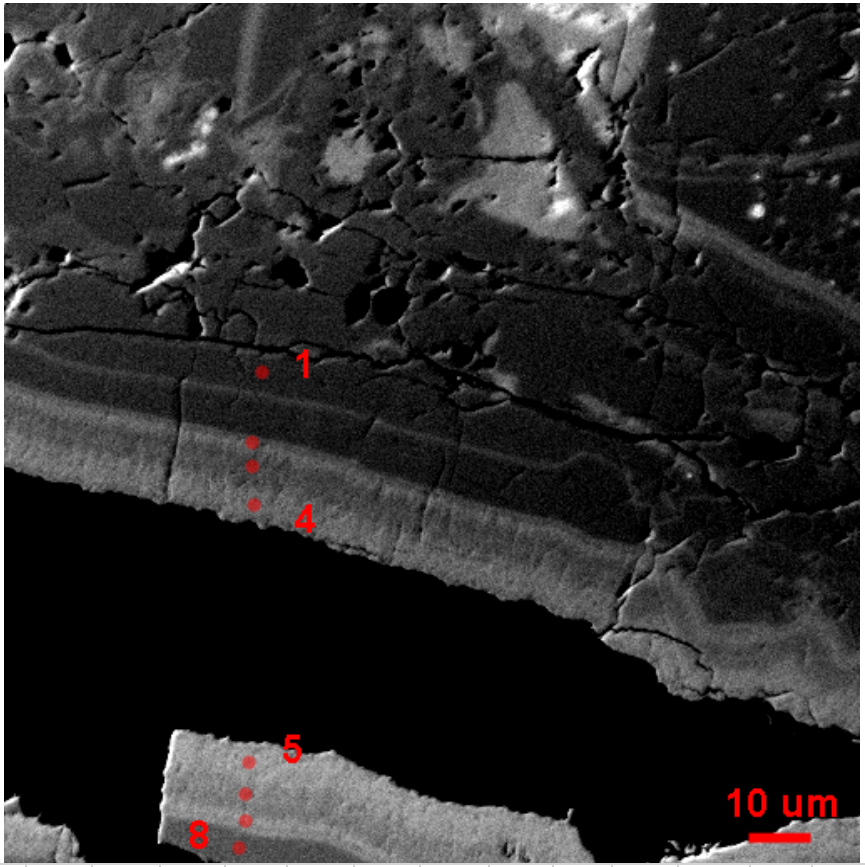

No.	Ag	Au	Na	Hg	Tl	As	Pb	Cu	Se	Bi	Co	Zn	W	Ni	Si	Te	Fe	Al	Sb	Ti	Sn	Mo	S	Ca	Total
1	0	0	0.004	0	0.028	0.004	0	0.005	0	0	0.069	0	0.017	0	0	0	45.222	0	0.015	0	0.02	0.64	54.423	0	100.447
2	1.191	0	0.001	0	0.044	5.78	0	0	0	0	0.05	0	0	0	0	0	41.692	0	0.014	0.01	0.015	0.621	49.438	0	98.856
3	0.083	0	0.001	0.001	0.096	5.058	0	0	0	0	0.055	0.009	0.011	0	0	0	42.747	0.001	0.008	0	0.021	0.631	52.046	0	100.768
4	0.771	0	0.019	0	0.061	7.29	0	0.003	0	0	0.051	0	0.026	0	0	0	40.847	0	0.003	0.019	0.027	0.595	50.158	0	99.87
5	0.668	0.01	0.009	0	0.072	7.525	0	0	0	0	0.054	0.002	0.025	0	0	0	41.114	0	0.009	0	0.024	0.592	50.146	0	100.25
6	0.197	0	0.004	0	0	5.791	0	0.003	0	0	0.062	0	0	0	0	0	42.325	0	0.012	0	0.022	0.615	51.797	0	100.828
7	1.246	0	0.006	0	0.062	4.473	0	0.012	0	0	0.056	0.003	0.001	0	0	0	42.631	0.001	0	0.006	0.02	0.627	51.898	0	101.042
8	0	0	0	0	0.049	0	0	0	0	0	0.051	0.024	0	0	0	0	46.085	0.001	0.011	0	0.02	0.656	54.735	0	101.632

PG1423-2456 Grain 4
Manto

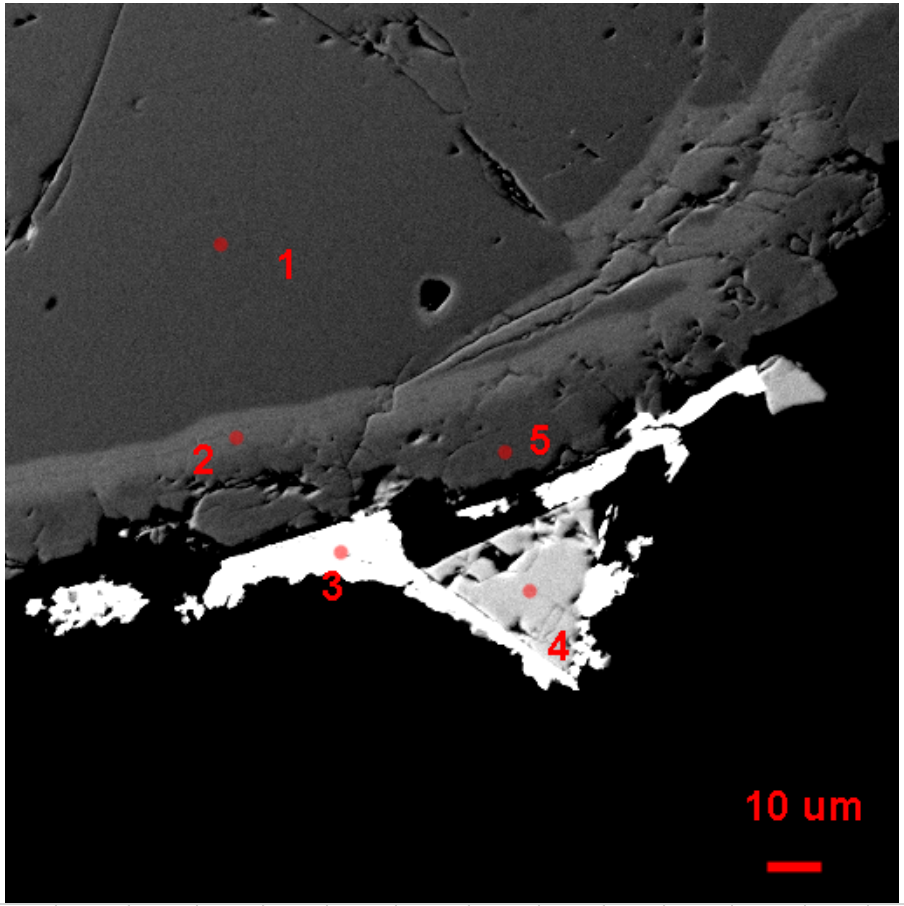

No.	Ag	Au	Na	Hg	Tl	As	Pb	Cu	Se	Bi	Co	Zn	W	Ni	Si	Te	Fe	Al	Sb	Ti	Sn	Mo	S	Ca	Total
1	0	0.013	0.016	0	0.031	0	0	0	0	0	0.064	0.008	0.023	0	0	0	45.909	0.005	0.012	0.007	0.017	0.673	54.681	0	101.459
2	0	0	0.023	0	0.022	6.416	0	0	0	0	0.044	0	0.027	0	0	0	41.743	0	0.012	0	0.018	0.612	51.379	0	100.296
3	**0**	**0**	**0.022**	**0**	**0**	**0**	**48.451**	**0.009**	**0**	**0**	**0**	**0**	**0**	**0.005**	**1.96**	**0.023**	**1.22**	**0.797**	**0**	**0.016**	**0.027**	**0.022**	**9.975**	**0.147**	**62.674**
4	0	0.961	2.951	0	0	0	0	0	0.001	0	0.004	46.851	0.035	0	0	0	12.715	0	0.02	0	0.023	0.472	34.696	0	98.729
5	0	0	0.015	0	0.022	0	0	0	0	0	0.065	0.022	0.044	0	0	0	45.472	0	0.009	0	0.019	0.682	54.465	0	100.815

AX12-1704 Grain 1
Helen Zone

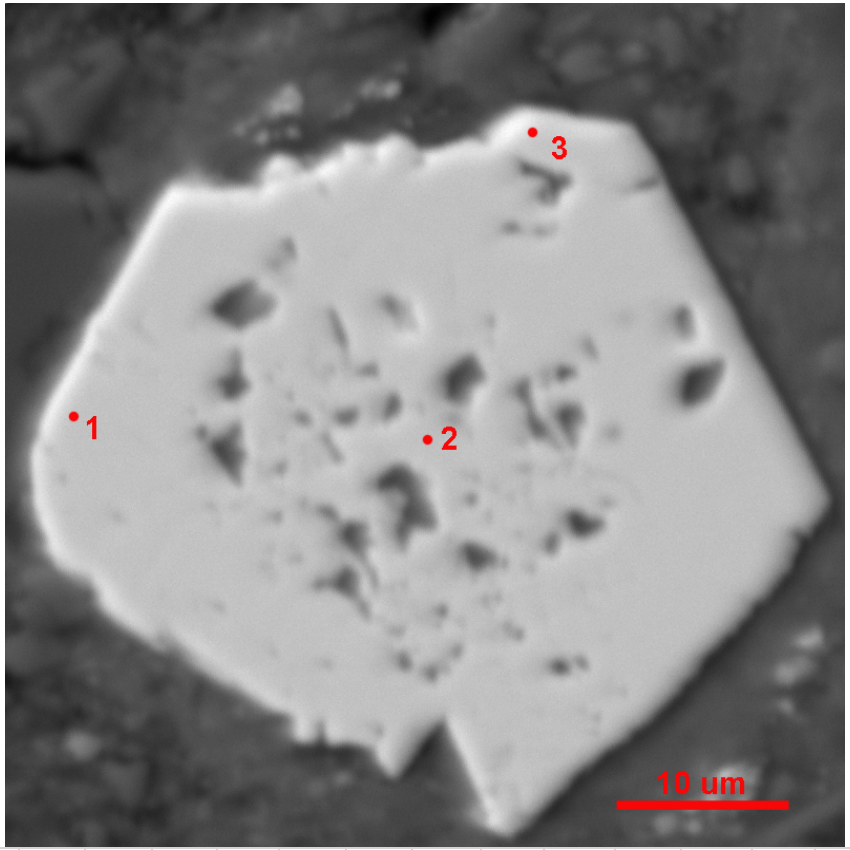

No.	Ag	Au	Na	Hg	Tl	As	Pb	Cu	Se	Bi	Co	Zn	W	Ni	Si	Te	Fe	Al	Sb	Ti	Sn	Mo	S	Ca	Total
1	**0.036**	**0.167**	**0**	**0.024**	**0.061**	**0.045**	**0**	**0.091**	**0.002**	**0.051**	**0.034**	**0.018**	**0**	**0.036**	**14.274**	**0.005**	**13.785**	**7.469**	**0.045**	**0.039**	**0.003**	**0.195**	**15.179**	**3.005**	**54.564**
2	0	0.009	0.017	0.006	0.07	0.025	0	0.014	0	0	0.055	0.006	0	0.056	1.829	0	42.563	0.706	0.032	0	0.007	0.61	49.19	0.008	95.203
3	0	0	0.014	0	0.049	0.012	0	0.031	0	0	0.09	0	0	0.052	3.798	0	40.787	0.207	0.015	0	0.016	0.583	46.98	1.335	93.969

AX12-1704 Grain 2
Helen Zone

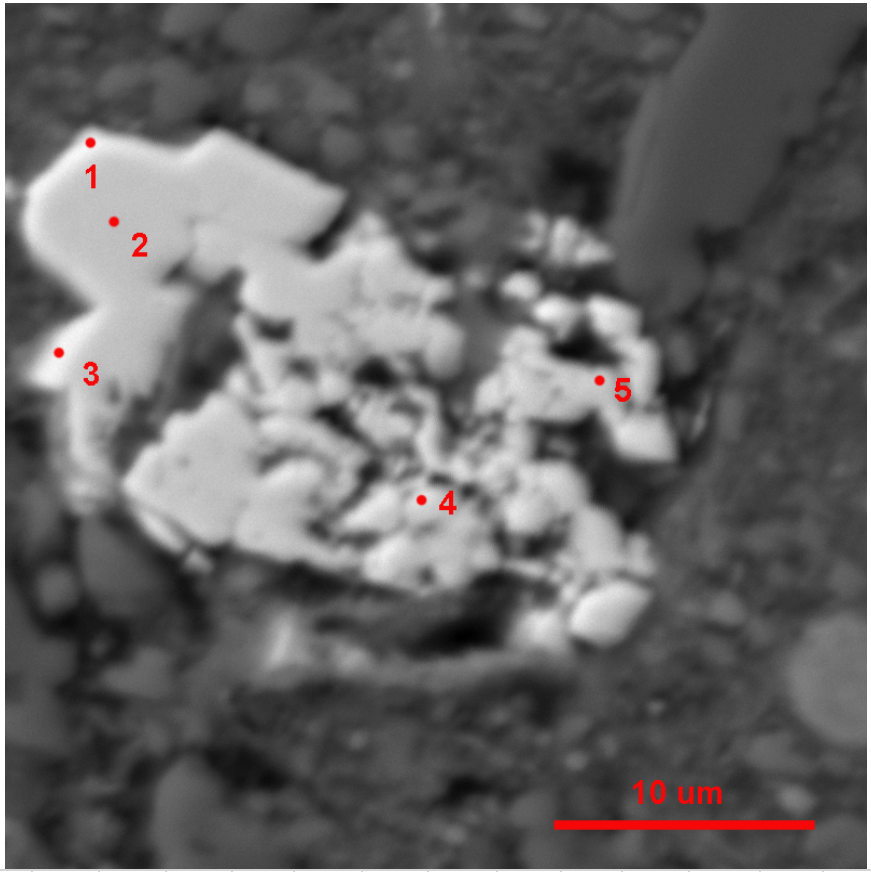

No.	Ag	Au	Na	Hg	Tl	As	Pb	Cu	Se	Bi	Co	Zn	W	Ni	Si	Te	Fe	Al	Sb	Ti	Sn	Mo	S	Ca	Total
1	0	0.003	0.018	0	0.015	0.011	0	0.019	0.004	0	0.115	0.034	0	0.051	0.978	0	44.166	0.342	0.007	0.008	0.023	0.602	50.9	0.173	97.469
2	0	0.022	0.008	0	0	0	0	0.002	0	0.024	0.064	0	0	0	0.119	0	44.745	0.019	0.003	0	0.021	0.653	52.936	0.043	98.659
3	0	0.017	0.015	0	0.043	0.009	0	0.017	0	0.015	0.063	0.025	0	0.018	0.3	0	44.422	0.084	0.013	0	0.025	0.649	51.252	0.119	97.086
4	0	0	0.029	0.03	0.048	0.01	0	0.045	0	0	0.065	0	0.011	0.05	0.089	0	42.592	0.019	0.021	0.004	0.025	0.647	50.176	0.09	93.951
5	0	0	0	0	0.059	0.018	0	0.034	0	0	0.092	0.092	0	0.072	0.531	0	39.442	0.084	0.021	0.117	0.008	0.584	47.127	1.647	89.928

AX12-1704 Grain 4
Helen Zone

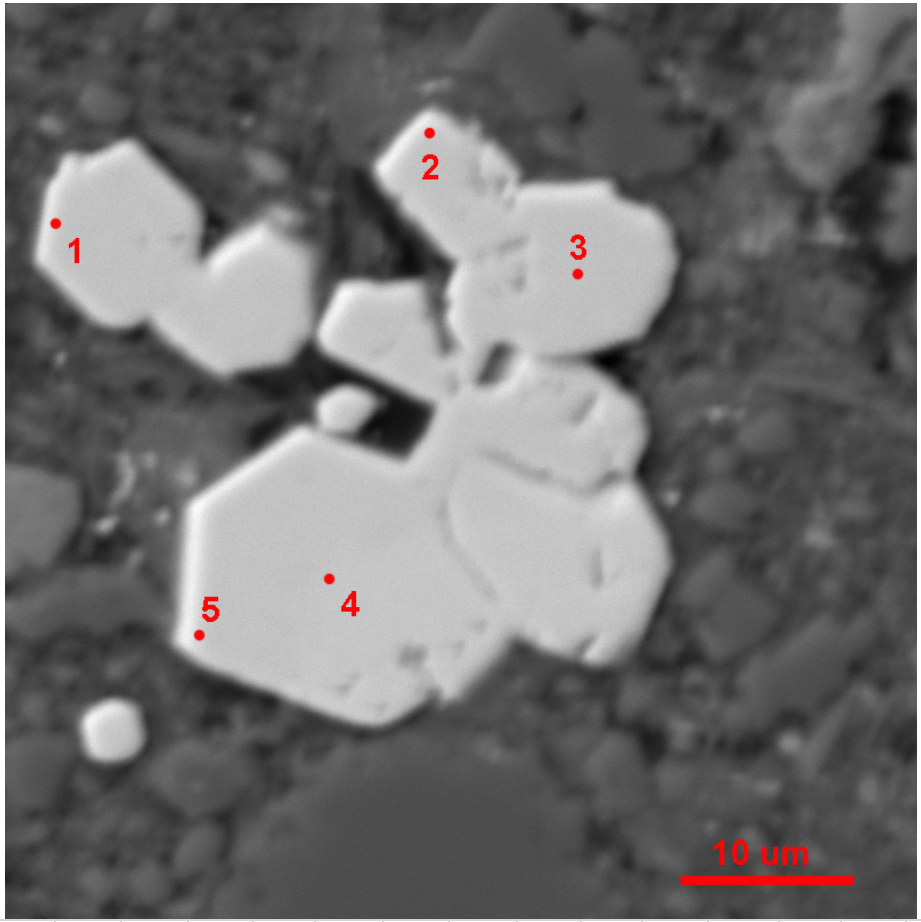

No.	Ag	Au	Na	Hg	Tl	As	Pb	Cu	Se	Bi	Co	Zn	W	Ni	Si	Te	Fe	Al	Sb	Ti	Sn	Mo	S	Ca	Total
1	0	0.021	0	0	0.053	0.004	0	0	0	0	0.04	0	0	0	0.108	0	45.137	0.021	0.01	0.024	0.025	0.655	53.243	0.021	99.362
2	0	0	0.005	0	0.029	0	0	0.007	0	0	0.061	0	0	0.006	0.149	0	45.379	0.056	0.012	0.001	0.02	0.639	53.685	0.017	100.066
3	0	0.011	0	0	0.026	0.001	0	0.021	0	0	0.046	0	0.002	0.02	0.072	0	45.275	0.009	0.012	0.027	0.02	0.65	53.611	0.038	99.841
4	0	0.014	0	0	0.067	0	0	0.002	0	0	0.058	0	0	0	0.027	0	45.686	0.001	0.014	0	0.019	0.668	53.58	0	100.136
5	0	0.015	0	0.003	0.005	0	0	0.013	0.007	0.002	0.06	0.025	0	0.015	0.174	0	45.235	0.041	0.011	0.003	0.017	0.637	53.138	0.024	99.425

AX12-1704 Grain 5
Helen Zone

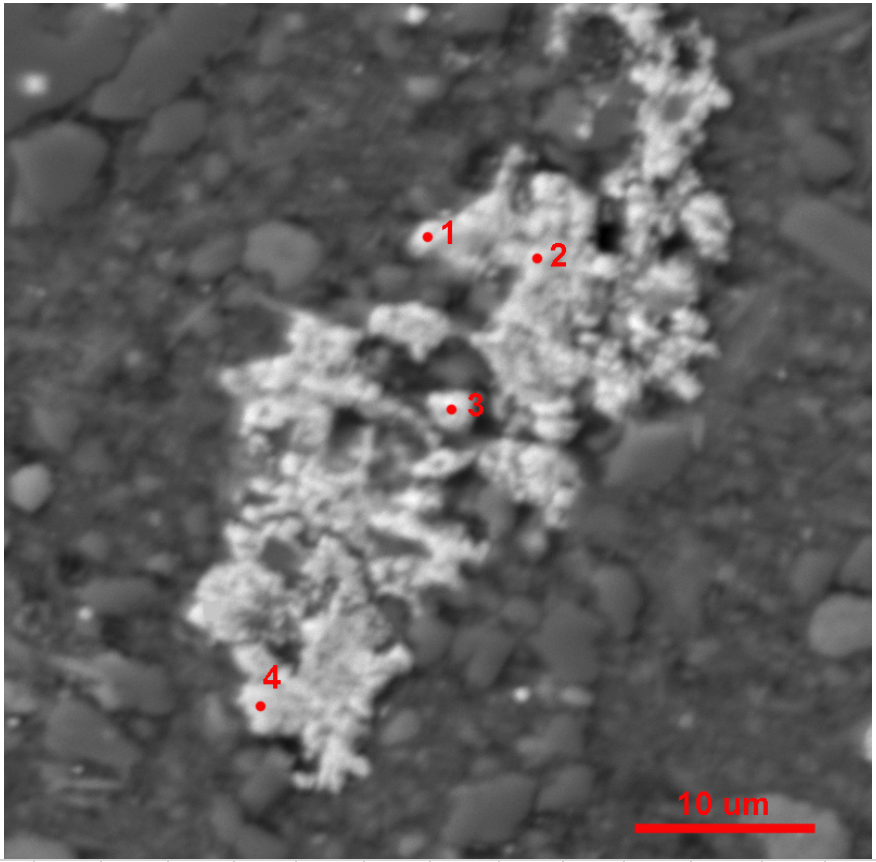

No.	Ag	Au	Na	Hg	Tl	As	Pb	Cu	Se	Bi	Co	Zn	W	Ni	Si	Te	Fe	Al	Sb	Ti	Sn	Mo	S	Ca	Total
1	0	0	0.03	0.002	0.072	0.017	0	0.05	0	0	0.069	0.016	0	0.105	1.884	0	42.666	0.509	0.01	0.009	0.008	0.628	51.141	0.124	97.34
2	0	0	0.171	0.007	0.109	0.074	0	0.081	0	0	0.065	0.059	0	0.086	0.466	0	41.798	0.23	0.019	0.006	0.015	0.62	47.265	0.13	91.201
3	**0**	**0.02**	**0.102**	**0.022**	**0.063**	**0.031**	**0**	**0.174**	**0**	**0**	**0.07**	**0.047**	**0**	**0.054**	**1.325**	**0**	**35.284**	**0.334**	**0.022**	**0.032**	**0.009**	**0.415**	**34.415**	**0.358**	**72.777**
4	**0**	**0**	**0.031**	**0.02**	**0.014**	**0.026**	**0**	**0.021**	**0**	**0.005**	**0.014**	**0.033**	**0**	**0.008**	**17.06**	**0**	**8.024**	**1.034**	**0.037**	**0.23**	**0.003**	**0.145**	**11.875**	**1.152**	**39.732**

AX12-1704 Grain 6
Helen Zone

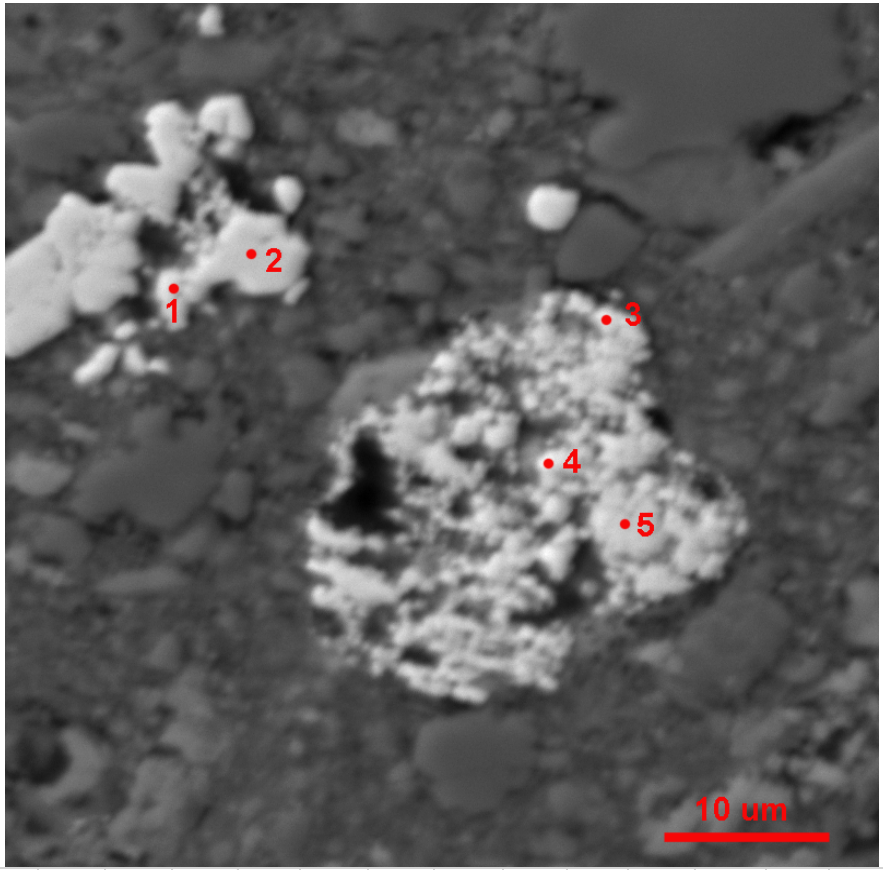

No.	Ag	Au	Na	Hg	Tl	As	Pb	Cu	Se	Bi	Co	Zn	W	Ni	Si	Te	Fe	Al	Sb	Ti	Sn	Mo	S	Ca	Total
1	**0**	**0.002**	**0.027**	**0.008**	**0.033**	**0.01**	**0.009**	**0.032**	**0**	**0**	**0.026**	**0.163**	**0**	**0**	**18.15**	**0**	**12.424**	**2.56**	**0.056**	**0.192**	**0**	**0.198**	**16.073**	**5.067**	**55.03**
2	0	0	0.03	0	0.01	0.004	0	0.012	0	0	0.098	0.03	0	0.032	1.422	0	43.562	0.16	0.014	0.004	0.019	0.671	51.757	0.127	97.952
3	0	0.013	0.072	0.035	0.046	0.041	0	0.086	0	0	0.061	0.106	0	0.203	2.209	0	39.612	0.865	0.027	0.072	0.007	0.592	45.882	0.881	90.81
4	0	0	0.024	0.011	0.058	0.047	0	0.035	0	0	0.054	0.101	0	0.106	1.847	0	38.942	0.983	0.038	0.064	0.015	0.552	44.38	0.521	87.778
5	0	0	0.039	0	0.014	0.034	0	0.039	0	0	0.067	0.098	0	0.156	1.593	0	38.322	0.634	0.028	0.311	0.01	0.552	43.155	0.407	85.459

AX12-1704 Grain 9
Helen Zone

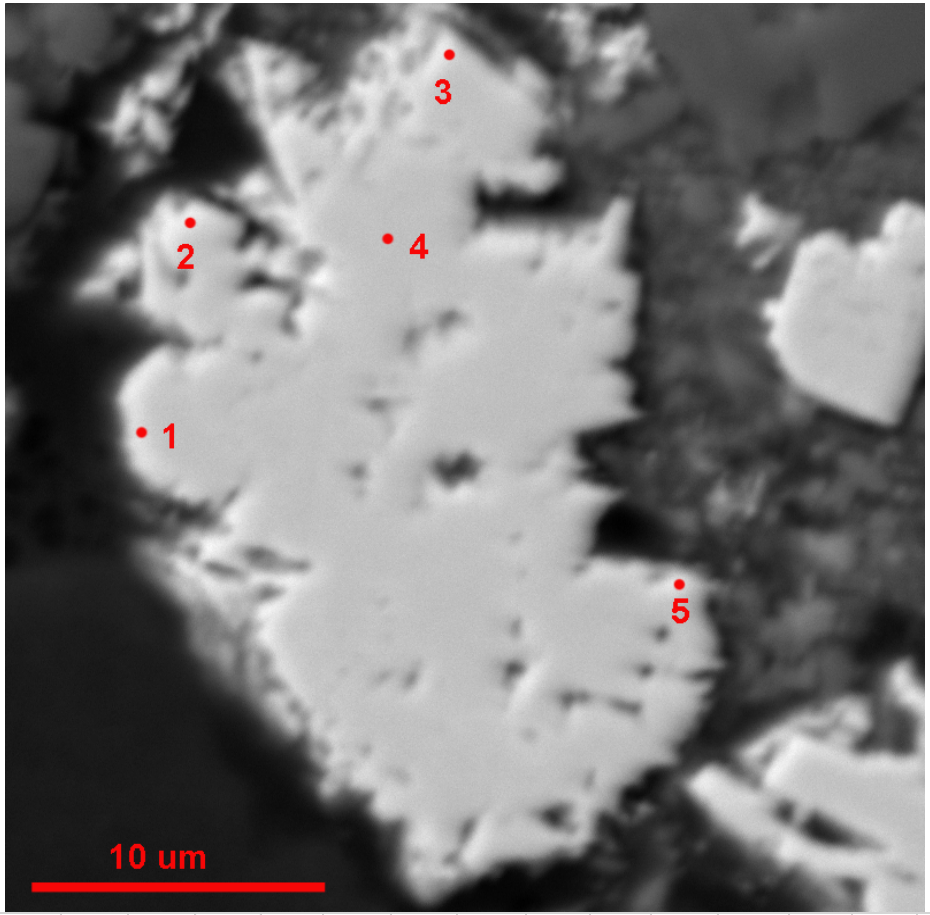

No.	Ag	Au	Na	Hg	Tl	As	Pb	Cu	Se	Bi	Co	Zn	W	Ni	Si	Te	Fe	Al	Sb	Ti	Sn	Mo	S	Ca	Total
1	0	0.013	0	0.018	0.076	0.536	0	0.034	0	0	0.066	0	0	0	0.027	0	45.451	0	0.142	0	0.038	0.655	52.555	0	99.611
2	0	0.006	0	0.014	0.007	0.276	0	0.045	0	0.004	0.057	0.024	0	0	0.091	0	44.761	0.006	0.078	0.015	0.026	0.65	51.488	0.018	97.566
3	0	0.004	0	0.011	0.118	1.187	0	0.048	0	0	0.059	0	0.002	0	0.064	0	44.569	0.008	0.105	0	0.05	0.658	52.058	0.004	98.945
4	0	0	0.004	0.031	0.231	1.976	0	0.034	0	0	0.056	0.005	0.013	0	0.034	0	43.956	0.005	0.161	0.025	0.038	0.654	51.386	0	98.609
5	0	0	0.028	0.055	0.082	0.868	0	0.041	0	0	0.055	0.038	0	0	1.855	0	40.387	0.583	0.134	0.032	0.03	0.581	46.501	0.555	91.825

Appendix E.
Vein Descriptions from Collected 2201 Zone Samples

Hole	Footage	Gangue	Gangue 2	Gangue 3	Sulfide	Sulfide 2	Sulfide 3	Sulfide 4	Sulfide 5	dominant (sulfide or gangue)	width (mm)
PG14-23	1529.8	cc			py					g	2
PG14-23	1609.5	cc			py	sph	gn	cpy?		s	3.5
PG14-23	1615.5	cc			py	sph	gn			s	3
PG14-23	1617	cc			sph	py	gn			G	1.5
PG14-23	1623.5	cc			py	sph	gn			G	4.5
PG14-23	1630	cc?			py	sph	gn			S	5.5
PG14-23	1646.5	cc			barren						1.5
PG14-23	1657	cc			py	sph	gn			S	6.5
PG14-23	1665	cc			py	sph	gn			g	2.5
PG14-23	1684.5	cc	sid	eu-qtz	py	sph	gn			g	1.0 - 5.0
PG14-23	1697	cc			py	sph	gn			s	3
PG14-23	1706.8	cc	qtz	sid	sph	py	gn			g	2.5
PG14-23	1710	cc			py	sph	gn			s	2.5
PG14-23	1711.5	qtz	sid	cc	py	sph					4.5
PG14-23	1731.5	cc			py	sph	gn				1
PG14-23	1742.5	qtz	sid	cc	py	sph	gn				3.5
PG14-23	1742.6	qtz	sid	cc	py	sph	gn				10.5
PG14-23	1742	qtz	sid	cc	py	sph	gn			g	3.0 - 6.0
PG14-23	1743	cc	sid		py	sph	gn?			g	3.5
PG14-23	1749	qtz	sid	cc	py	sph	aspy			g	3.5
PG14-23	1875.5	cc			py	gn	sph			g	1.5
PG14-23	1886.5	qtz	sid	cc	py	sph	po	gn		g	33
PG14-23	1896.5	qtz	sid		py	sph				g	4
PG14-23	1928	cc			py	sph	gn	cpy		s	1.5
PG14-23	1950	qtz			py	po	sph	cpy		g	12.0 - 15.0
PG14-23	1954.5	cc			py					g	1
PG14-23	1954.4	cc			py					g	1
PG14-23	1991	qtz			py	cpy?	sph			G	3.5
PG14-23	1993	qtz			sph	py				G	3.5
PG14-23	2004	qtz	cc	sid?	py	sph	gn			S	33
PG14-23	2057	cc			py	cpy?				s	1.75
PG14-23	2124	cc			py	sph	cpy	po		S	2
PG14-23	1750	cc			py	sph	gn			S	4
PG14-23	1769	qtz			py	sph				g	4.5
PG14-23	1775	sid	qtz		py	gn					2

PG14-23	**1778.4**	**qtz**	**sid**		**py**	**sph**				**s**	**4**
PG14-23	**1778.5**	**qtz**	**cc**	**sid?**	**py**	**sph**				**s**	**3.5**
PG14-23	**1784**	**cc**	**qtz**	**sid?**	**py**	**sph**	**gn**	**cpy**		**g**	**4.0 - 6.0**
PG14-23	**1809**	**cc**			**py**	**sph**	**gn**			**g**	**2**
PG14-23	**1851.5**	**qtz**	**cc**		**py**	**sph**	**cpy**			**s**	**3**
PG14-23	**2450.5**	**cc**			**py**	**sph**					**25**
PG14-23	**2229**	**cc**	**sid**		**py**					**g**	**1.5**
PG14-23	**2317**	**cc**			**barren?**						**1.5**
PG14-23	**2723**	**cc**			**barren**						**4**
PG14-23	**2773**	**cc**			**barren**						**1**
PG14-23	**2784**	**cc**			**barren**						**5.5**
PG14-23	**2841**	**cc**			**py**	**sph**	**gn**			**s**	**2**
PG14-23	**2904**	**?**			**sph**	**py**	**gn**			**S**	**20**
PG14-23	**2919**	**sid**	**cc**		**py**	**sph**				**g**	**1**
PG14-15	**2417**	**qtz**			**sph**	**py**	**gn**			**s**	**1.5**
AX-46	**2746.3**	**qtz**	**sid**		**py**					**g**	**2.5**
AX-46	**2110.5**	**cc**			**py**	**gn**	**sph**			**g**	**4**
AX-46	**2198**	**cc**			**py**	**sph**					**<1**
AX-46	**2895.3**	**qtz**			**py**	**sph**				**g**	**1.5**
AX-46	**2889.7**	**qtz**			**py**	**gn**	**sph**			**equal**	**1**
AX-46	**2894**	**qtz**	**cc**	**sid**	**py**	**dark sulfide thread**				**g**	**3**
AX-46	**2888**	**qtz**			**po**	**py?**				**g**	**1.5**
AX-46	**2920.5**	**qtz**	**cc**		**py**	**po**				**g**	
PG14-14	**2436**	**cc (ferroan?)**			**sph**	**py**				**G**	**13**
PG14-14	**2428.5**	**cc**			**sph**	**py**					**1.5**
PG14-14	**2440**	**qtz?**	**cc**		**py**	**sph**				**S**	**4**
PG-02	**2105**	**cc**			**barren**						**10**
PG-02	**2147.5**	**cc**			**py**	**sph**	**gn**			**s**	**4**
PG-02	**2065.8**	**cc**	**dol?**		**po**	**py**	**sph**	**cpy**			**25**
AX-46	**2642.3**	**qtz**			**py**	**sph**	**aspy**	**cpy**		**s**	**3**
AX-46	**2646.8**	**cc**			**sph**	**py**	**gn**			**s**	**2.5**
AX-46	**2684**	**qtz**	**cc**	**sid**	**py**	**sph**	**aspy**	**cpy**			**1**
AX-46	**2665.7**	**qtz**	**cc**		**sph**	**aspy**	**py**	**cpy**		**s**	**2.0 - 6.0**
AX-46	**2675.5**	**qtz**	**sid**		**py**	**sph**	**po**	**cpy**		**s**	**2.5**
AX-46	**2666.5**	**qtz**	**sid**		**aspy**	**py**	**sph**	**cpy**		**s**	**4.0 - 6.0**
AX-46	**2710.8**	**qtz**	**sid**		**py**	**sph**	**aspy**	**cpy**		**s**	**1.5**
AX-46	**2762.5**	**qtz**	**sid**		**sph**	**gn**	**cpy**	**py**		**s**	**1.5**
PG14-05	**1989.3**	**cc**			**py**	**sph**				**g**	**10**
PG14-05	**1967.5**	**cc**			**barren**						**1**

PG14-05	2279	qtz	sid		aspy	py	sph	po	gn	s	15
PG14-05	2292	qtz	cc	sid	aspy	gn	py	sph	cpy	equal	3
PG14-05	2293.8	sid	qtz		py	sph	hem?			equal	7
PG14-05	2294	qtz	cc	sid	py	aspy	sph	cpy	po	s	1
PG14-05	2296.5	cc			py	sph	aspy	cpy		s	2.0-4.0
AX-53	2485.2	cc	sericite?	qtz	py					g	1.5
AX-53	2457.5	cc	sericite?	qtz	py					g	1.5
AX-53	2367	cc			py	sph				G	2.5
PG14-15	1876	cc			py					g	3.5
PG14-15	1616.5	qtz	sid		py	sph	cpy	gn	po?	s	30
PG14-15	2204a	qtz	cc	sid	py	sph	cpy			g	2.0-5.0
PG14-15	2204b	qtz?	cc?		py	sph	po?	cpy		S	2.0-4.0
PG14-15	2235.5	cc			py	sph	gn	cpy?		s	20
PG14-15	2236	cc			py	sph	gn			s	20
PG14-15	2242	qtz	sid	cc	py	sph				g	2
PG14-15	2243.5	qtz	sid	cc	py	sph				S	1.0-5.0
PG14-15	1944	cc			py					g	5
PG14-15	1863	cc			py	sph	gn			g	3.5
PG14-15	1862.7	cc			py		sph			g	2.5
PG14-15	3382.7a	qtz	sid		aspy	py				S	10
PG14-15	3382.7b	qtz	sid		py	sph	aspy			s	2.0-7.0
PG14-15	3383.4	qtz	sid	cc	py	po	sph	aspy		s	5.0-7.0
PG14-15	3385.5	qtz	sid		aspy	py	po			s	1.0-5.0
PG14-15	2463.3	qtz			py	sph	cpy	po		S	14
PG14-15	2491	qtz	sid		py	po	sph	aspy		s	15.0-20.0
PG14-15	2486.5a	qtz	sid	cc	py	po	gn			s	1.5
PG14-15	2486.5b	qtz	sid?	cc	py	sph	gn	po?	VG	g	3.0-5.0
PG14-15	2486.5c	sid	sid		dark fine-grained sulfs					G	2.5
PG14-15	2487.4a	qtz	sid	sid	py	sph	po	cpy		s	13
PG14-15	2487.4b	qtz	sid	sid	py	sph	po			s	7
PG14-15	2487.4c	qtz	sid?		py	sph?				s	1
PG14-15	2492a	qtz	sid	sid	py	sph	gn			s	4
PG14-15	2492b	sid			py					g	1
PG14-15	2513.6	qtz	sid	sid	py	gal	cpy	aspy	VG	s	150
AX-51	2611.8a	qtz	sid		aspy	gn	cpy	VG	py	g	5.5
AX-51	2611.8b	qtz			py	sph	cpy	aspy		s	1.0-3.0
AX-51	2848.5	qtz	sid		sph	aspy	py	cpy		S	17

AX-51	2872.8	qtz	sid		py	sph	gn			S	1
AX-51	2867.5	qtz	sid		sph	aspy	py			s	3.5
PG14-15	2557	qtz	sid		aspy	py	sph	cpy		s	16
PG14-15	2573.3	qtz	sid		py	aspy				S	15
PG14-15	2587.4	qtz			py	sph	cpy	gn	po	equal	5.5
PG14-15	2608.5	qtz	sid		py	sph	gn			g	1.5
AX-35	1780	cc			py					equal	10
PG14-15	3315.6	qtz	sid	sid	py	sph	cpy	gn		s	2
PG14-15	3322	qtz	sid		gn?	py?					2.5
PG14-15	3331	qtz	cc		py	po	sph?			g	4
PG14-15	3340.7	qtz	cc		py					g	2
PG14-15	3352.2a	qtz	sid	sid	barren						6
PG14-15	3352.2b	qtz	sid		py	sph				equal	2.5
PG14-15	3346.4	qtz	sid	sid	py	sph	po	aspy?		s	5
PG14-03	2714.3	cc			barren						2
PG14-03	2751	sid	sid		py	sph	po			S	9
PG14-03	2761.8	cc	qtz		py	sph	gn			s	3.5
AX-46	2114	qtz	sid		py	sph				g	5
PG14-10	2652.5				py	aspy	cpy			S	35
PG14-05	1887.5	cc			py	sph				g	2
AX-53	1237	sid?	sid?		py					s?	<1
AX-53	1320.5	sid	cc		py					s?	<1
PG-02	2182.8a	qtz	sid		barren						3
PG-02	2182.8b	qtz	sid		sph	py	gn			equal	1.5
PG-02	2232.2	qtz	sericite?		py					s	<1
PG-02	2301.8	qtz	sid	sid	py	aspy	sph	gn			6
PG-02	2535.5	qtz	sid	sid	py	aspy	cpy	sph	gn	g	5
PG-02	2536.7	qtz	sid		py	aspy	cpy	sph			9
AX-51	2591.8	sid	sid		py	sph	gn			s	4.0-10.0
AX-51	2600	qtz	sid		py	sph				s	3.5
AX-51	2591a	qtz	sid		py	po				S	2.0-5.0
AX-51	2591b	sid	qtz		py	sph				s	1
AX-51	2605.2	qtz			py	sph	cpy			s	6
AX-51	2615.5	qtz			sph	py	cpy			g	1.5
AX-51	2857.8	qtz	sid		aspy	py	sph			g	2
PG1425A	1641	cc			py	gn	sph			g	
PG1425A	1570	cc			py	sph	gn			s	
PG1425A	2738.5	cc	?		py	sph	gn			S	1.5
PG1425A	2750	cc	sid	qtz							
PG1425A	2818.5	cc									
PG1425A	2925	sid	qtz								

PG1425A	**2962**	**qtz**	**sid**								
PG1425A	**2178**	**qtz**									
PG1425A	**2183**	**qtz**	**Fe dol**	**sid**							
PG1425A	**2587.5**	**cc**	**qtz**								
PG1425A	**2572**	**qtz**	**cc**								
PG1425A	**2561**	**cc?**									
PG1425A	**2484.2**	**cc**									
PG1425A	**2411**	**cc**	**sid?**								
PG1425A	**2227**	**qtz**									

Appendix F.
R Scripts for Geochemical Modeling

All scripts are written for the CHNOSZ package for R (Dick, 2019). http://www.chnosz.net/

Jeff Dick assisted with the language for some of the following examples and others are based off demos on the CHNOSZ web site as suggested by W. Bonner in 2018-2019.

Script E.1

To plot gold solubility on logfO_2-pH plots with sulfur species predominance fields (Figs. 31, 32).

```
# gold solubility contours on logfO2-pH diagram
# adapted from demo by J. Dick
# After Williams-Jones et al., 2009, Fig. 3
# doi:10.2113/gselements.5.5.281


# modify to use thermodynamic properties recommended by Pokrovski et al. 2014
mod.obigt("Au(HS)2-", G = 3487, H = 4703, S = 77.46, Cp = 3.3, V = 75.1, a1 = 12.3373, a2 = 22.3421, a3 = 3.0317, a4 = -3.7026, c1 = -53.6010, c2 = 31.4030, omega = 0.7673)
mod.obigt("AuCl2-", G = -36795, H = -46664, S = 47.16, Cp = -26.4, V = 68.6, a1 = 11.4774, a2 = 20.2425, a3 = -2.2063, a4 = -3.6158, c1 = 27.0677, c2 = -22.440, omega = 0.8623)
mod.obigt("AuCl", G = -3184, H = -2077, S = 41.73, Cp = -15.1, V = 53.1, a1 = 9.0294, a2 = 14.2654, a3 = 0.1430, a4 = -3.3687, c1 = -2.6993, c2 = -6.1162, omega = 0)
mod.obigt("Au+", G = 39000, H = 45182, S = 16.5, Cp = 0.58, V = 31.4, a1 = 6.1161, a2 = 7.1520, a3 = 2.9389, a4 = -3.0747, c1 = 7.7764, c2 = -2.9158, omega = 0.1390)
mod.obigt("Au(HS)", G = 8344, H = 13193, S = 50.86, Cp = 1.8, V = 56.5, a1 = 9.4965, a2 = 15.4057, a3 = -0.3052, a4 = -3.1459, c1 = -38.1356, c2 = 19.6524, omega = 0.0)

# define temperature (degrees C), pressure (bar), grid resolution
T <- 180
P <- "Psat"
res <- 600
# make smooth (TRUE) or sharp (FALSE) transitions between basis species
blend <- TRUE

# set up system
basis(c("Au", "Cl-", "H2S", "H2O", "oxygen", "H+", "Fe"))
species(c("Au(HS)2-", "AuCl2-", "AuCl", "Au+", "Au(OH)2-", "AuOH", "AuHS"))
# this get us close to total S = 0.01 m
basis("H2S", -2)
# calculate solution composition for 1 mol/kg NaCl
NaCl <- NaCl(T = T, P = P, m_tot=1)
basis("Cl-", log10(NaCl$m_Cl))
# calculate affinity with changing basis species
bases <- c("H2S", "HS-", "HSO4-", "SO4-2")
m <- mosaic(bases, pH = c(2, 10, res), O2 = c(-53, -34, res), T = T, P = P, IS = NaCl$IS, blend = blend)
# calculate and plot solubility
s <- solubility(m$A.species)
# convert to ppb
s <- convert(s, "ppb")
```

```
diagram(s, type="loga.balance", levels = c(1, 10, 100, 1000))
# show predominance fields
diagram(m$A.bases, add=TRUE, col = "red", col.names = "red", limit.water = FALSE, lty = 2, italic = TRUE)
diagram(m$A.species, add=TRUE, col = "goldenrod4", col.names = "goldenrod4", limit.water = FALSE, lwd = 2, bold = TRUE)
```

Script E.2
To plot silver solubility on logfO_2-pH plots with sulfur species predominance fields (Figs. 31, 32).

```
#adapted from Script E.1


# modify to use thermodynamic properties recommended by Pokrovski et al. 2014
mod.obigt("Ag(HS)2-", G = 287, H = -6636, S = 49.00, Cp = 3.348, V = 42.82, a1 = 7.8651, a2 = 11.4225, a3 = 1.2604, a4 = -3.2512, c1 = 13.9576, c2 = -2.3624, omega = 0.6367)
mod.obigt("AgCl2-", G = -51350, H = -60092, S = 49.78, Cp = -16.6, V = 37.1, a1 = 7.1327, a2 = 9.8065, a3 = 1.8947, a4 = -3.1844, c1 = 4.8953, c2 = -6.7789, omega = 0.6667)
mod.obigt("AgCl", G = -17399, H = -18810, S = 32.067, Cp = -5.328, V = 21.631, a1 = 4.2750, a2 = 3.7555, a3 = 4.2739, a4 = -2.9343, c1 = 3.0441, c2 = -4.1199, omega = 0)


# define temperature (degrees C), pressure (bar), grid resolution
T <- 180
P <- "Psat"
res <- 600
# make smooth (TRUE) or sharp (FALSE) transitions between basis species
blend <- TRUE

# set up system
basis(c("Ag", "Cl-", "H2S", "H2O", "oxygen", "H+"))
species(c("Ag(HS)2-", "AgCl2-", "AgCl", "Ag+", "Ag(OH)2-", "AgOH", "AgHS"))
# this get us close to total S = 0.01 m
basis("H2S", -2)
# calculate solution composition for 1 mol/kg NaCl
NaCl <- NaCl(T = T, P = P, m_tot=1)
basis("Cl-", log10(NaCl$m_Cl))
# calculate affinity with changing basis species
bases <- c("H2S", "HS-", "HSO4-", "SO4-2")
m <- mosaic(bases, pH = c(2, 10, res), O2 = c(-53, -34, res), T = T, P = P, IS = NaCl$IS, blend = blend)
# calculate and plot solubility
s <- solubility(m$A.species)
# convert to ppb
s <- convert(s, "ppb")
diagram(s, type="loga.balance", levels = c(0.01, 0.1, 1, 10, 100, 1000, 10000))
# show predominance fields
diagram(m$A.bases, add=TRUE, col = "red", col.names = "red", limit.water = FALSE, lty = 2, italic = TRUE)
diagram(m$A.species, add=TRUE, col = "skyblue4", col.names = "skyblue4", limit.water = FALSE, lwd = 2, bold = TRUE)
```

Script E.3
To plot total Au solubility (Fig. 29). Adapted from CHNOSZ demo "gold.R: Au solubility calculations"

```
# CHNOSZ/demo/gold.R: Au solubility calculations
# 20181101 jmd first version
# 20181109 add calculation of K+ molality
# 20190127 update Au species in OBIGT, not here

# modify to use thermodynamic properties recommended by Pokrovski et al. 2014
mod.obigt("Au(HS)2-", G = 3487, H = 4703, S = 77.46, Cp = 3.3, V = 75.1, a1 = 12.3373, a2 = 22.3421,
a3 = 3.0317, a4 = -3.7026, c1 = -53.6010, c2 = 31.4030, omega = 0.7673)
mod.obigt("AuCl2-", G = -36795, H = -46664, S = 47.16, Cp = -26.4, V = 68.6, a1 = 11.4774, a2 = 20.2425,
a3 = -2.2063, a4 = -3.6158, c1 = 27.0677, c2 = -22.440, omega = 0.8623)
mod.obigt("AuCl", G = -3184, H = -2077, S = 41.73, Cp = -15.1, V = 53.1, a1 = 9.0294, a2 = 14.2654, a3
= 0.1430, a4 = -3.3687, c1 = -2.6993, c2 = -6.1162, omega = 0)
mod.obigt("Au+", G = 39000, H = 45182, S = 16.5, Cp = 0.58, V = 31.4, a1 = 6.1161, a2 = 7.1520, a3 =
2.9389, a4 = -3.0747, c1 = 7.7764, c2 = -2.9158, omega = 0.1390)
mod.obigt("Au(HS)", G = 8344, H = 13193, S = 50.86, Cp = 1.8, V = 56.5, a1 = 9.4965, a2 = 15.4057, a3
= -0.3052, a4 = -3.1459, c1 = -38.1356, c2 = 19.6524, omega = 0.0)


# set up system
# use H2S here: it's the predominant species at the pH of the QMK buffer -- see sulfur()
basis(c("Al2O3", "quartz", "Fe", "Au", "K+", "Cl-", "H2S", "H2O", "oxygen", "H+"))
# set molality of K+ in completely dissociated 0.5 molal KCl
# NOTE: This value is used only for making the legend;
# activities corrected for ionic strength are computed below
basis("K+", log10(0.5))

# create a pH buffer
mod.buffer("QMK", c("quartz", "muscovite", "K-feldspar"), "cr", 0)

# define colors for Au(HS)2-, AuHS, AuOH, AuCl2-
# after Williams-Jones et al., 2009
# (doi:10.2113/gselements.5.5.281)
col <- c("#ED4037", "#F58645", "#0F9DE2", "#22CC88")

# log(m_Au)-T diagram like Fig. 2A of Williams-Jones et al., 2009 and Fig. 8a of Pokrovski et al., 2014
# (doi:10.2113/gselements.5.5.281)
# (doi:10.1144/SP402.4)
Au_T2 <- function() {
  species(c("Au(HS)2-", "AuHS", "AuOH", "AuCl2-"))
  # total S = 0.01 m
  basis("H2S", -2)
  # apply PPM buffer for fO2
  basis("O2", "PPM")
  # apply QMK buffer for pH
  basis("H+", "QMK")
  # estimate solution composition for 1.5 m NaCl and 0.5 m KCl
  chl <- chloride(T = seq(150, 550, 10), P = 1000, m_NaCl = 1.5, m_KCl = 0.5)
```

```
  #  # calculate affinity and solubility, considering speciation of sulfur
  #  bases <- c("H2S", "HS-", "SO4-2", "HSO4-")
  #  m <- mosaic(bases, T = seq(150, 550, 10), `Cl-` = log10(chl$m_Cl), `K+` = log10(chl$m_K), P = 1000,
IS = chl$IS)
  #  s <- solubility(m$A.species)
  a <- affinity(T = seq(150, 550, 10), `Cl-` = log10(chl$m_Cl), `K+` = log10(chl$m_K), P = 1000, IS =
chl$IS)
  s <- solubility(a)
  # make diagram and show total log molality
  diagram(s, ylim = c(-10, -3), col = col, lwd = 2, lty = 1)
  diagram(s, add = TRUE, type = "loga.balance", lwd = 3, lty = 2)
  # make legend and title
  dP <- describe.property("P", 1000)
  dNaCl <- expression(italic(m)[NaCl] == 1.5)
  dKCl <- expression(italic(m)[KCl] == 0.5)
  legend("topleft", c(dP, dNaCl, dKCl), bty = "n")
  dH2S <- expr.species("H2S", value = 0.01, molality = TRUE)
  dO2 <- describe.basis(ibasis = 9)
  dpH <- describe.basis(ibasis = 10)
  legend(300, -3, c(dH2S, dO2, dpH), bty = "n")
  title(main=("After Williams-Jones et al., 2009, Fig. 2A"), font.main = 1)
}

Au_T2()
```

Script E.4
To plot total Ag solubility (Fig. 30). Adapted from CHNOSZ demo "gold.R: Au solubility calculations"

```
# modify to use thermodynamic properties recommended by Pokrovski et al. 2014
mod.obigt("Ag(HS)2-", G = 287, H = -6636, S = 49.00, Cp = 3.348, V = 42.82, a1 = 7.8651, a2 = 11.4225,
a3 = 1.2604, a4 = -3.2512, c1 = 13.9576, c2 = -2.3624, omega = 0.6367)
mod.obigt("AgCl2-", G = -51350, H = -60092, S = 49.78, Cp = -16.6, V = 37.1, a1 = 7.1327, a2 = 9.8065,
a3 = 1.8947, a4 = -3.1844, c1 = 4.8953, c2 = -6.7789, omega = 0.6667)
mod.obigt("AgCl", G = -17399, H = -18810, S = 32.067, Cp = -5.328, V = 21.631, a1 = 4.2750, a2 = 3.7555,
a3 = 4.2739, a4 = -2.9343, c1 = 3.0441, c2 = -4.1199, omega = 0)


# set up system
# use H2S here: it's the predominant species at the pH of the QMK buffer -- see sulfur()
basis(c("Al2O3", "quartz", "Fe", "Ag", "K+", "Cl-", "H2S", "H2O", "oxygen", "H+"))
# set molality of K+ in completely dissociated 0.5 molal KCl
# NOTE: This value is used only for making the legend;
# activities corrected for ionic strength are computed below
basis("K+", log10(0.5))

# create a pH buffer
mod.buffer("QMK", c("quartz", "muscovite", "K-feldspar"), "cr", 0)
```

```
# define colors for Ag(HS)2-, AgHS, AgCl2-
col <- c("#ED4037", "#F58645", "#22CC88")



Ag_T2 <- function() {
  species(c("Ag(HS)2-", "AgHS", "AgCl2-"))
  # total S = 0.01 m
  basis("H2S", -2)
  # apply PPM buffer for fO2
  basis("O2", "PPM")
  # apply QMK buffer for pH
  basis("H+", "QMK")
  # estimate solution composition for 1.5 m NaCl and 0.5 m KCl
  chl <- chloride(T = seq(150, 550, 10), P = 1000, m_NaCl = 1.5, m_KCl = 0.5)
  #  # calculate affinity and solubility, considering speciation of sulfur
  #  bases <- c("H2S", "HS-", "SO4-2", "HSO4-")
  #  m <- mosaic(bases, T = seq(150, 550, 10), `Cl-` = log10(chl$m_Cl), `K+` = log10(chl$m_K), P = 1000,
IS = chl$IS)
  #  s <- solubility(m$A.species)
  a <- affinity(T = seq(150, 550, 10), `Cl-` = log10(chl$m_Cl), `K+` = log10(chl$m_K), P = 1000, IS =
chl$IS)
  s <- solubility(a)
  # make diagram and show total log molality
  diagram(s, ylim = c(-10, -3), col = col, lwd = 2, lty = 1)
  diagram(s, add = TRUE, type = "loga.balance", lwd = 3, lty = 2)
  # make legend and title
  dP <- describe.property("P", 1000)
  dNaCl <- expression(italic(m)[NaCl] == 1.5)
  dKCl <- expression(italic(m)[KCl] == 0.5)
  legend("topleft", c(dP, dNaCl, dKCl), bty = "n")
  dH2S <- expr.species("H2S", value = 0.01, molality = TRUE)
  dO2 <- describe.basis(ibasis = 9)
  dpH <- describe.basis(ibasis = 10)
  legend(300, -3, c(dH2S, dO2, dpH), bty = "n")
}

Ag_T2()
```